AD NUMBER
AD855385
LIMITATION CHANGES
TO: **Approved for public release; distribution is unlimited.**
FROM: **Distribution authorized to U.S. Gov't. agencies and their contractors; Administrative/Operational Use; MAR 1969. Other requests shall be referred to Rocket Propulsion Lab., Edwards AFB, CA.**
AUTHORITY
AFRPL ltr 29 Sep 1971

AFRPL-TR-69-129

FINAL REPORT
DEVELOPMENT OF CASTABLE CARBONACEOUS MATERIALS FOR SOLID ROCKET NOZZLES

THIOKOL CHEMICAL CORPORATION
WASATCH DIVISION

Technical Report AFRPL-TR-69-129

March 1969

ROCKET PROPULSION LABORATORY
RESEARCH AND TECHNOLOGY DIVISION
AIR FORCE SYSTEMS COMMAND
Edwards, California

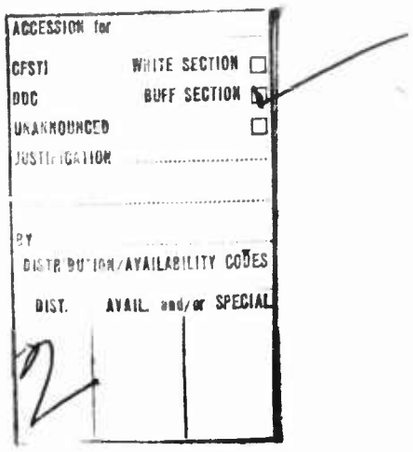

SPECIAL NOTICE

When U. S. Government drawings, specifications, or other data are used for any purpose other than a definitely related Government procurement operation, the Government thereby incurs no responsibility nor any obligation whatsoever, and the fact that the Government may have formulated, furnished, or in any way supplied the said drawings, specifications, or other data, is not to be regarded by implication or otherwise, or in any manner licensing the holder or any other person or corporation, or conveying any rights or permission to manufacture, use, or sell any patented invention that may in any way be related thereto.

AFRPL-TR-69-129 Contract AF 04(611)-11417

FINAL REPORT
DEVELOPMENT OF CASTABLE CARBONACEOUS MATERIALS FOR SOLID ROCKET NOZZLES

Prepared by

THIOKOL CHEMICAL CORPORATION
WASATCH DIVISION
Brigham City, Utah

Stanley H. Cardall Richard C. Laramee

TECHNICAL REPORT AFRPL-TR-69-129

March 1969

Prepared for

ROCKET PROPULSION LABORATORY
RESEARCH AND TECHNOLOGY DIVISION
AIR FORCE SYSTEMS COMMAND
Edwards, California

Publications No. 0469-23540B

FOREWORD

This report was prepared by Wasatch Division of Thiokol Chemical Corporation, Brigham City, Utah, under Contract AF 04(611)-11417. The work was administered under direction of the Air Force Rocket Propulsion Laboratory, Motor Component Development Branch, with W. F. Payne and R. Schoner as the project engineers. This report covers the program research and development performance period from March 1966 thru March 1969.

This program was conducted at the Wasatch Division under the management of E. L. Bennion with E. L. Gray as the technical project manager. Others participating in the program were: S. H. Cardall, Materials Development and Nozzle Manufacture; and Mr. R. C. Laramee, Nozzle Design and Performance Analysis.

Publication of this report does not constitute Air Force approval of its findings and conclusions. It is published only for the dissemination of results and for the exchange and stimulation of ideas.

This technical report has been reviewed and is approved.

Charles R. Cooke
Chief, Solid Rocket Division

ABSTRACT

Three basic material formulations designated T-2610, T-4120, and T-4113 were evaluated by laboratory testing and static firing in test motors with nozzles having a throat diameter of approximately 4 inches. In total, six nozzles were fabricated and static tested. Nozzle No. 1, which was fabricated of conventional nozzle materials, was used as a baseline. The remaining five nozzles were constructed using the castable carbonaceous materials. Nozzles No. 1, 2, and 3 functioned successfully. Nozzle No. 4 malfunctioned due to material failure. Both a motor and nozzle malfunction occurred during the test of Nozzle No. 5. A motor failure prevented accurate evaluation of Nozzle No. 6. Performance data from the six nozzle tests indicate that the materials will require additional development effort; however, the accumulative results for materials T-2610 and T-4120 continue to be encouraging and warrant additional evaluation effort.

TABLE OF CONTENTS

LIST OF ILLUSTRATIONS

LIST OF ILLUSTRATIONS (Cont)

LIST OF ILLUSTRATIONS (Cont)

LIST OF ILLUSTRATIONS (Cont)

LIST OF ILLUSTRATIONS (Cont)

LIST OF ILLUSTRATIONS (Cont)

LIST OF ILLUSTRATIONS (Cont)

LIST OF ILLUSTRATIONS (Cont)

LIST OF TABLES

LIST OF TABLES (Cont)

SECTION I
INTRODUCTION

Previous materials investigation had demonstrated that a category of castable or moldable carbonaceous materials offers significant cost and fabrication advantages over contemporary ablative nozzle materials. Although these advantages had been demonstrated, material performance had not been thoroughly evaluated. This program was funded to demonstrate the performance of these materials prior to their consideration for use in solid propellant rocket motor nozzles, as well as to provide a performance comparison to the reinforced plastic ablatives commonly in use.

The specific objectives of this program were to develop low pressure moldable or castable carbonaceous material(s) for utilization in a solid propellant rocket motor by (1) characterizing the material, (2) developing processing techniques, (3) establishing process controls, and (4) developing repair techniques for rejectable parts.

The program objectives were accomplished by means of a thorough laboratory investigation conducted to determine the optimum material formulations and processing techniques. This laboratory effort was then complemented by subscale nozzle static tests. A program block diagram is presented in Figure 1.

For purposes of discussion, the program results have been treated in two phases: Phase I, Material and Process Optimizations and Phase II, Subscale Nozzle Evaluation. These phases are contained in Sections II and III, respectively.

The work reported in Section II of the report resulted in the establishment of optimized material formulations for the inlet, throat backup, throat and exit cone nozzle insulation components. Fabrication techniques and processing parameters such as molding, pressure, and cure temperatures were established. Mechanical property design data were determined for these materials. In addition, nozzle repair materials and techniques were developed.

From the laboratory studies conducted, two low cost carbonaceous materials (T-2610 and T-4120) were considered as candidate nozzle insulation materials. The T-2610 has characteristics suitable for use as a throat and exit cone insulation. The T-4120, developed specifically for curing at moderate pressure, is suitable for exit cone application. These formulations consist basically of graphite powder and phenolic resin.

A third low cost material (T-4113) was designed for nozzle inlet applications; T-4113 incorporates an acrylonitrile butadiene rubber into the graphite powder and phenolic resin. This material was compounded to provide a specific elongation in the nozzle inlet liner.

Section III of the report provides a summary of the subscale nozzle phase. This phase included the design, manufacture, and test firing of six nozzles with a normal 4 in. diameter throat. Post-test nozzle performance was analyzed for comparative erosion, thermal, and structural information. The first subscale nozzle used conventional nozzle insulation materials and was used for control purposes. The other five nozzles were made with a variation of the proposed low cost carbonaceous materials and processes.

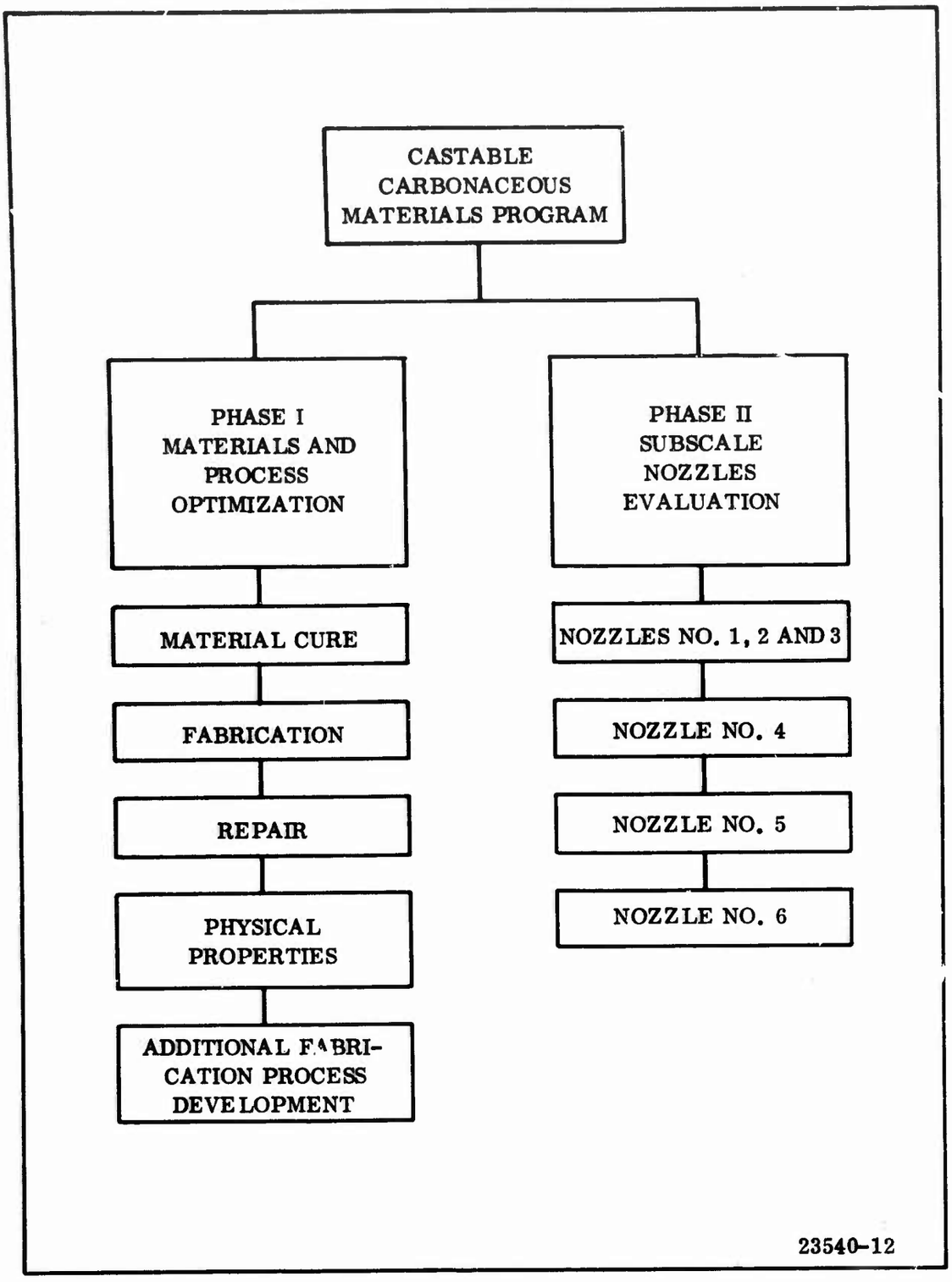

Figure 1. Program Block Diagram

SECTION II
PHASE I--MATERIALS AND PROCESS OPTIMIZATION

Based on laboratory evaluations, two low cost carbonaceous materials (T-2610 and T-4120) were selected as candidate nozzle insulation materials. The T-2610 was planned for use as a throat and exit cone insulation and the T-4120, which was developed specifically for curing at moderate pressure, was planned for exit cone application. These materials are basically formulations of graphite powder and phenolic resin.

A third low cost material (T-4113) was designed for nozzle inlet applications; T-4113 incorporates an acrylonitrile butadiene rubber into the graphite powder and phenolic resin. This material was compounded to provide a specific elongation in the nozzle inlet liner.

A. MATERIAL CURE

This section of the program involved the effects of curing laboratory test samples and nozzle components made of Low Cost Carbonaceous Materials (LCCM) formulations at various temperatures and pressures.

To simulate the internal stresses occurring in the material during the manufacture of large nozzles, laboratory flat slab and cylindrical test samples were prepared. The cylindrical samples were made by hand packing the material on the outside or inside of steel cylinders (7.5 in. ID and 8.5 in. OD) and then curing under appropriate conditions. The flat slabs and cylinders were cut into specimens to obtain density, tensile strength, tensile modulus, elongation and coefficient of thermal expansion data. The test matrix in Table I describes the cure system variables and the number of tests required.

Data obtained for the above optimization studies are listed in Tables II thru IV. The values given represent averages of several test specimens from each sample.

Only those cure systems providing acceptable physical properties were tested for relative erosion performance in the TU-379 motor test (Figure 2).

The three LCCM insulations were made into adapter cones, throats and exit cones for testing in the TU-379 materials test motor in accordance with the materials optimization erosion test matrix outlined in Table V.

As specified, three nozzle components were molded simultaneously in a multicavity mold or machined from a single block of material. Two components of

TABLE I

MATERIALS CURE OPTIMIZATION, PHYSICAL TEST DATA MATRIX

Variables -

T-4120 filled phenolic resin, low pressure cure
T-2610 filled phenolic resin, high pressure cure
T-4113 filled NBR-phenolic, low pressure cure

Five cure pressures, $\overline{P}_c$

0, 15, 200, 500, and 1,000 psi (nominal)

Two cure temperatures

170° F and 300° F (nominal)

Three cure processes-pressure application methods, P_M

internal cylinder
external cylinder
flat slab

Cure Temp (° F)	Material	$\overline{P}_c$ / P_M	Number of Test Specimens/Variables Combination*								
			0 (psi)		15 (psi)		200 (psi)			500 (psi)	1,000 (psi)
			Int Press.	Ext Press.	Int Press.	Ext Press.	Int Press.	Ext Press.	Flat Slab	Flat Slab	Flat Slab
170	T-4120		3	2	2	3	2	2	3	2	2
170	T-4113		2**	3	3	--	2	--	3	--	--
300	T-4120		--	--	2	3	2	--	3	2	--
300	T-2610		--	--	--	--	2	2	3	2	3
300	T-4113		--	--	--	2	--	--	3	--	--

*When three samples are listed, the third specimen was postcured.
**Specimens were unsatisfactory for testing purposes.

TABLE II

PHYSICAL PROPERTIES OF T-4113 MATERIAL

Process Variables			Physical Properties*				
Cure Temperature	Fabrication Method	Cure Pressure (psi)	Density (gm/cc)	Elongation (Percent)	Tensile Strength (psi)	Tensile Modulus	CTE (cm/cm/°C x 10^{-5})
						Values x 10^3	
170° F	External Drum	0	1.05 to 1.13	4.6 to 5.2	272 to 333	2.06 to 2.46	4.4 to 4.7
			1.09 Avg	4.9 Avg	303 Avg	2.26 Avg	4.6 Avg
			1.07**	0.6**	552**	3.08**	4.7**
						Values x 10^6	
	Internal Drum	0	← Visually Unsatisfactory*** →				
		15	1.49 to 1.54	0.02 to 0.03	285 to 555	1.00 to 1.16	2.4 to 2.8
			1.52 Avg	0.02 Avg	320 Avg	1.08 Avg	2.6 Avg
		200	← Visually Unsatisfactory*** →				
						Values x 10^5	
	Flat Slab	200	1.40 to 1.43	3.0 (Soft)	71 (Soft)	(Soft)	(Soft)
			1.42 Avg				
			1.41**	0.6**	589**	1.40**	2.44**
300° F	External Drum	15	1.17 to 1.17	7.0 to 11.0	34 to 36	(Soft)	3.4 to 5.0
			1.17 Avg	9.0 Avg	35 Avg		3.7 Avg
	Internal Drum	15	0.96 to 1.0	10.0 to 20.0	18 to 28	(Soft)	2.7 to 3.3
			0.99 Avg	15.0 Avg	23 Avg		2.9 Avg
						Values x 10^5	
	Flat Slab	200	1.51 to 1.53	4.2 to 6.2	408 to 461	1.19 to 1.34	1.46 to 2.76
			1.52 Avg	5.2 Avg	434 Avg	1.26 Avg	2.11 Avg
			1.54**	3.2**	534**	1.48**	2.28**

*The low and high values listed are each average values from four specimens.

**Postcured.

***Visually unsatisfactory samples contain numerous voids and were not suitable for testing.

TABLE III

PHYSICAL PROPERTIES OF T-4120 MATERIAL

Process Variables			Physical Properties*				
Cure Temperature	Fabrication Process	Cure Pressure (psi)	Density (gm/cc)	Elongation (Percent)	Tensile Strength (psi)	Tensile Modulus (10^6)	CTE (cm/cm/°C x 10^{-5})
170° F	External Drum	0	1.433 to 1.586 1.512 Avg	0.04 to 0.09 0.06 Avg	647 to 1,610 1,128 Avg	1.84 to 2.25 2.04 Avg	1.99 to 2.35 2.17 Avg
		15	1.530 to 1.564 1.547 Avg	0.10 to 0.10 0.10 Avg 0.07**	1,284 to 1,558 1,421 Avg	1.31 to 1.80 1.56 Avg 1.90**	1.99 to 2.68 2.34 Avg 1.75**
		200	1.755 to 1.770 1.763 Avg	0.07 to 0.13 0.10 Avg	1,423 to 2,147 1,785 Avg	2.08 to 2.22 2.15 Avg	2.49 to 5.11 3.80 Avg
	Internal Drum	0	1.592 to 1.560 1.576 Avg 1.465**	0.09 to 0.09 0.09 Avg 0.07**	1,376 to 1,860 1,608 Avg 528**	1.51 to 1.71 1.61 Avg 1.08**	2.10 to 2.17 2.14 Avg 1.49**
		15	1.449 to 1.467 1.458 Avg	0.08 to 0.08 0.08 Avg	375 to 546 460 Avg	0.97 to 1.27 1.12 Avg	5.77 to 6.73 6.25 Avg
		200	1.575 to 1.624 1.600 Avg	0.06 to 0.08 0.07 Avg	684 to 907 796 Avg	1.11 to 1.42 1.26 Avg	2.19 to 4.25 3.22 Avg
	Flat Slab	200	1.613 to 1.647 1.630 Avg 1.623**	0.03 and Broke 0.07**	532 and Broke 1,181**	1.53 and Broke 1.76**	3.42 to 4.05 3.74 Avg 1.43**
		500	1.760 to 1.781 1.770 Avg	0.03 to 0.05 0.04 Avg	1,670 to 1,675 1,672 Avg	1.69 to 1.81 1.75 Avg	1.86 to 2.71 2.28 Avg
		1,000	1.818 to 1.819 1.818 Avg	0.11 to 0.15 0.13 Avg	2,702 to 3,082 2,892 Avg	1.74 to 2.15 1.94 Avg	2.20 to 2.63 2.42 Avg
300° F	External Drum	15	1.531 to 1.552 1.542 Avg 1.515**	0.09 to 0.15 0.12 Avg 0.14**	1,755 to 2,042 1,798 Avg 1,717**	1.60 to 2.34 1.97 Avg	2.41 to 2.78 2.60 Avg 3.00**
	Internal Drum	15	1.459 to 1.477 1.468 Avg	0.08 to 0.15 0.11 Avg	804 to 1,466 1,135 Avg	0.84 to 1.64 1.24 Avg	1.79 to 1.82 1.80 Avg
		200	1.675 to 1.676 1.676 Avg	0.14 to 0.16 0.15 Avg	2,022 to 2,665 2,344 Avg	1.47 to 1.92 1.64 Avg	2.40 to 2.84 2.62 Avg
	Flat Slab	200	1.648 to 1.656 1.652 Avg 1.621**	0.11 to 0.16 0.14 Avg 0.14**	1,548 to 1,868 1,708 Avg 2,265**	1.30 to 1.38 1.34 Avg 1.45**	1.36 to 1.54 1.45 Avg 1.43**
		500	1.664 to 1.752 1.708 Avg	0.15 to 0.16 0.16 Avg	2,815 to 2,875 2,845 Avg	1.42 to 1.75 1.58 Avg	2.26 to 2.66 2.46 Avg

*The low and high values listed are each average values from four specimens.
**Postcured.

TABLE IV

PHYSICAL PROPERTIES OF T-2610 MATERIAL

Process Variables			Physical Properties*				
Cure Temperature	Fabrication Process	Cure Pressure (psi)	Density (gm/cc)	Elongation (Percent)	Tensile Strength (psi)	Tensile Modulus (10^6)	CTE (cm/cm/°C x 10^{-5})
300° F	External Drum	200	← Visually Unsatisfactory** →				
	Internal Drum	200	← Visually Unsatisfactory** →				
	Flat Slab	500	1.46 to 1.55 1.50 Avg	8.0 and Broke	39 and Broke	Broke	1.68 to 2.39 2.04 Avg
		1,000	1.62 to 1.79 1.70 Avg 1.72***	0.11 to 0.13 0.12 Avg 0.15***	1,426 to 1,861 1,644 Avg 2,027***	1.40 to 1.51 1.46 Avg 1.40***	1.93 to 2.24 2.08 Avg 2.06***

*The low and high values listed are each average values from four specimens.
**Visually unsatisfactory samples contain numerous voids and were not suitable for testing.
***Postcured.

TABLE V

MATERIALS OPTIMIZATION EROSION MATRIX

Material	Cure Temperature (° F)	Cure Pressure (psi)	Part S/N		
			Inlet*	Throat	Exit Cone
T-4113	170	0	169**, 173**		
		15	174		
		200	165**, 168**		
	300	15	179		
T-4120	170	0			30
		15		177	175, 176
		200		166**	167**
	300	15		180	37
		200		172	178
		500		171	2, 332
T-2610	300	1, 000		164, 164**	

*Adapter
**Postcured

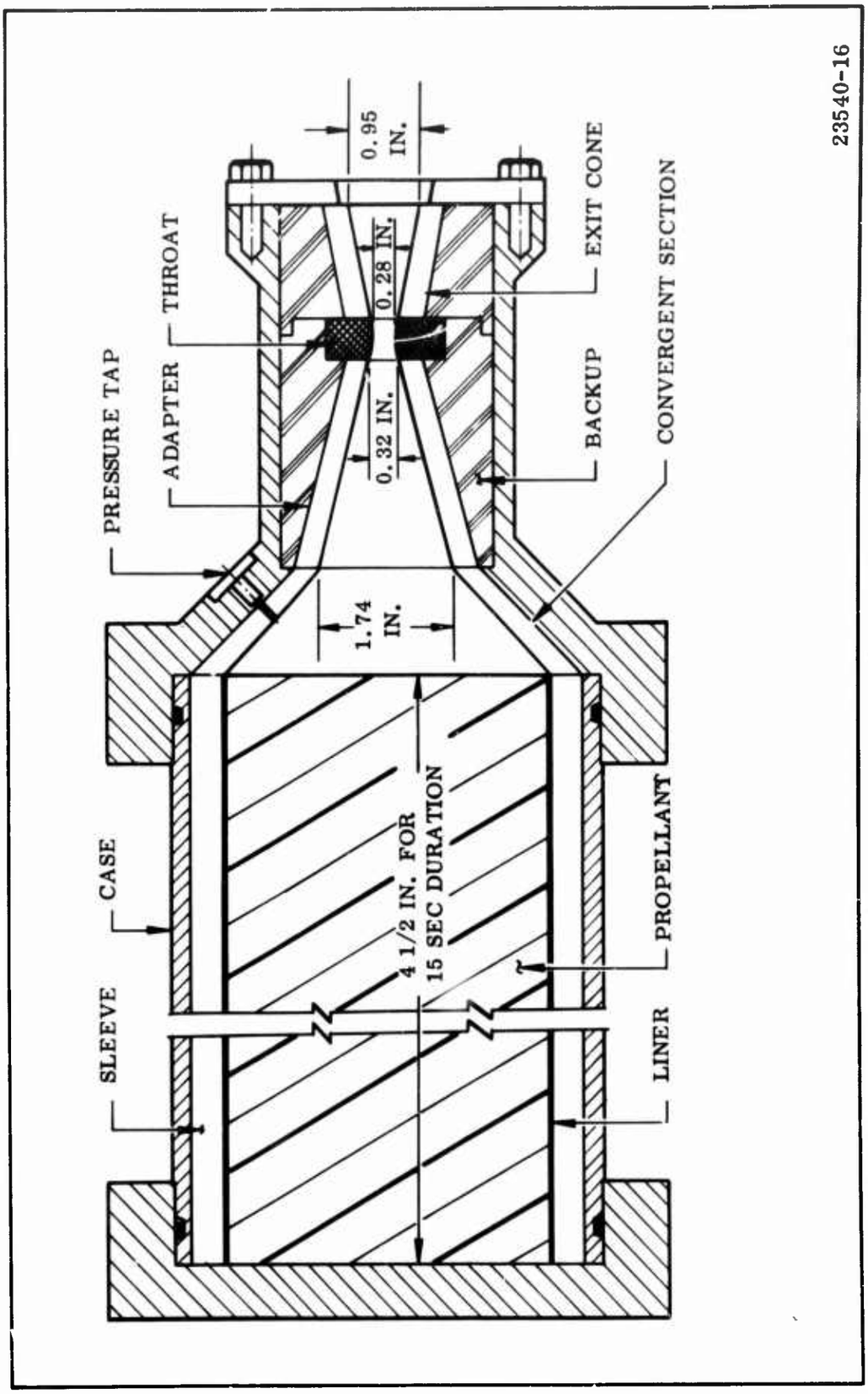

Figure 2. TU-379 Materials Test Motor

each material were fired in the TU-379 motor and one test specimen was held in reserve for verification or for a different material combination. Erosion of the adapter and exit cone was determined by measuring the volumetric increase at 0.1 in. longitudinal increments. Erosion rate was determined by converting this volumetric change to a radial change and dividing by the motor burning time. The average rate was calculated by an arithmetic average of the four stations nearest the throat. Erosion of the throat was determined by photographing the fired throat, measuring the area with a planimeter and comparing this to the original area.

The results of the motor tests with the motor operating parameters and material process parameters are presented in Table VI.

The material/cure combinations used in the test motors were selected to provide comparative rather than basic erosion data for nozzle design, i.e., systems were assembled to duplicate those possible in large nozzle tests.

Laboratory testing of the T-4113 inlet material was very limited prior to the initiation of this development program. Additional laboratory studies were required to develop the optimum material formulation for the nozzle inlet application. The test matrix in Table VII describes the formulations that were evaluated and the tests conducted.

Data obtained for the inlet optimization studies are shown in Table VIII.

The inlet material formulation study was initiated to run concurrently with the physical property testing of the materials optimization studies to allow possible improvement of the inlet formulation.

Physical test data from the optimization and inlet material formulation studies showed the T-4113 material containing 25 percent resin content to be the prime candidate insulation for nozzle inlet application. It was noted when the polymer content was reduced to 20 percent, the "wetting" capability of the resin was not sufficient to thoroughly wet the filler material, resulting in a very dry mix and brittle properties as evidenced by the test data. When the polymer content was increased to 30 percent, a very wet mix resulted. This condition leads to difficulty in achieving volatiles removal necessary for material processing.

The physical properties and the performance of the three low cost ablative materials for subscale nozzle evaluation can be summarized as follows.

> T-2610--Best performance was obtained when the material was cured at 1,000 psi and 300° F. Post cure of the material results in increased tensile strength and slightly reduced erosion rate. This material performed well in throat and exit cone applications.
>
> T-4120--The performance of parts cured at 170° F was equal to those cured at 300° F. Physical and erosion properties were moderately improved by increasing cure

TABLE VI

MATERIALS OPTIMIZATION EROSION PERFORMANCE

Motor Parameters			Material and Process Parameters							Material Performance	
Test No.*	Burn Time (sec)	Average Pressure (psi)	Part and S/N	Material**	Cure Temp (°F)	Cure Pressure (psi)	Cure Time (hr)	Postcure Temp (°F)	Postcure Time (hr)	Average Erosion Rate (mil/sec)	Throat Area Increase (sq in.)***
802	16.16	30	A-168P	T-4113	170	200	6	300	12	3.87	
803	16.94	326								3.90	
			T-177	T-4120	170	15	42				0.61
											0.71
			E-167P	T-4120	170	200	6	170	48	0.61	
										0.69	
804	16.16	399	A-173P	T-4113	170	0	26	300	12	3.98	
805	16.41	381								3.34	
			T-166P	T-4120	170	200	6	170	48		0.50
											0.47
			E-178	T-4120	300	200	4			0.08	
										0.30	
806	14.37	582	A-165	T-4113	170	200	6	170	64	2.48	
807	15.43	498								1.46	
			T-164	T-2610	300	1,000	4				0.24
											0.30
			E-37	T-4120	300	15	4			0.92	
										0.99	
808	17.80	312	A-174	T-4113	170	15	42			3.22	
809	16.61	315								4.56	
			T-180P	T-4120	300	15	4	300	4		0.99
											0.84
			E-2331	T-2610	300	1,000	1			0.14	
										0.11	
810	18.20	274	A-169	T-4113	170	0	26	170	64	2.94	
811	14.82	423								2.73	
			T-172	T-4120	300	200	4				0.81
											0.44
			E-30	T-4120	170	0	66			0.76	
										0.39	
812	16.00	457	A-179P	T-4113	300	15	4	300	12	6.11	
813	15.51	467								5.77	
			T-171	T-4120	300	500	4	300	4		0.41
											0.44
			E-175	T-4120	170	15	42			0.22	
										1.56	
814	14.41	527	A-1366	MX-4925†	300	1				0.91	
815	15.81	533								0.95	
			T-164P	T-2610	300	1,000	4	300	4		0.18
											0.24
			E-176P	T-4120	170	15	42	300	12	1.17	
										0.73	

*Propellant TP-H1011 16% Al, 86% solids.
**A - adapter cone, T - throat, E - exit cone.
***Original area = 0.56 sq in.
†Carbon fiber phenolic.

TABLE VII

INLET MATERIAL FORMULATION OPTIMIZATION MATRIX

CANDIDATE INSULATION

T-4113

MATERIALS FOR OPTIMIZATION STUDY

Phenolic resin, Durez 10694

NBR, Hitco 158

Graphite particles - Great Lakes 1008

Graphite particles - Great Lakes 1012

VARIABLES

Total polymer content (%)	20	25	30
Ratio, phenolic resin to NBR	1.3:1	1:1	0.7:1
Ratio, particle size (1008 to 1012)	5:1	3:1	1:1

TEST REQUIREMENTS

Density, tensile strength and modulus, and erosion rate

MATERIAL FORMULATION TEST MATRIX

Total polymer (%)		20			25			30		
Ratio, phenolic resin to NBR		1.3:1	1:1	0.7:1	1.3:1	1:1	0.7:1	1.3:1	1:1	0.7:1
					Part S/N					
Ratio, graphite particles (1008 to 1012)	1:1	--	--	--	T-3740	T-3713	--	--	--	--
	3:1	--	T-4113-20	T-4140-20	T-4140	T-4113	T-4141	T-4140-30	T-4113-30	--
	5:1	--	--	--	--	T-4913	--	--	--	--

TABLE VIII

PHYSICAL PROPERTIES OF INLET MATERIALS

Parts Fabricated	S/N	Material	Staging Temp (°F)	Cure Temp (°F)	Pressure Cure (psi)	Post Cure (°F)	Density* (gm/cc)	Tensile** Strength (psi)	Tensile** Modulus (psi)	Elongation** (%)	Average* Erosion Rate (mil/sec)
Flat Slab (5 by 10 in.)	67	T-4113-20	170	300	10	---***					
Adapter Cone TU-379	67-1	T-4113-20				---***					
Flat Slab (5 by 10 in.)	66	T-4141-20	170	300	10	---***					
Adapter Cone TU-379	66-1	T-4141-20	170	300	10	---***					
Flat Slab (5 by 10 in.)	53	T-3740	170	300	10	3 hr at 300	1.335	419	5.43×10^3	3.5	
Adapter Cone TU-379	49	T-3740	170	300	10	4 hr at 300					
Flat Slab (5 by 10 in.)	54	T-3713	170	300	10	3 hr at 300	1.359	388	3.82×10^3	5.2	
Adapter Cone TU-379	50	T-3713	170	300	10	4 hr at 300					
Flat Slab (5 by 10 in.)	52	T-4140	170	300	10	3 hr at 300					
Adapter Cone TU-379	48	T-4140	170	300	10	5 hr at 300					
Flat Slab (5 by 10 in.)	57	T-4113	170	300	200	--	1.460	229	1.43×10^3	62.0	
Adapter Cone TU-379	41	T-4113		300	10	4 hr at 300					
Flat Slab (5 by 10 in.)	51	T-4141	170	300	10	3 hr at 300	1.407	264	2.34×10^3	4.1	
Adapter Cone TU-379	51-1	T-4141	170	300	10	5 hr at 300					
Flat Slab (5 by 10 in.)	64	T-4140-30	170	300	10	--†		892	1.41×10^5	0.12	
Adapter Cone TU-379	64-1	T-4140-30	170	300	10	--	1.096				
Flat Slab (5 by 10 in.)	65	T-4113-30	170	300	10	--†					
Adapter Cone TU-379	65-1	T-4113-30	170	300	10	--†					
Flat Slab (5 by 10 in.)	62	T-4913	170	200	10	4 hr at 300	1.346	58	0.56×10^3	34.0	
Adapter Cone TU-379	62-1	T-4913	170	200	10	4 hr at 300					
Flat Slab (5 by 10 in.)	63	T-4941	170	200	10	4 hr at 300	1.369	72	0.50×10^3	57.5	
Adapter Cone TU-379	63-1	T-4941	170	200	10	4 hr at 300					
Adapter Cone TU-379	39	T-4113	170	300	200	--					1.74
Adapter Cone TU-379	40	T-4113	170	300	200	--					0.00
Adapter Cone TU-379	41	T-4113	170	300	10	4 hr at 300					4.91

*Average of three test specimens.
**Average of four test specimens.
***Too brittle for testing.
†Too soft for testing.

pressures rather than cure temperatures. However, the difference is not significant enough to warrant a high pressure cure in fabricating large nozzle components. This material performed best as an exit cone insulation.

T-4113--This material demonstrated the high elongation required for nozzle adapter or inlet areas. It has a lower tensile strength and higher erosion rate than does T-2610 or T-4120. The 170° F cure and post cure were superior to the high temperature (300° F) cure.

B. FABRICATION PROCESS

The objective of this portion of the program was to determine the effects of adding reinforcement to the basic formulation to (1) provide higher structural integrity, (2) improve cure systems and processing techniques, and (3) establish processing controls. Reinforcement variations included use of carrier cloth and phenolic honeycomb cells. Tests were conducted to measure density, tensile strength, and composite beam strength.

Flat slabs using the three candidate materials were fabricated with glass cloth reinforcement, with paper phenolic honeycomb reinforcements and without reinforcement. The test matrix for these samples is given in Table IX.

The glass cloth used in this effort was a glass* fabric with an open weave. All three materials had to be applied by hand troweling and working into the cloth. It was impossible to apply the material by dipping, and application with a doctor blade was not successful. The blade merely wiped the material over the cloth. Possibly these techniques could be used if the compounds were carried in a very high solvent content mix and the solvent then evaporated, as is done in normal phenolic impregnated glass cloth production. However, particle separation would likely occur.

Similar difficulties were encountered in using the paper phenolic honeycomb. The T-4113 could be poured into the cells but the other two materials do not have low viscosities and had to be hand forced into each cell. The paper phenolic honeycomb used was 0.5 in. cell by 0.75 in. thick with 19 percent resin from Hexcel Products. The original test plan called for manufacturing cylinders similar to those used in the cure optimization studies Because of the problems mentioned, this effort did not proceed any further.

The flat slabs were all of a standard 5 by 10 by 0.5 in. size. After cure, they were cut into test specimens of 2 and 3 in. widths. The 2 in. specimen was bonded to a 0.10 in. thick steel plate with Epon 913 and tested as a flat beam. Figure 3 shows the testing arrangement. The load was applied at a rate of 0.05 in. per minute and the specimen was loaded until obvious failure by load decrease or until the composite deflected 0.5 inch. The load deflection curves are presented in Figures 4 thru 8 . In each family, a curve is also presented for the nonreinforced material bonded to the steel and for the plain steel plate.

*Bean Style No. 32.

TABLE IX

FABRICATION PROCESS DEVELOPMENT MATRIX

Cure Temp (° F)	Materials	Cure Pressure (psi) 0	15	200	500	1,000
170	T-4120	HC*	FG**	FG		HC
			HC	HC		
170	T-4113		FG			
			HC			
170	T-2610		HC			
300	T-4120	HC		HC		HC
				FG		FG
				NR***		
300	T-4113			FG		
				NR		
300	T-2610					HC
						NR

*HC denotes honeycomb reinforced.
**FG denotes fiberglass reinforced.
***NR denotes nonreinforced.

NOTE:

All specimens contained five layers per inch of thickness except for the 200 psi cured T-4113, FG composite which contained 50 layers per inch of thickness.

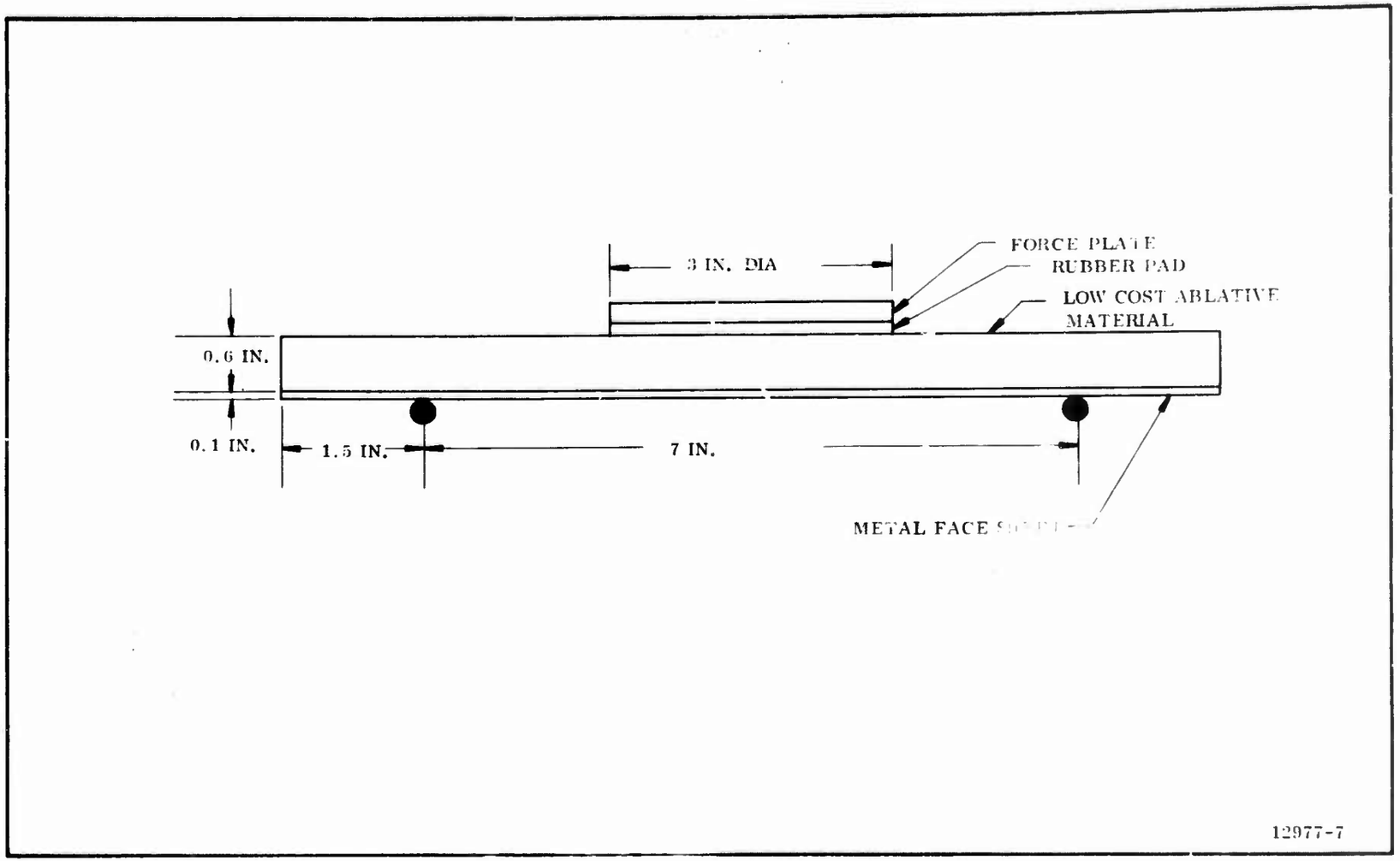

Figure 3. Composite Beam Test Equipment Arrangement

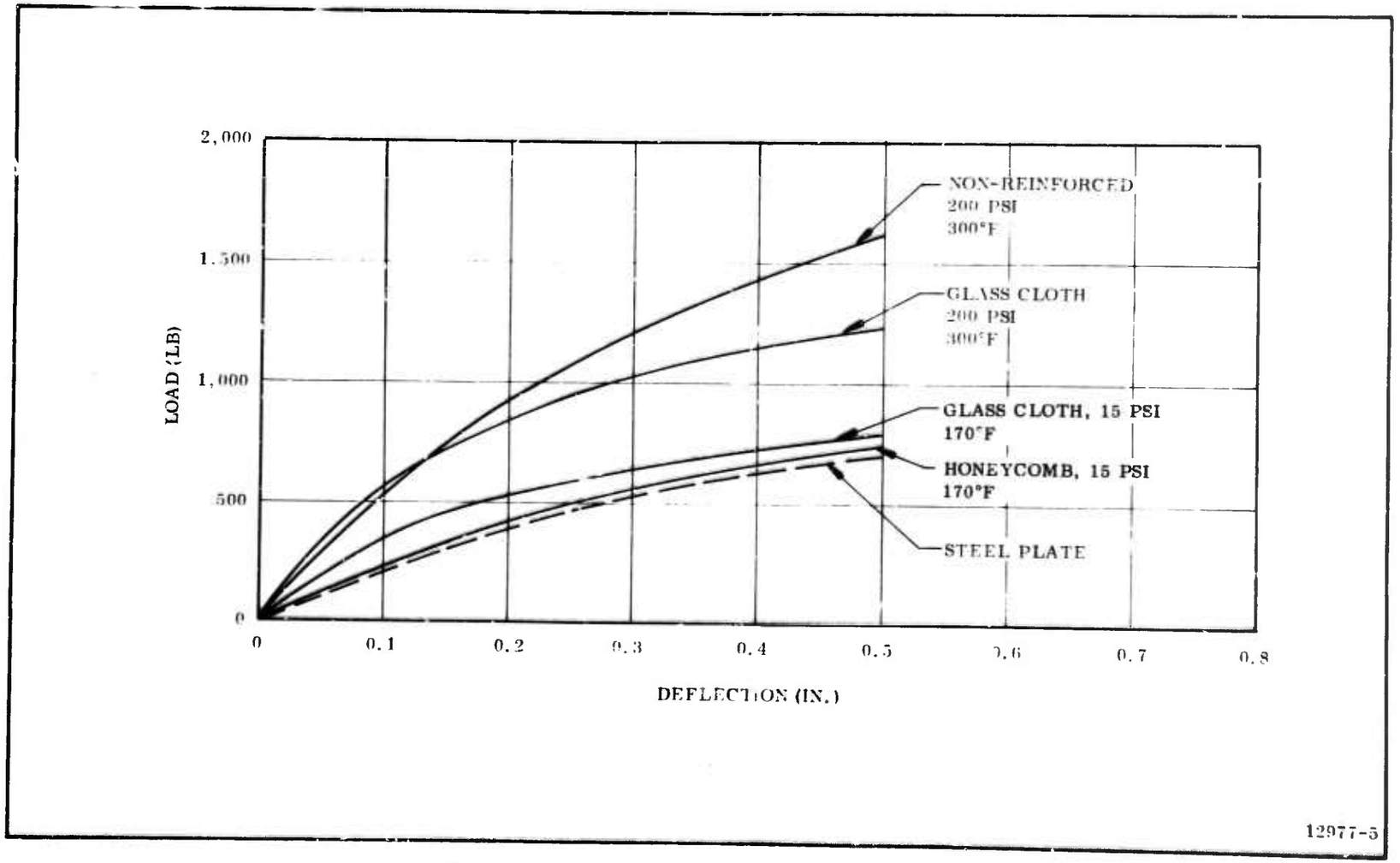

Figure 4. Composite Beam Tests, T-4113

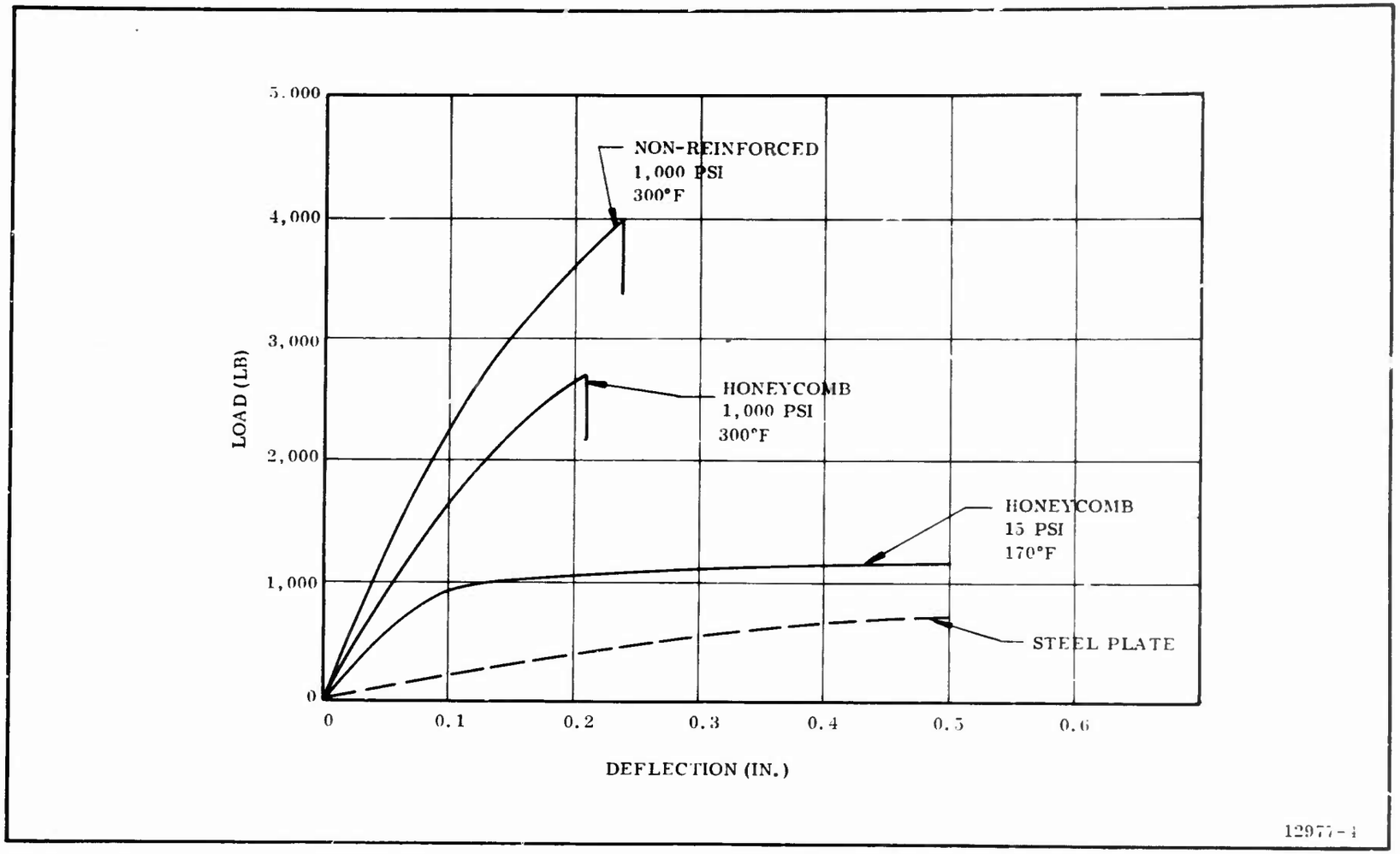

Figure 5. Composite Beam Tests, T-2610

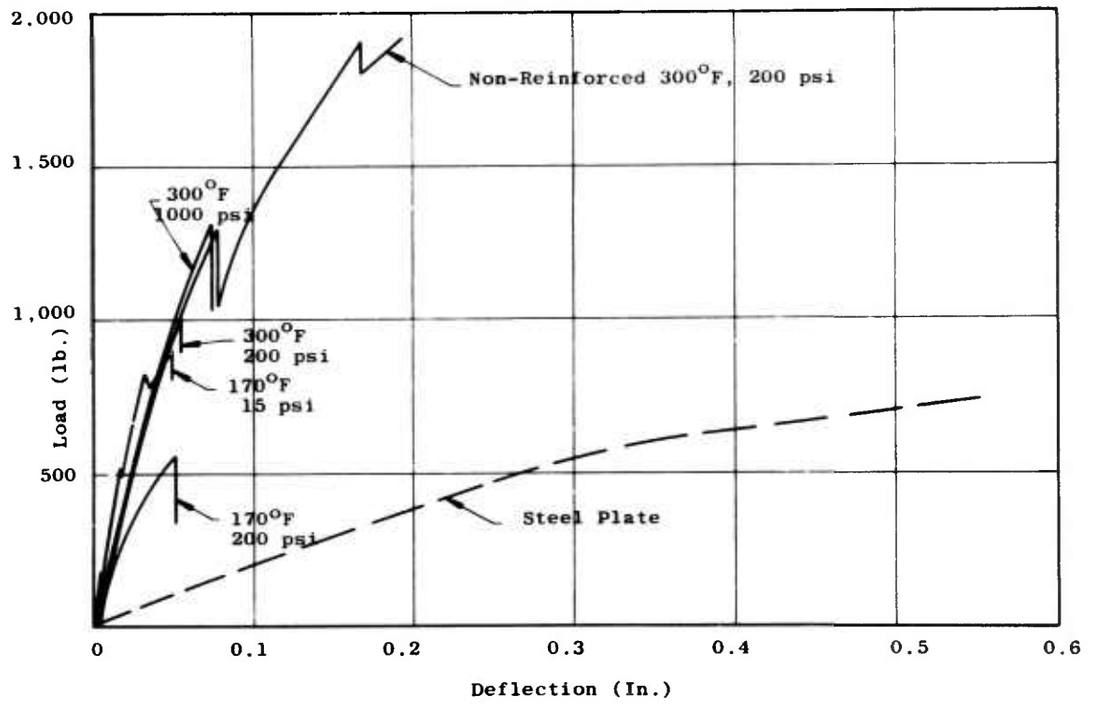

NOTE: ALL SPECIMENS WERE GLASS CLOTH REINFORCED EXCEPT AS NOTED.

Figure 6. Composite Beam Tests, T-4120

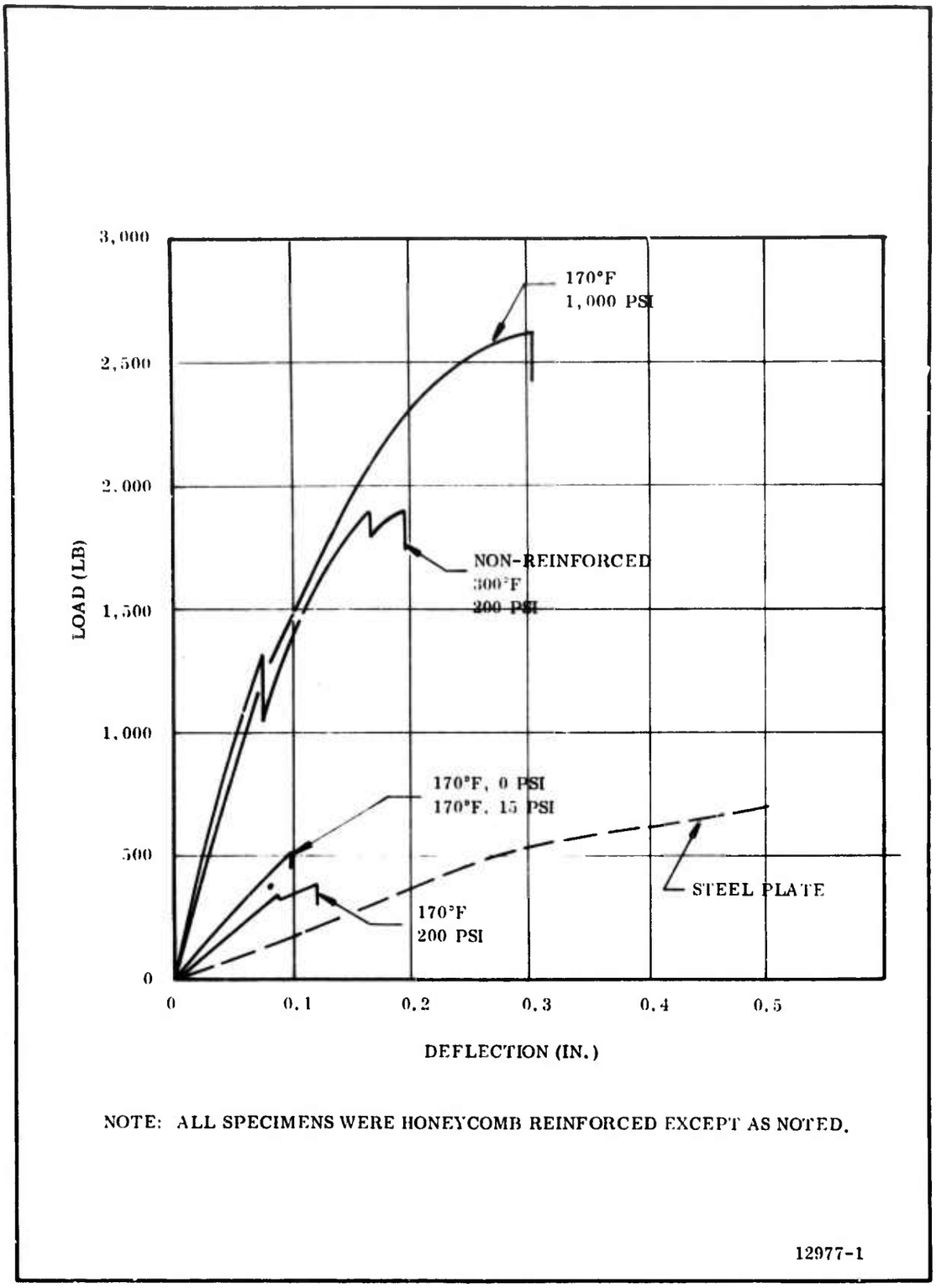

Figure 7. Composite Beam Tests, T-4120

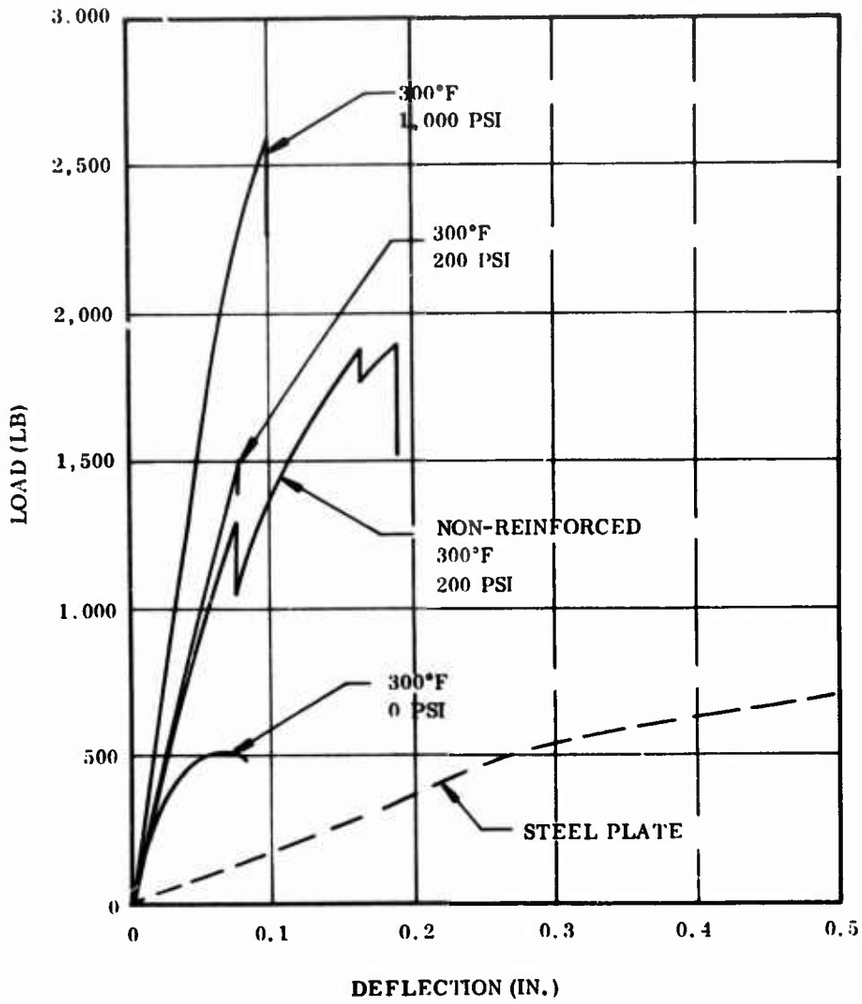

NOTE: ALL SPECIMENS WERE HONEYCOMB EINFORCED EXCEPT AS NOTED.

12977-3

Figure 8. Composite Beam Tests, T-4120

The results of the T-4113 material tests (Figure 4) show that neither reinforcement adds to the base material strength. The higher cure pressures create better "wet out" of the reinforcement and improve strength. The materials tested did not delaminate, crack or separate from the steel.

The results of the T-2610 composite beam tests (Figure 5) are similar to those for the T-4113. The one sample cured at 170° F was prepared only for a comparison value. The T-2610 formulation was not designed for cure at this temperature. The material did not fail, but moved with the steel similar to the T-4113. The remaining T-2610 specimens failed by complete cracking of the material. The T-2610 material would not adhere properly to the glass cloth and no slabs of this type were made.

Figures 6 thru 8 show the load deflection curves for the T-4120 material. The nonreinforced material failed in stages with the initial failure occurring at a load of 1,300 psi and final failure at 1,900 psi. With one minor exception, the glass cloth or honeycomb reinforcement did not improve the properties of the beam. All glass cloth specimens had initial failures in the 600 to 1,300 lb load range. The honeycomb specimens showed a definite relationship of increasing strength with cure pressure, but only one specimen (300° F, 1,000 psi) had an improvement in properties.

Photographs of the tested specimens are presented in Figures 9 thru 13. Figure 9 shows the four T-4113 specimens. All of the specimens remained bonded to the steel. The nonreinforced material did not crack but the other three materials showed some cracking with a more pronounced effect on the lower temperature and pressure specimens. The T-2610 (Figure 10), which is a more rigid material than the T-4113, was not designed to take the strain of this test. The nonreinforced T-2610 failed by cracking across the midpoint of the specimen. Specimens with the honeycomb reinforcement failed along the honeycomb cell walls. The photographs show the change in material uniformity when a reinforcement is used and when the material is cured at a low pressure.

The nonreinforced T-4120 material cracked across the midpoint of the specimen and upon continued deflection separated from the steel (Figures 11 thru 13). The honeycomb reinforced specimen (cured at 1,000 psi) failed in a similar manner, but all other honeycomb specimens failed by a material/cell wall separation with individual cell units breaking loose from the steel. The glass cloth specimens failed by delaminating along the cloth layers. Figure 13 shows an additional problem associated with the glass cloth, which is common to all three compounds. The cloth layers in the cure slabs have extensive waviness. Milling the slabs to true flatness often results in cutting through these cloth layers.

The nonreinforced materials were studied for technique improvements with regard to component manufacture. Care was taken not to create laminar planes while hand packing materials into molds for curing at low pressure (0 to 15 psi). No problems existed in thin sections, but in thicknesses over 1 in., the material had to be applied in layers so that voids could be worked out. The best technique

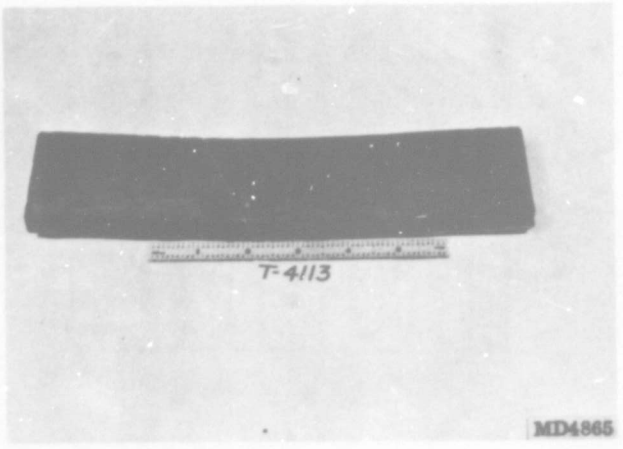

a. Nonreinforced 300° F, 200 psi

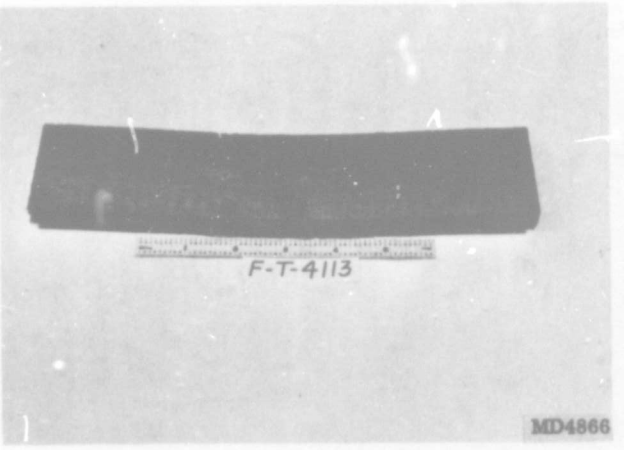

b. Fiberglass Reinforced 300° F, 200 psi

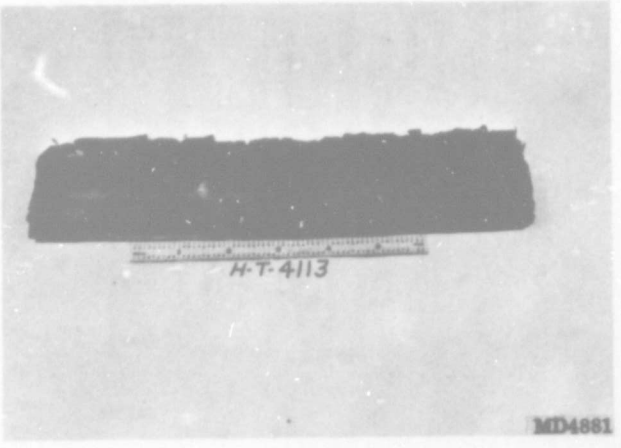

c. Honeycomb Reinforced 170° F, 15 psi

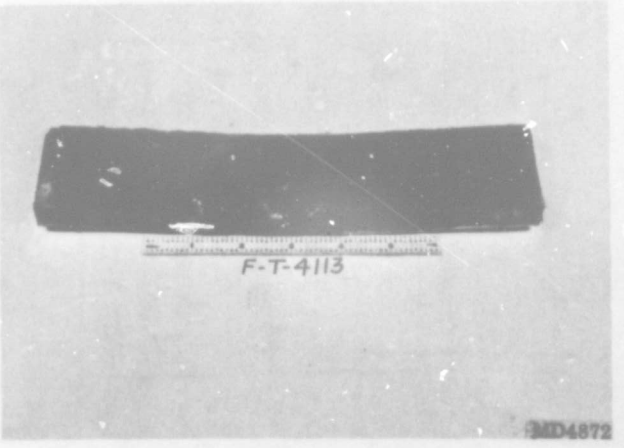

d. Fiberglass Reinforced 170° F, 15 psi

Figure 9. Composite Beam Specimens, T-4113

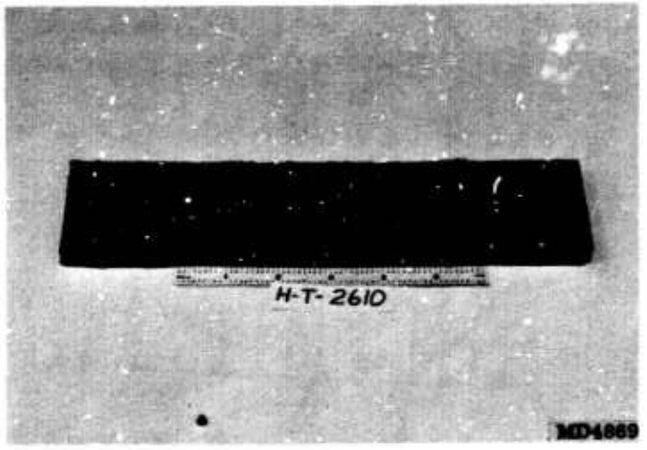

a. Nonreinforced 300° F, 1,000 psi

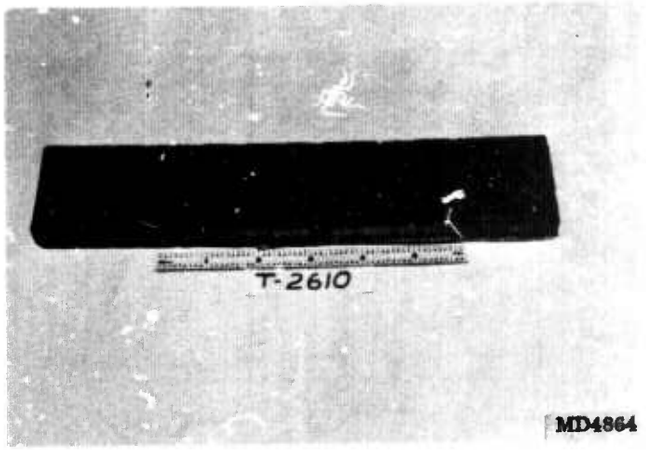

b. Honeycomb Reinforced 300° F, 1,000 psi

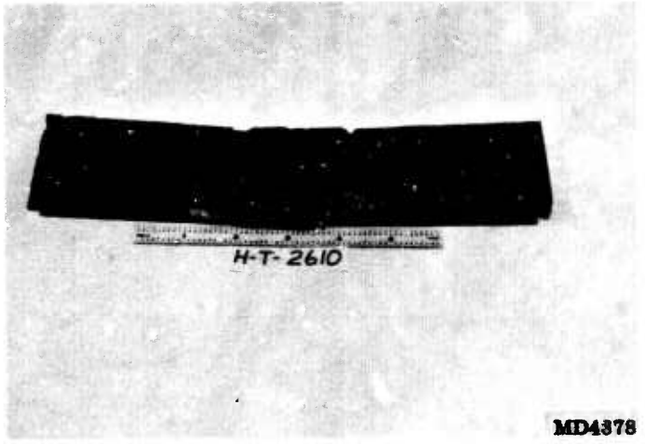

c. Honeycomb Reinforced 170° F, 15 psi

Figure 10. Composite Beam Specimens, T-2610

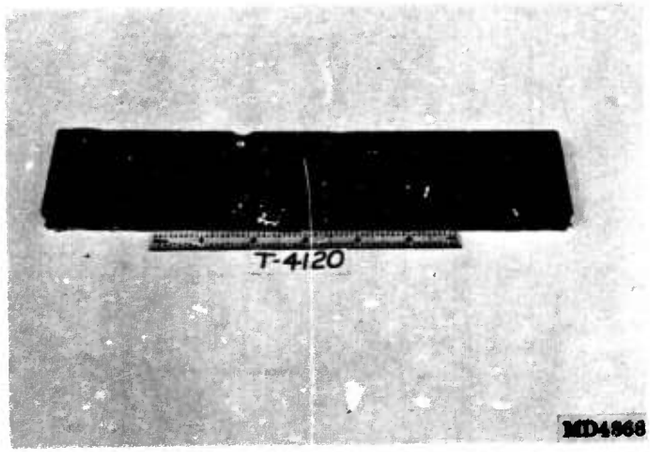

a. Nonreinforced 300° F, 200 psi

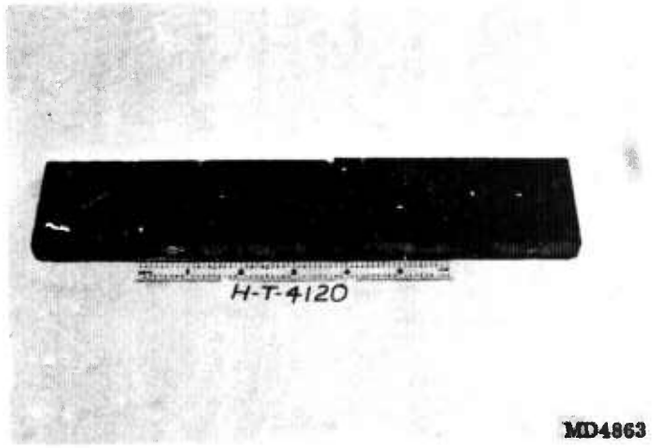

Honeycomb Reinforced 300° F, 1,000 psi

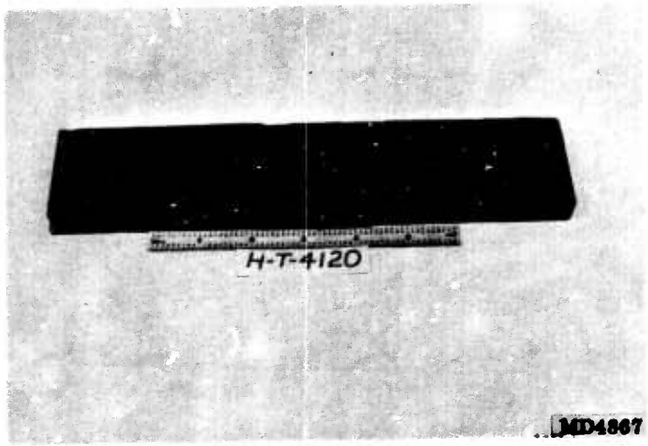

c. Honeycomb Reinforced 300° F, 200 psi

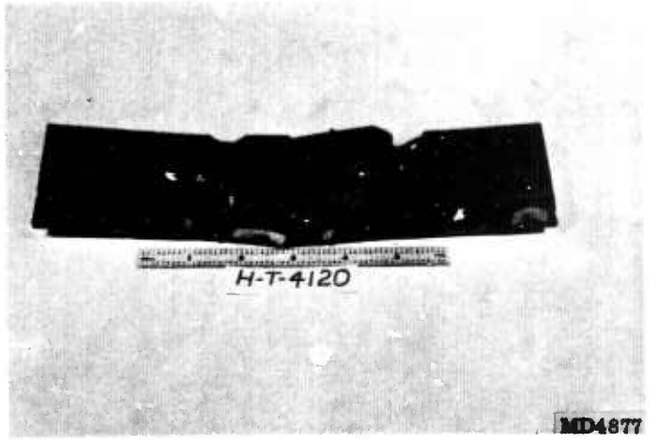

d. Honeycomb Reinforced 300° F, 0 psi

Figure 11. Composite Beam Specimens, T-4120

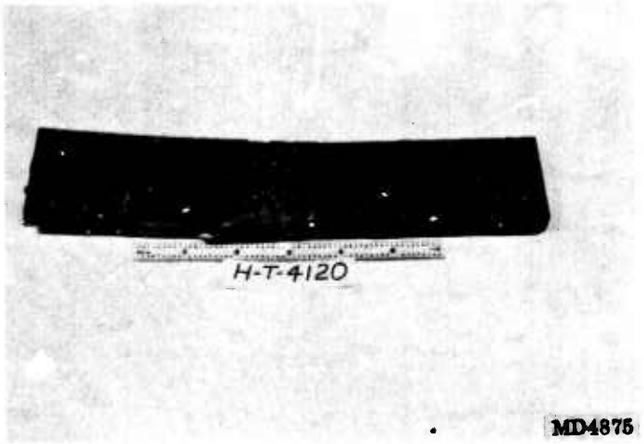

a. Honeycomb Reinforced 170° F, 1,000 psi

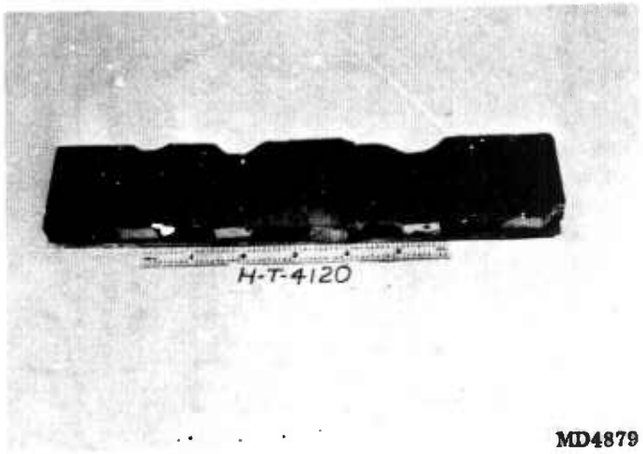

b. Honeycomb Reinforced 170° F, 200 psi

c. Honeycomb Reinforced 170° F, 15 psi

d. Honeycomb Reinforced 170° F, 0 psi

Figure 12. Composite Beam Specimens, T-4120

a. Glass Cloth Reinforced 300° F, 1,000 psi

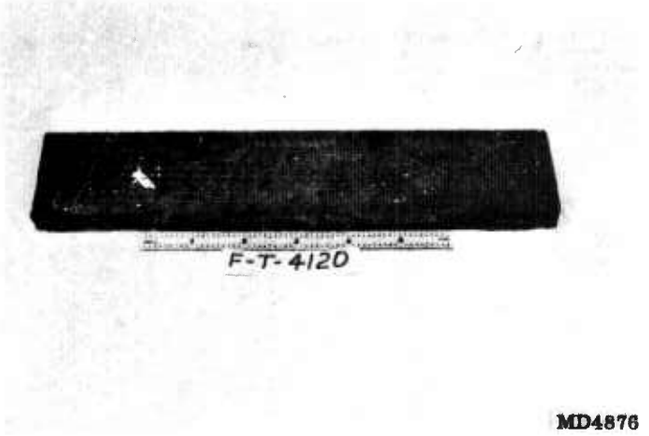

b. Glass Cloth Reinforced 300° F, 200 psi

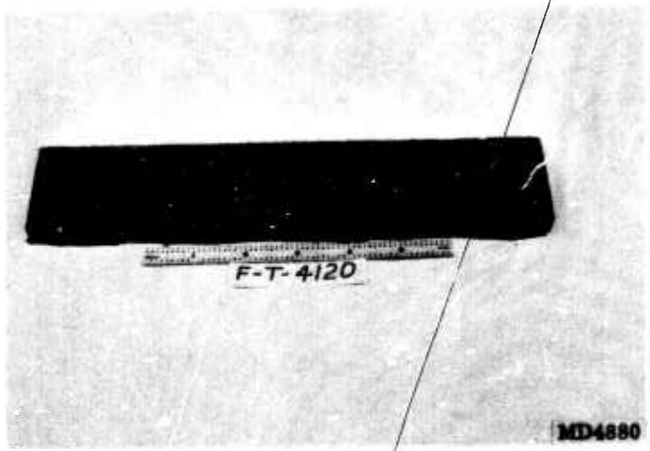

c. Glass Cloth Reinforced 170° F, 200 psi

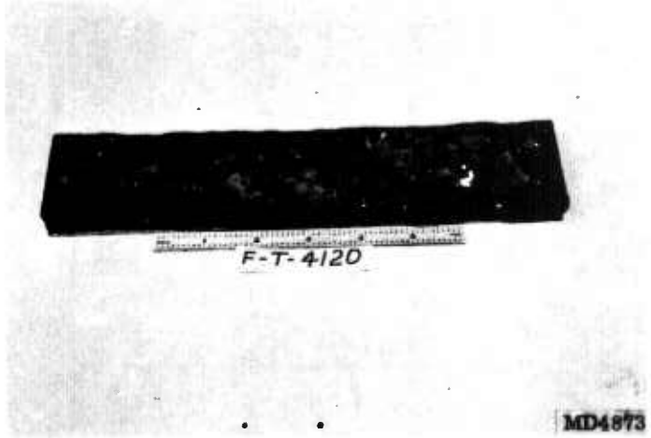

d. Glass Cloth Reinforced 170° F, 15 psi

Figure 13. Composite Beam Specimens, T-4120

appeared to be pressure packing by hand. Tamping systems, such as a pneumatic hammer, were tried but they tended to aggravate the laminar condition. As each layer was applied and tamped, a skin formed. When the next layer was applied, an unbonded plane occurred. At higher cure pressure (200 psi and above), laminar conditions were not a problem. The higher pressure moved the material and caused flow between the layers.

The T-2610 was originally developed for a high temperature, high pressure cure (300° F, 1,000 psi). Attempts to mold the material at 170° F and high pressure (200 psi and above) were not successful. At this temperature, the cure time was greatly extended and the pressure caused the resin to flow out of the die. A fully positive mold would be required to cure under these conditions.

The quality of the test samples and parts made with nonreinforced material was somewhat affected by the degree of staging prior to molding. Staging of the T-2610 material was necessary to remove the solvent volatiles prior to molding to accomplish processing at 300° F and 1,000 psi (for quality) in a confined mold. Attempts to mold without staging were completely unsatisfactory, resulting in samples full of voids and cracks.

The uncured T-4120 was a very viscous mix containing approximately 8 percent solvent. This material was cured in a vacuum bag either with or without autoclave pressure. As a result, the volatiles were removed during the preheat and initial cure cycle. Staging was therefore not used on any test samples or parts made of this material.

The T-4113 with the NBR solution contained a much higher solvent content (32 percent) than the T-4120. This material required staging for two purposes. First, staging was required to increase the viscosity to make the material easier to handle. In its bare state, the material tended to slump, even on moderately sloping surfaces. Second, the curing material formed a skin after 1/4 hr at 170° F, thus preventing the escape of a high amount of volatiles. During staging at 170° F, the T-4113 material, spread as thin layers on metal sheets, formed a skin and had to be broken up several times to provide freshly exposed surface for solvent evaporation.

Some of the samples in the cure optimization studies were prepared by applying the T-4113 to the mold cylinder in thin layers and allowing each layer to dry. The resulting samples were either completely unsatisfactory or had densities in the 1.0 to 1.2 gm/cc range, while properly staged samples had densities of 1.4 to 1.5 gm/cc.

The remaining 3 in. wide portion of each slab was machined into a tensile specimen in accordance with Figure 14. This size specimen was selected to be similar to a standard plastic tensile specimen and yet include, in the gage width, an assurance of multiple honeycomb cells. For comparison purposes, all materials were machined to the same size.

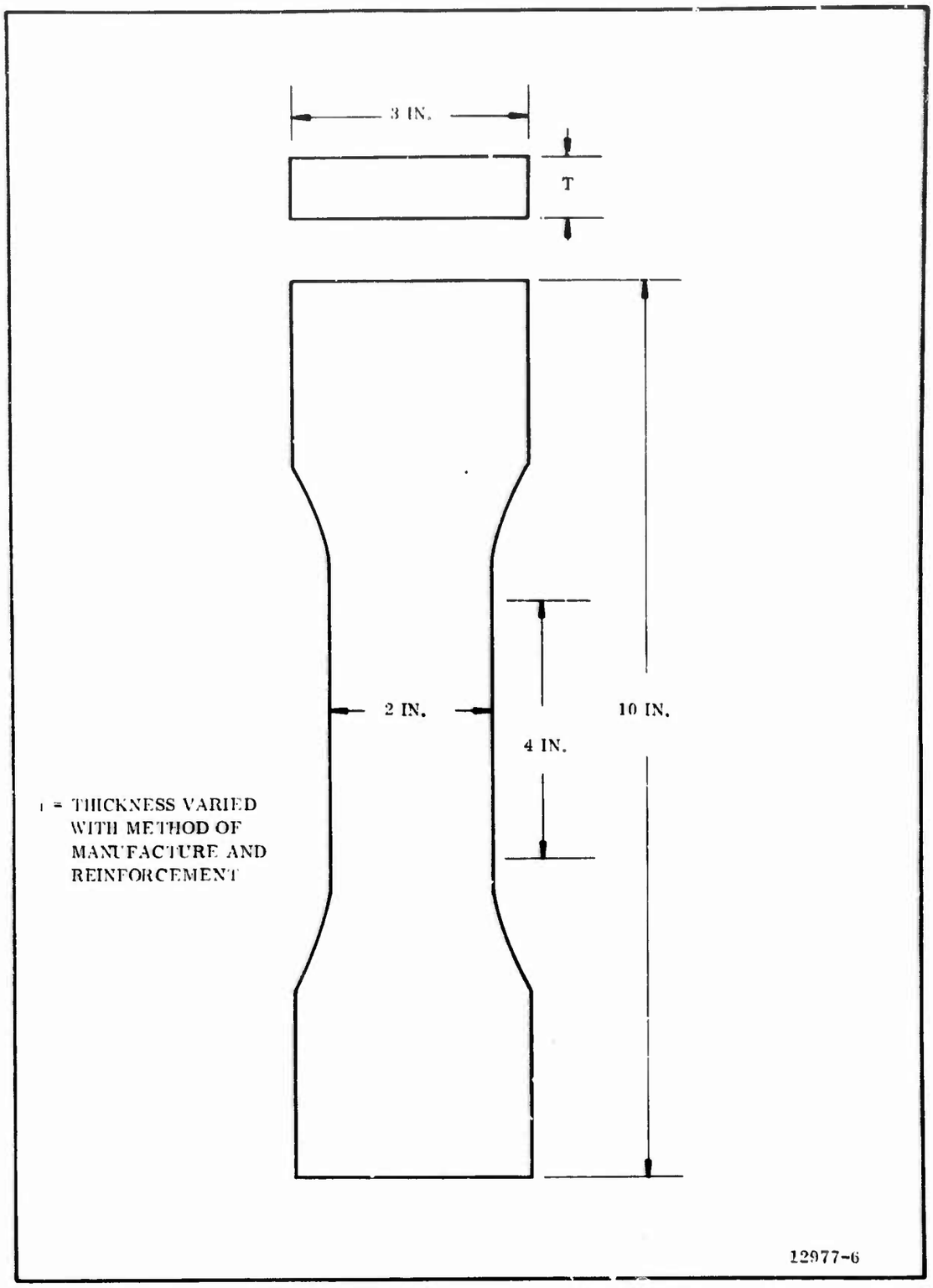

Figure 14. Fabrication Process Development Tensile Specimen

The density measurements were made in specimens taken from ends of the beam and tensile test slabs.

The density and tensile test data for the composite materials are presented in Table X. The tensile strength values for the nonreinforced materials are not directly comparable to those reported previously in the cure optimization studies since the composite material tensile specimens were not of standard size. For the three base materials, the tensile strength measured on the two types of specimen compare as follows when the materials are cured under similar conditions:

Material	Standard Tensile Specimen (psi)	Special Tensile Specimen (psi)
T-4113	634	687
T-4120	2,265	910
T-2610	2,027	1,725

As with the beam test data, the higher cure pressures increased the tensile strength of the composites. The T-4120 data are presented graphically in Figure 15. This pressure relationship was not apparent in the nonreinforced material properties. However, in the reinforced materials, the pressure presumably created a better resin-reinforcement wetout with resultant improved properties.

Generally, the inclusion of reinforcements did not improve the physical properties of the base materials, but it does appear that a reinforcement can be used without degrading the base material and some side advantage may be gained.

C. REPAIR MATERIAL

The carbonaceous materials developed should be reparable to eliminate the costly rejection of components due to defects observed during manufacture or after end item delivery. Therefore, this effort included the development and evaluation of materials that could be used to repair the selected base material without degrading nozzle performance or reliability.

The capability to make repairs in the three low cost ablative materials (T-4120, T-2610, and T-4113) was evaluated using a low pressure, 170° F cure technique.

This work was divided into two phases. The purpose of Phase I was to obtain an adhesive system that would provide a bond strength between the base material and the steel adhesion discs greater than the cohesive structural strength of the base material and proposed repair materials. Phase II was to develop bond data and erosion data of the repair materials to the base materials.

Test slabs (5 by 10 by 1 in.) of the three insulation materials were prepared under conditions developed in the materials optimization studies. Adhesion test specimens were prepared in which the base materials were bonded to themselves and to steel adhesion discs with various adhesion combinations. Figures 16 and 17 show the test specimens for the two phases. Table XI presents the tensile adhesion data obtained in the Phase I study.

TABLE X

PHYSICAL PROPERTIES OF REINFORCED MATERIALS

Process Conditions						Physical Properties		
						Density (gm/cc)		
Est. No.	Base Material	Reinforcement	Cure Temp (° F)	Cure Pressure (psi)	Cure Time (hr)	Average*	Range	Tensile Strength (psi)
134	4120	Honeycomb	170	0	21.25	1.43	1.40 to 1.45	U**
150	4120	Honeycomb	170	15	23.50	1.53	1.51 to 1.55	27
154	4120	Honeycomb	170	200	19.50	1.59	1.56 to 1.63	70
140	4120	Honeycomb	170	1,000	16.75	1.83	1.83 to 1.83	1,165
142	4120	Honeycomb	300	0	5.75	1.47	1.46 to 1.48	27
137	4120	Honeycomb	300	200	15.50	1.59	1.57 to 1.63	500
125	4120	Honeycomb	300	1,000	5.0	1.79	1.78 to 1.79	647
159	4120	None	300	200	17.50	1.68	1.66 to 1.73	910
152	4120	Glass Cloth	170	15	23.50	1.55	1.54 to 1.56	301
156	4120	Glass Cloth	170	200	19.50	1.52	1.47 to 1.56	536
143	4120	Glass Cloth	300	200	5.25	1.53	1.46 to 1.58	612
126	4120	Glass Cloth	300	1,000	5.0	1.66	1.65 to 1.68	962
130	4113	Honeycomb	170	15	66.0	1.21	1.20 to 1.24	14
132	4113	Glass Cloth	170	15	66.0	1.33	1.29 to 1.37	U
145	4113	Glass Cloth	300	200	5.25	1.48	1.46 to 1.47	3,050
162	4113	None	300	200	19.0	1.56	1.49 to 1.63	687
121	2610	Honeycomb	170	15	66.0	1.19	1.18 to 1.22	272
122	2610	Honeycomb	300	1,000	7.25	1.64	1.62 to 1.67	1,100
163	2610	None	300	1,000	6.50	1.84	1.84 to 1.85	1,725

*Average of three tests.
**U denotes unsatisfactory for test.

TABLE XI

BASE MATERIAL ADHESION DATA

Base Material	Cure Cycle	Adhesive				Tensile Adhesion (psi)			Type of Failure
		Type	Hour	°F	psi	No. of Specimens	Range	Average	
T-4120	170° F at 15 psi for 48 hr	Epon 913	4	170	0	3	1,750 to 1,960	1,828	100% cohesive T-4120
		UF-3195	5	170	0	3	1,895 to 1,990	1,931	100% cohesive T-4120
		T-4120 and silica tape	4	300	0	3	750 to 975	862	95% adhesive to silica tape
T-4113	170° F at 15 psi for 48 hr/plus 74 hr at 170° F at 0 psi	Epon 913	3	170	0	3	159 to 218	185	100% cohesive in T-4113 base
		T-4113 resin	151	170	0	3	300 to 495	400	100% cohesive in T-4113 base
		T-4113 without base	137	170	0	3	48 to 253	179	75% cohesive in T-4113 adhesive
T-2610	300° F at 1,000 psi for 4 hr	Epon 913	3	170	0	3	1,470 to 2,240	1,860	95% cohesive T-2610

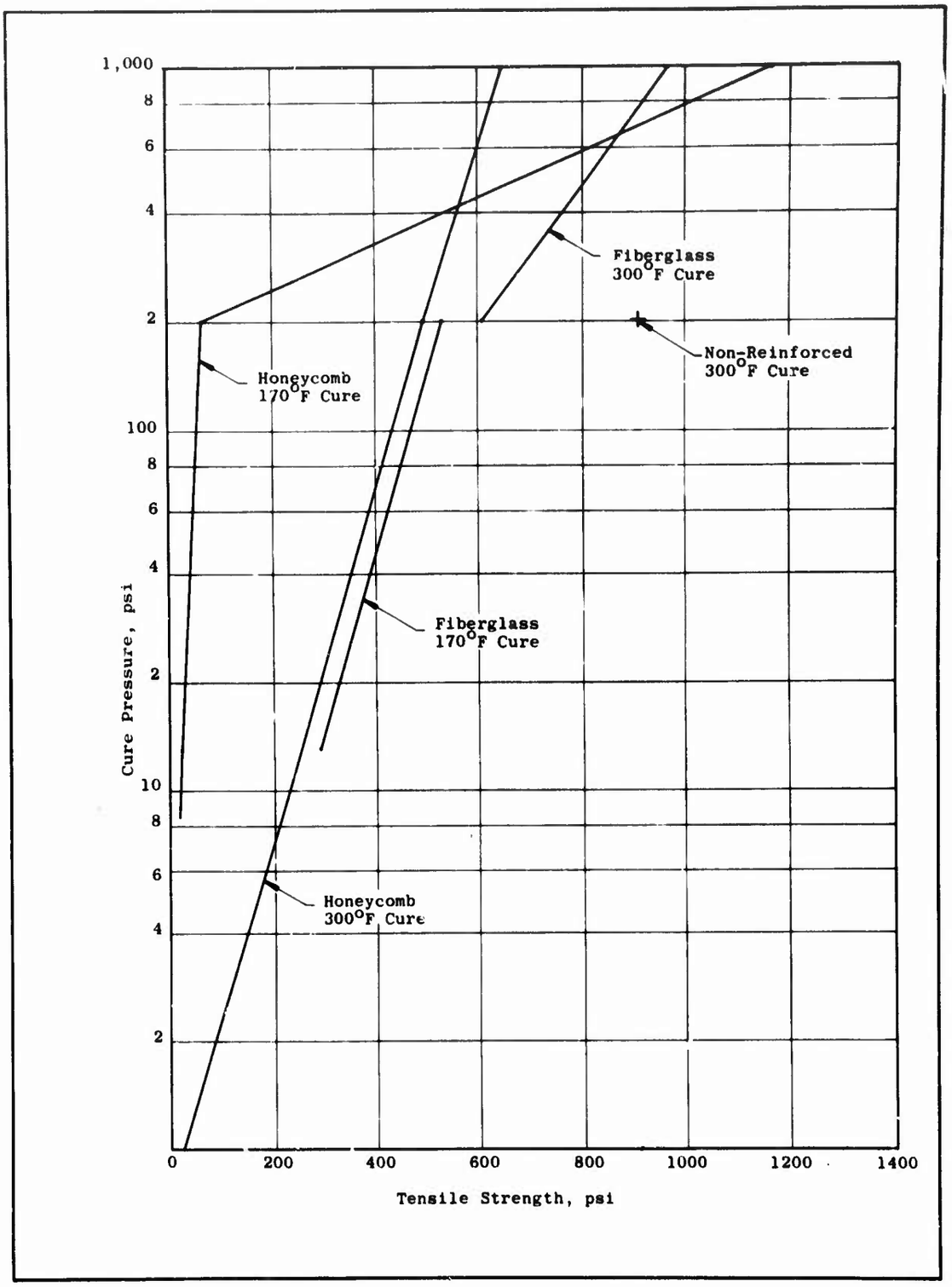

Figure 15. Tensile Strength, T-4120 Reinforced

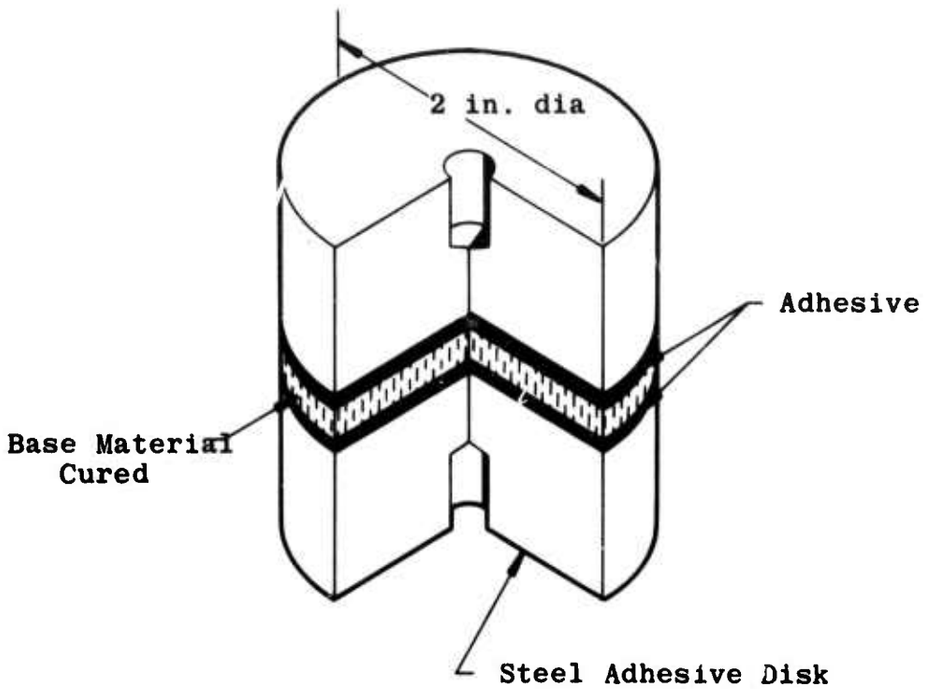

PROCEDURE: Mold base material
Cut into disks
Mill surfaces flat
Bond into assembly

Figure 16. Repair Material Adhesion Specimen, Phase I

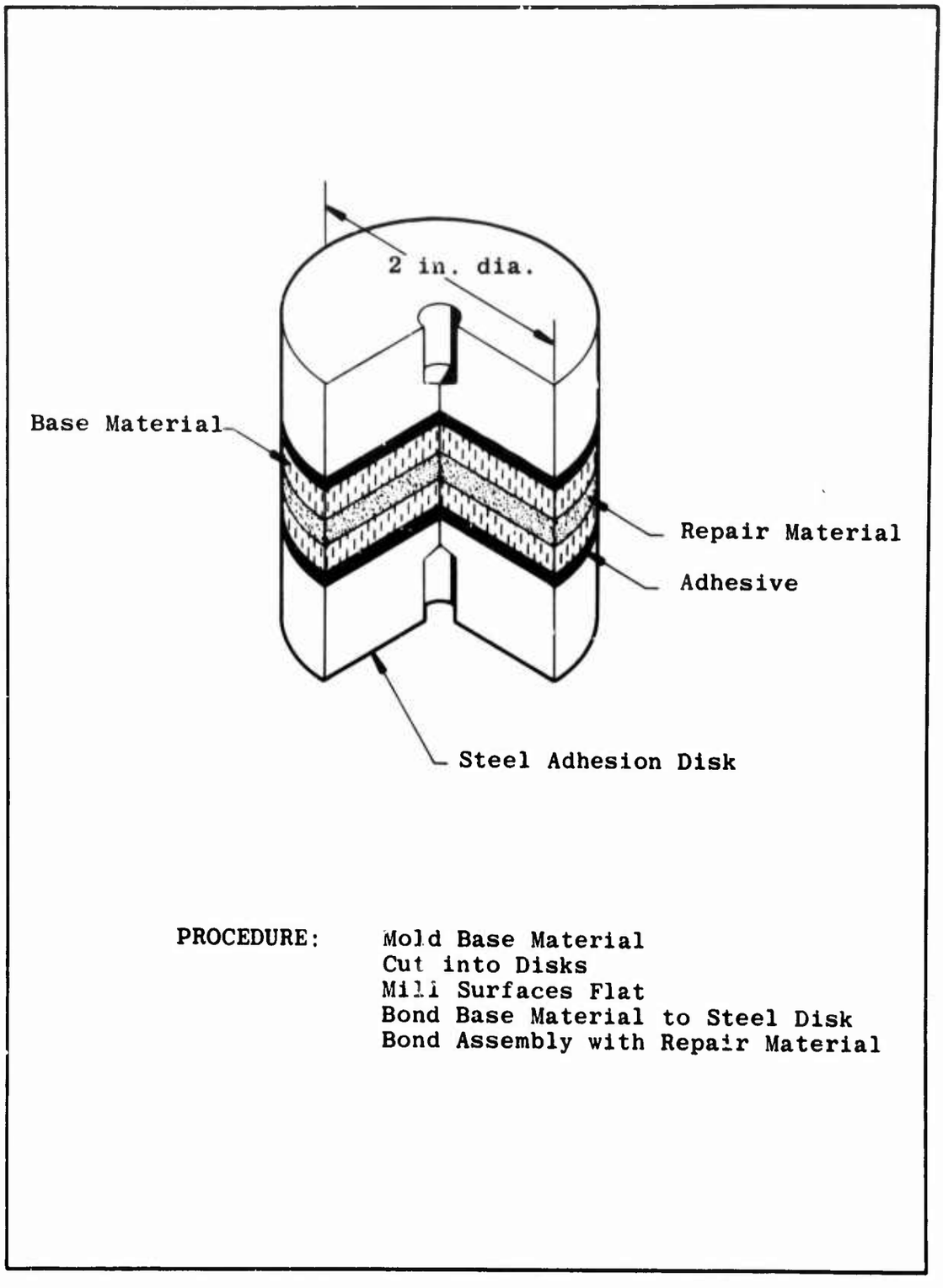

Figure 17. Repair Material Adhesion Specimen, Phase II

For the T-4113 base material, the T-4113 resin system (without filler) provided a better bond to steel than the Epoxy (Epon 913) adhesive. However, both adhesive systems yielded a cohesive type failure in the T-4113 material and the epoxy system was selected for specimen preparation because it has a much shorter cure cycle. The same adhesive was therefore selected for all of the base materials.

The Phase II repair materials adhesion data are presented in Table XII. These data show that for each base material, a repair material can be used and cured in place at a pressure of 15 psi or lower and 170° F. These conditions are obtainable in most field operations by vacuum bag and heating blanket arrangements. The candidate repair materials were test fired in the TU-379 motor by making intentional defects and repairs in adapters and exit cones. This study was performed by (1) drilling and filling 0.5 and 0.25 in. diameter holes in the inlet (adapter) and exit cone, respectively, and (2) machining and filling a 0.25 in. wide longitudinal groove in the inlet of the TU-379 motor.

The matrix for the erosion tests of the repairs is as follows:

Base Material	Repair Material	Cure Cycle (hr)	Cure Cycle (°F)	Cure Cycle (psi)	Location of Repair	Type of Repair
T-4120	T-4120	48	170	0	Adapter	0.5 in. hole, 0.25 in. longitudinal groove
T-4120	T-4120	48	170	0	Exit Cone	0.25 in. hole
T-4113	T-4113	72	170	0	Adapter	0.5 in. hole, 0.25 in. longitudinal groove
T-2610	T-4120	42	170	0	Adapter	0.5 in. hole, 0.25 in. longitudinal groove

Table XIII shows the TU-379 repair matrix and erosion rates. The erosion rates shown are for the base material since the repairs were not made in the area normally measured and reported. The rates are reported only to show that the base material performance is comparable to that previously obtained, indicating the repairs had no effect on performance. Visual examination of the repairs show that uniform erosion exists between the base and repair material and no channeling or gouging occurred at the repair interfaces. All repairs were well bonded in place to the base materials.

D. PHYSICAL PROPERTIES

Physical properties of the selected base and repair materials and associated cure systems, using processing and fabrication techniques proven during prior subtask efforts were determined for the range of temperature from ambient to 600° F. The test matrix shown in Table XIV identifies the planned physical properties testing effort. Test slabs (4 by 10 by 1 in.) of the three insulation materials were prepared using processing and fabrication techniques listed below.

TABLE XII

REPAIR MATERIALS ADHESION DATA

Base Material	Adhesive	Repair Material Type	Cure Hour	Cure °F	Cure psi	No. of Specimens	Tensile Adhesion (psi) Range	Tensile Adhesion (psi) Average	Type of Failure
T-4120	Epon 913	T-4120	48	170	0	3	1,035 to 1,710	1,250	90% cohesive in repair material
		T-4120	48	170	15	3	534 to 1,500	1,091	80% cohesive in repair material
		T-4113	48	170	0	3	74 to 126	103	80% cohesive in repair material
		T-4113	48	170	15	3	1,112 to 221	181	100% cchesive in repair material
T-4113	Epon 913	T-4113	209	170	0	3	21 to 93	64	100% adhesive
		T-4113	48 +161	170 170	15 0	3	144 to 205	174	70% cohesive in repair material
T-2610	Epon 913	T-4120	48	170	0	3	980 to 1,460	1,180	66% adhesive in T-4120
		T-4120	48	170	15	3	581 to 1,190	855	100% adhesive in T-4120

TABLE XIII

LCCM REPAIR MATERIAL EROSION PERFORMANCE

TU-379 Motor Number	Base Material	Cure Temp (°F)	Cure Pressure (psi)	Repair Material	Cure Temp (°F)	Cure Pressure (psi)	Avg Rate of Erosion (mils/sec)*
			Adapter Cone:				
848/849	T-4120	170	0	T-4120	170	0	3.29 2.98
850/851	T-4120	170	15	T-4120	170	0	4.22 **
852/853	T-4113	170	15	T-4113	170	0	4.70 5.20
854/855	T-2610	300	1,000	T-4120	170	0	0.20 **
			Exit Cone:				
848/849	T-4120	170	0	T-4120	170	0	0.78 +0.33
850/851	T-4120	170	15	T-4120	170	0	+0.93 2.16
852/853	T-2610	300	1,000	No Repair	--	--	0.44 +0.43
854/855	T-4120	170 170	200 15	No Repair	--	--	3.80 1.76

*The + sign indicates increase in thickness due to char swelling.
**Cones physically damaged after test, unsatisfactory for measurement.

TABLE XIV

MATERIALS DESIGN DATA MATRIX

Physical Property	Temperature at Measurement (°F)	Minimum No. of Specimens per Base Material	Remarks
Density	72	5	*
Weight Loss	72 to 600	1	**
Tensile Strength, Modulus and Elongation	72, 300, 600	9	3 per temperature
Compressive Strength and Modulus	72, 300, 600	9	3 per temperature
Coefficient of Thermal Expansion	72 to 600	2	**
Specific Heat	72 to 600	1	**
Thermal Conductivity	100	1	--

*Elevated temperature values can be calculated by use of weight loss and CTE data.
**Each specimen tested over entire temperature range.

Material	Cure Cycle		
	Pressure (psi)	Temperature (° F)	Time (hr)
T-4113	15	170	150
T-4120	15	170	48
T-2610	1,000	300	3

The physical test properties are shown in Tables XV thru XIX and Figures 18 thru 21. The methods utilized to determine the physical properties are given below.

1. DENSITY

The density was determined using calculated weight and dimensional measurements at room temperature. Density at elevated temperatures can be calculated from room temperature density and the subsequently measured weight loss and coefficient of thermal expansion data.

2. THERMAL CONDUCTIVITY

Thermal conductivity testing was performed utilizing a Cenco-Finch thermal conductivity apparatus. A sample (2 by 2 by 1/4 in.) was placed between the heat source vessel (boiling water) and the receiver. Contact was assured through utilization of a 4 kg weight on top of the source vessel. Heat flow through the sample was then determined through monitoring thermocouple readings (° F) from the source and receiving vessels.

3. COEFFICIENT OF LINEAR THERMAL EXPANSION

The coefficient of thermal expansion of the three materials was measured at various heating rates to approximately 600° F. The expansion was measured in a dilatometer using specimens 2 in. long by 0.5 in. in diameter. The control of the equipment was by time rather than temperature and thus the endpoint temperature varied somewhat from that desired.

The T-2610 (300° F cure) was tested at heating rates of 150, 500, and 400° F/hr. The results of these tests are shown in Figure 18. The expansion curves are similar for all three heating rates but the initial expansion to contraction change occurs at higher temperatures with the higher heating rates, probably due to nonuniform crossection temperature.

The test data for the T-4120 are plotted in Figure 19. The 150° F/hr heating rate curve is similar in shape to that for the T-2610 except that the expansion to contraction transition occurs at a lower temperature, quite probably due to the T-4120 being cured at 170° F rather than 300° F. The lower temperature cured specimens quite probably are undergoing continued cure and this may explain the continued shrinkage at the 4,000° F/hr heating rate.

TABLE XV

DENSITY DESIGN DATA

Base Material	Test Temperature (°F)	Density (gm/cc) Test Values	Average
T-2610	72	1.686	1.706
		1.738	
		1.702	
		1.766	
		1.737	
T-4113	72	1.406	1.346
		1.370	
		1.373	
		1.329	
		1.251	
T-4120	72	1.592	1.595
		1.585	
		1.574	
		1.603	
		1.621	

TABLE XVI

TENSILE STRENGTH DESIGN DATA

Base Material	Test Temperature (°F)	Tensile Strength (psi) Test Values	Average
T-2610	72	2,970 2,905 2,905	2,926
	300	1,695 1,960 1,330	1,661
	600*		
T-4113	72	184 363 524 403 412	437
	300	97 113 81 56 61	81
	600	293 346 363 371 387	352
T-4120	72	3,420 2,400 1,140	2,320
	300	1,020 645 767	810
	600	146	146

*Gripping of specimens at 600° F test temperature created fracture of specimens.

TABLE XVII

COMPRESSIVE PROPERTIES DESIGN DATA

Base Material	Test Temperature (°F)	Compressive Strength (psi)		Compressive Modulus (psi x 10^5)	
		Test Values	Average	Test Values	Average
T-2610	72	12,050	11,916	4.76	4.49
		11,650		4.12	
		12,050		4.58	
	300	5,020	5,040	1.86	1.87
		5,300		1.89	
		4,800		1.86	
	600	3,000	2,820	0.88	0.85
		2,380		0.83	
		2,080		0.83	
T-4113	72	169	130	0.063	0.067
		168		0.071	
		53			
	300	32	30		
		20			
		38			
	600	925	821	0.23	0.16
		890		0.18	
		650		0.08	
T-4120	72	8,430	8,185	4.72	4.56
		7,720		4.38	
		8,470		4.58	
	300	1,910	2,043	5.10	5.49
		2,280		5.54	
		1,940		5.84	
	600	6,840	6,673	3.77	3.71
		7,130		3.36	
		6,050		4.00	

TABLE XVIII

THERMAL CONDUCTIVITY DESIGN DATA

Base Material	Test Temperature (°F)	Thermal Conductivity (Btu/ft-hr-°F)
T-2610	100	0.490
T-4113	100	0.656
T-4120	100	0.886

TABLE XIX

SPECIFIC HEAT DESIGN DATA

Base Material	Test Temperature (°F)	Specific Heat (Btu/lb-°F) Test Values	Average
T-2610	150	0.3235	0.3306
		0.3376	
	200	0.3706	0.3783
		0.3771	
		0.3873	
	300	0.3606	0.3528
		0.3437	
		0.3540	
	500	0.3626	0.3683
		0.3730	
		0.3693	
	600	0.3659	0.3704
		0.3717	
		0.3736	
T-4113	150	0.2905	0.2991
		0.3077	
	200	0.3431	0.3449
		0.3484	
		0.3432	
	300	0.3479	0.3476
		0.3474	
	500	0.2706	0.2684
		0.2677	
		0.2672	
	600	0.2994	0.2933
		0.2710	
		0.3094	
T-4120	150	0.2723	0.2677
		0.2631	
	200	0.2940	0.3005
		0.3174	
		0.2900	

TABLF XIX (Cont)

SPECIFIC HEAT DESIGN DATA

Base Material	Test Temperature (°F)	Specific Heat (Btu/lb-°F) Test Values	Average
T-4120 (Cont)	300	0.2939	0.3143
		0.3296	
		0.3193	
	500	0.2475	0.2504
		0.2479	
		0.2558	
	600	0.3252	0.3017
		0.3068	
		0.2822	
		0.2927	

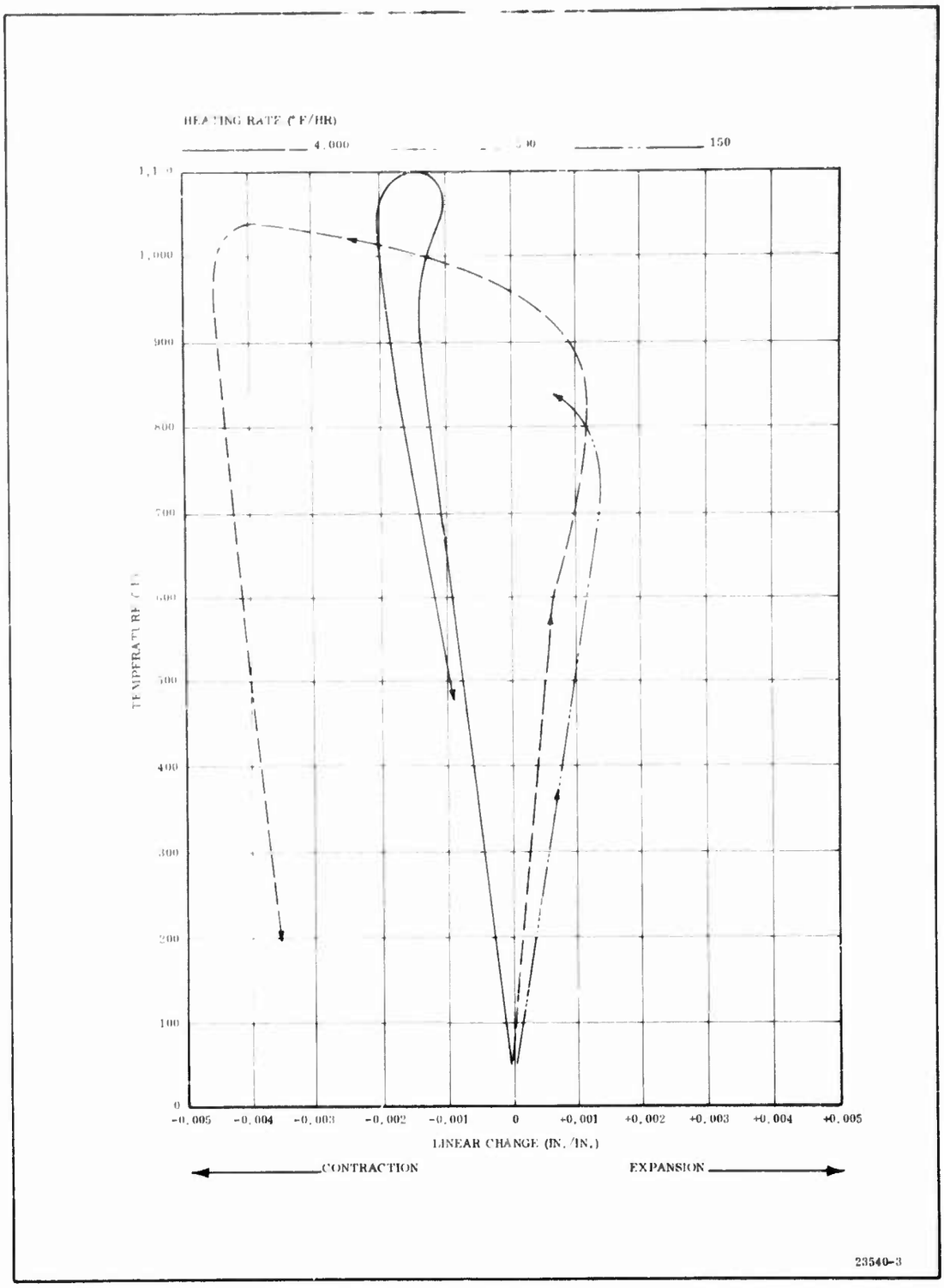

Figure 18. Linear Thermal Expansion, T-2610 Rerun

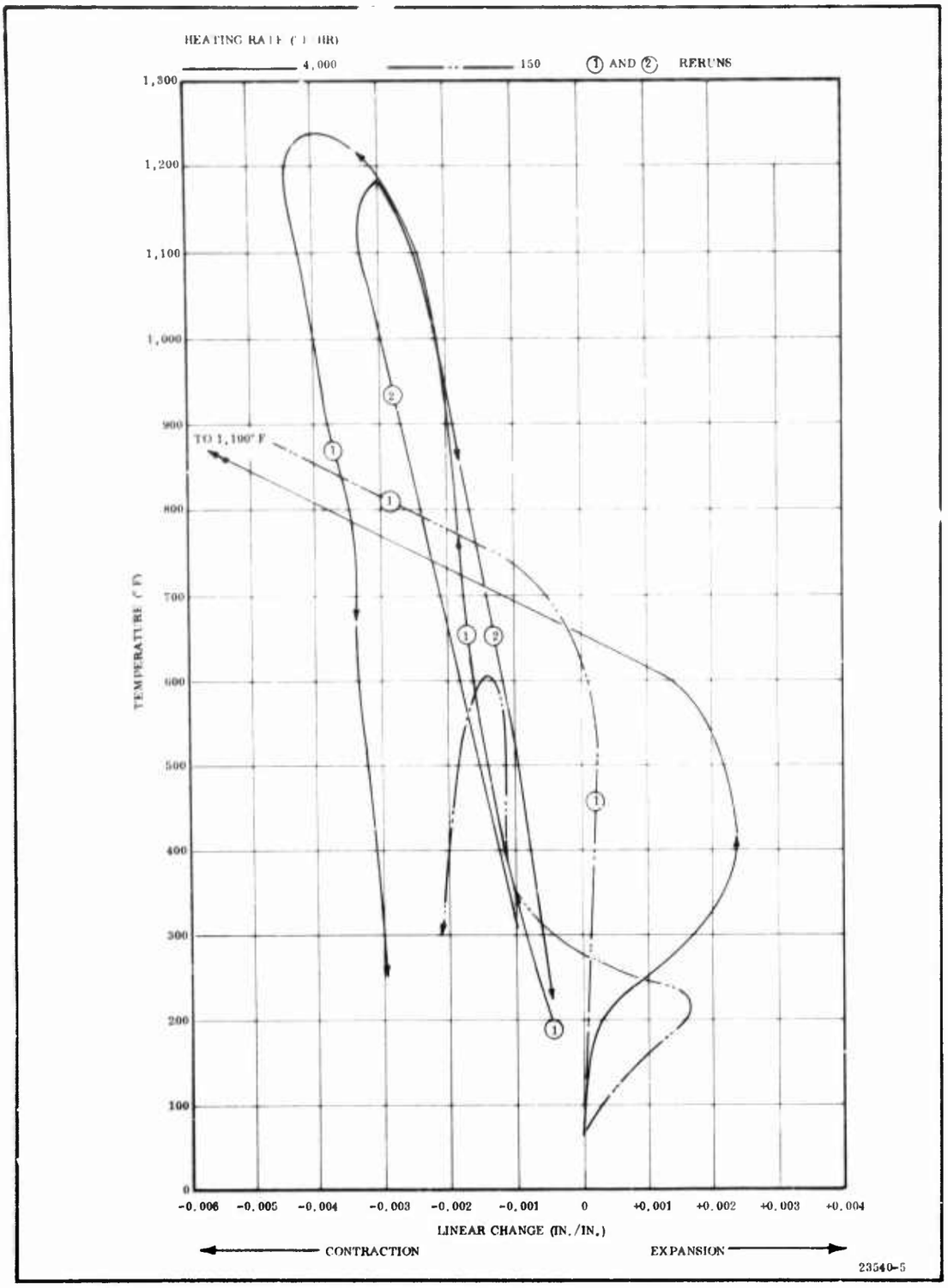

Figure 19. Linear Thermal Expansion, T-4120

The results of the T-4113 (170° F cure) are presented in Figure 20 and are similar to those for the T-4120.

4. WEIGHT LOSS

The weight loss test involved raising the temperature of a test specimen at a constant rate and monitoring the weight loss of the specimen. Figure 21 shows the weight loss of the three materials to 600° F.

5. TENSILE STRENGTH

Tensile strength was determined by Standard ASTM Testing Methods. A dumbbell shaped specimen was machined from the material of 0.5 in. nominal thickness. Specimens were pulled to failure at the desired temperature on the Riehle Tensile Tester.

E. ADDITIONAL FABRICATION PROCESS DEVELOPMENT

The additional fabrication effort was added to the program by an addendum to the Program Plan. Its scope was to study the possibility of incorporating chopped fibers into the T-4113 to improve the char retention characteristics.

Attempts were made to add chopped rayon or glass fibers to the T-4113 formulation in various quantities and fiber lengths. A maximum of 3 percent of the fibers could be added to the basic T-4113 formulation before the mixer, a 10 qt Hobart with a flat beater, failed to operate properly. Fiber contents beyond this level required added solvent to insure proper blending of components. Fibers over 3 in. in length could not be adequately mixed into the formulation without gathering or balling up, regardless of the amount of solvent added or the mixing speed; therefore, further studies were restricted to fibers of 1 in. or less in length.

A 13 percent level of fiber reinforcement was selected for the T-4113 insulation and the T-4120 was also tested with the fiber reinforcements.

Material formulations, T-4113 and T-4120, containing various quantities of fiber and fiber length were hand packed in 5 by 10 by 1 in. molds and cured at 170° F and ambient pressure. Unsatisfactory parts resulted with T-4113 containing 13 percent fiber reinforcement when cured at ambient pressures. The parts were of a poor construction and nonuniform in texture, although similar parts fabricated of T-4120 were visually satisfactory. Based on these results, a cure cycle of 300° F and 200 psi was selected for curing the T-4113 with 13 percent chopped rayon and glass in TU-379 adapter cones and test slabs (4 hr cure). The erosion and physical data are shown in Table XX. The erosion rate was much greater than expected and was 3 to 4 times as high as the nonreinforced material. To evaluate this poor performance, the previously test fired, nonreinforced T-4113 was re-examined. These data, summarized in Table XXI, show that curing or post curing

HEATING RATE (°F/HR)
500
150
(1) RERUNS
TO 650° F
TO 95° F
1,200
1,100
1,000
900
800
700
600
500
400
300
TEMPERATURE (°F)

Figure

A

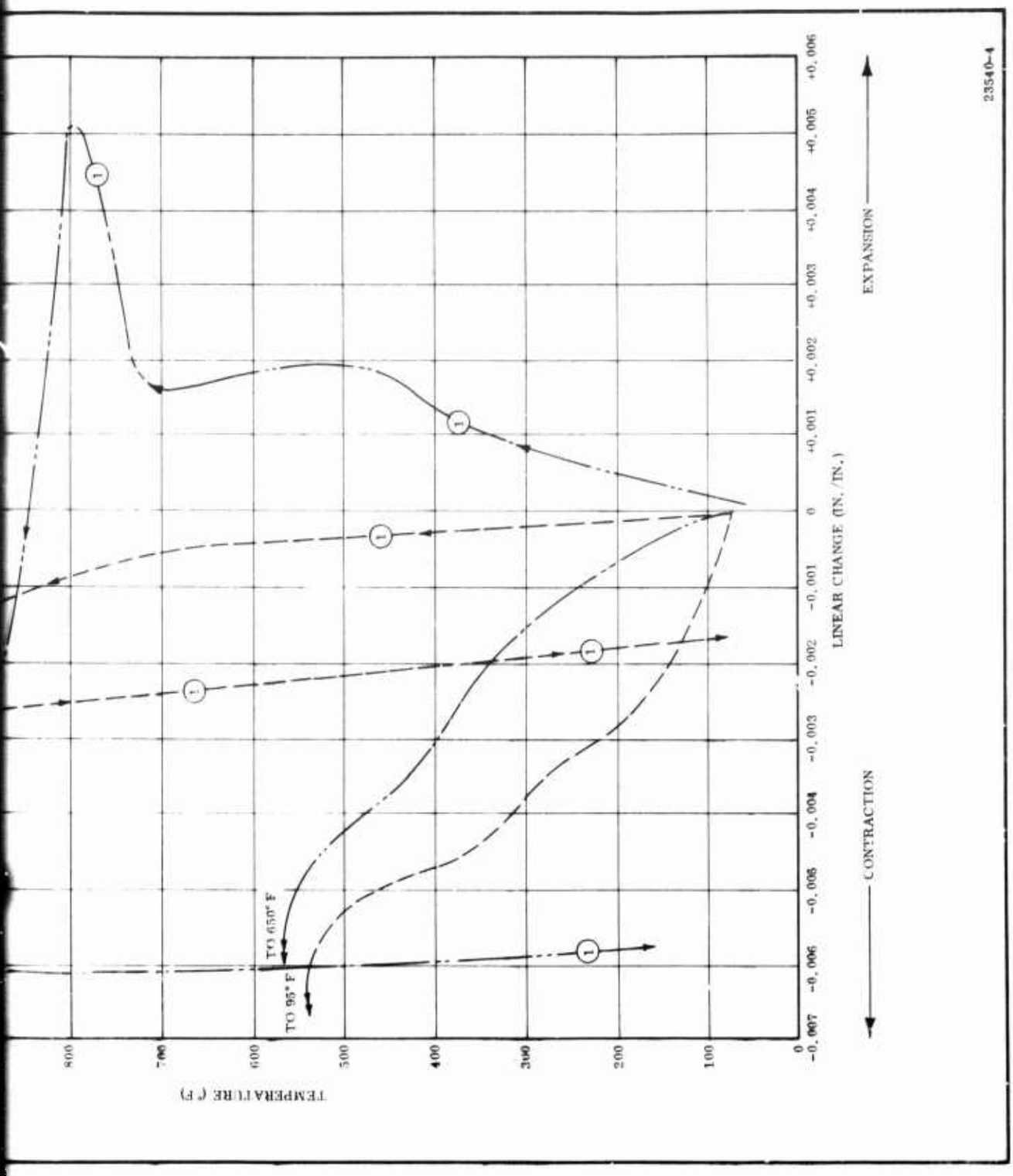

Figure 20. Linear Thermal Expansion, T-4113

B

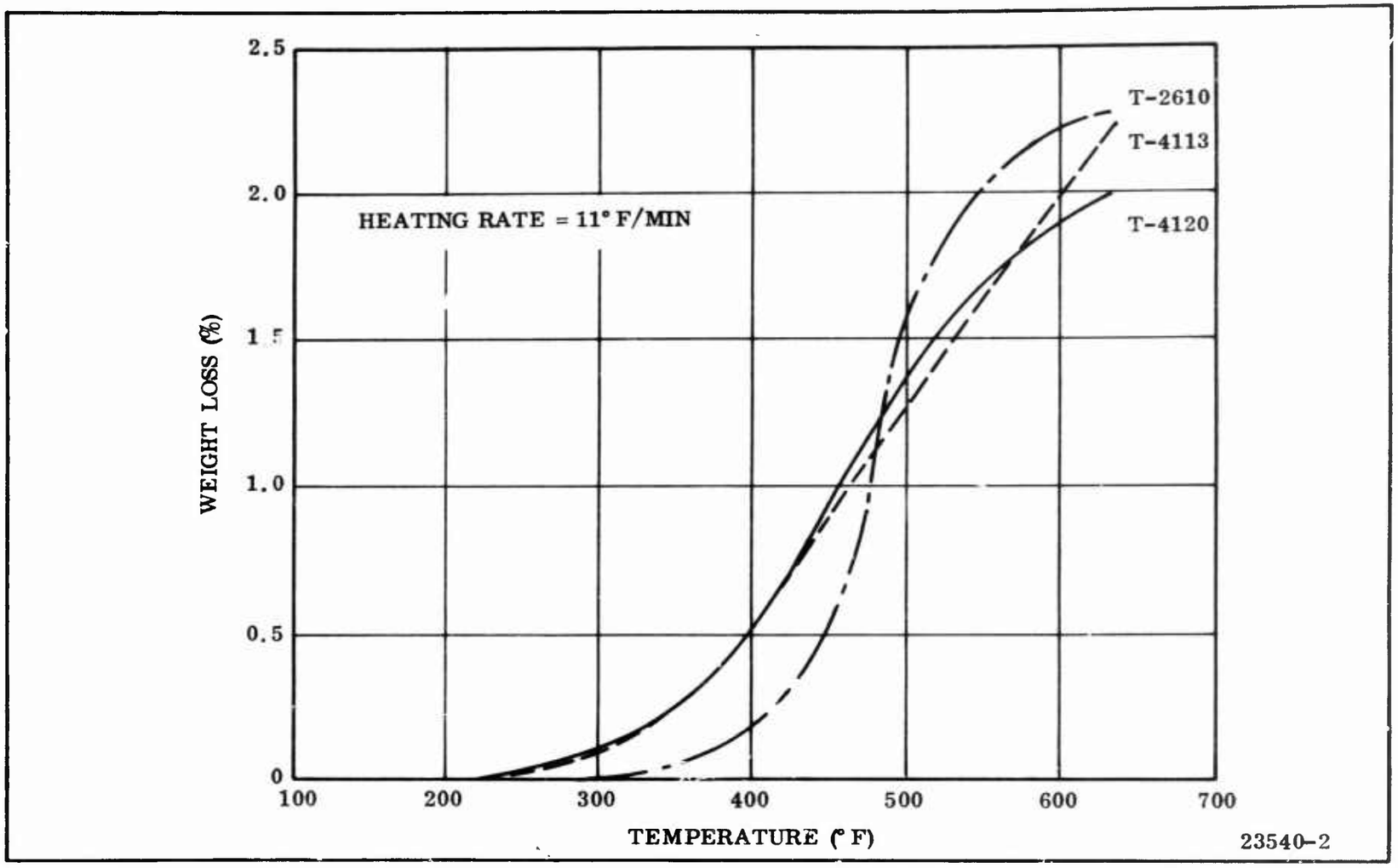

Figure 21. LCCM Weight Loss

TABLE XX

MATERIAL PROPERTIES, REINFORCED T-4113

Properties	13 Percent Rayon (3/4 in.)	13 Percent Glass (3/4 in.)
Cure Cycle		
Temperature (°F)	300	300
Pressure (psi)	200	200
Density (gm/cc)	1.36	1.11
Tensile Strength (psi)	276	445
Elongation (percent)	3.1	11.0
Erosion Rate (mils/sec)	13 16	12 10

TABLE XXI

T-4113 EROSION DATA

TU-379 ADAPTER

Test No.	Cure Cycle Pressure (psi)	Cure Cycle Temperature (°F)	Cure Cycle Time (hr)	Post Cure Cycle Temperature (°F)	Post Cure Cycle Time (hr)	Total Time (hr) at 170° F	Total Time (hr) at 300° F	Erosion Rate (mils/sec) Individual	Erosion Rate (mils/sec) Average
808/809	15	170	42	--	--	42	--	3.22 4.56	3.89
810/811	0	170	26	170	64	90	--	2.94 2.73	2.84
806/807	200	170	6	170	64	70	--	2.48 1.46	1.97
802/803	200	170	6	300	12	6	12	3.87 3.90	3.88
804/805	200	170	26	300	12	26	12	3.98 3.34	3.66
812/813	15	300	4	300	12	--	16	6.11 5.77	5.94

VACUUM STAGED

Motor Test No.	Material	Resin (percent)	Glass Fiber Reinforcement (percent)	Cure Temperature (°F)	Cure Pressure (psi)	Erosion Rate (mils/sec)
893/894	T-4113	30	15	300	200	7.24 7.80
895/892	T-4113	30	8	300	200	5.00 4.45

at 300° F is actually detrimental to the material performance. With the data grouped by the maximum process temperature, the average erosion rates are:

Maximum Process Temperature (° F)	Average Erosion Rate (mils/sec)
170	2.82
300	4.39

These results indicated that the 300° F temperature may have contributed to the high erosion rates and that the resin content used was insufficient for adequate fiber wetting and bonding. Therefore, TU-379 adapter cones were made with variations in resin content and fiber reinforcement. In the TU-379 motor, all parts were severely eroded and several were burned through, indicating an erosion rate of over 20 mils/sec. The increased resin content and lower cure temperature obviously did not offer any improvement. On visual appearance, the glass parts were superior to the rayon specimens as the glass eroded uniformly while the rayon was gouged. Again, this could be due to the cure temperature difference.

Normally, T-4113 material is staged before molding at 170° F for 1.5 to 2 hr and is broken up every 15 min (as a thin skin forms) to allow for solvent release. With the fibrous material though, the 170° F staging was not desirable because the thin solvent free skin forms and the fibrous material is difficult to break up. The material was, therefore, staged at ambient conditions for 4 to 5 hr with an occasional stirring. It was realized that a portion of the solvent would remain in the material at the time of specimen fabrication, but it was expected that the remaining solvent would be removed by vacuum during the earlier stages of cure. However, the cured parts contained as much as 7 percent solvent (apparently due to surface blocking). To eliminate the problem of retained solvent, a 2,500 gm T-4113 type mix containing 375 gm of fiberglass in 1,000 ml of methyl ethyl ketone was staged under a vacuum system (3 in. Hg) at ambient temperature for 4 hr. This T-4113 material had an ideal packing consistency.

Formulation mixes using the above technique were made of the T-4113 material using various resin contents and fiberglass reinforcement. TU-379 adapter cones were fabricated at 300° F and 200 psi, with the 300° F cure selected to reproduce the previous glass tests and allow a much shorter cure time. Table XXI shows the processing parameters and erosion rates. The vacuum staged parts were definitely improved over previous parts and approached the nonreinforced parts in erosion resistance.

Additional mixes of the T-4113 type material without fiber reinforcement were made using the same staging cycle. The recovered solvent vapor was condensed and collected in a dry ice trap. The measured amount removed was 73 percent by weight of the total solvent content. The T-4113 vacuum staged material was then hand packed into a 5 by 10 by 1 in. mold and cured at 300° F and 200 psi. The tensile and density properties of this slab are given (page 56) with the properties of nonvacuum T-4113 staged material shown for comparison.

Material	Cure Temperature (° F)	Cure Pressure (psi)	Tensile Strength (psi)	Elongation (%)	Modulus (psi x 10^5)	Density (gm/cc)
T-4113 Vac	300	200	939	6.77	2.8	1.49
T-4113	300	200	434	5.2	1.3	1.52

SECTION III
PHASE II--SUBSCALE NOZZLE EVALUATION

A. INTRODUCTION

The basic subscale nozzle was designed within the limits of (1) the interface requirements of the Edwards Air Force Base (EAFB) char motor, (2) operating conditions of 700 psi average chamber pressure with 30 to 60 sec action time, and (3) propellant supplied by EAFB. The test motor has a 44 in. diameter and contains an uncured end burning polycarbutene type propellant with 68 percent ammonium perchlorate and 17 percent aluminum.

The three low-cost materials developed during the materials process optimization studies were tested on five subscale nozzles. A sixth nozzle (No. 1) using state-of-the-art ablative plastics was also tested as a baseline.

The discussion of this program phase has been divided into four subsections. Subscale Nozzles No. 1, 2 and 3 are discussed as a group because they were designed, manufactured and tested concurrently. Nozzles No. 4, 5 and 6 are discussed individually because they were designed and manufactured sequentially based on the preceding nozzle performances.

B. NOZZLES NO. 1, 2 AND 3

1. DESIGN

The insulation design in the nozzle assembly was purposely made ultraconservative to allow for unexpected material problems with the low cost materials and to allow for up to 60 sec firings, should long duration tests be desirable in later subscale tests.

Performance of the Nozzle No. 1 was as predicted. Erosion and thermal profiles are presented in Figures 22 thru 25.

The predicted temperature profiles were obtained using an IBM 7040 computer program for two dimensional axisymmetric transient temperature prediction. Erosion profiles were predicted using a plot of measured erosion rates correlated with convective heat transfer coefficients (ref Appendix A, Sections A thru C). The convective heat transfer coefficients for various locations in the nozzle were obtained as a part of the thermal analysis using the Bartz' equation. Motor operation parameters used are shown below:

$$P_c = 700 \text{ psia}$$

$$T_o = 6,200°R$$

$$t_a = 30 \text{ sec}$$

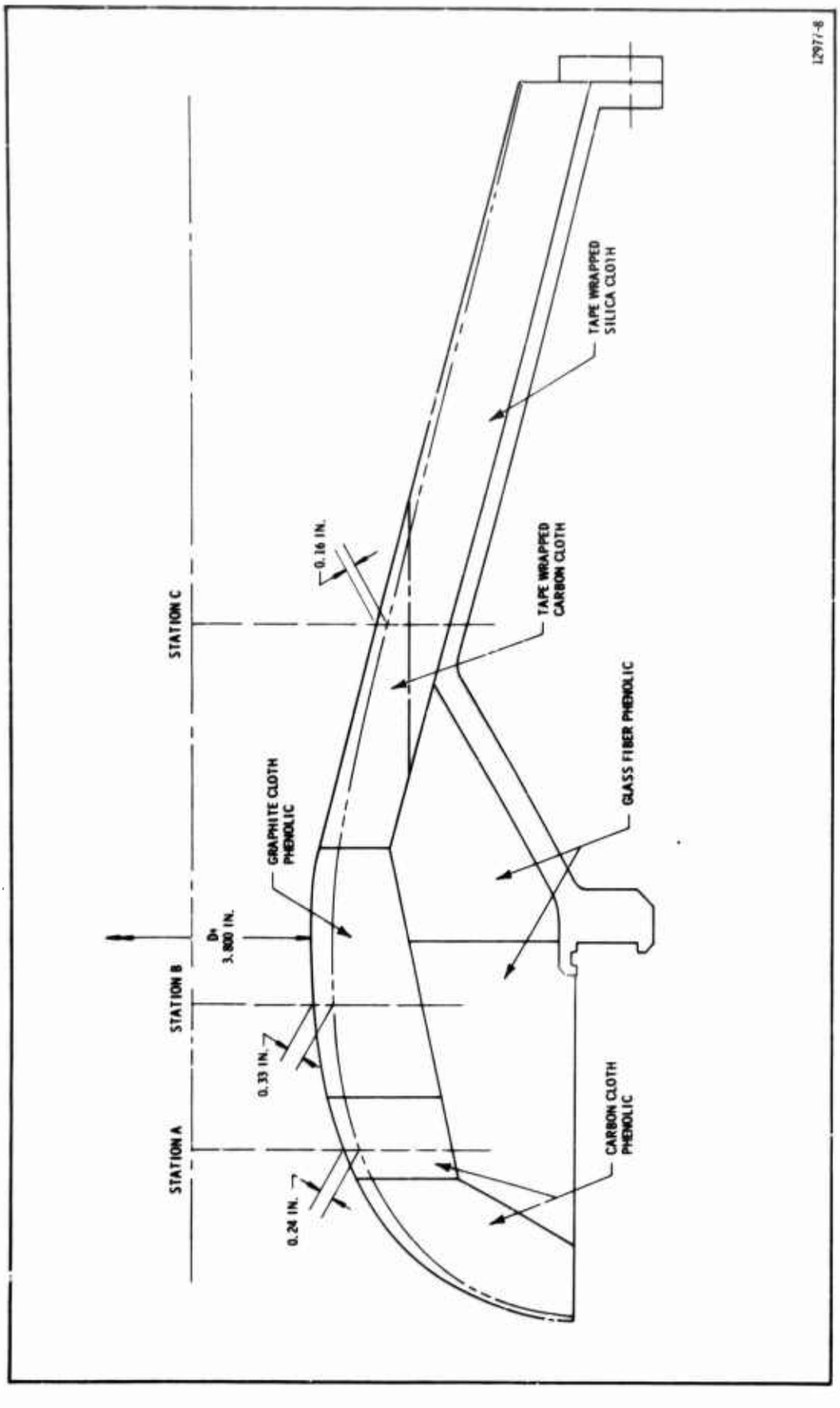

Figure 22. Predicted Erosion Profile, Nozzle No. 1

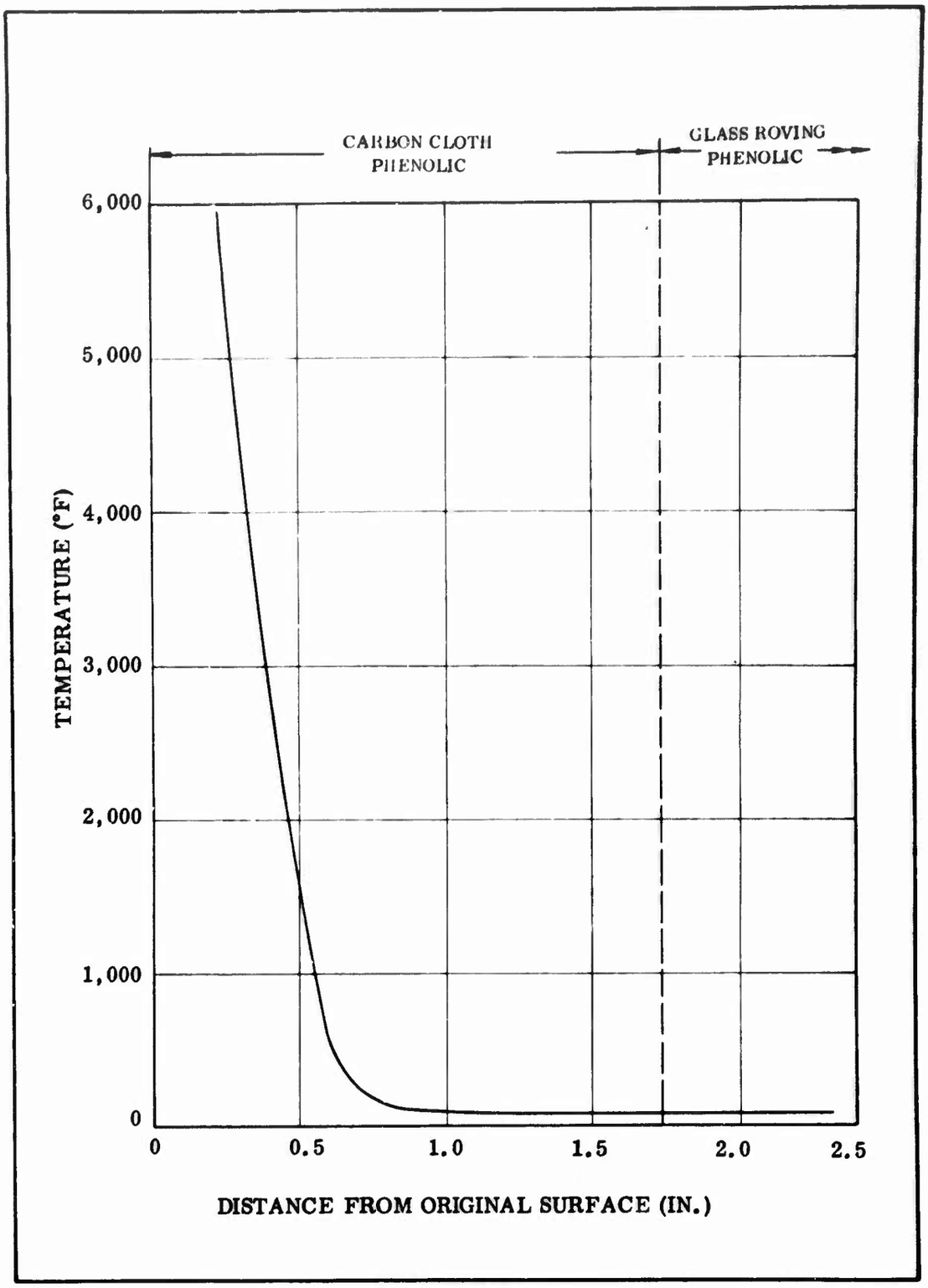

Figure 23. Predicted Thermal Profile, Nozzle No. 1, Station A, 30 Sec

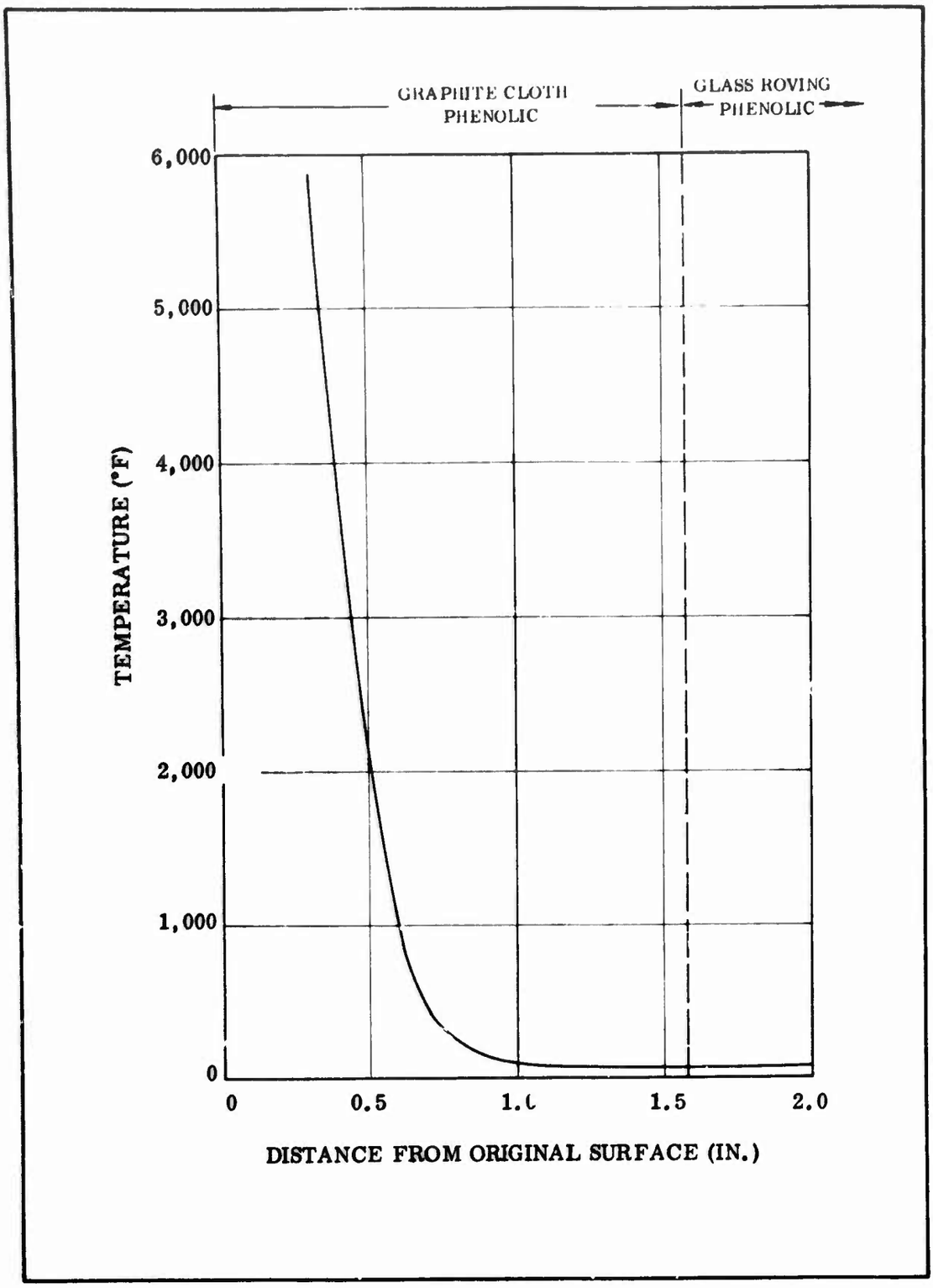

Figure 24. Predicted Thermal Profile, Nozzle No. 1, Station B, 30 Sec

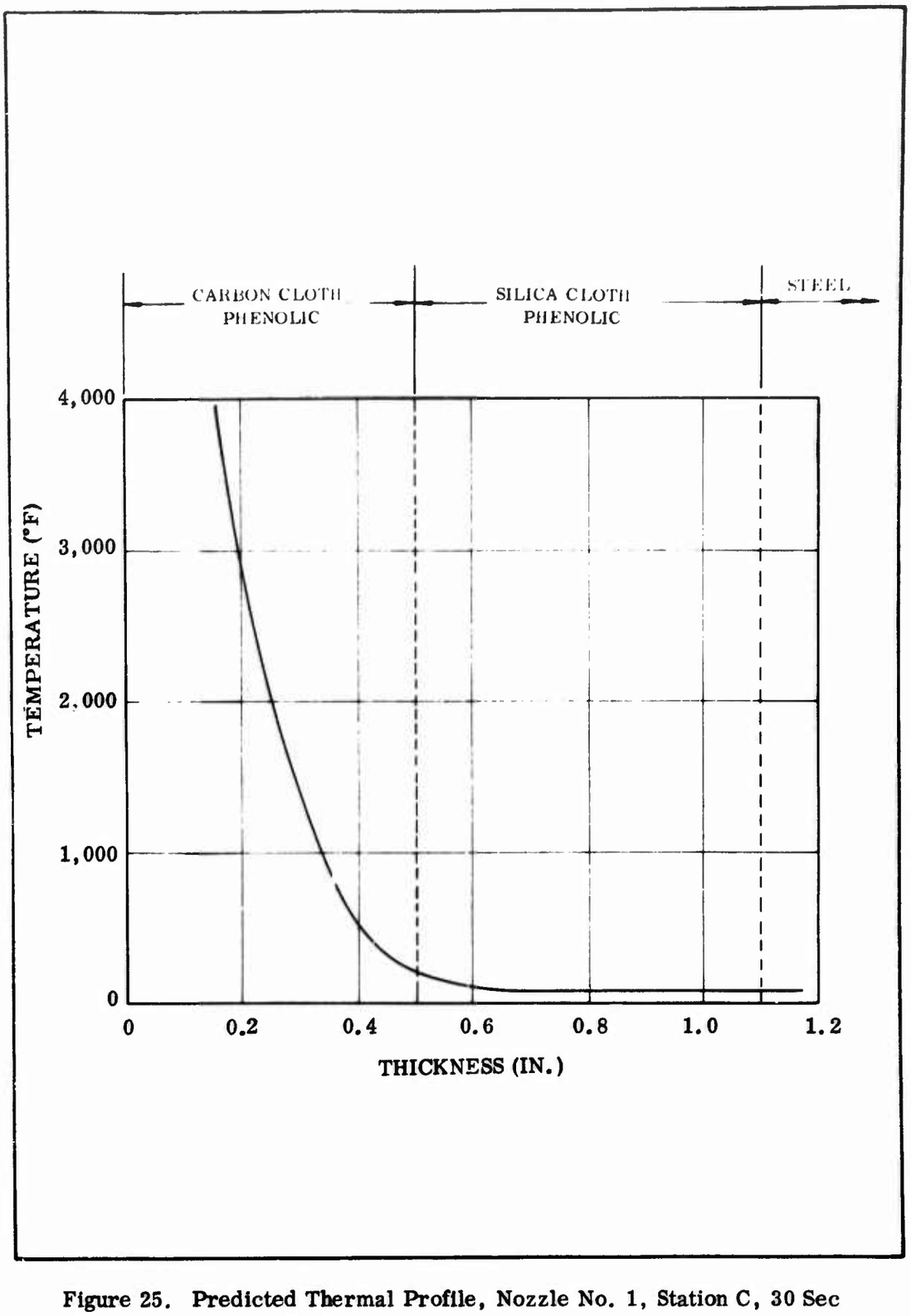

Figure 25. Predicted Thermal Profile, Nozzle No. 1, Station C, 30 Sec

Limited data were available for the test propellant; thus, thermal properties of the combustion gases were assumed to be similar to those of TP-H1011 propellant combustion products.

2. FABRICATION

The component materials and fabrication methods for the first three subscale nozzles (No. 1, 2 and 3) are reviewed in Table XXII. Figure 26 illustrates the nozzle design showing the components and instrumentation location.

Nozzle No. 1 was manufactured without problems. Originally, the exit cone was to be of a rosette construction, but it was changed to a tape wrap parallel to the centerline at the direction of RPL in order to produce a part more representative of the construction used in large nozzles. This change necessitated purchasing the part from an outside source. The part had several minor discrepancies but was accepted for use. The carbon-silica interface was not normal to the internal surface as designed, but was parallel to the centerline. Also, several wrinkles and minor voids visible on the internal surface apparently were caused by the material slipping on the mandrel during cure. Figure 27 shows the steel nozzle body in the final condition, except for the holes in the aft retainer flange and the instrumentation holes. Figure 28 shows the assembled nozzle prior to final machining.

The components and assembly for Nozzle No. 2 were completed without problems. Figures 29 thru 32 show the nozzle components prior to assembly into the nozzle shell.

The throat and inlet for Nozzle No. 3 were fabricated without difficulties, but problems were encountered with the throat backup. It was originally planned that this part be of T-4120 similar to that in Nozzle No. 2. This part was made by hand packing the material in a 14 in. diameter steel drum and curing it as a solid billet. However, the cured part had cracks and delaminations. Additional attempts were made to produce a solid billet and also a cylinder with an open 5 in. diameter center hole. Some improvements in quality were obtained, but generally the moldings were not considered usable. The throat backup was then made from the T-4113 and the first attempt resulted in an excellent part. The exit cone for this nozzle was initially made by hand packing the T-4120 in the assembled nozzle and curing it in place. The first attempt at this produced a good exit cone, but separations appeared between the exit cone and the steel shell. The T-4120 was machined out and the same procedure was again used with a slower cooldown cycle after cure. Separations occurred as before. The separations were minor in both cases, but during firing they could have resulted in cone cracking where the steel did not support the insulation. The problem of separation was associated with poor adhesion of the T-4120 to the steel and/or to material shrinkage during cure. Since in both trials, the exit cone itself was satisfactory, a glass-epoxy mold was made, and the exit cone was cured external to the nozzle. It was then bonded into the nozzle body. Figures 33 thru 36 show the nozzle components prior to assembly and final machining.

The assembled and machined nozzles were instrumented with thermocouples in accordance with the design drawing. Each thermocouple hole was individually

TABLE XXII

NOZZLE FABRICATION MATRIX

Nozzle No.	Features	Nozzle Body	Entrance Forward	Entrance Aft	Throat	Throat Backup	Exit Cone Forward	Exit Cone Aft
1	Material	Steel	FM-5063, Carbon Cloth Phenolic	FM-5063, Carbon Cloth Phenolic	FM-5064, Graphite Cloth Phenolic	Durez 16771, Glass Roving Phenolic	FM-5063, Carbon Cloth Phenolic	FM-5067, Silica Cloth Phenolic
	Fabrication Process	Roll and Weld	1/2 by 1/2 chopped sq molded at 2,000 psi, 310°F	Rosette perpendicular to centerline, molded at 1,300 psi, 325°F	Rosette perpendicular to centerline, molded at 1,275 psi, 325°F	Chopped 1/2 in. lengths, molded at 2,000 psi, 290°F	Tape wrap parallel to centerline, autoclave cured at 215 psi, 310°F	Tape wrap parallel to centerline, autoclave cured at 215 psi, 310°F
2	Material	Steel	T-4113 (One piece)		FM-5064, Graphite Cloth Phenolic	T-4120, cured as solid billet at 0 psi, 170°F, 72 hr	T-2610, molded as solid billet at 500 psi, 305°F, 5 hr	
	Fabrication Process	Roll and Weld	Staged 1.5 hr at 170°F, cured as solid billet at 300°F, 200 psi, 4 hr		Rosette perpendicular to centerline, molded at 1,275 psi, 325°F			T-4120, hand packed in assembled nozzle at 15 psi, 170°F, 22 hr
3	Material	Steel	T-4113		T-2610	T-4113	T-4120 (One piece)	
	Fabrication Process	Roll and Weld	Staged 1.5 hr at 170°F, cured as solid billet at 300°F, 200 psi, 4 hr		Staged 4 hr at 200°F, molded at 1,000 psi, 300°F, 2 hr	Staged 1.5 hr at 170°F cured at 200 psi, 6 hr, 300°F	Cured in epoxy mold at 15 psi, 170°F, 64 hr	
4	Material	Steel	T-4113	T-4113	T-4120	T-4113	T-4120	T-4120
	Fabrication Process	Roll and Weld	Staged at 170°F, cured as solid billet at 170°F 15 psi		Cured at 300°F, 200 psi	Cured at 170°F, 0 psi	Cured at 170°F, 15 psi, rubber expansion washer between forward exit and aft exit cone, liner UF-1149 installed between steel shell and T-4120 insulation	
5	Material	Steel	T-4113	T-4113	T-2610	T-4113	T-2610	T-4120
	Fabrication Process	Roll and Weld	Vacuum staged, cured at 300°F, 200 psi, 4.5 hr		Cured at 300°F, 1,000 psi	Cured at 300°F, 200 psi, 4.5 hr	Cured at 300°F, 1,000 psi Glass cloth phenolic liner installed between steel shell and insulation	Cured at 170°F, 15 psi
6	Material	Steel	T-2610	T-2610	High Density Graphite	Silica Cloth Phenolic	T-2610	T-2610
	Fabrication Process	Roll and Weld	Cured 300°F, at 1,000 psi as solid billet, over OD of material was installed silica cloth phenolic ring	Cured at 300°F, 1,000 psi as solid billet			Each cured at 1,000 psi, 300°F, as solid billets and machined to contour Silica cloth phenolic sleeve bonded between T-2610 insulation and steel shell	

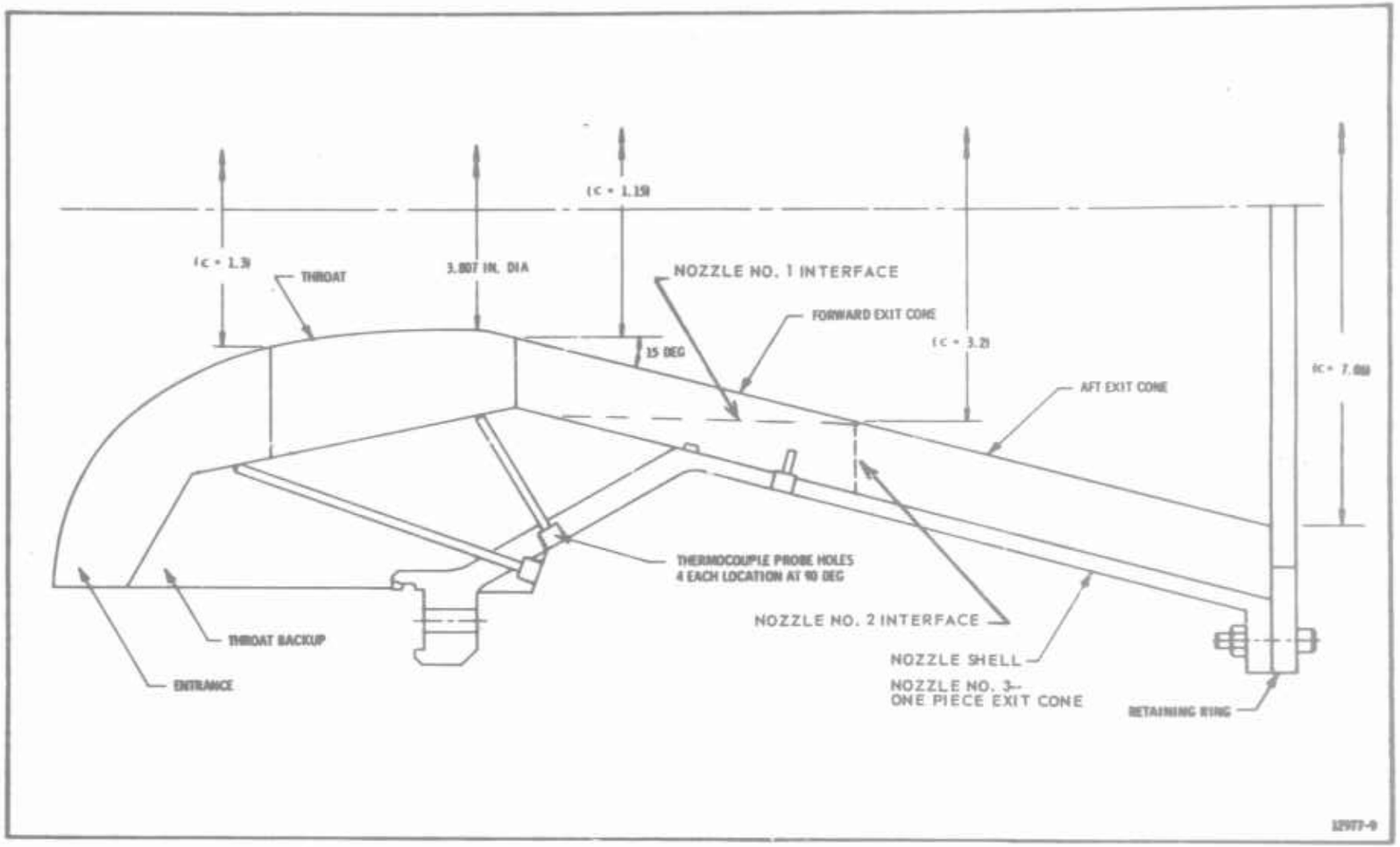

Figure 26. Nozzle Assembly, No. 1, 2, and 3

Figure 27. Nozzle Body

Figure 28. Nozzle No. 1

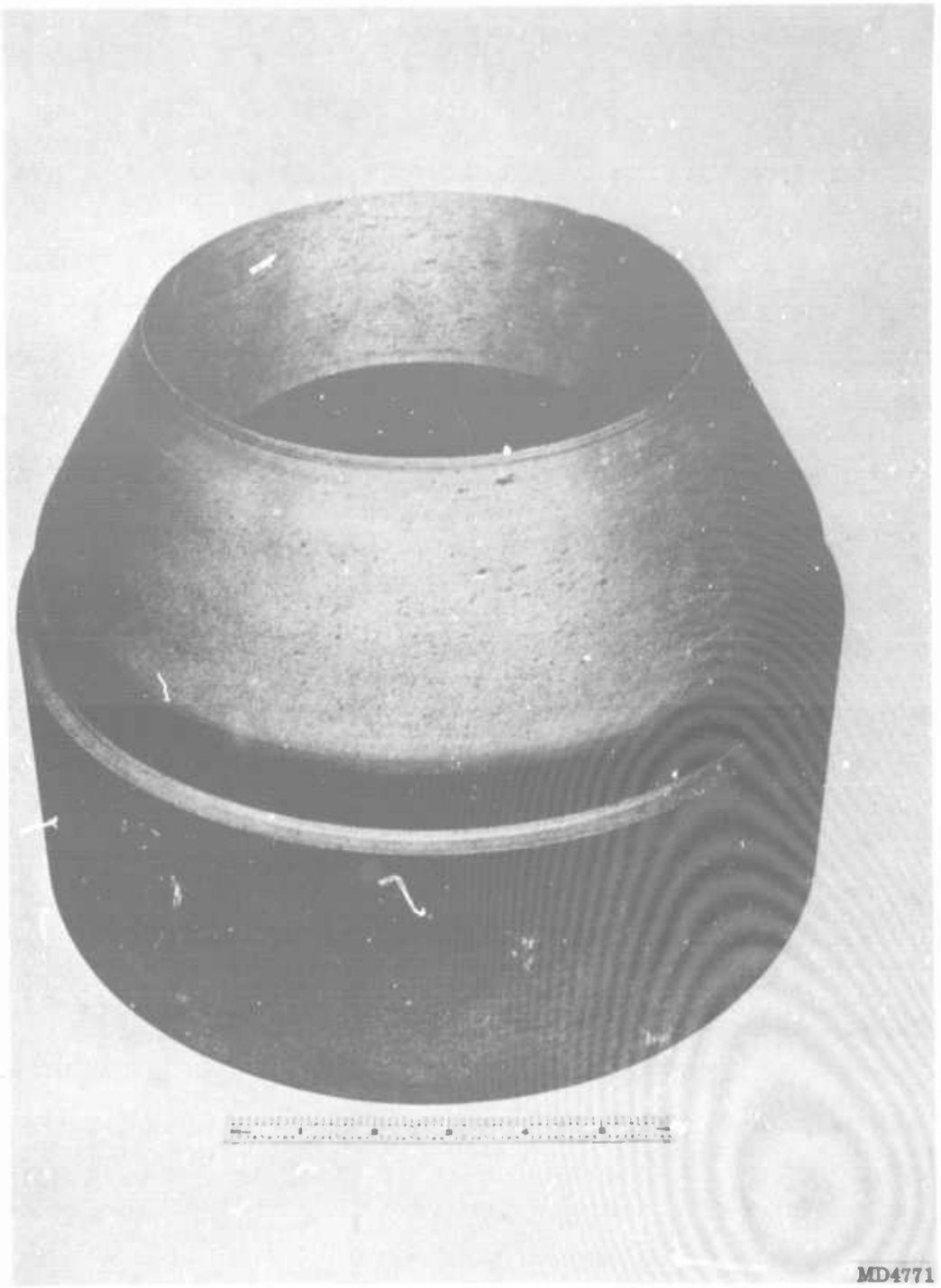

Figure 29. Nozzle No. 2 Inlet

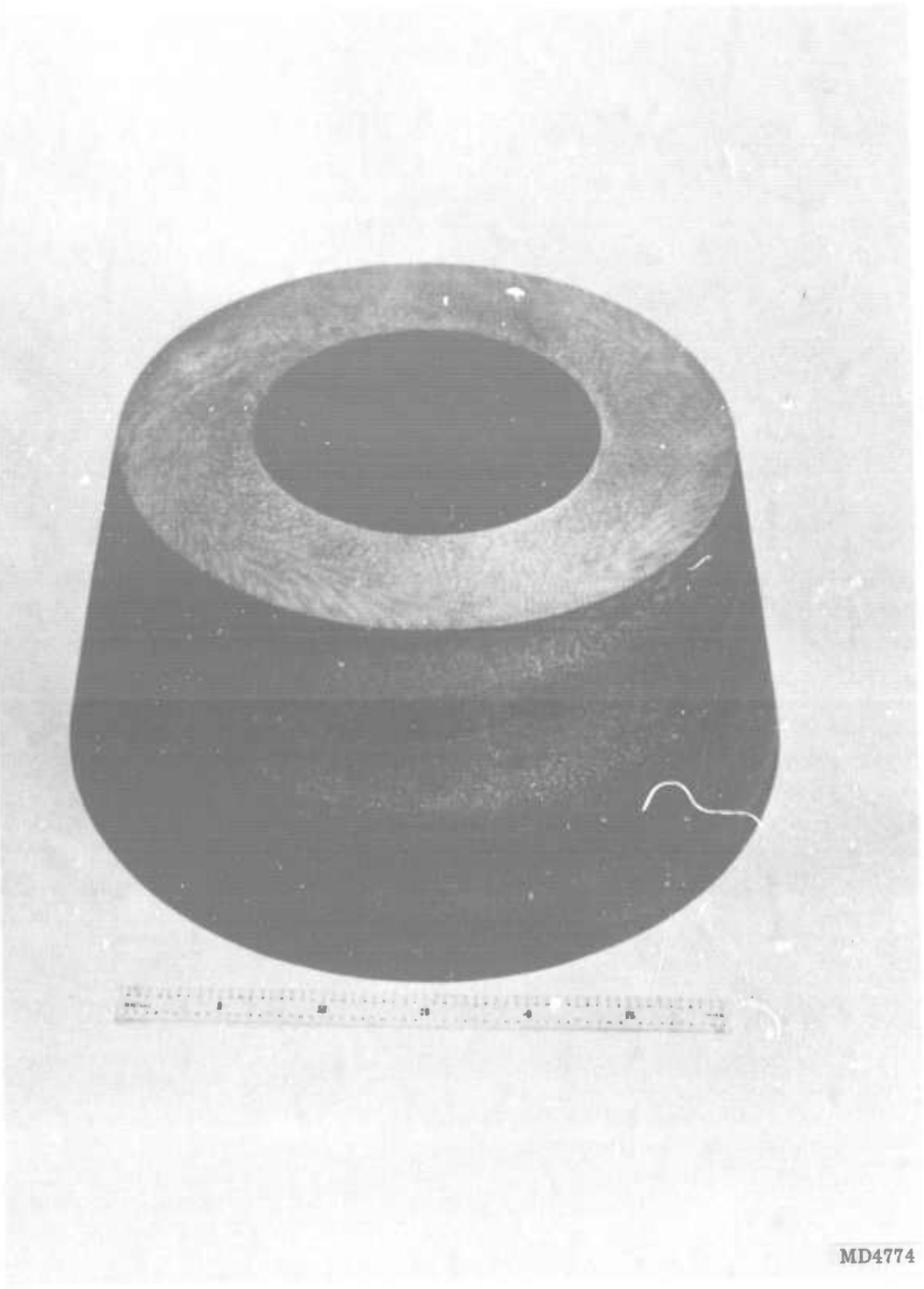

Figure 30. Nozzle No. 2 Throat

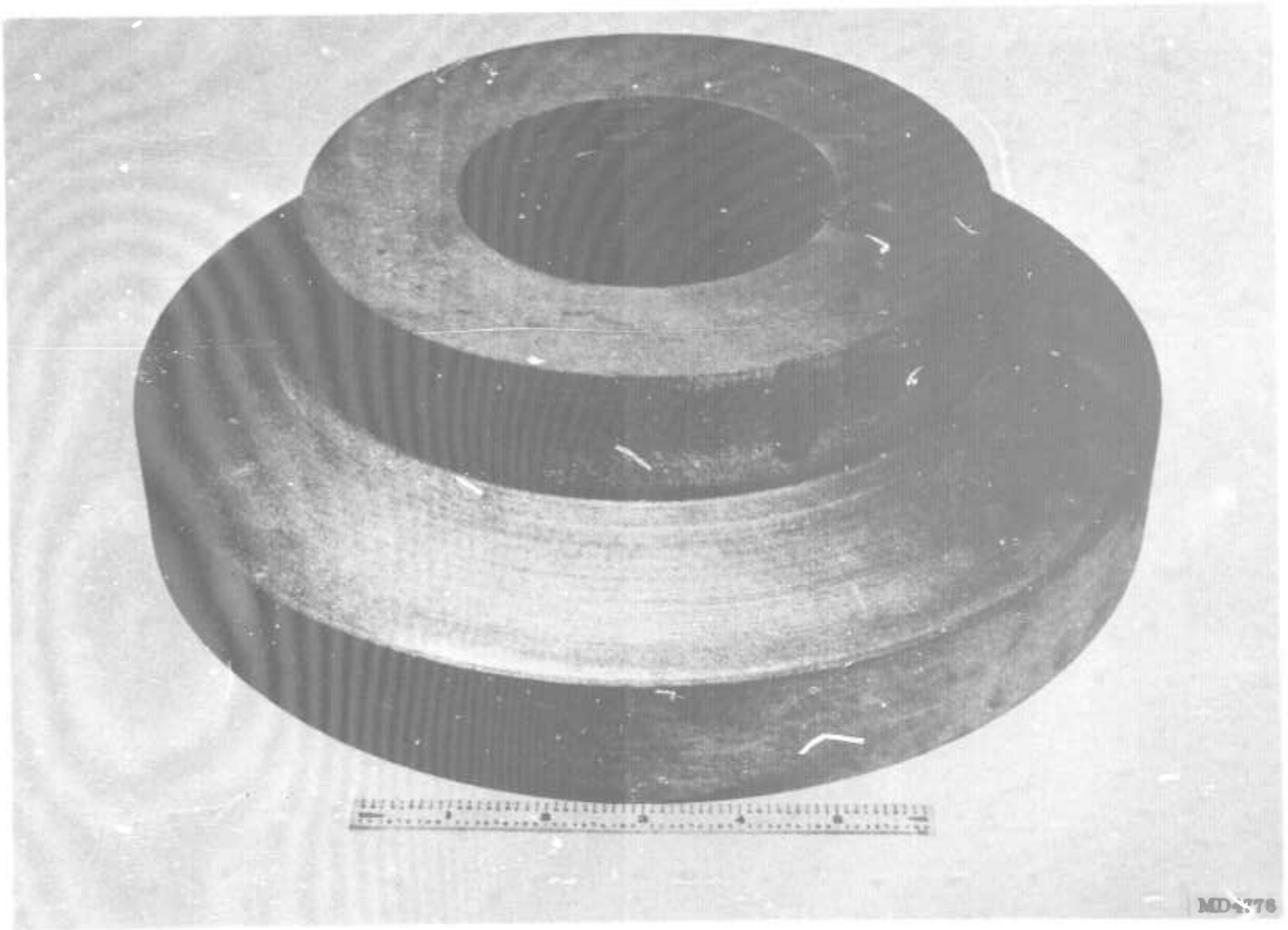

Figure 31. Nozzle No. 2 Throat Backup

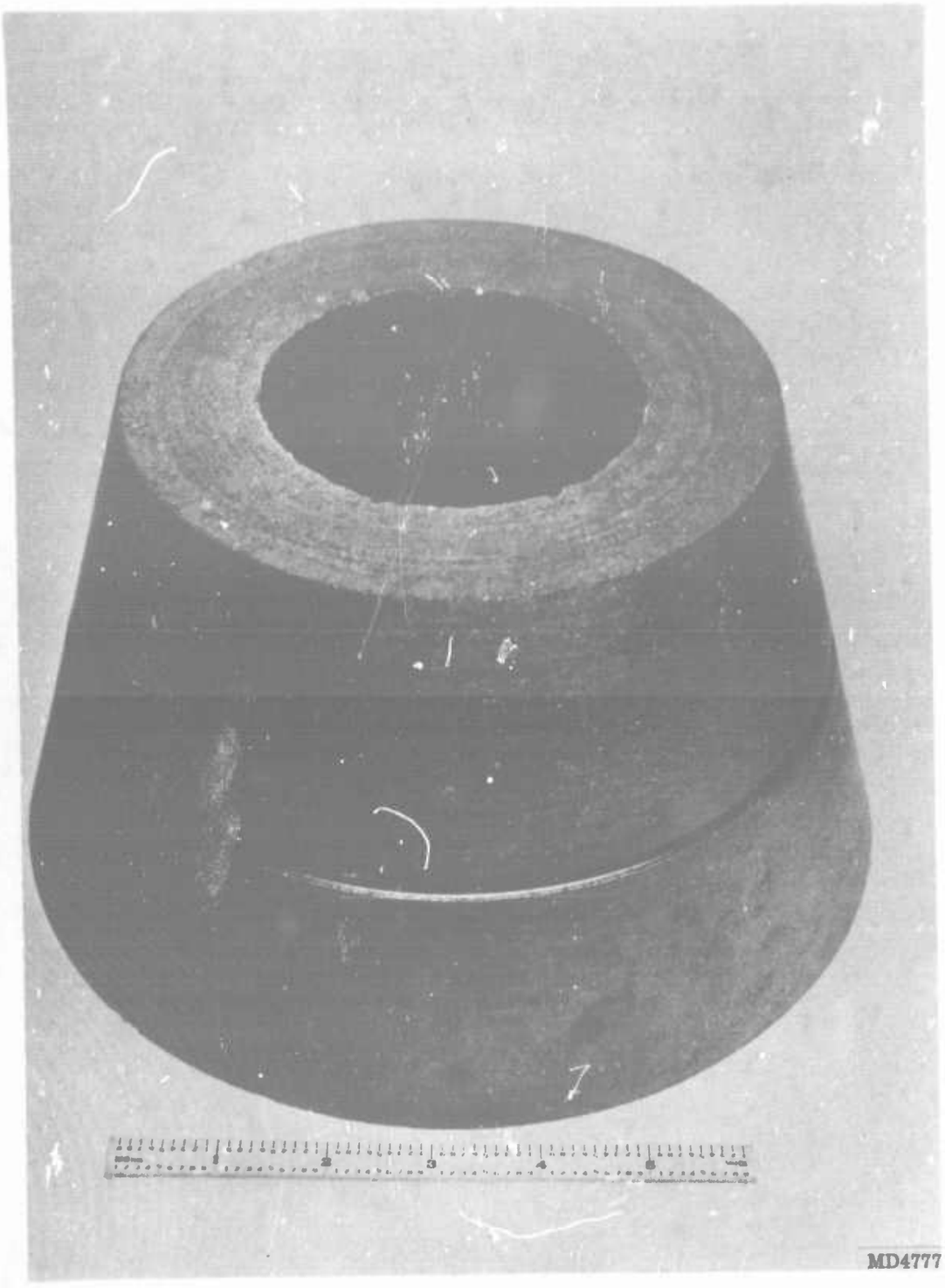

Figure 32. Nozzle No. 2 Forward Exit Cone

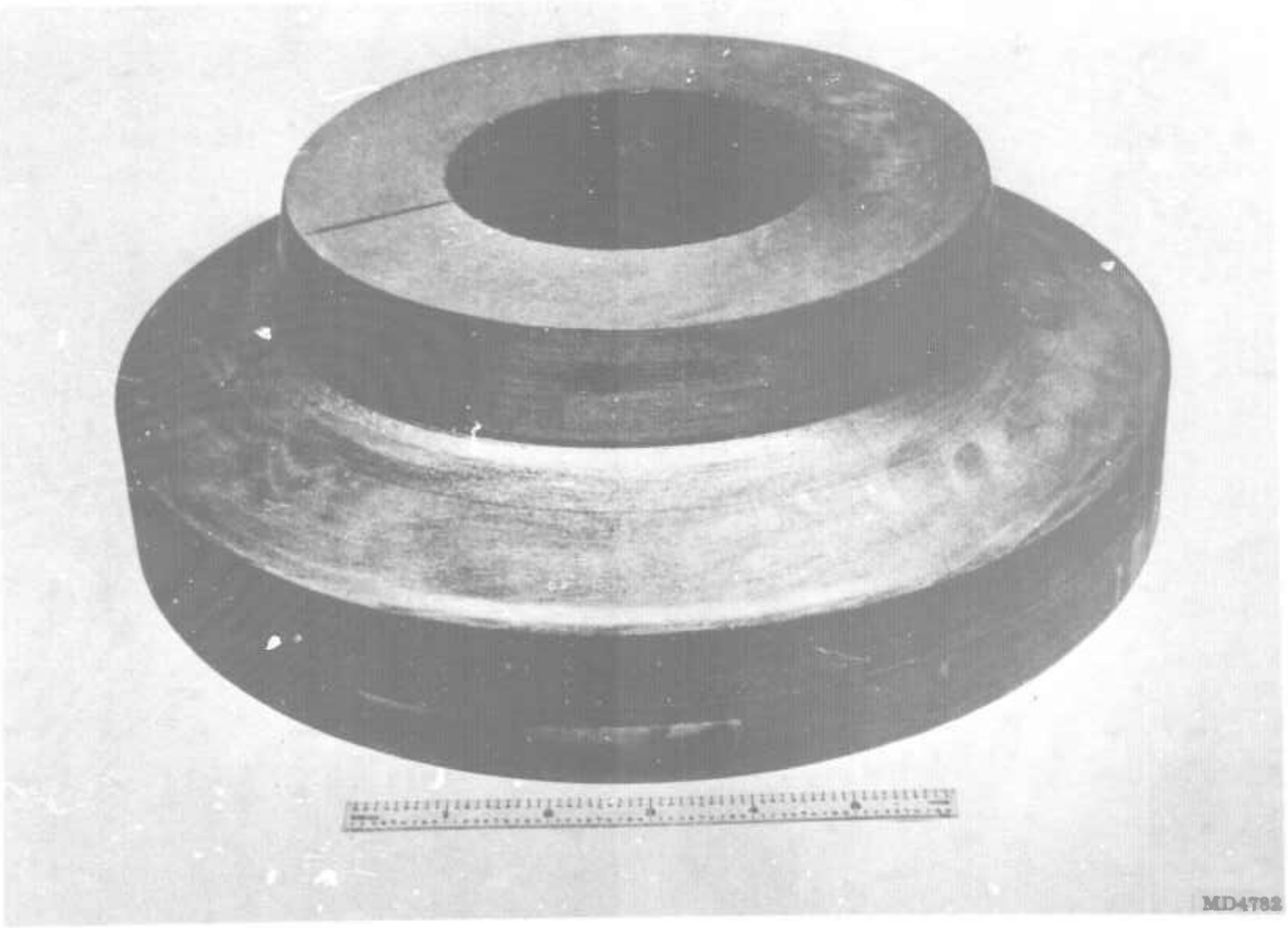

Figure 33. Nozzle No. 3 Inlet

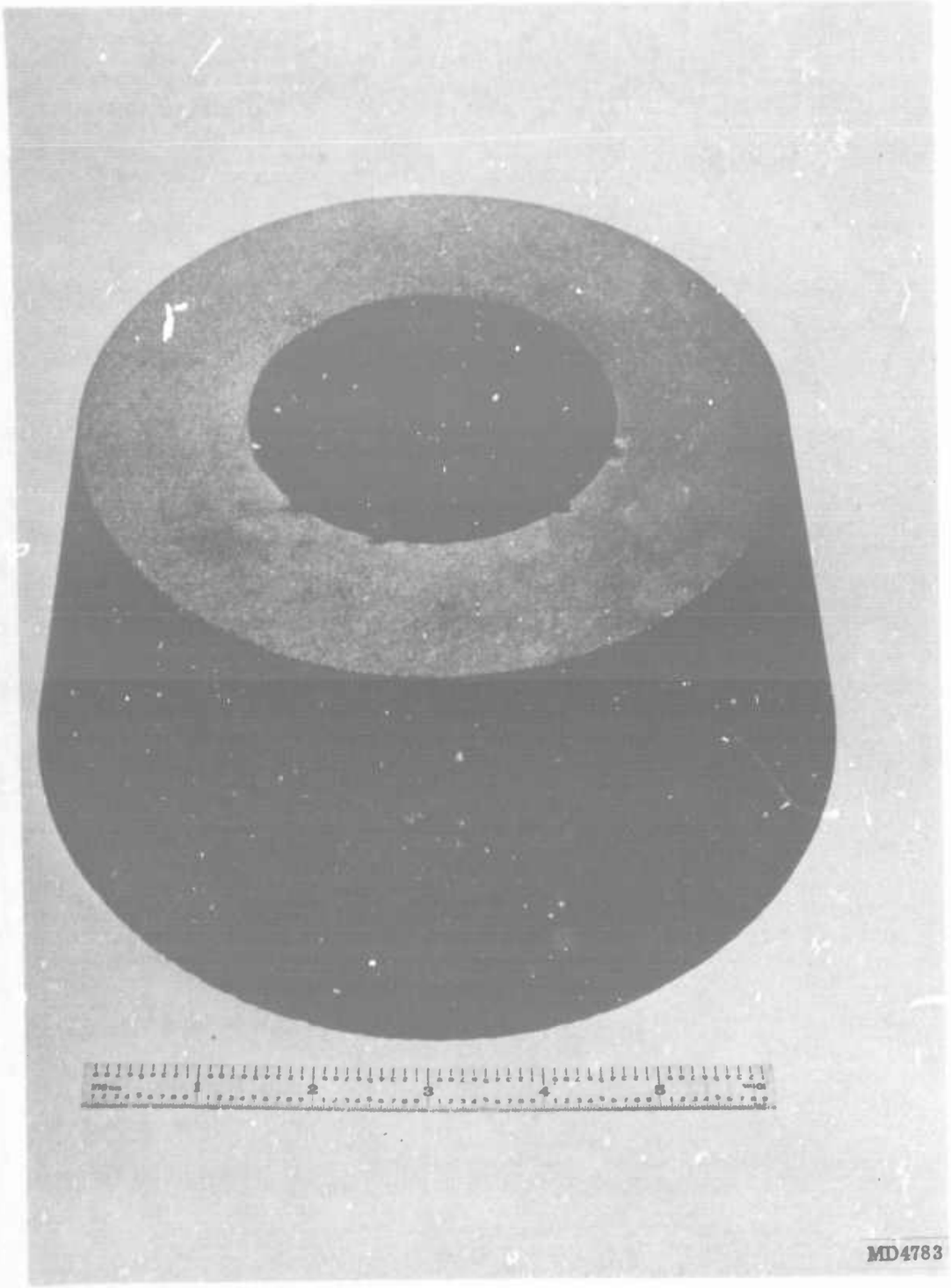

Figure 34. Nozzle No. 3 Throat

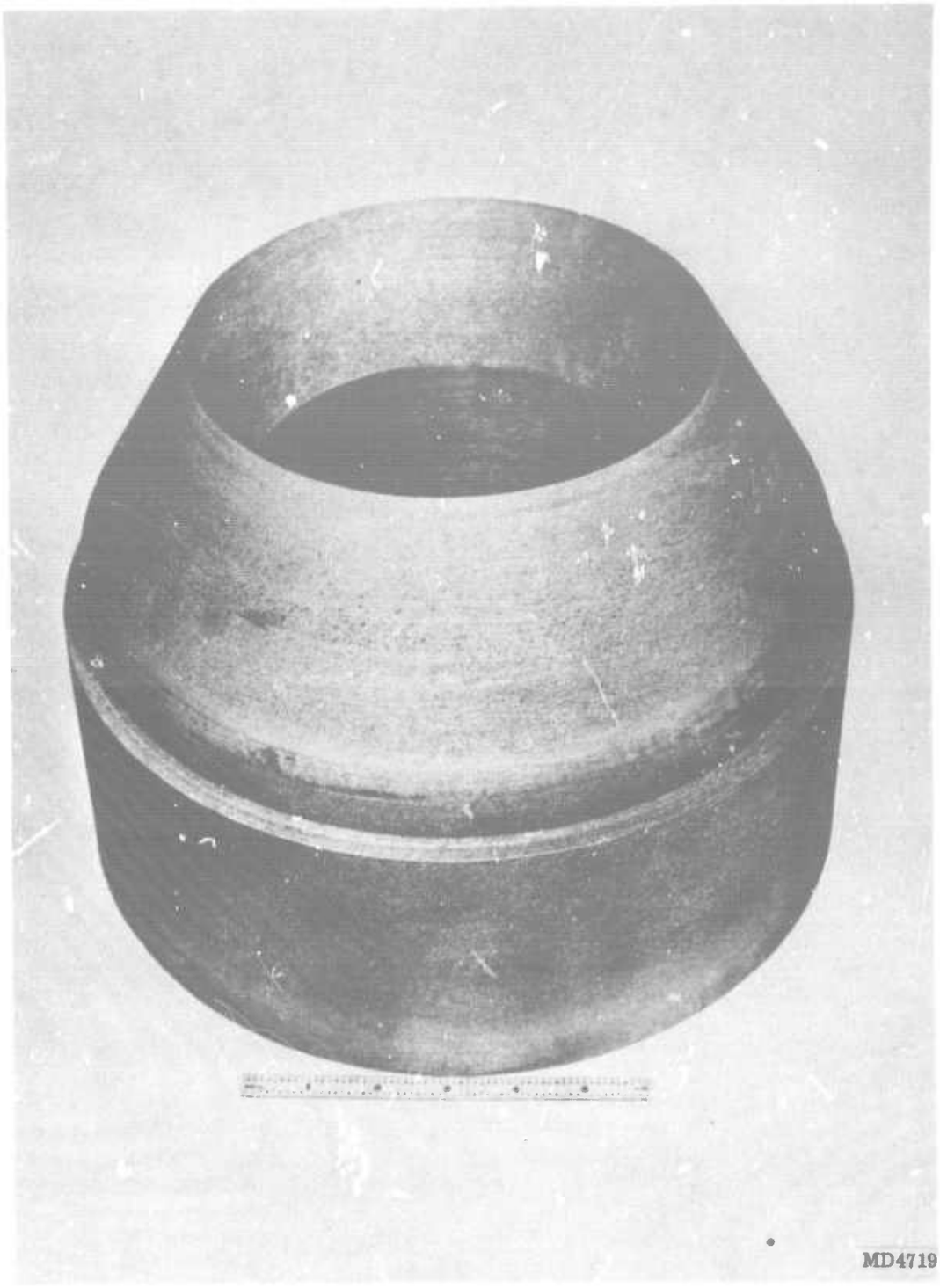

Figure 35. Nozzle No. 3 Throat Backup

Figure 36. Nozzle No. 3 Exit Cone

measured after drilling to accurately locate the point of temperature measurement for use in the postfire thermal analysis.

3. POST-TEST VISUAL EVALUATION

The nozzles were visually examined at the test site and again upon return to Thiokol. Photographs of the postfired nozzle assemblies were taken and the components were removed from the steel shell and photographed. Each nozzle component was sectioned into one 180 deg and two 90 deg segments; photographs were then taken and erosion and char measurements made.

Figures 37 thru 40 show Nozzle No. 1 prior to removal of the insulation from the steel. All of the components were in excellent condition with the exit cone having some gouging where wrinkles were present in the as-built exit cone. Figure 41 is a view of the throat entrance backup assembly and Figure 42 is a view of a longitudinal section. Figure 43 is a view of the longitudinal section of the exit cone.

Nozzle No. 2, prior to removal of the insulation from the steel shell is shown in Figures 44 thru 47. All materials performed satisfactorily with the inlet (T-4113) showing some local gouging and spalling of the char and some gouging at the inlet throat interface. Also the exit cones, both forward (T-2610) and aft (T-4120), had some fine thermal cracks. Figures 48 thru 50 are pictures of the throat-inlet backup after removal from the steel. Figure 48 shows particularly well how the inlet char layer separated from the virgin material. Figures 51 thru 55 are various views of the exit cone. The exit cones were extremely well bonded to the steel and considerable force was required to remove them, even after a heat soak at 350°F in an attempt to break the bond. Quite possibly, the open cracks seen in Figures 51 and 54 were caused or aggravated by the forceful rejection.

Subscale Nozzle No. 3 was very similar in appearance to Nozzle No. 2. The inlet char layer was gouged and spalled and the exit cone had fine thermal cracks. The performance of the T-2610 throat in this nozzle compared favorably to the performance of the graphite cloth phenolic on the first two nozzles. The throat was in excellent condition with only small local cracks in the charred layer. Figures 56 thru 63 are views of Nozzle No. 3

The motor ballistics of the three subscale nozzles are listed in Table XXIII.

4. EROSION EVALUATION

The erosion was determined by sectioning the static tested nozzle component at several locations and measuring the thickness of the residual material. The erosion is the difference between the original thickness (nominal and the measured residual material). The erosion profiles for Nozzles No. 1, 2 and 3 are shown in Figures 64, 65 and 66. The calculated erosion rate at various stations is summarized in Table XXIV using the web time for each motor. The nozzle erosion rate versus area ratio presented graphically in Figure 67 shows the LCCM to be equal or superior to the plastics in the throat and exit cone but not in the inlet. For Nozzles No. 2 and 3,

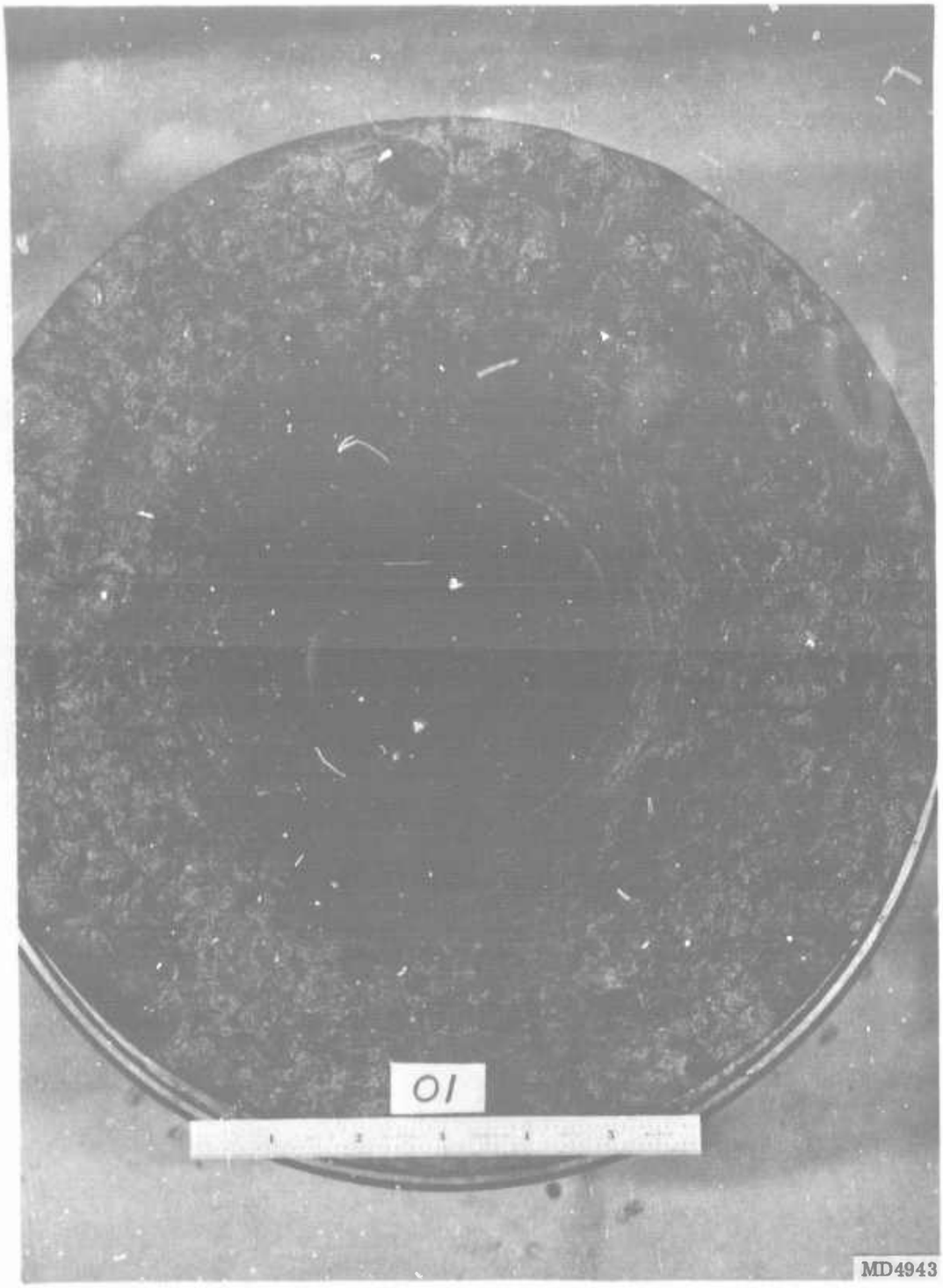

Figure 37. Nozzle No. 1 Postfired Condition, Forward View

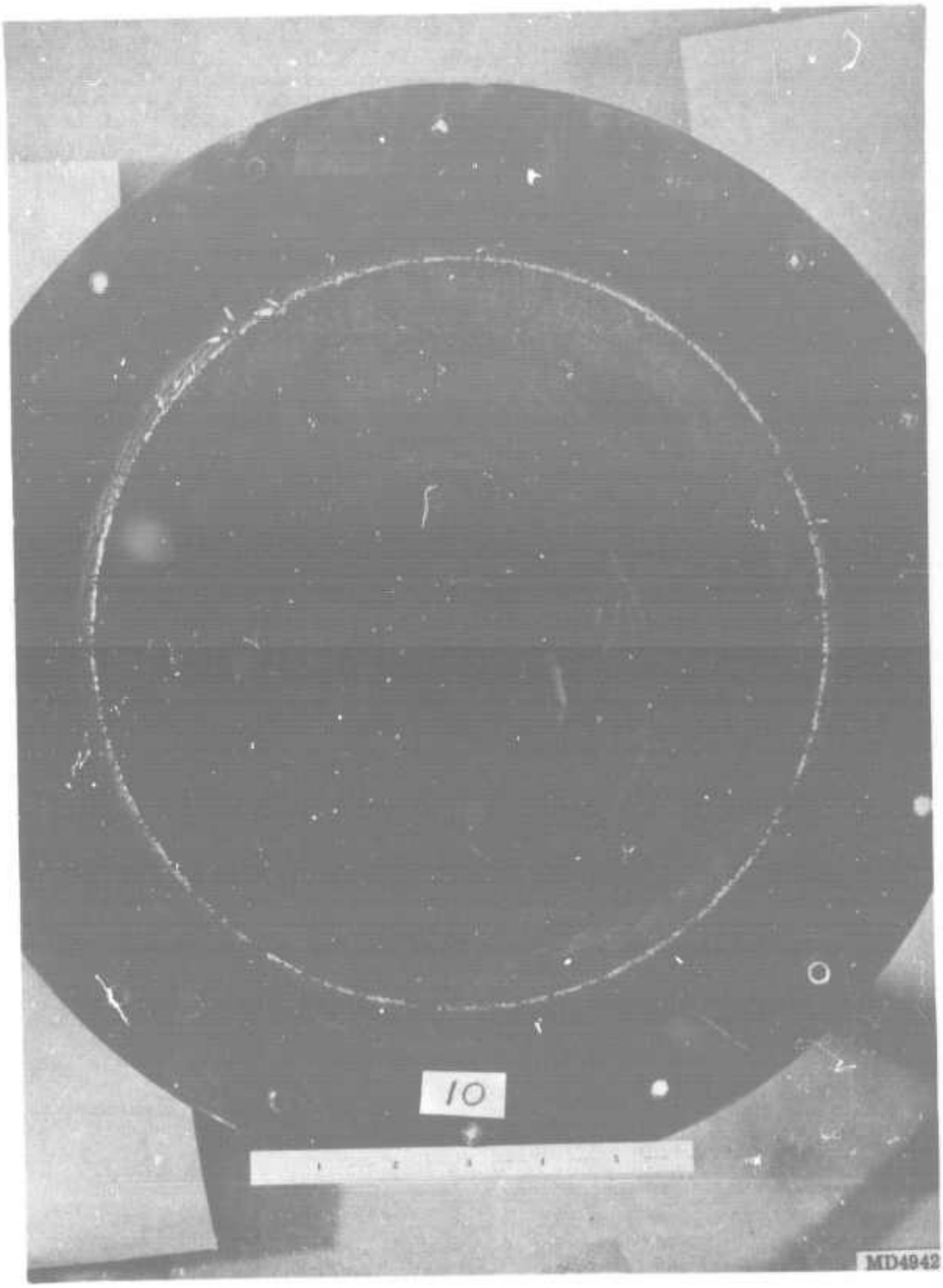

Figure 38. Nozzle No. 1 Postfired Condition, Aft View

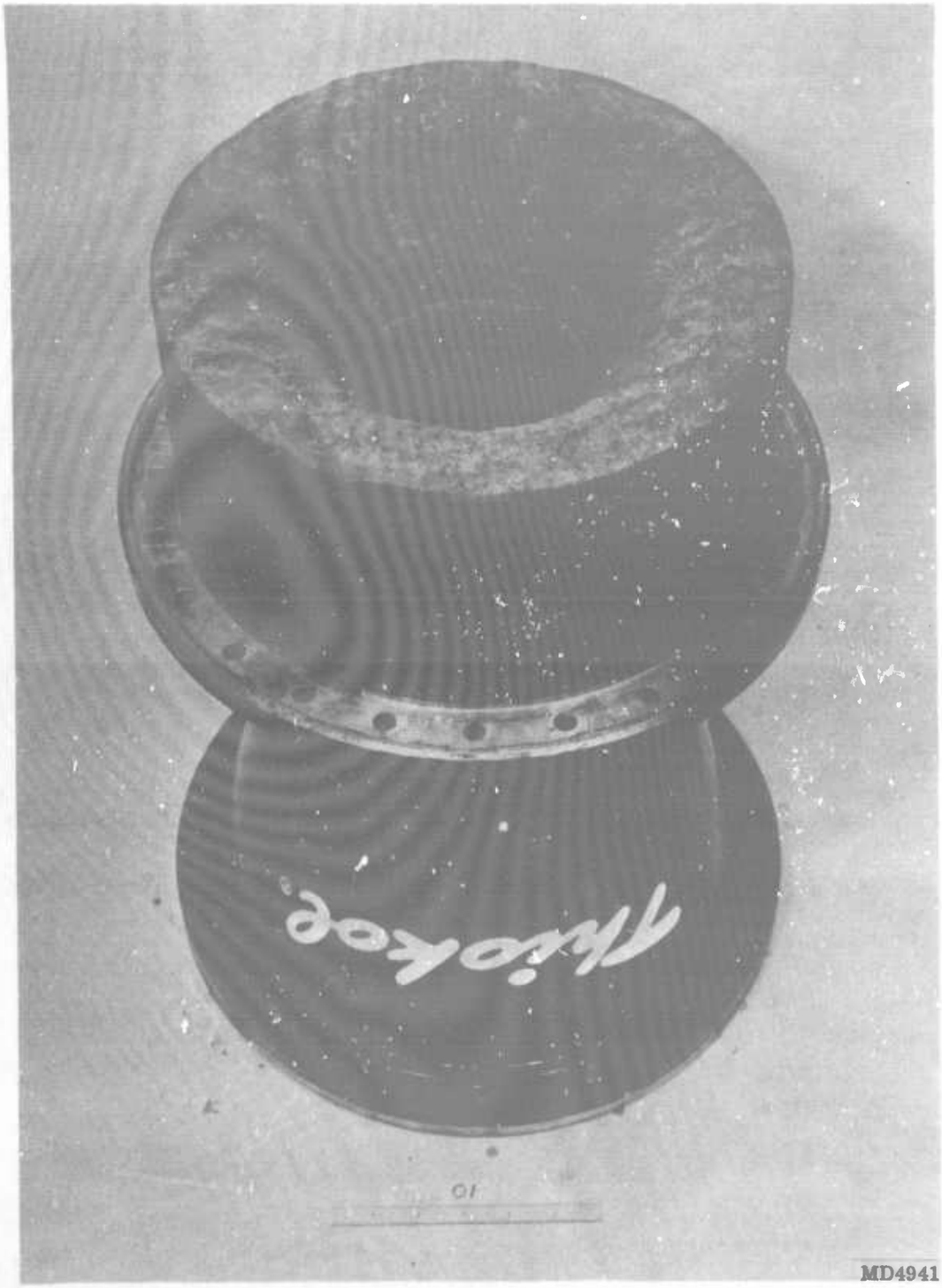

Figure 39. Nozzle No. 1 Postfired Condition

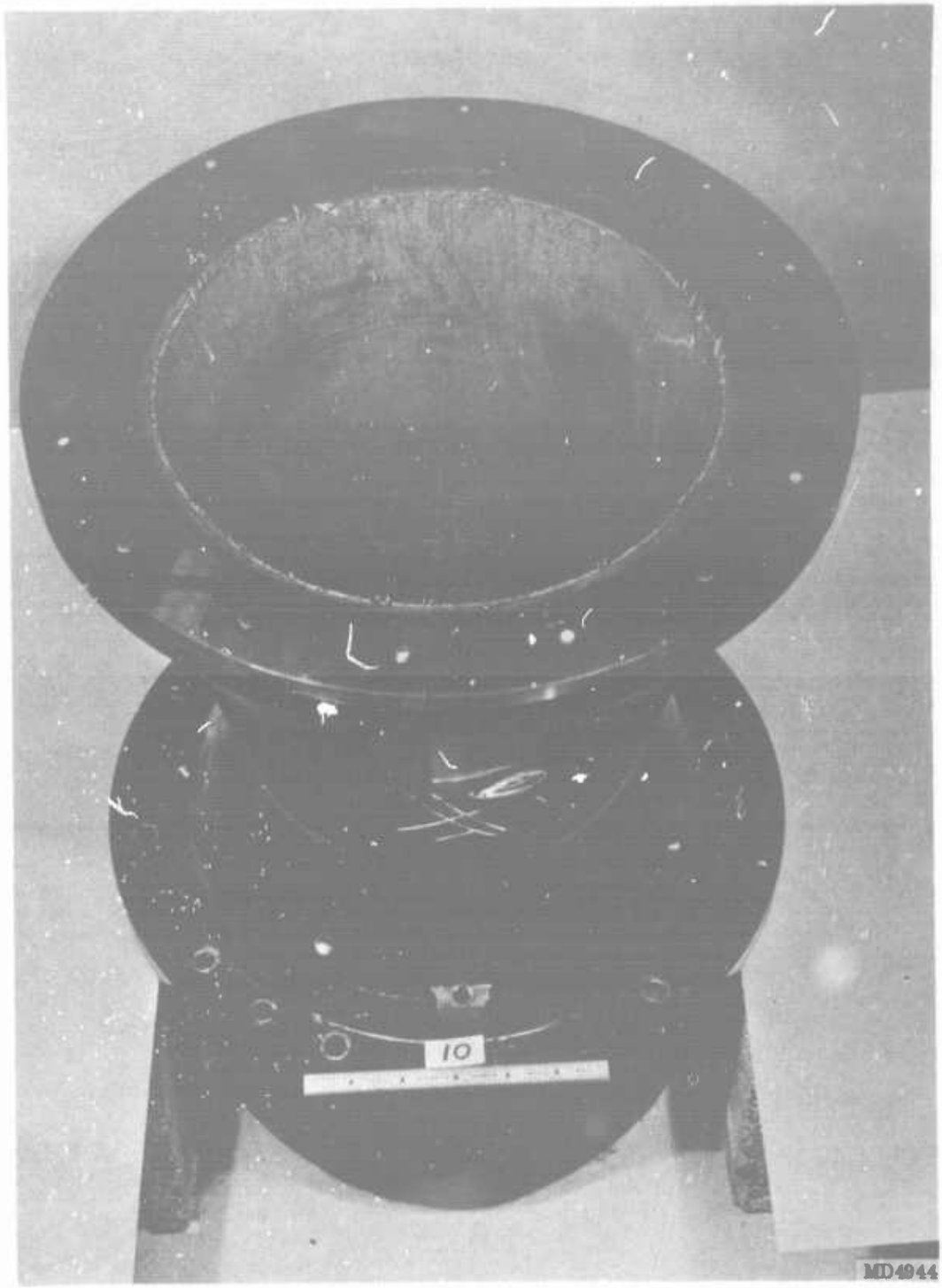

Figure 40. Nozzle No. 1 Postfired Condition, Aft End

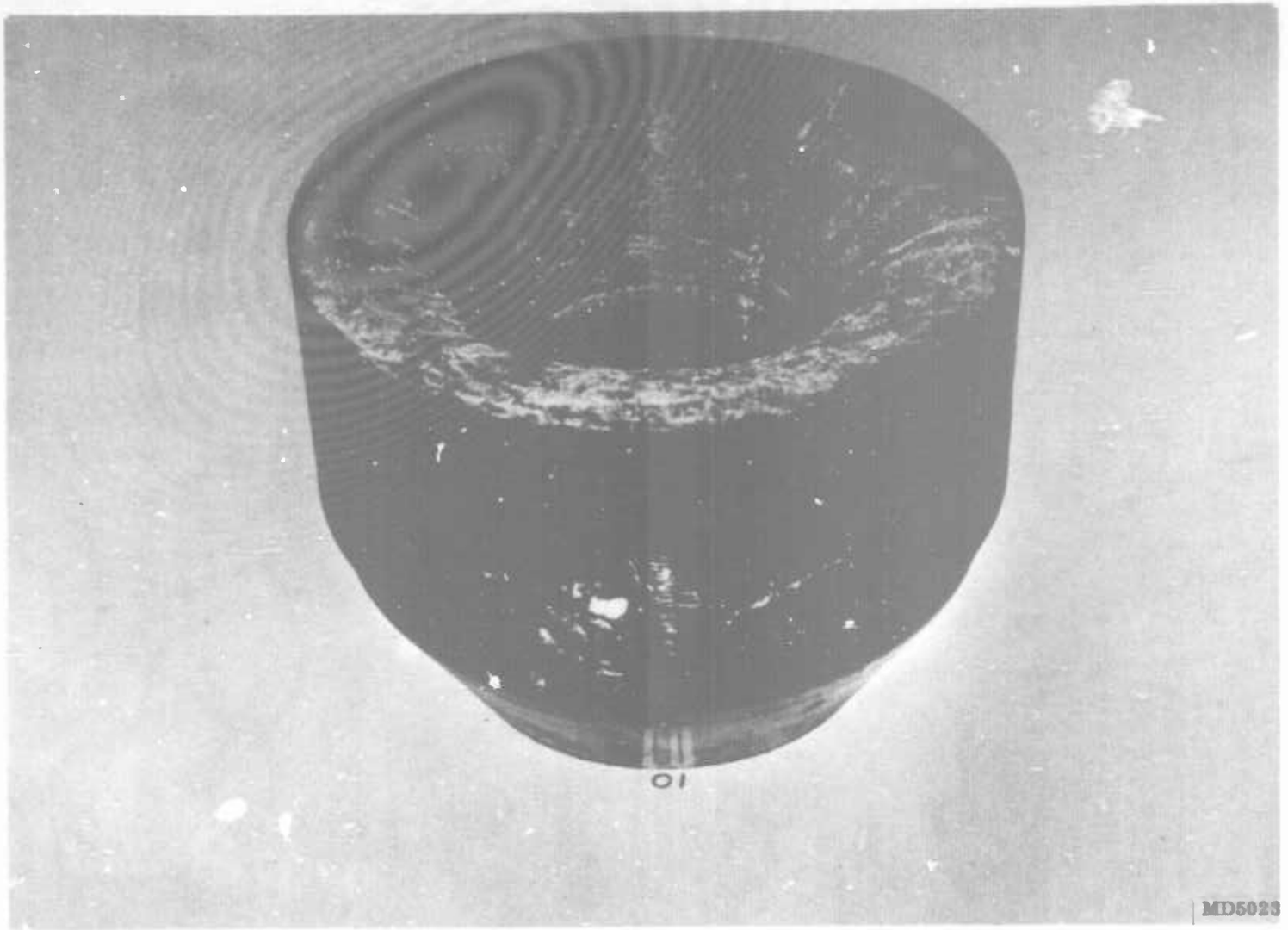

Figure 41. Nozzle No. 1 Postfired Condition, Inlet-Throat-Backup

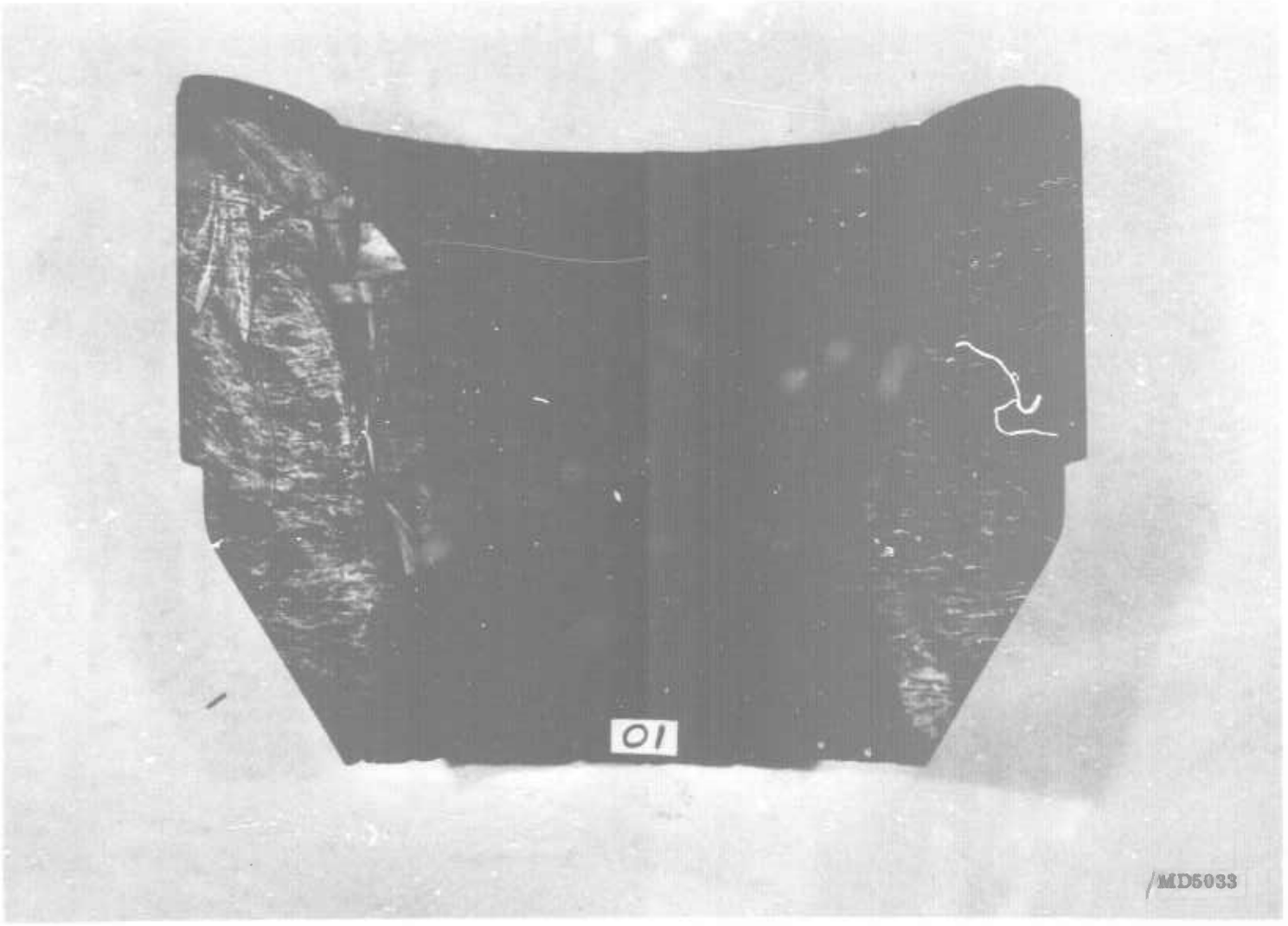

Figure 42. Nozzle No. 1 Postfired Condition, Inlet-Throat-Backup Section

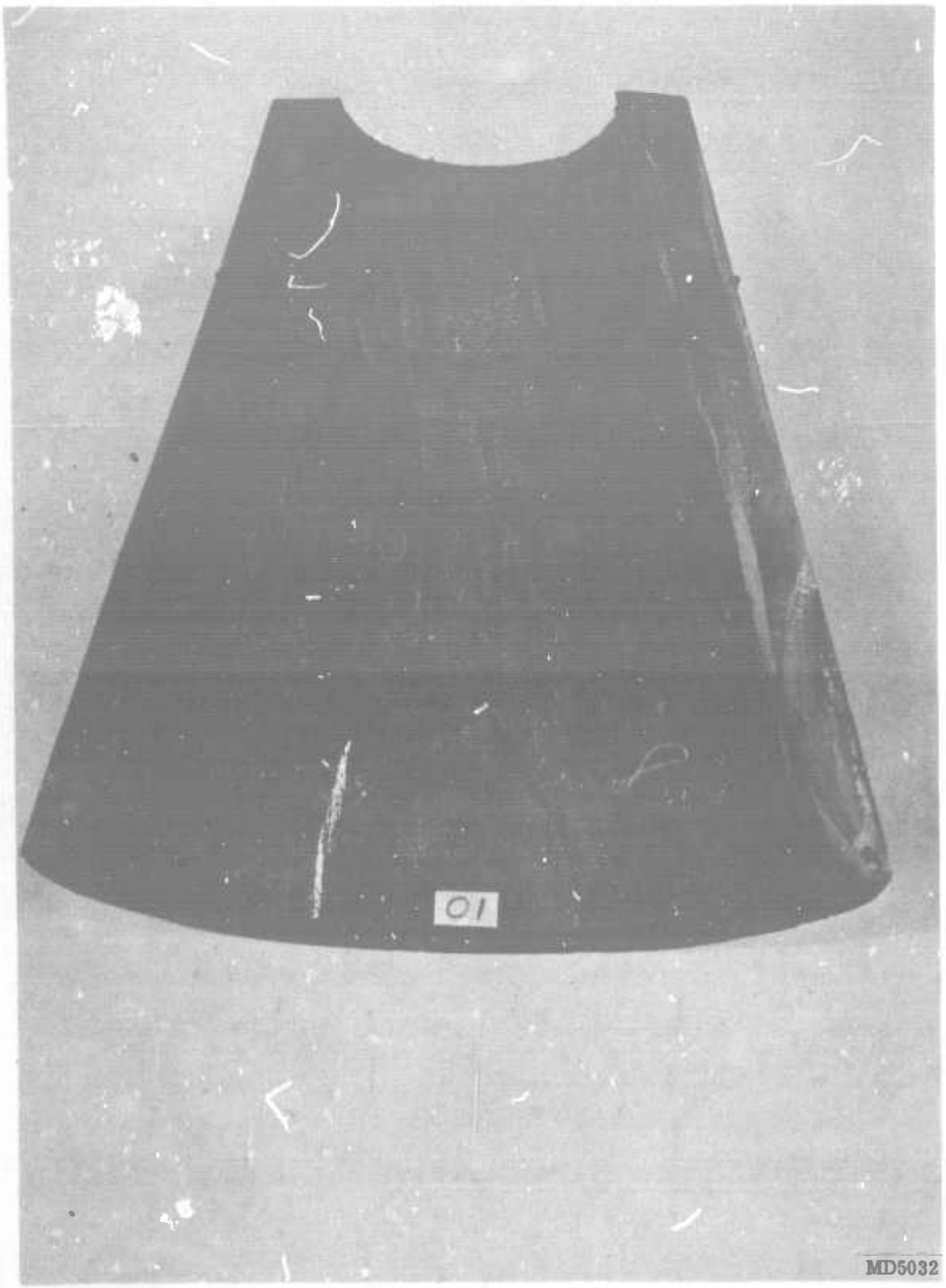

Figure 43. Nozzle No. 1 Postfired Condition, Exit Cone Section

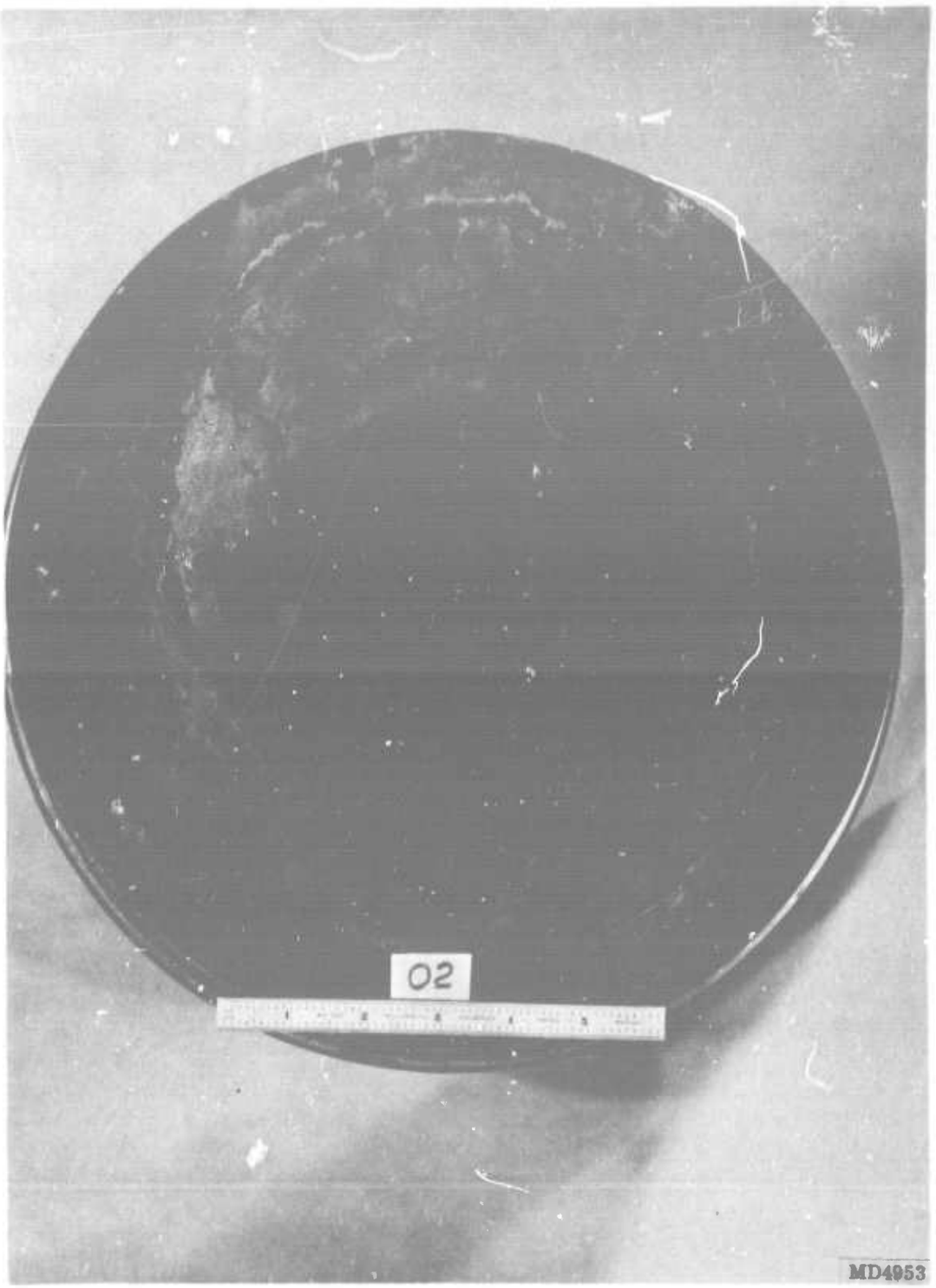

Figure 44. Nozzle No. 2 Postfired Condition, Forward View

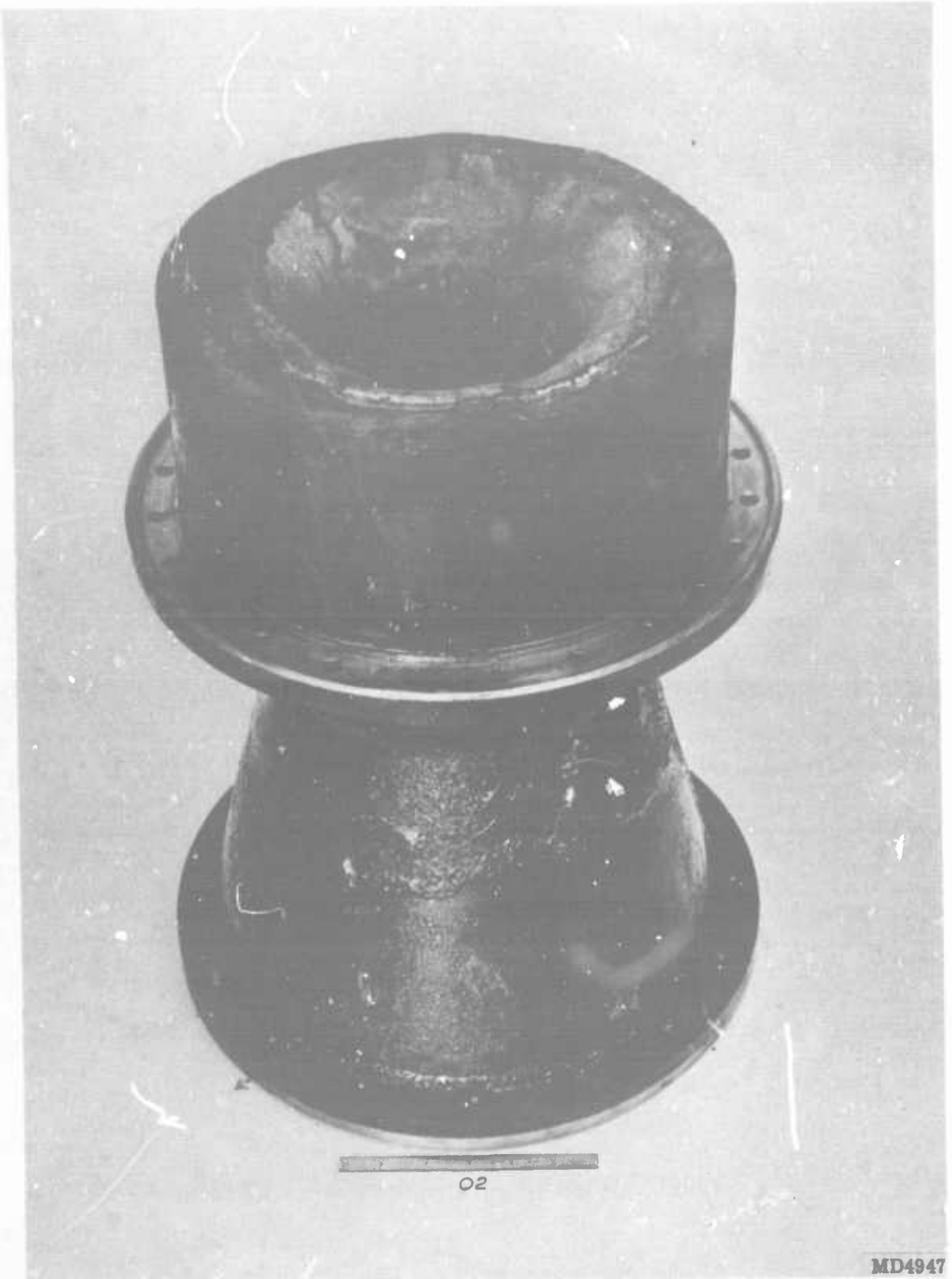

Figure 45. Nozzle No. 2 Postfired Condition, Entrance

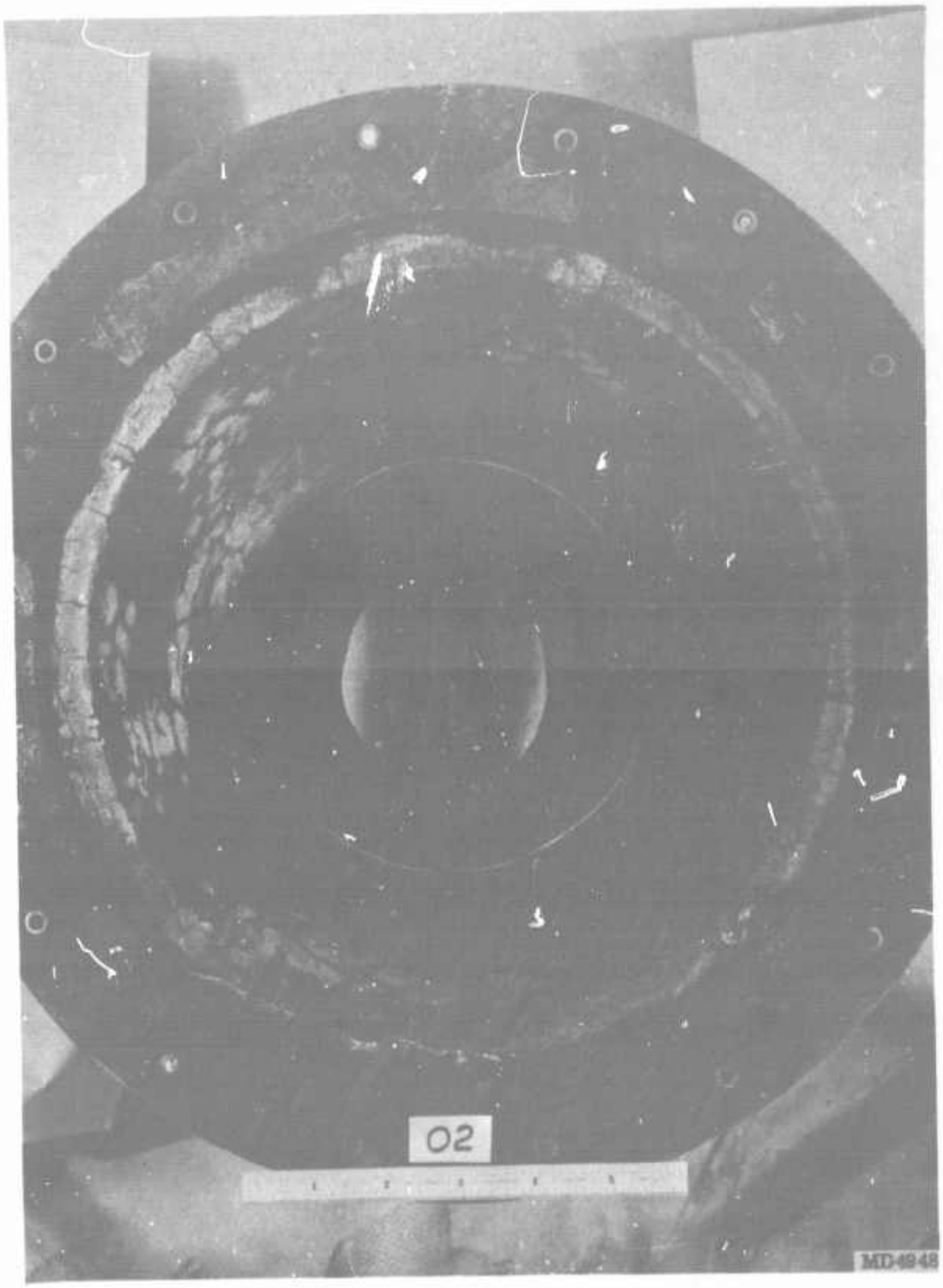

Figure 46. Nozzle No. 2 Postfired Condition, Aft View

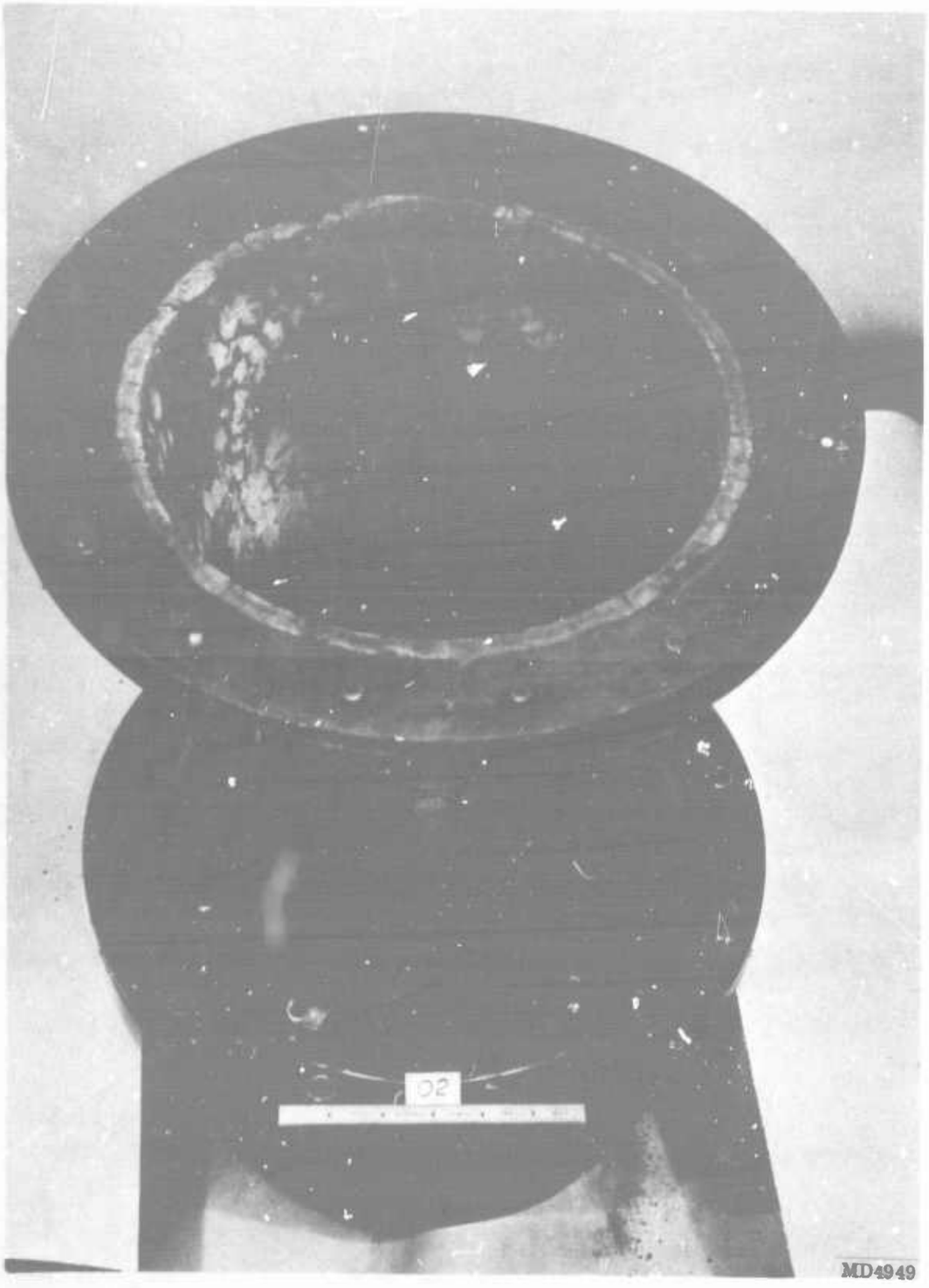

Figure 47. Nozzle No. 2 Postfired Condition, Aft End

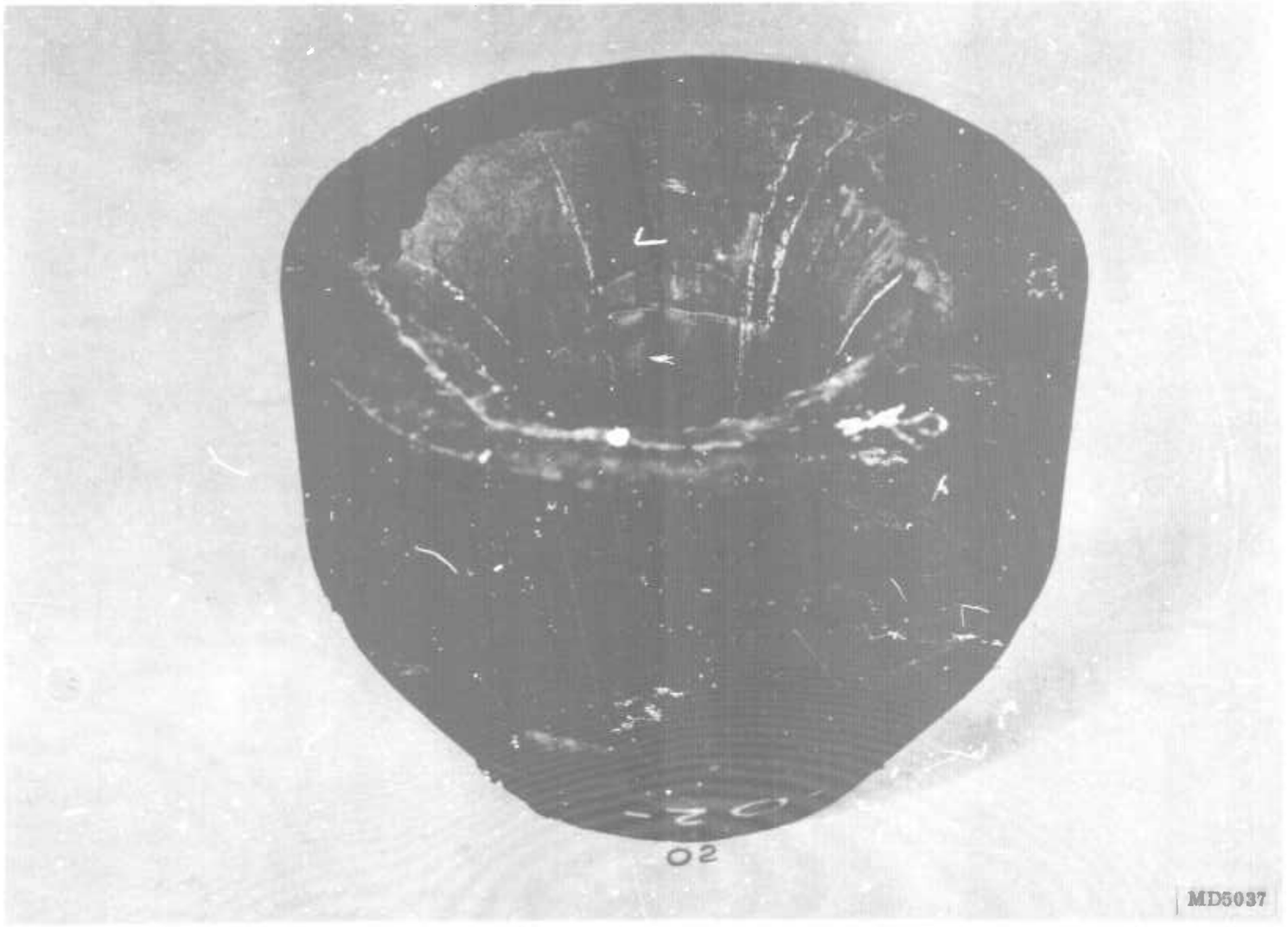

Figure 48. Nozzle No. 2 Postfired Condition, Inlet

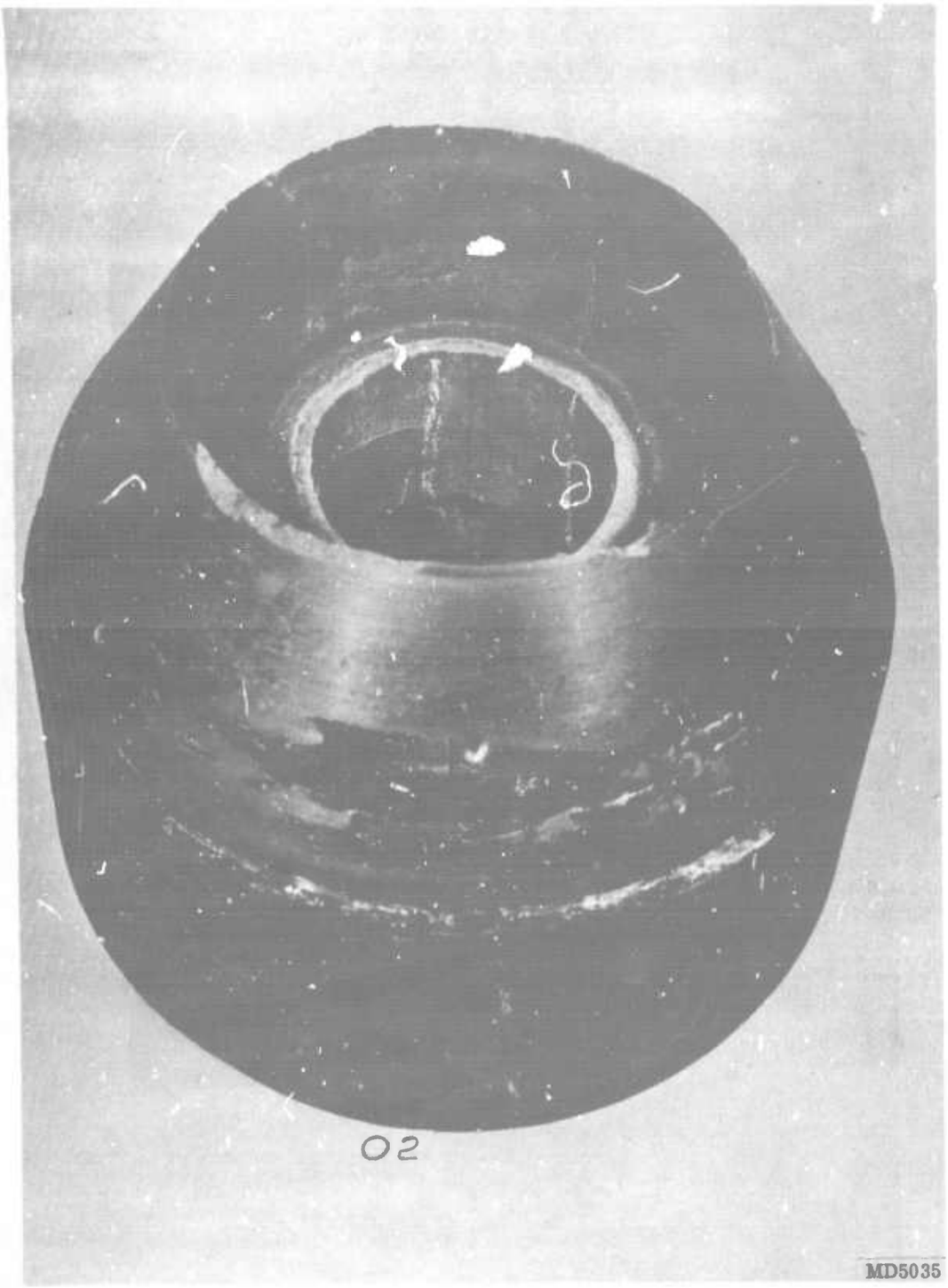

Figure 49. Nozzle No. 2 Postfired Condition, Inlet-Throat-Backup Assembly

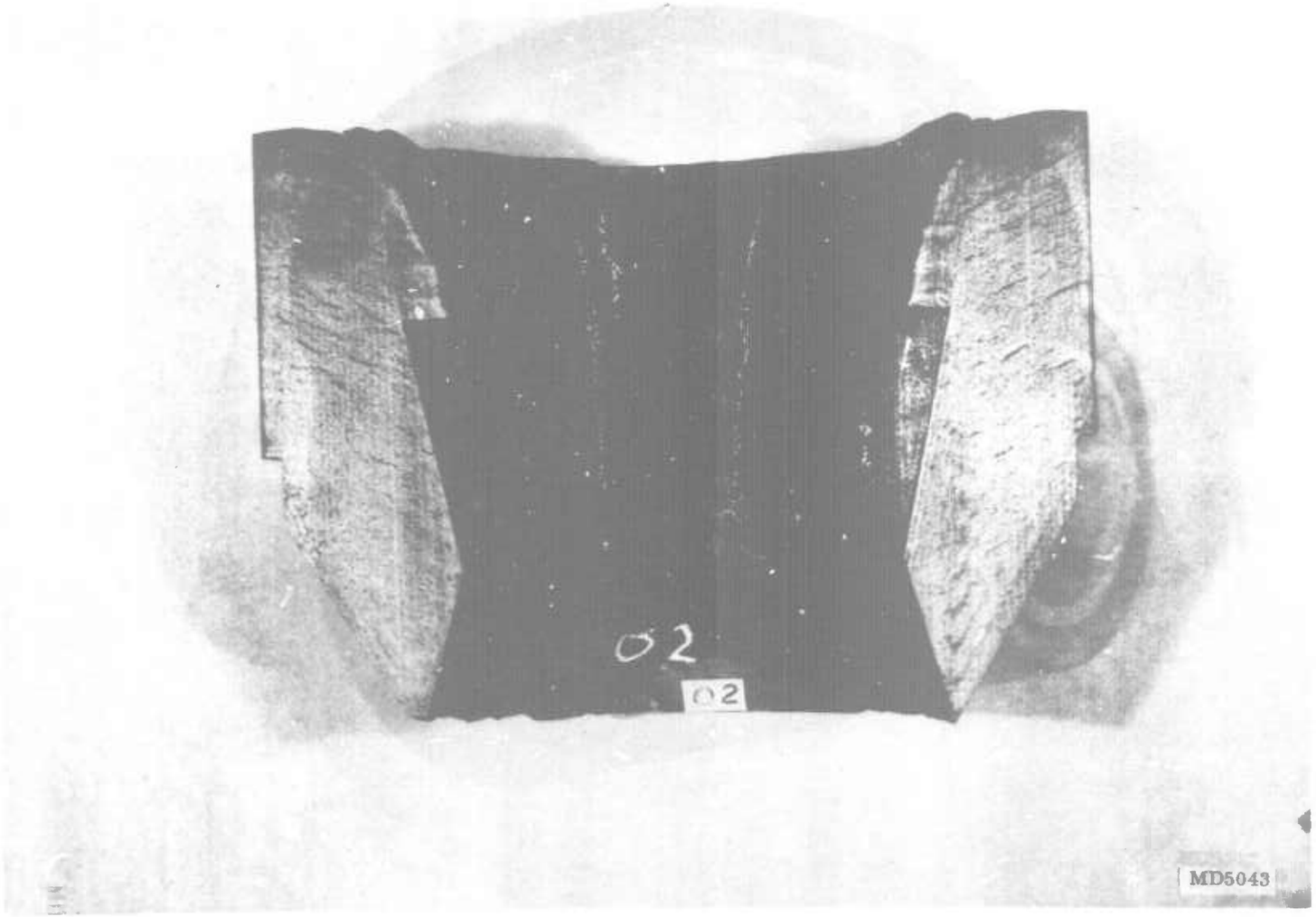

Figure 50. Nozzle No. 2 Postfired Condition, Throat Section

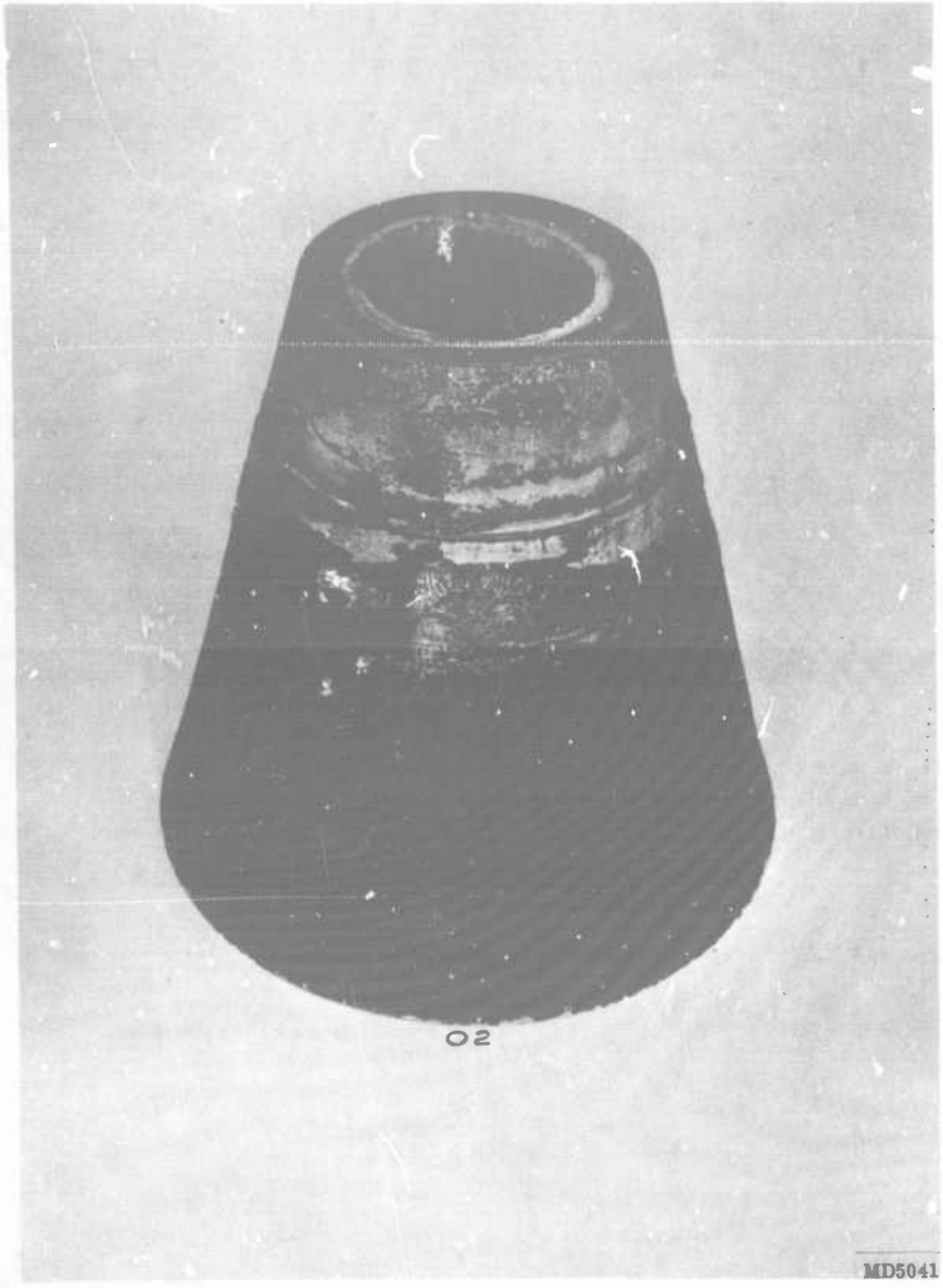

Figure 51. Nozzle No. 2 Postfired Condition, Exit Cone

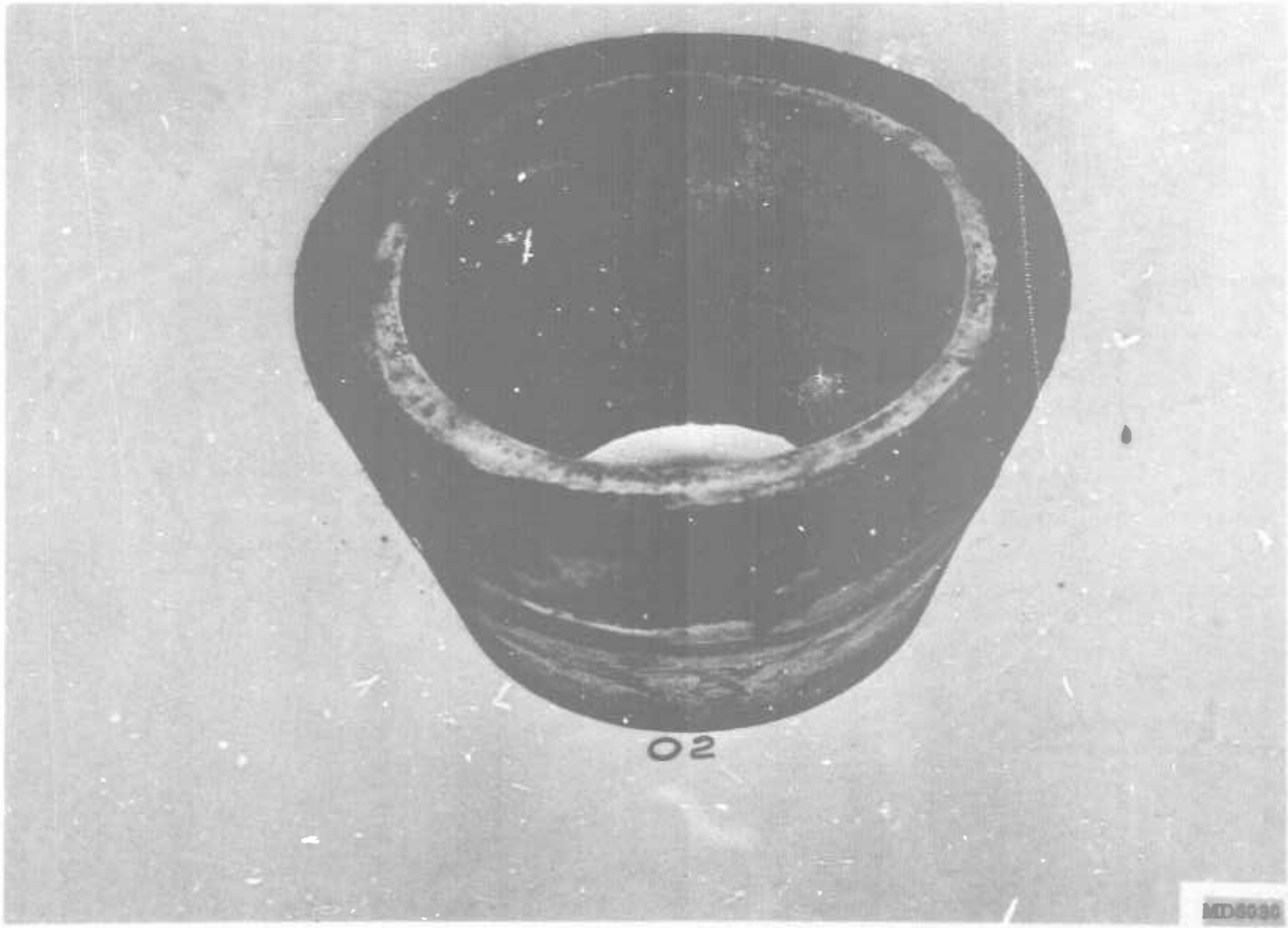

Figure 52. Nozzle No. 2 Postfired Condition, Forward Exit Cone

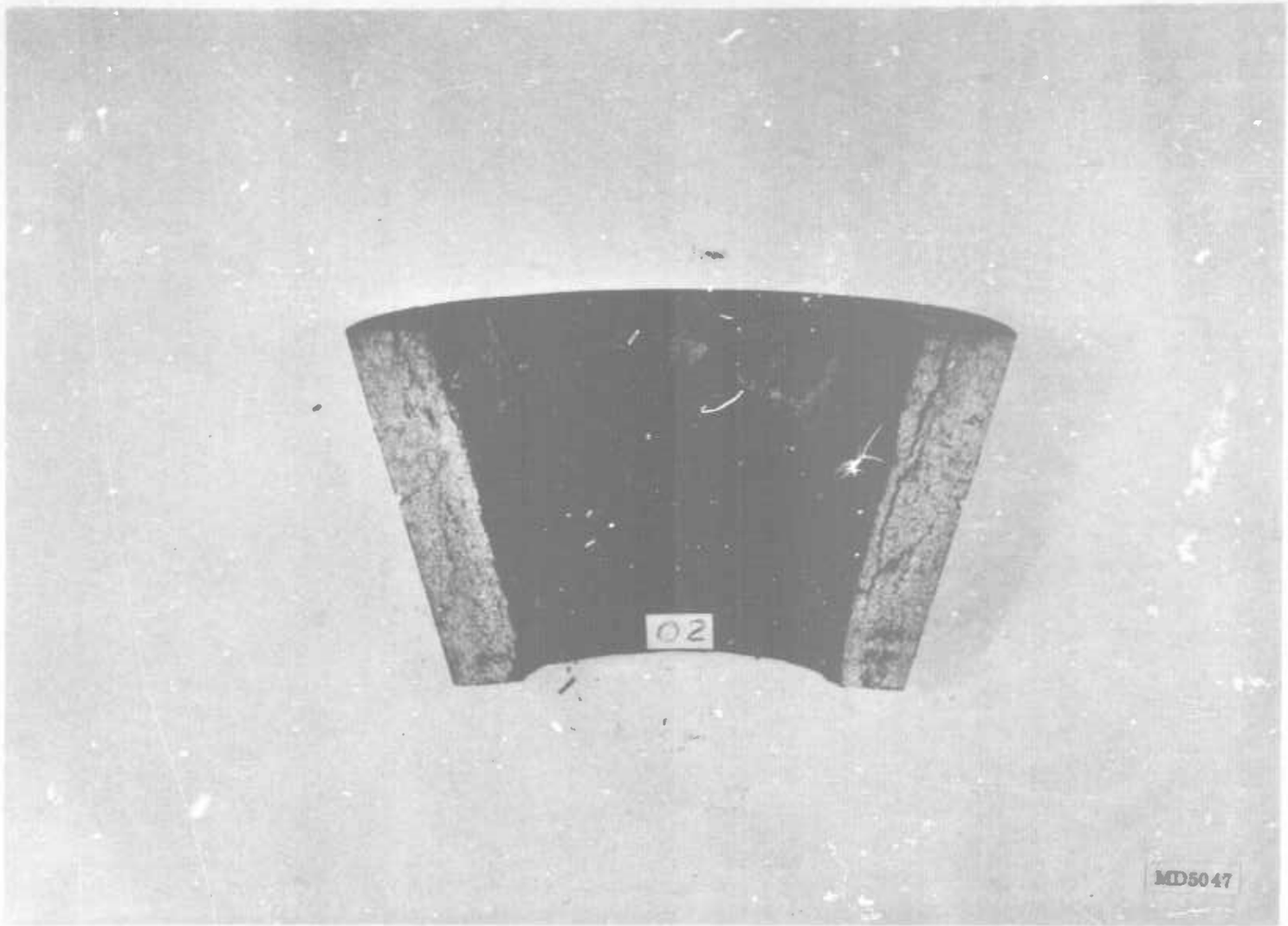

Figure 53. Nozzle No. 2 Postfired Condition, Forward Exit Cone Section

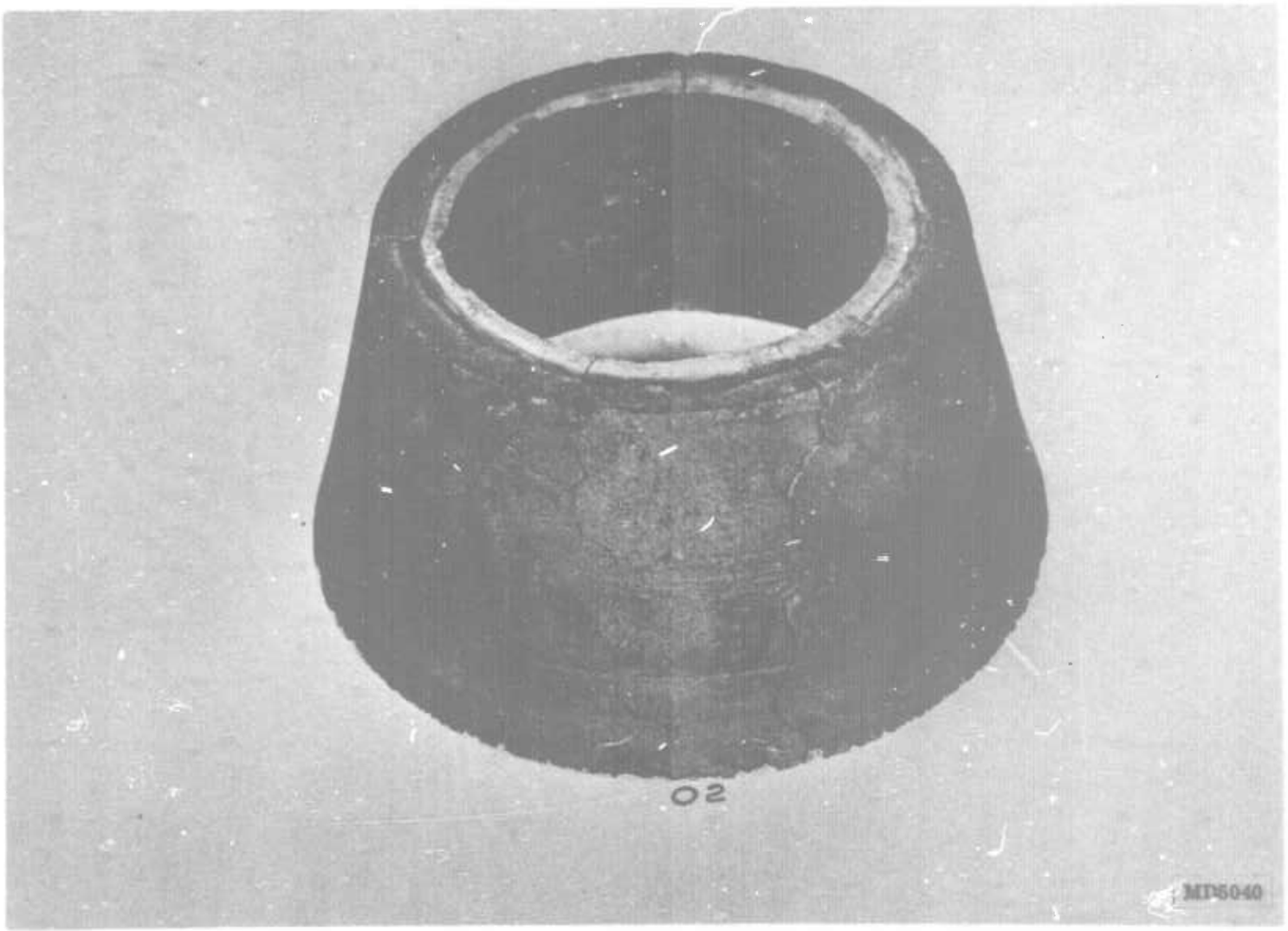

Figure 54. Nozzle No. 2 Postfired Condition, Aft Exit Cone

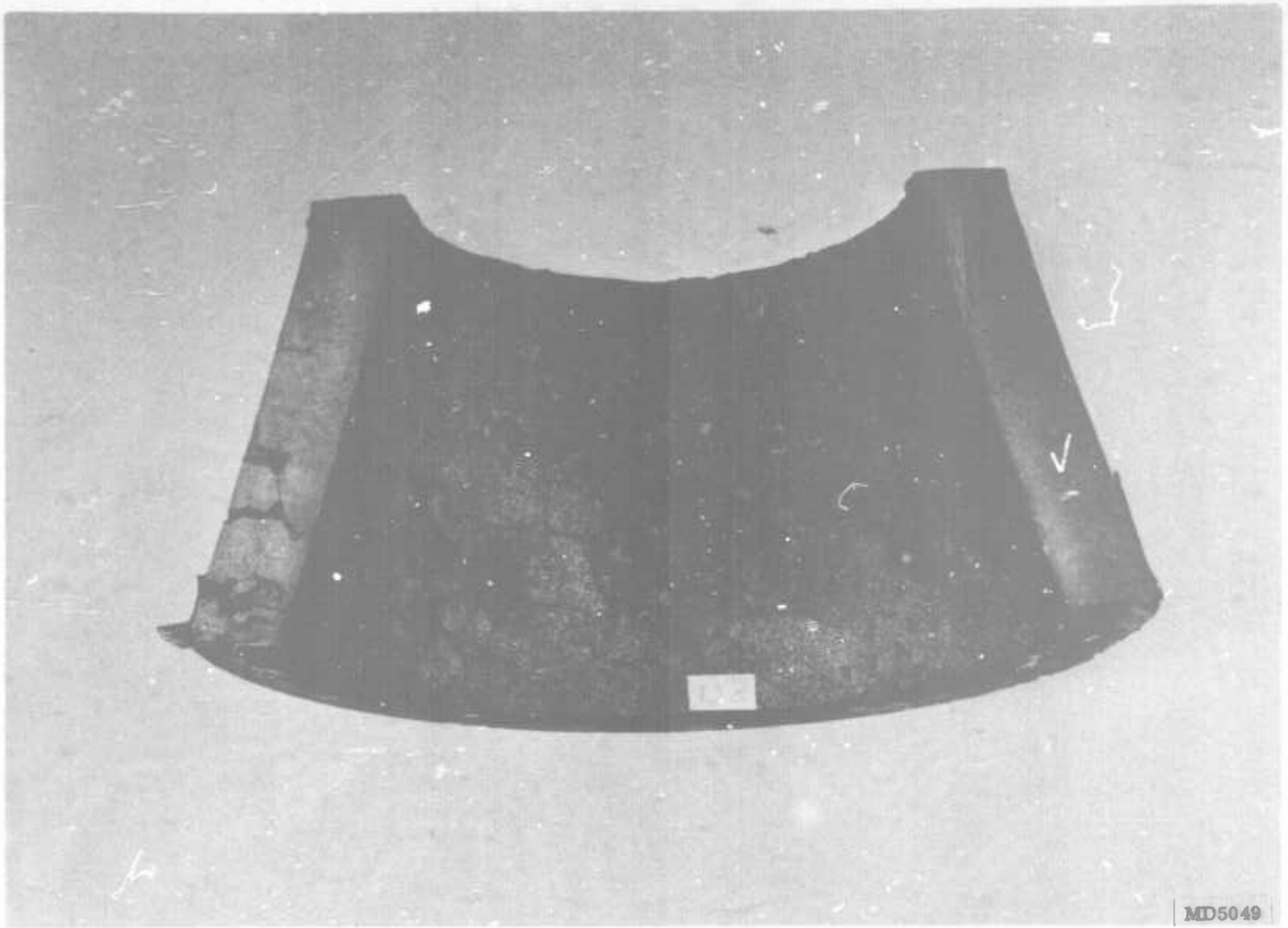

Figure 55. Nozzle No. 2 Postfired Condition, Aft Exit Cone Section

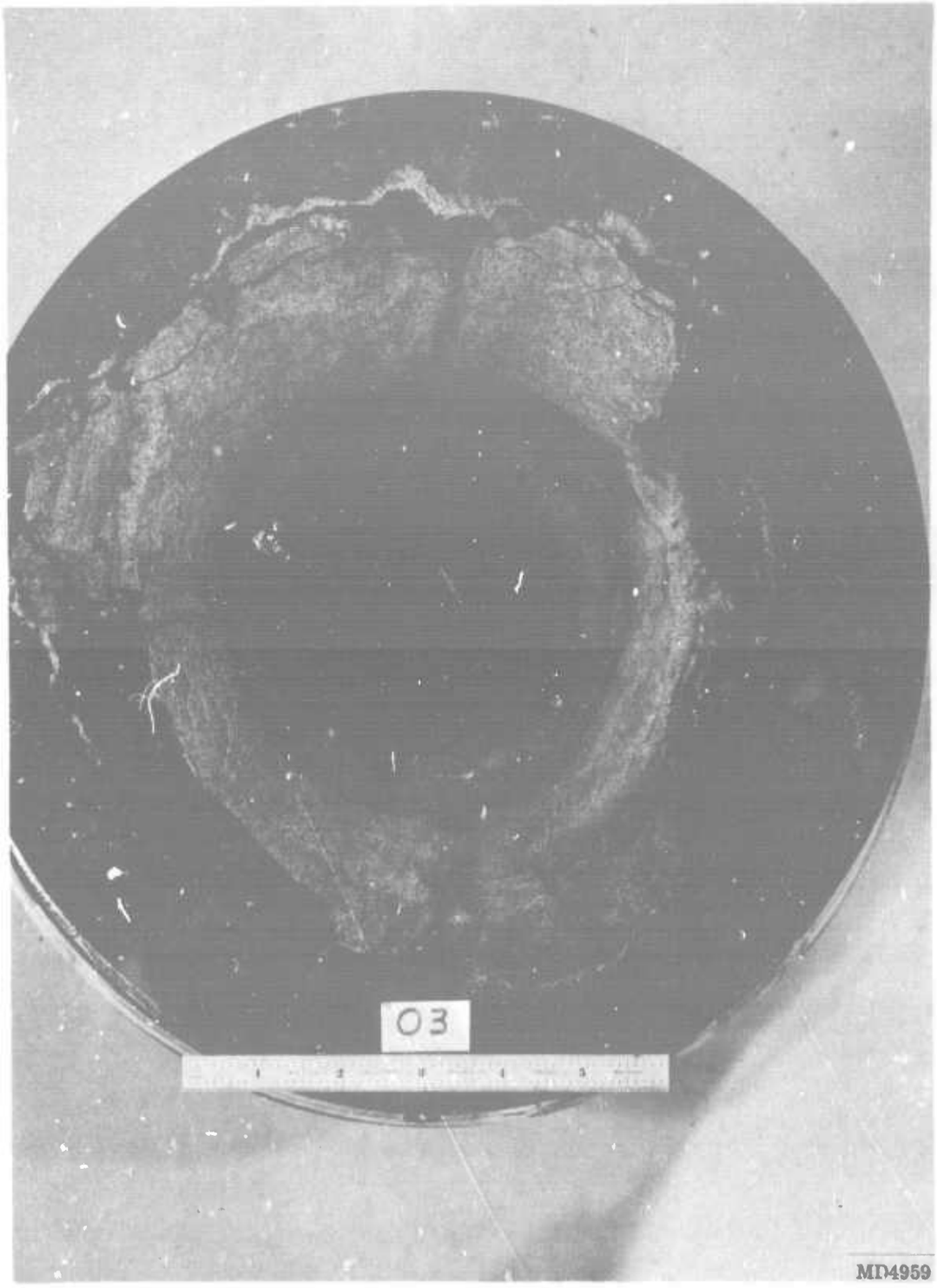

Figure 56. Nozzle No. 3 Postfired Condition, Forward View

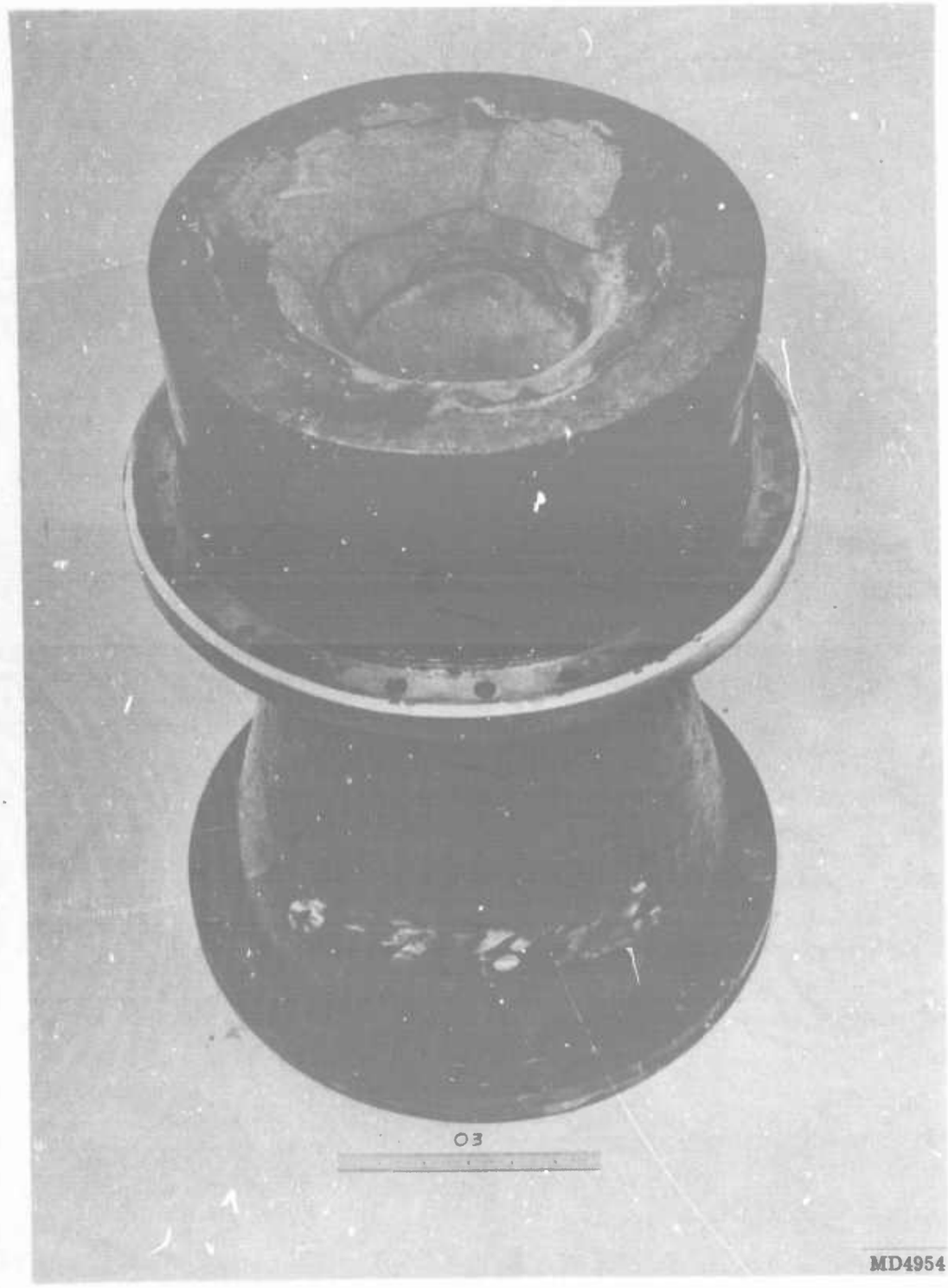

Figure 57. Nozzle No. 3 Postfired Condition, Inlet

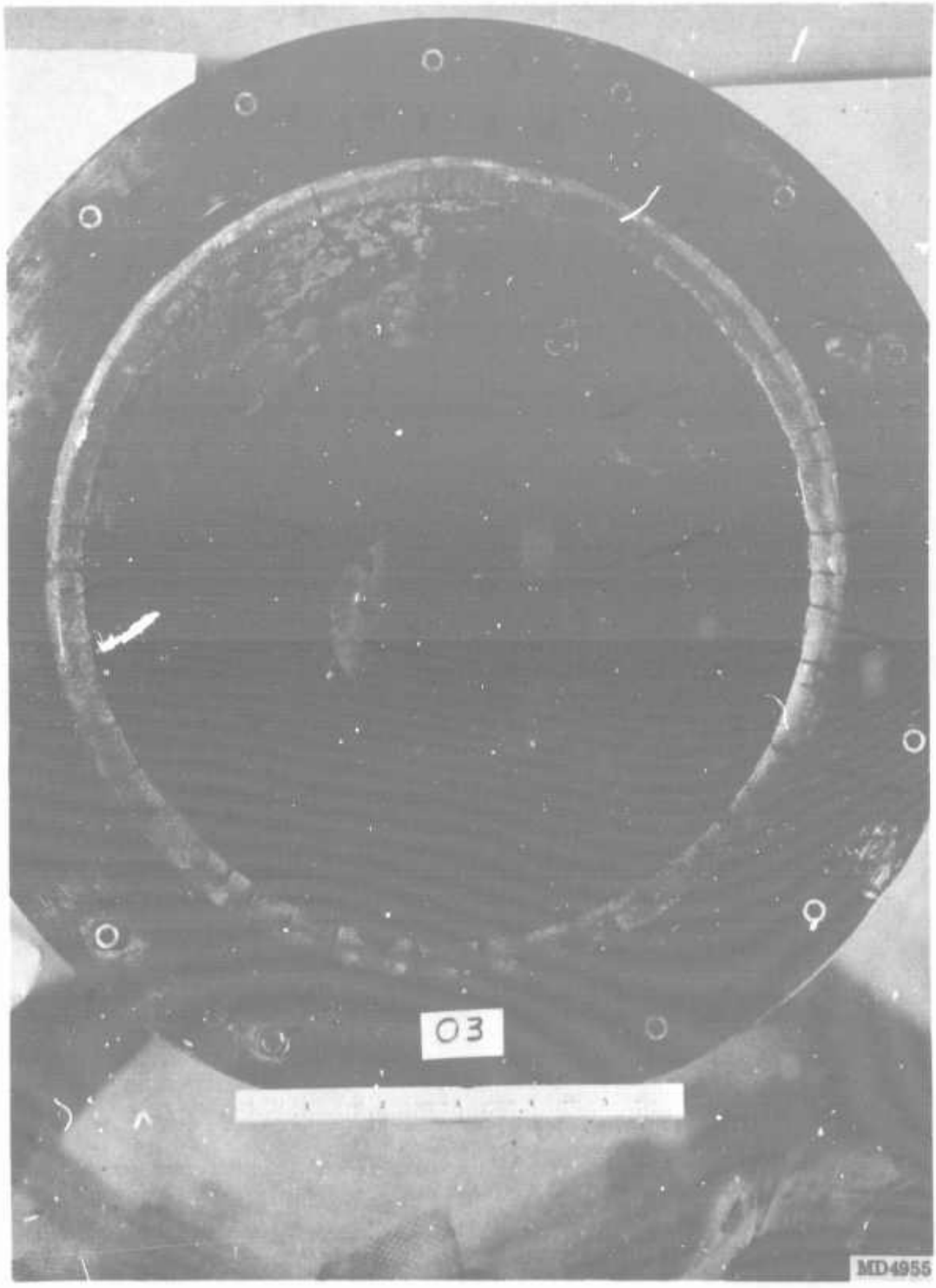

Figure 58. Nozzle No. 3 Postfired Condition, Aft View

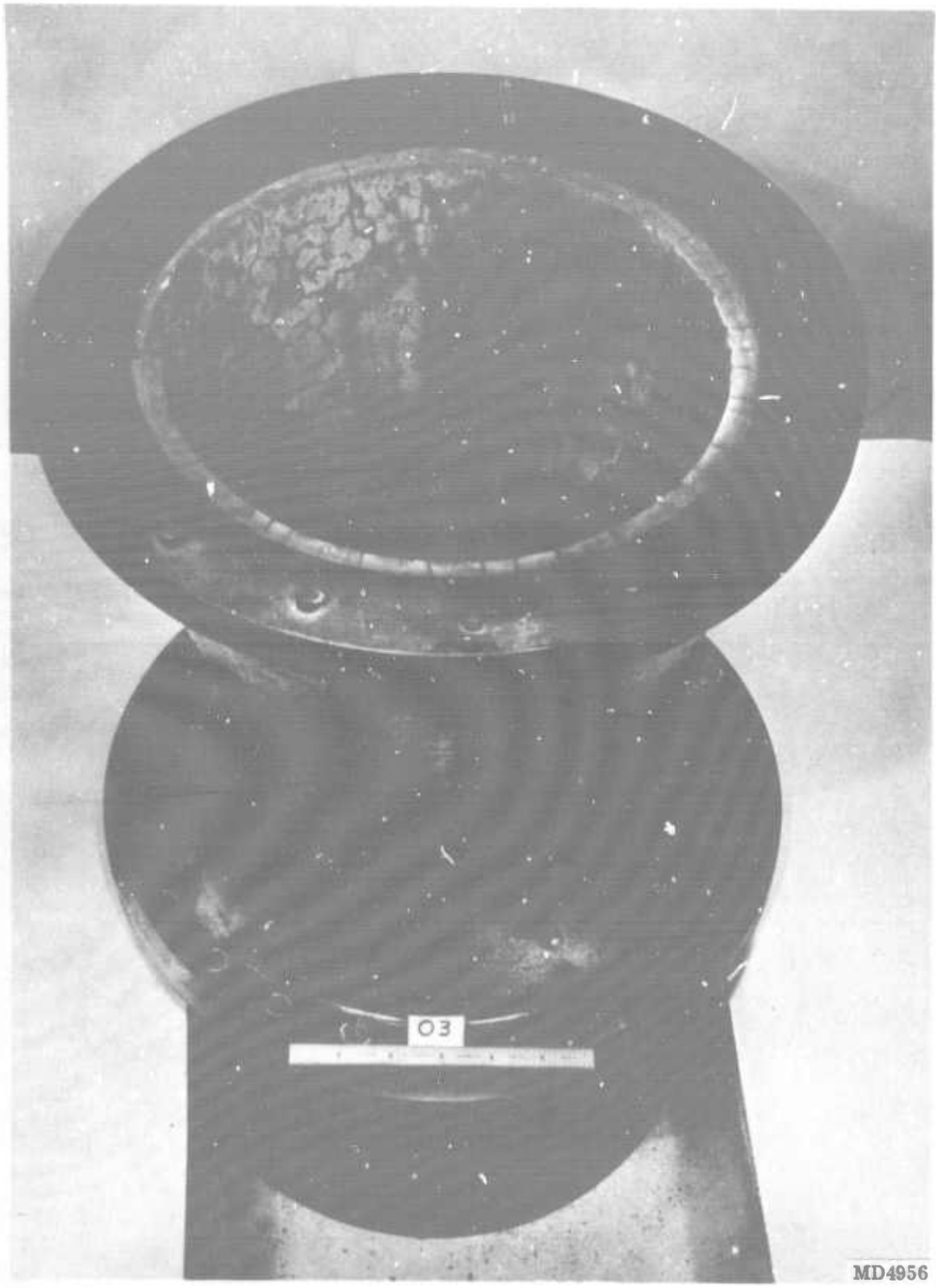

Figure 59. Nozzle No. 3 Postfired Condition, Aft End

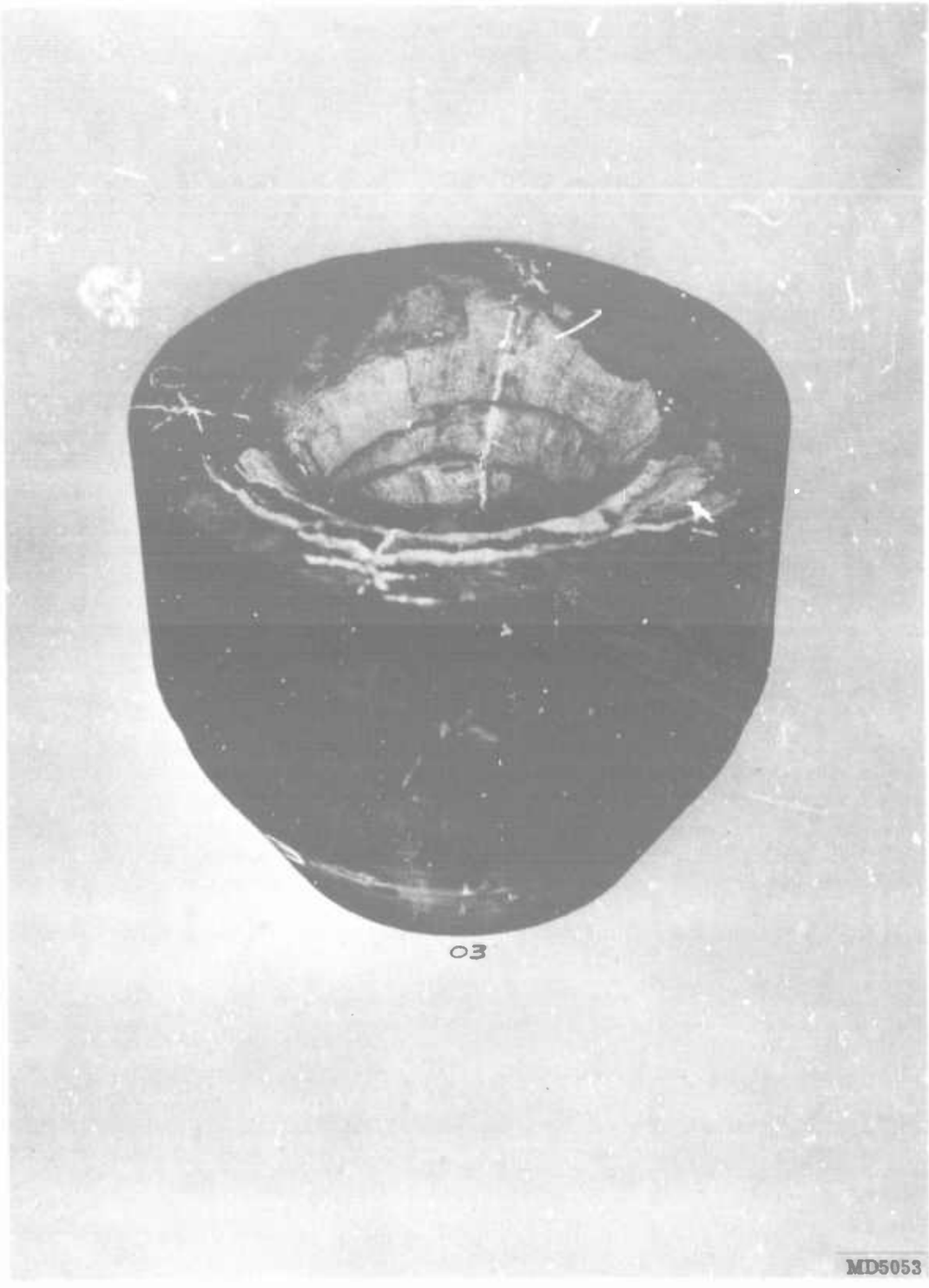

Figure 60. Nozzle No. 3 Postfired Condition, Inlet-Throat-Backup Assembly

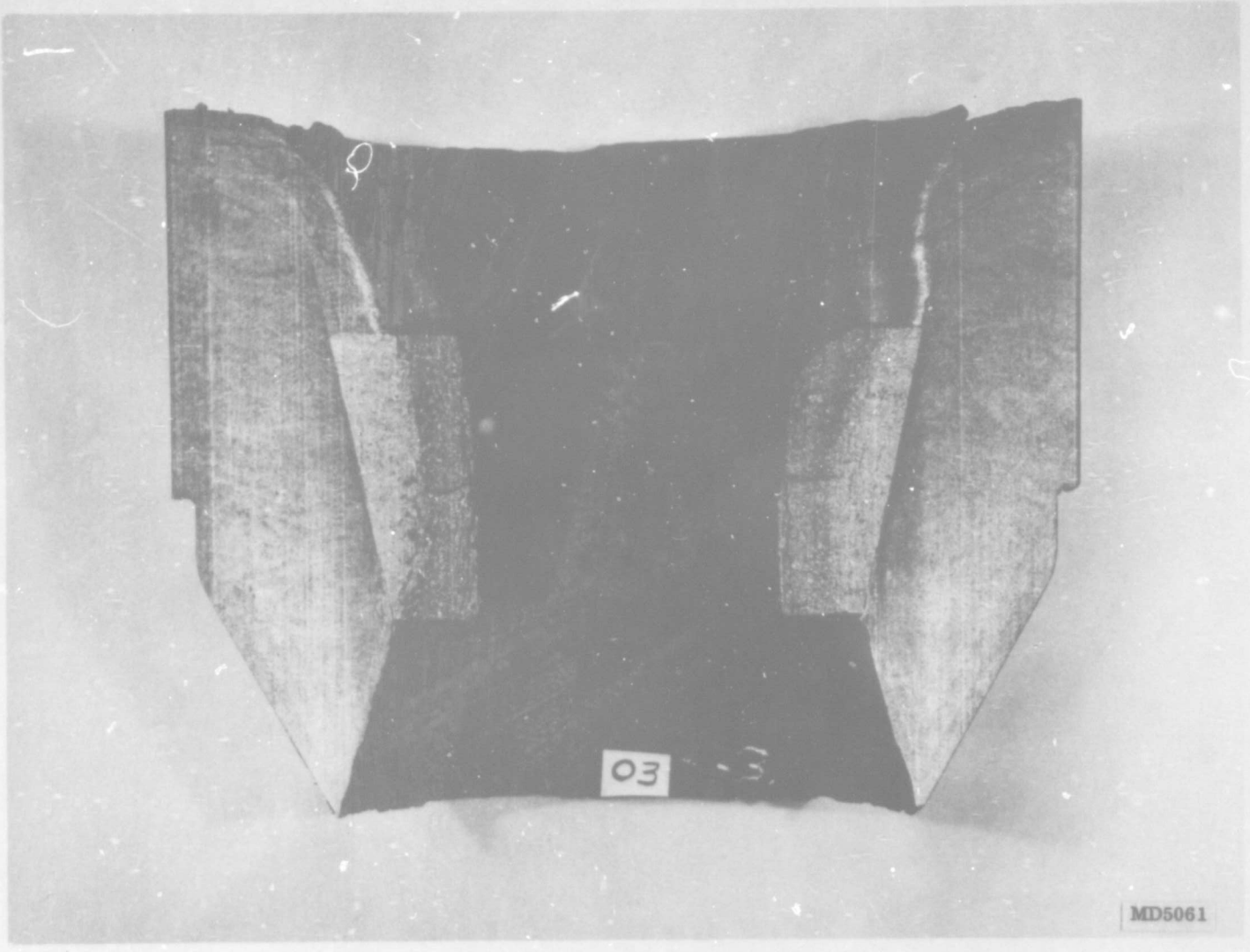

Figure 61. Nozzle No. 3 Postfired Condition, Inlet-Throat-Backup Section

Figure 62. Nozzle No. 3 Postfired Condition, Exit Cone

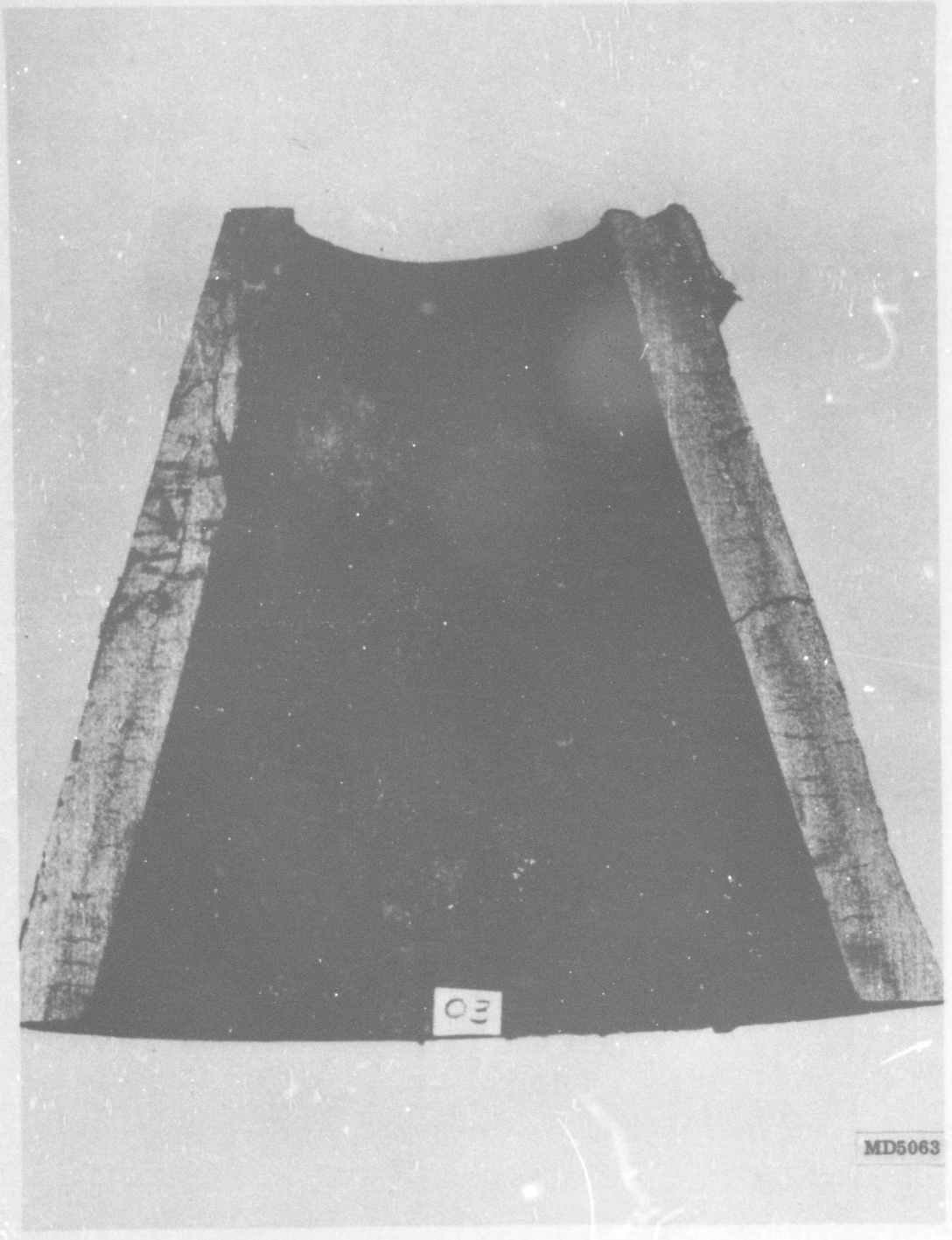

Figure 63. Nozzle No. 3 Postfired Condition, Exit Cone Section

TABLE XXIII

CHAR MOTOR BALLISTICS

Nozzle No. and Test Date	Average Throat Dia (in.) Initial	Average Throat Dia (in.) Final	Chamber Gas Temperature (°F)	Maximum Pressure (psia)	Average Pressure (psia)	Action Time (sec)
No. 3 Tested 10/4/66	3.807	4.086	5,643	646	552.2	27.55
No. 2 Tested 10/7/66	3.807	4.153	5,643	696	555.5	26.70
No. 1 Tested 10/12/66	3.807	4.052	5,643	721	575.5	25.40

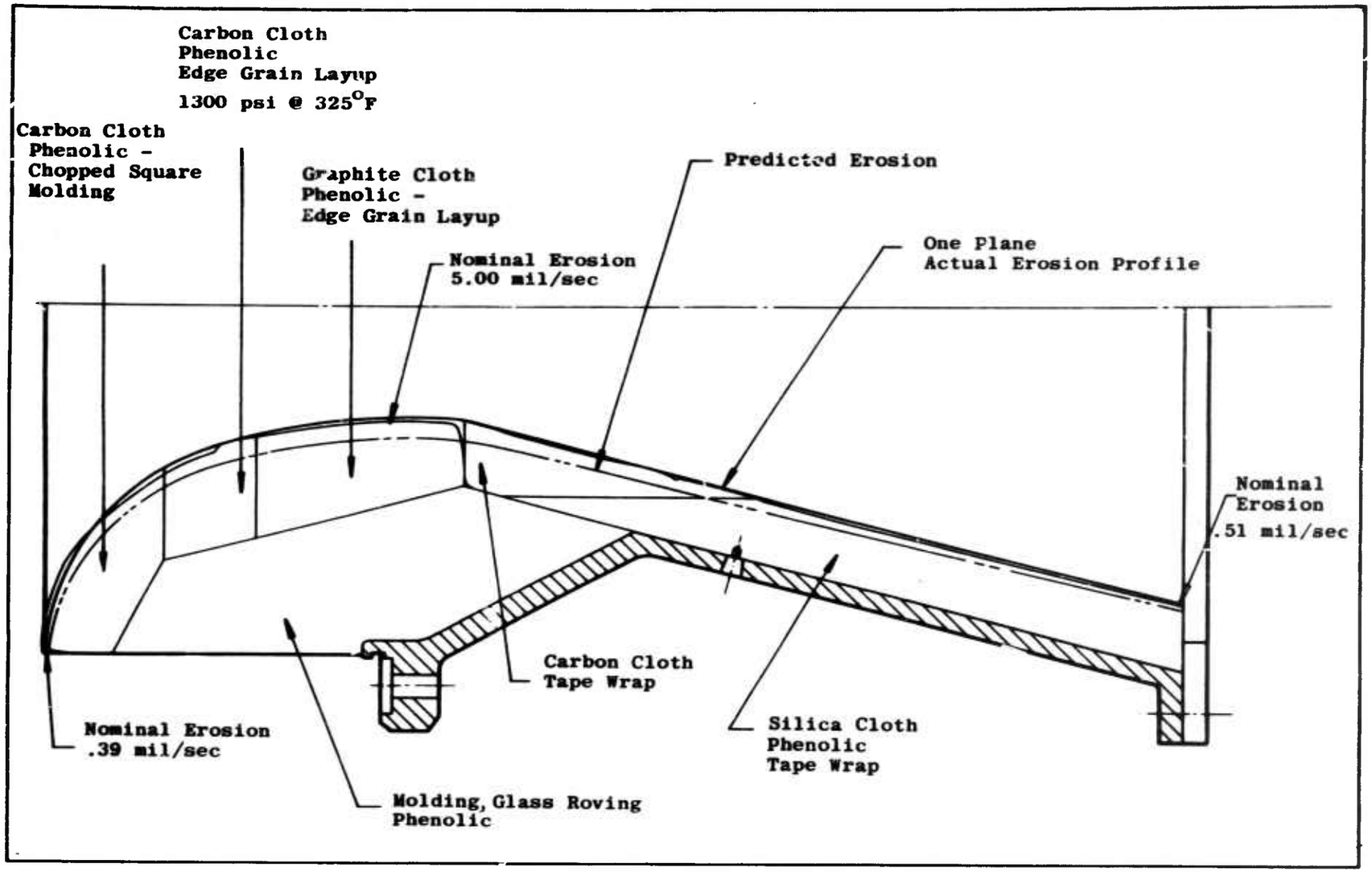

Figure 64. Nozzle No. 1 Erosion Profile

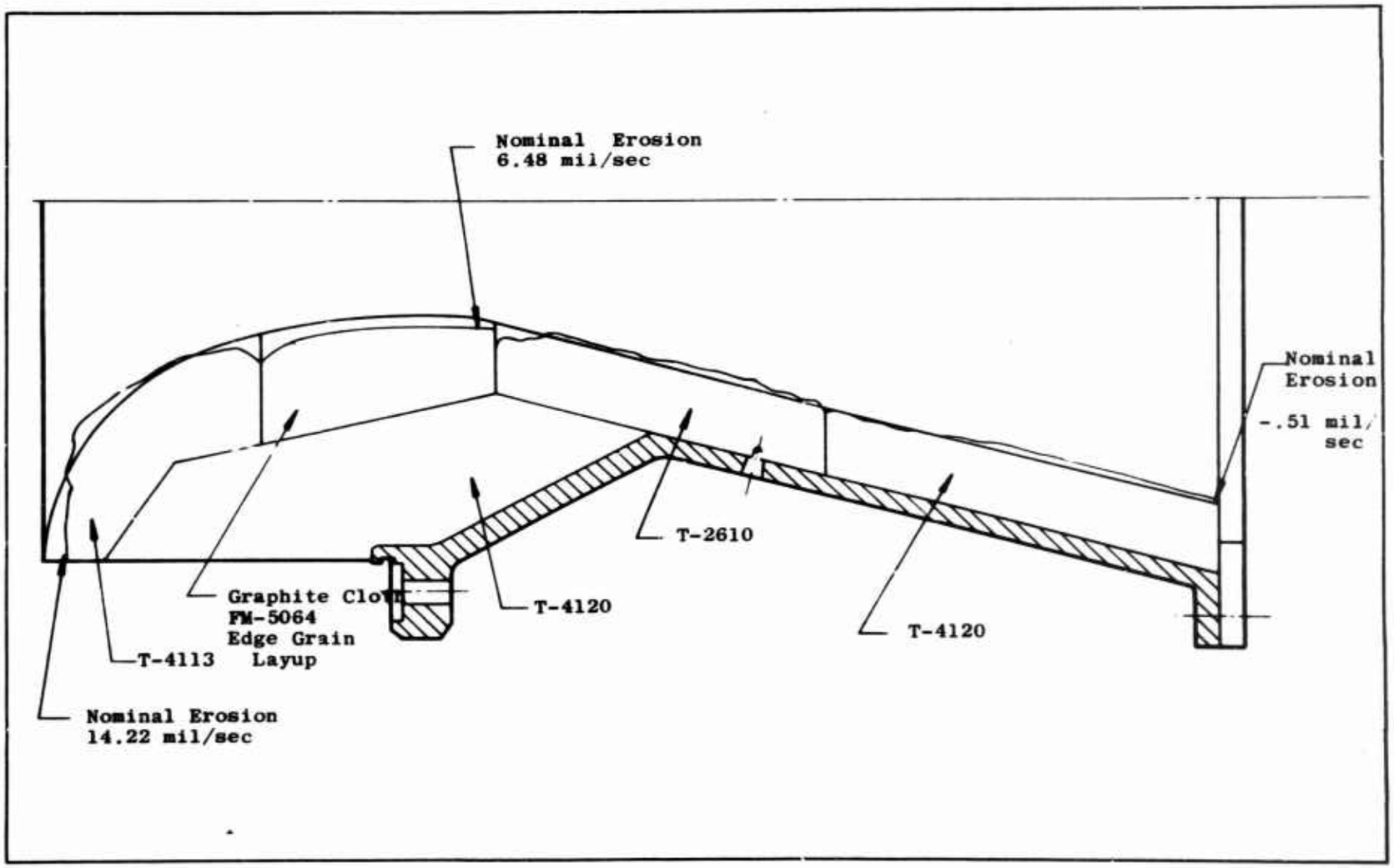

Figure 65. Nozzle No. 2 Erosion Profile

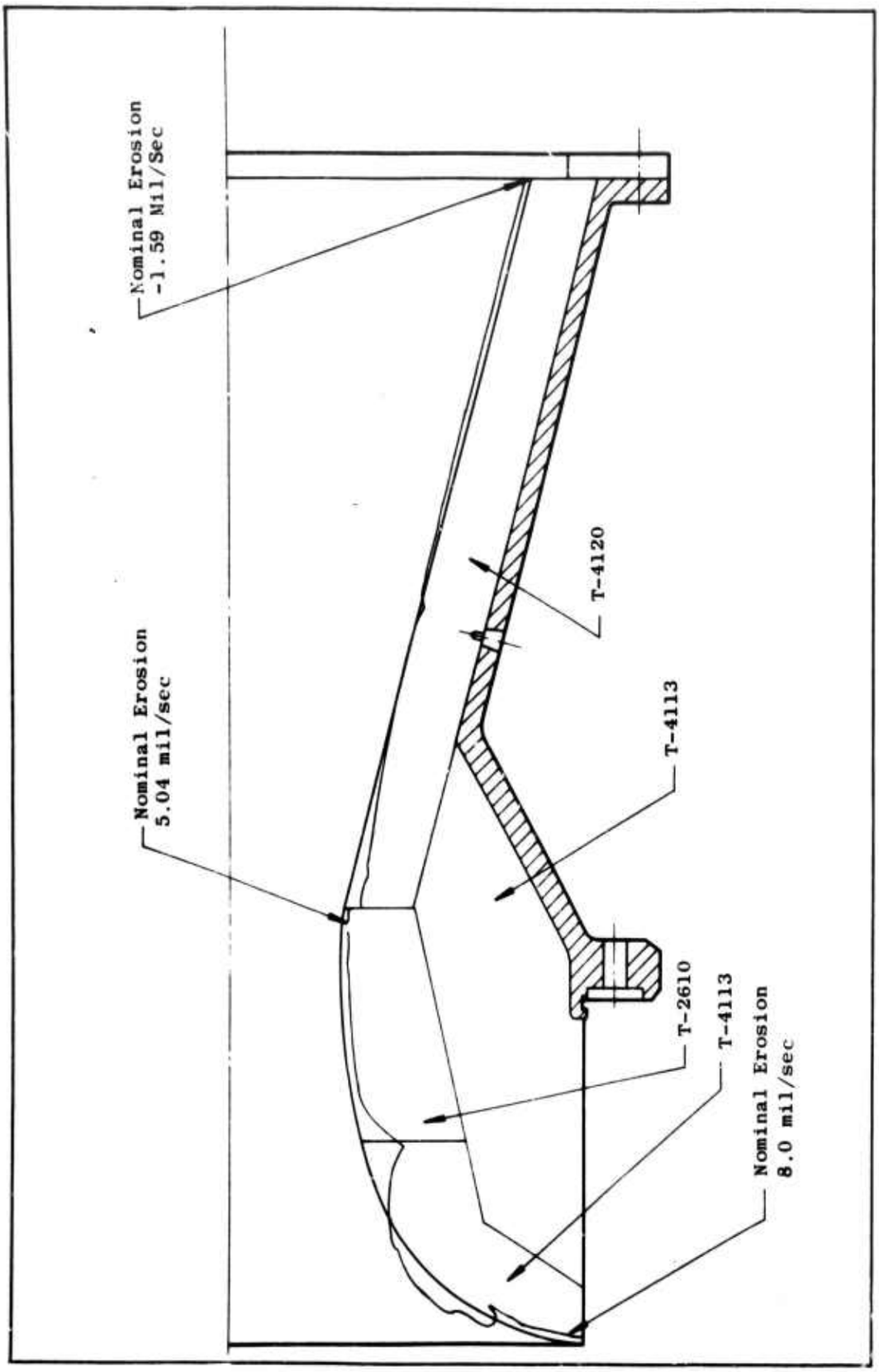

Figure 66. Nozzle No. 3 Erosion Profile

TABLE XXIV

NOZZLE EROSION RATES

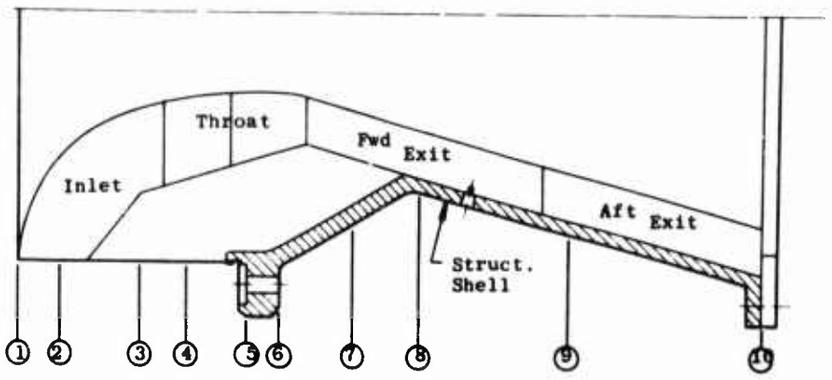

Nozzle		Location and Area Ratio									
		⊕ 1	2	3	4	5	⊕ 6	7	8	9	⊕ 10
		10.0	5.59	2.15	1.36	1.01	1.00	1.24	2.27	3.53	7.05
3	Min	+6.90					+4.93				-1.09
	Nom	+8.00	+4.36	-3.99	+17.05	+5.09	+5.04	+7.27	-1.09	-1.81	-1.59
	Max	+8.35					+5.16				-2.14
2	Min	+12.00					+4.92				-.18
	Nom	+14.22	+4.87	-1.87	+17.60	+6.37	+6.48	+2.62	-.75	-2.62	-.51
	Max	+15.00					+8.66				-.75
1	Min	0.00					+4.28				+.37
	Nom	+.39	-1.57	+1.97	+3.54	+5.52	+5.00	+1.97	+1.18	+4.33	+.51
	Max	+1.18					+5.53				+.75

\+ Material Erosion − Material Contraction ⊕ Six Measurements

All others one measurement.

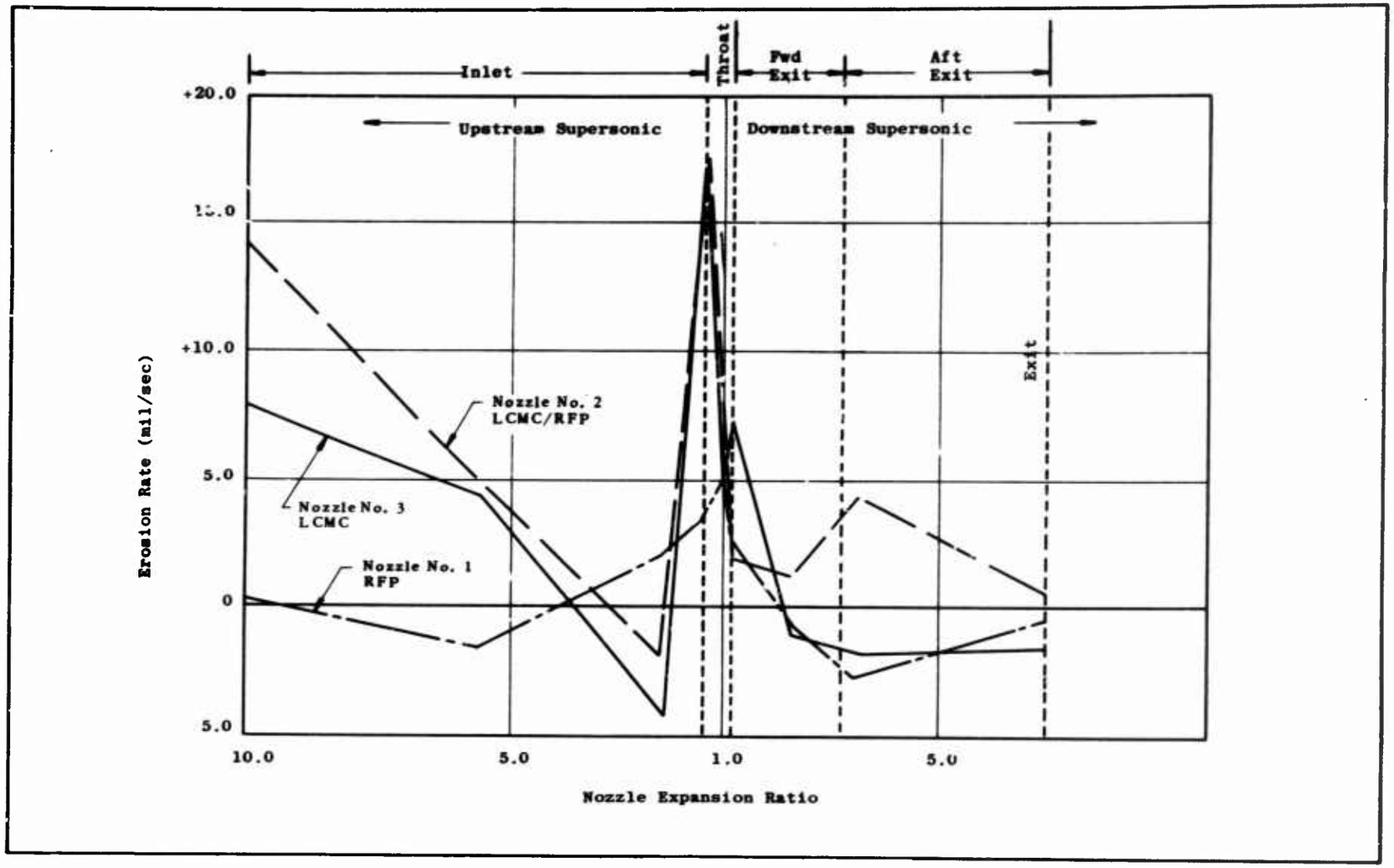

Figure 67. Material Erosion Rate

the high erosion rate at the inlet-nozzle interface was not plotted because the erosion consisted of localized gouging.

5. POSTFIRE PROPERTIES

Specimens were taken from the various locations of the nozzle components to determine part density. As much as possible, specimens were taken from either wholly virgin or wholly charred material. Tables XXV, XXVI and XXVII show the specimen locations and test results. As is expected, the specimens from the charred areas show lower density than those from the virgin specimens.

6. INSTRUMENTATION

Each of the three subscale nozzles were instrumented with 12 thermocouples as shown in Figure 68. The four thermocouples at Station A were at the inlet backup insulation interface; the four at Station B in the throat or at the throat backup interface; and the four at Station C at two depths in the exit cone. The temperature was continually recorded throughout the firing and during the post heat soak until approximately T+60 seconds. The measured temperatures at 30 and 60 sec are presented in Table XXVIII. The data for 30 sec is presented graphically in Figures 69, 70 and 71 for the three locations.

At all three stations, the temperature of the test materials was higher than that of the baseline ablative plastics. On the basis of temperatures of the three materials, the T-4113 had the lowest thermal conductivity and the T-2610 had the highest. This ranking is to be expected because of greater graphite particle packing at the higher cure pressures used for the T-2610.

7. ACTUAL VS PREDICTED PERFORMANCE

The three test nozzles were designed based on a thermal analysis of the baseline nozzle. The predicted thermal performance and actual measured temperatures are shown in Figures 72, 73 and 74 for the three measuring stations of Nozzle No. 1 and in Figure 75 for Station C in Nozzle No. 3. A prediction of erosion for the baseline nozzle was prepared during the design study. At all locations, the erosion measured was less than that predicted. The erosion rates predicted for the baseline nozzle (No. 1, reinforced plastic) were higher than the actual rates because the predicted values were not multiplied by the grain shape factor (GSF) which is approximately 0.50 for uncured, end burning grains (ref Appendix A, Sections A thru C and also Thiokol-Wasatch Document TWR-1710, "A Method for the Preliminary Sizing of Nozzle Liner"). The predicted and actual erosion rates for this nozzle at Stations 4, 5, and 8 (see Figure 22 and Table XXIV) are listed below.

Location	Predicted Erosion Rate (mils/sec)	Predicted Erosion Rate x GSF (mils/sec)	Actual Erosion Rate (mils/sec)
4	8.00	4.00	3.54
5	11.00	5.50	5.52
8	5.33	2.66	1.18

TABLE XXV

POSTFIRE DENSITY OF NOZZLE NO. 1

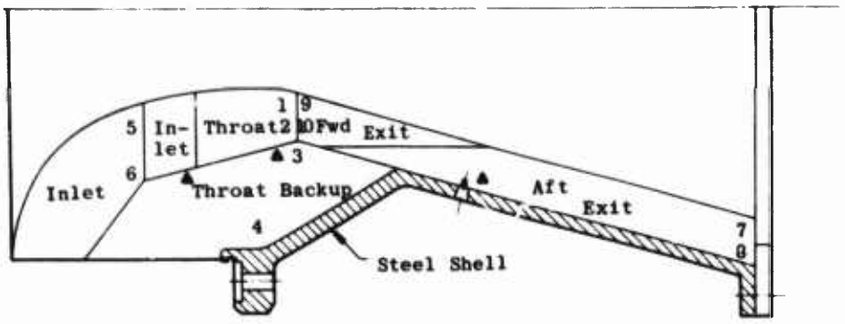

▲ Thermocouple Probes
4 each located at 90 deg

Specimen Location	Material	Postfire Density gm/cc
1. Throat	FM-5064	1.266
2. Throat	FM-5064	1.268
3. Throat Backup	Durez 16771	1.271
4. Throat Backup	Durez 16771	1.320
5. Inlet	FM-5063	1.321
6. Inlet	FM-5063	1.284
7. Aft Exit	FM-5067	1.672
8. Aft Exit	FM-5067	1.725
9. Fwd Exit	FM-5063	1.260
10. Fwd Exit	FM-5063	1.462

TABLE XXVI

POSTFIRE DENSITY OF NOZZLE NO. 2

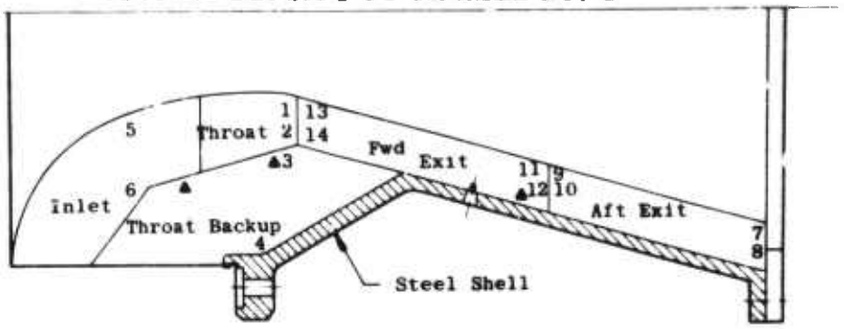

▲ Thermocouple Probes
4 each located at 90 deg

Specimen Location	Material	Postfire Density gm/cc
1. Throat	FM-5064	1.142
2. Throat	FM-5064	1.362
3 Throat Backup	T-4120	1.556
4 Throat Backup	T-4120	1.594
5 Inlet	T-4113	1.279
6. Inlet	T-4113	1.535
7. Exit - Aft	T-4120	1.322
8. Exit - Aft	T-4120	1.421
9. Exit - Aft	T-4120	1.299
10. Exit - Aft	T-4120	1.251
11. Exit - Fwd	T-2610	1.495
12. Exit - Fwd	T-2610	1.649
13. Exit - Fwd	T-2610	1.450
14. Exit - Fwd	T-2610	1.640

TABLE XXVII

POSTFIRE DENSITY OF NOZZLE NO. 3

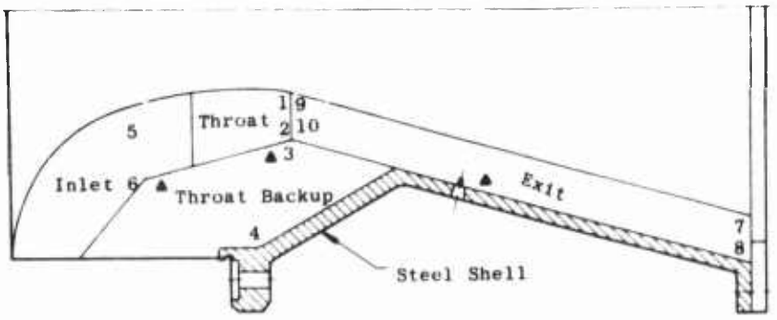

▲ Thermocouple Probes
4 ea. located at 90 deg

Location Index	Material	Postfire Density gm/cc
1. Throat	T-2610	1.562
2. Throat	T-2610	1.572
3. Throat Backup	T-4113	1.503
4. Throat Backup	T-4113	1.546
5. Inlet	T-4113	1.462
6. Inlet	T-4113	1.410
7. Exit - Aft	T-4120	1.375
8. Exit - Aft	T-4120	1.471
9. Exit - Fwd	T-4120	1.306
10. Exit - Fwd	T-4120	1.520

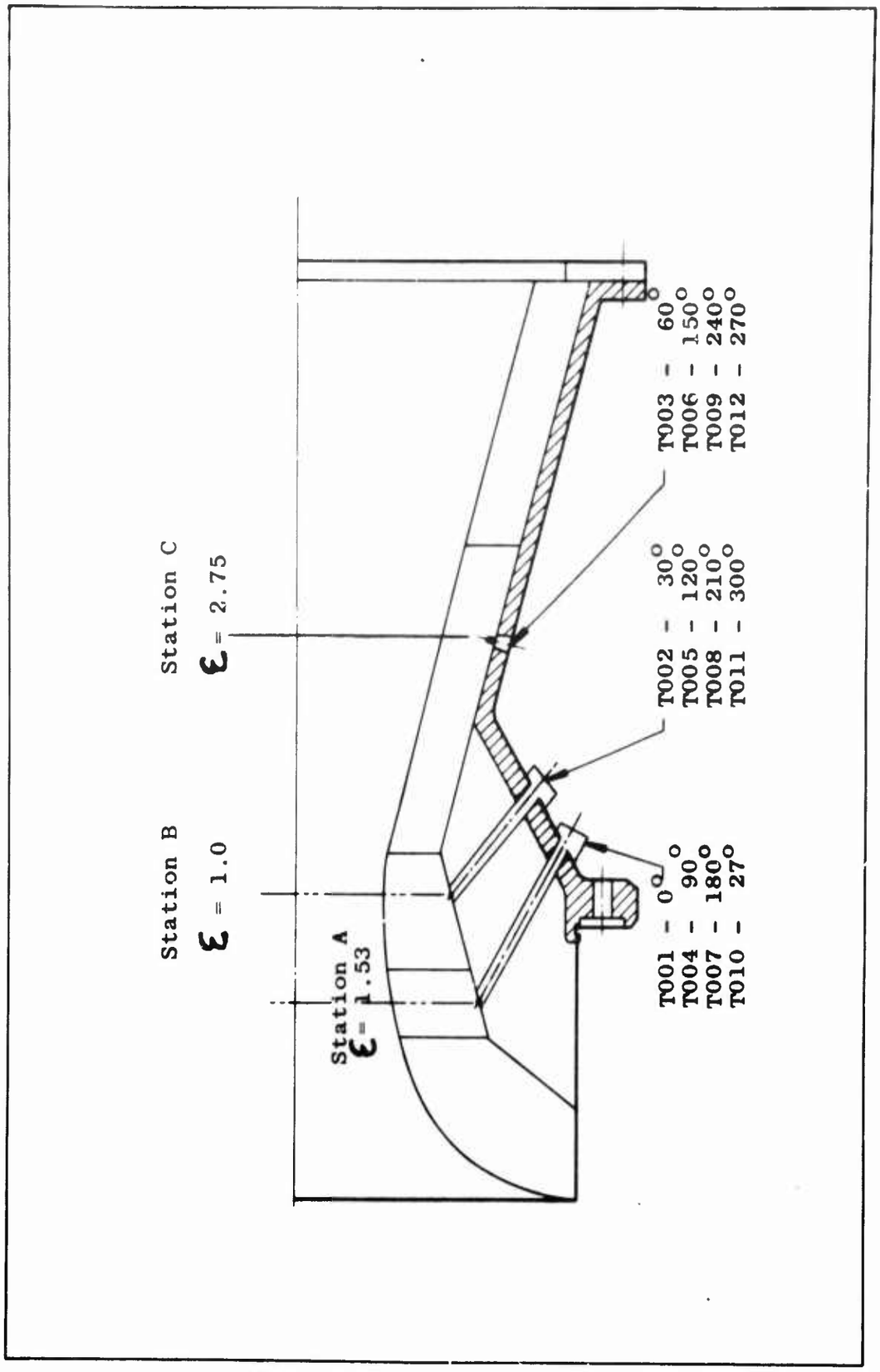

Figure 68. Nozzle Instrumentation Location

TABLE XXVIII

MEASURED NOZZLE TEMPERATURES

TEMPERATURE (°F)

NOZZLE NO.	Time (sec)	THERMOCOUPLE											
		T001	T002	T003	T004	T005	T006	T007	T008	T009	T010	T011*	T012
3	30	125	296	83	89	435	320	106	155	240	90	--	328
	59	214	356	113	134	850	755	174	255	550	136	--	722
2	30	100	78	196	118	81	342	220	78	285	112	--	410
	52	169	98	292	232	145	660	430	97	495	231	--	565
1	30	70	70	70	70	74	74	70	69	71	67	--	71
	63	70	72	73	71	192	83	70	79	73	69	--	83
Station		A	B	C	A	B	C	A	B	C	A	B	C
Distance from Surface (in.)		1.60	1.38	0.80	1.60	1.05	0.65	1.60	1.38	0.80	1.60	1.05	0.65

*Nonoperative

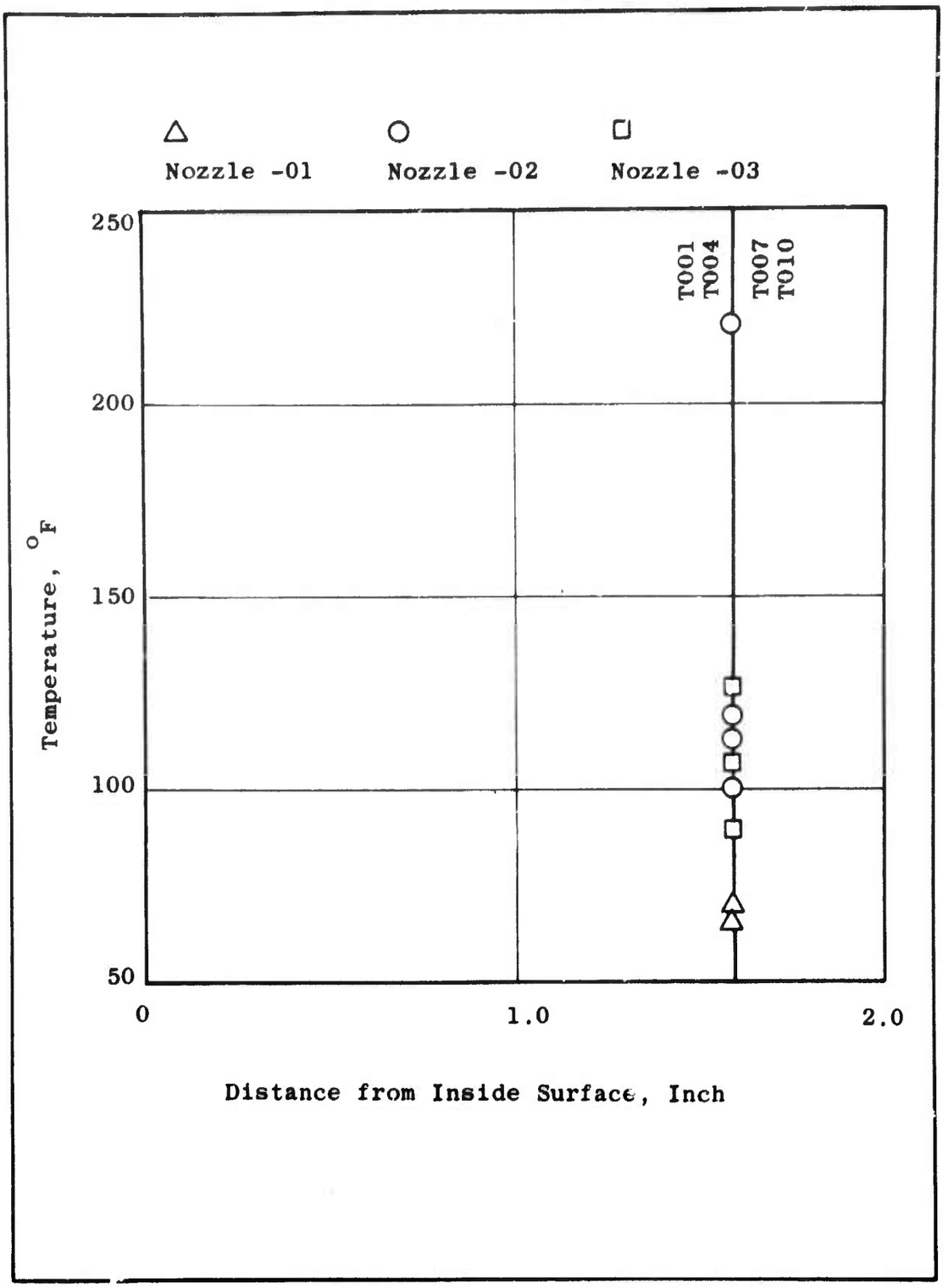

Figure 69. Temperature at Station A, 30 Sec

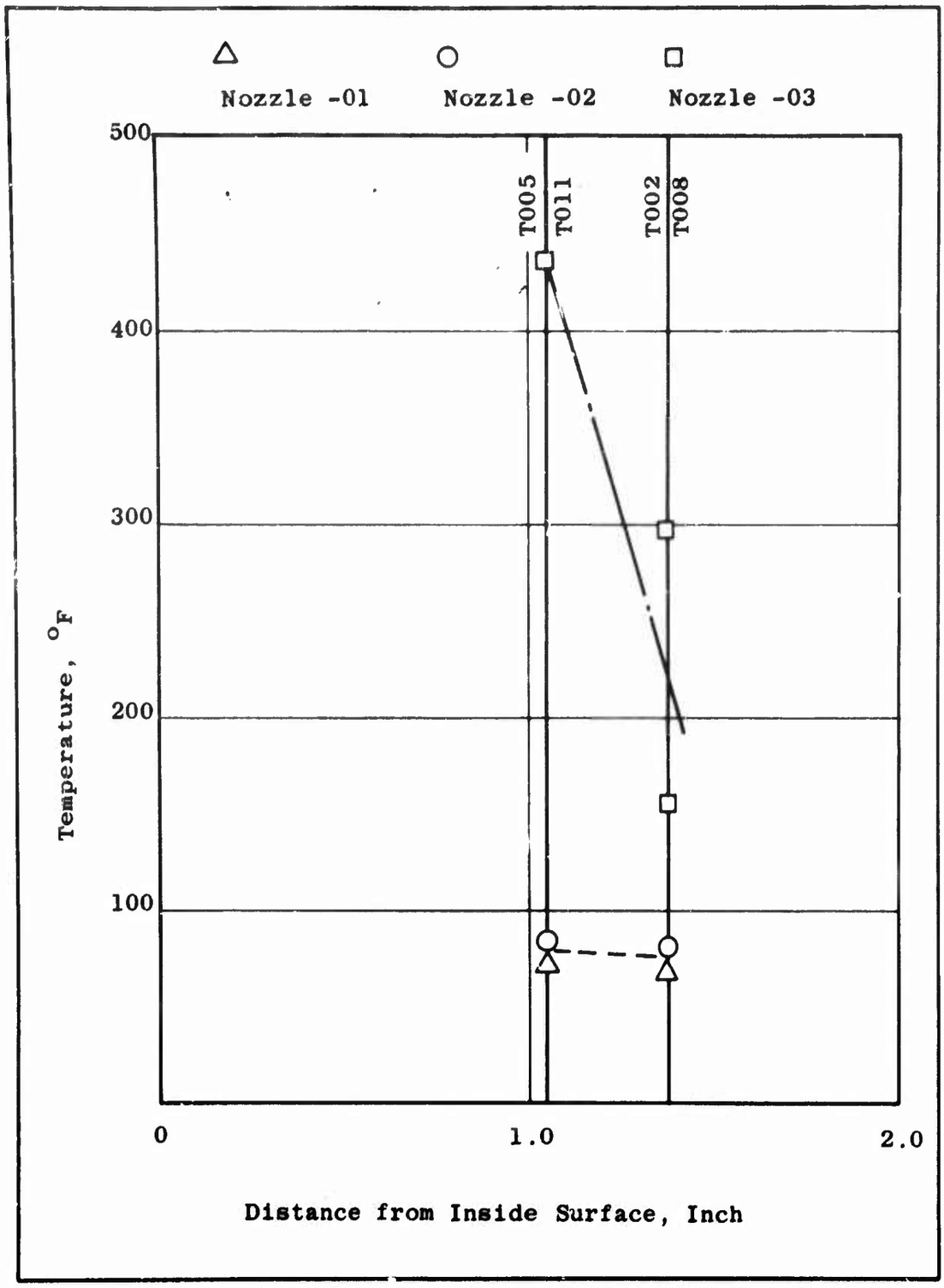

Figure 70. Temperature at Station B, 30 Sec

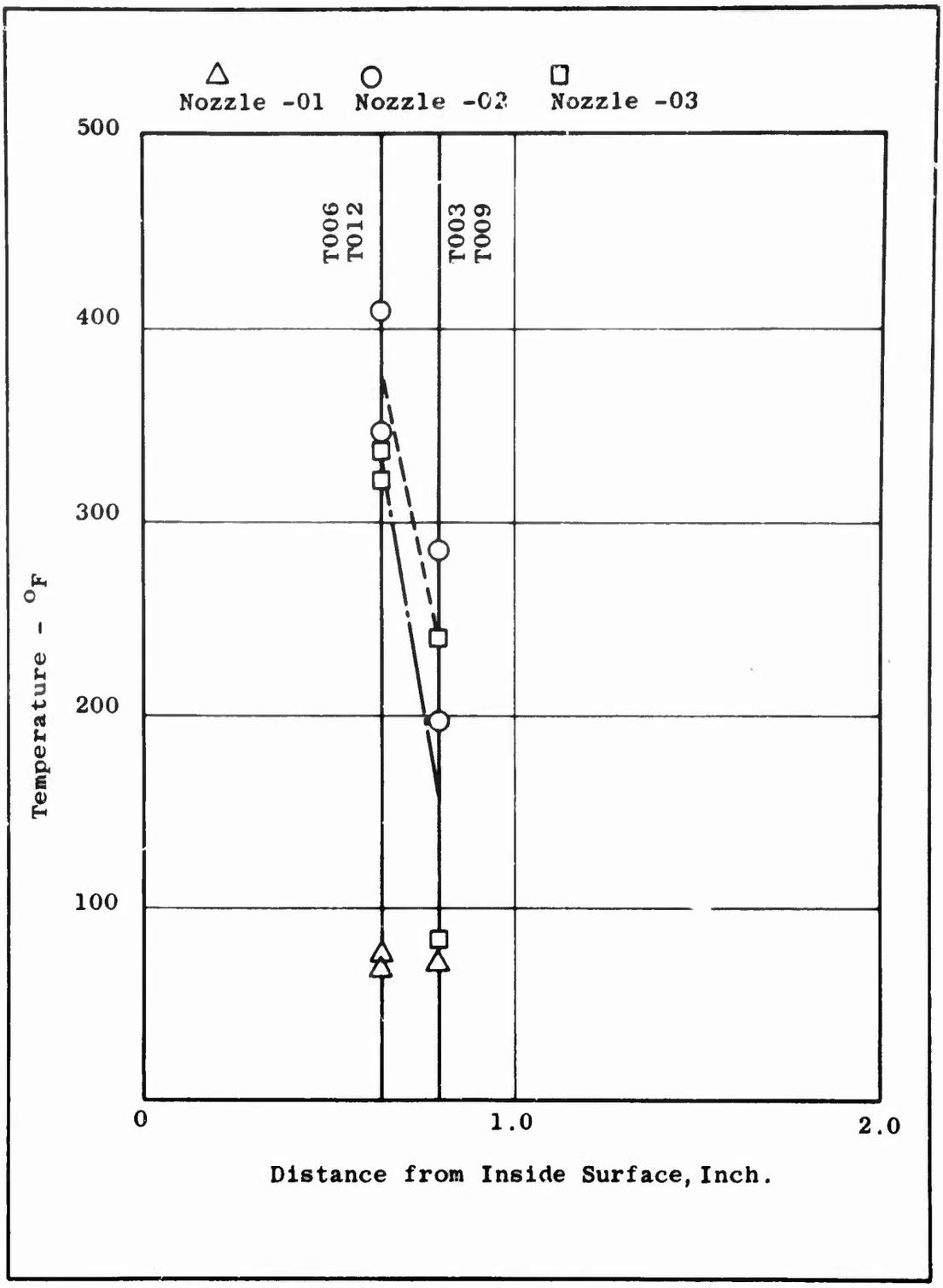

Figure 71. Temperature at Station C, 30 Sec

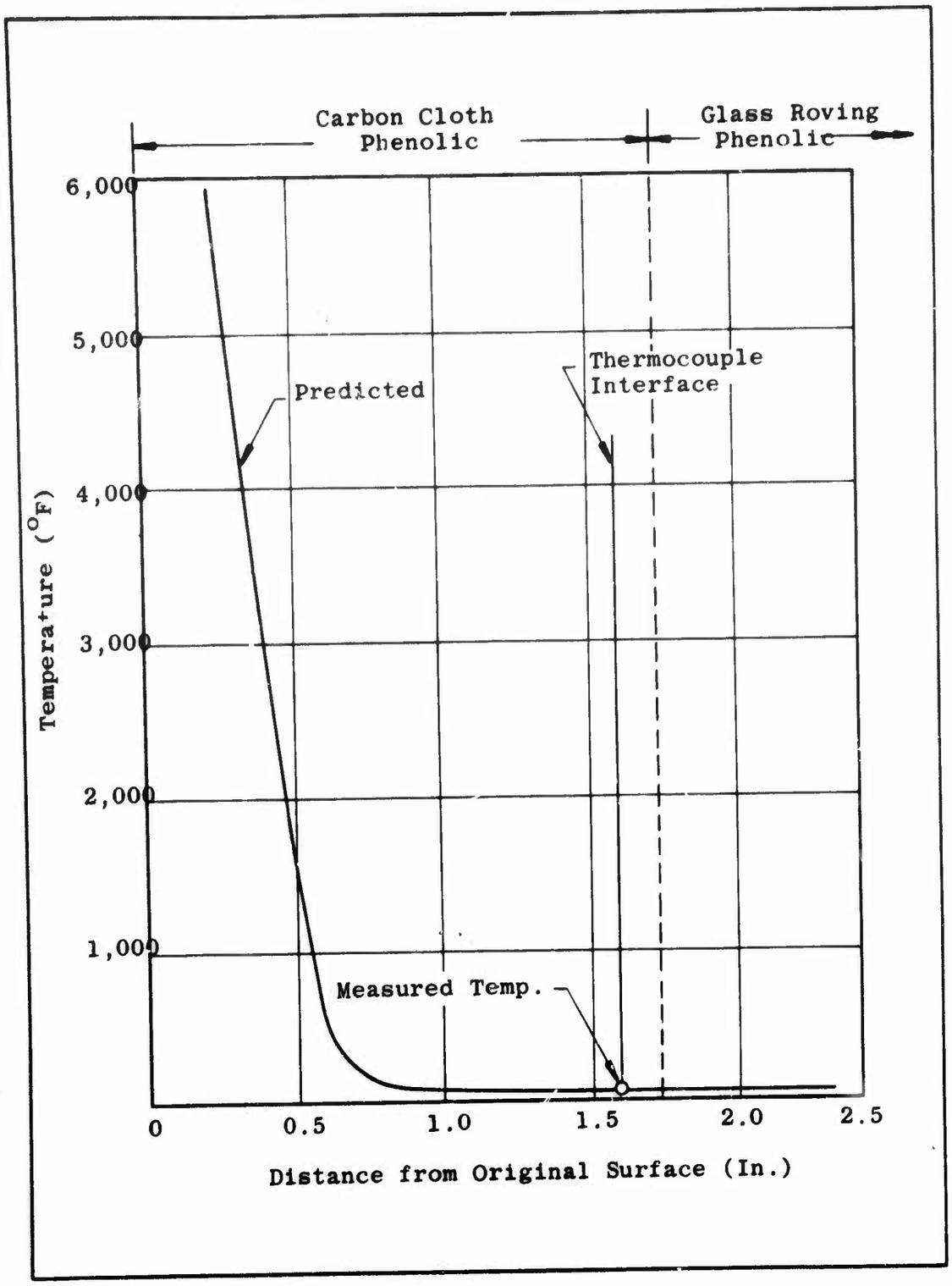

Figure 72. Thermal Profile, Nozzle No. 1, Station A, 30 Sec

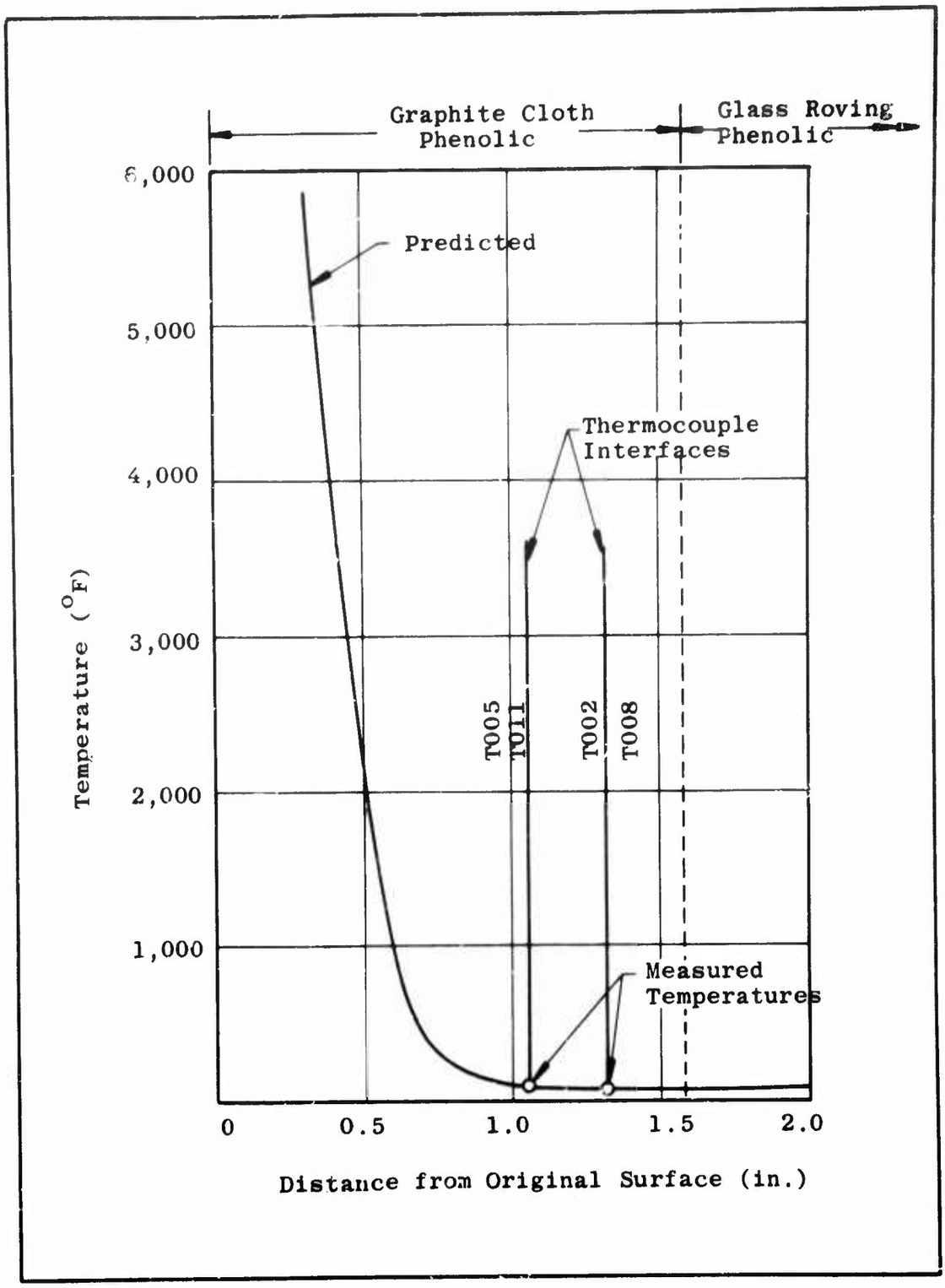

Figure 73. Thermal Profile, Nozzle No. 1, Station B, 30 Sec

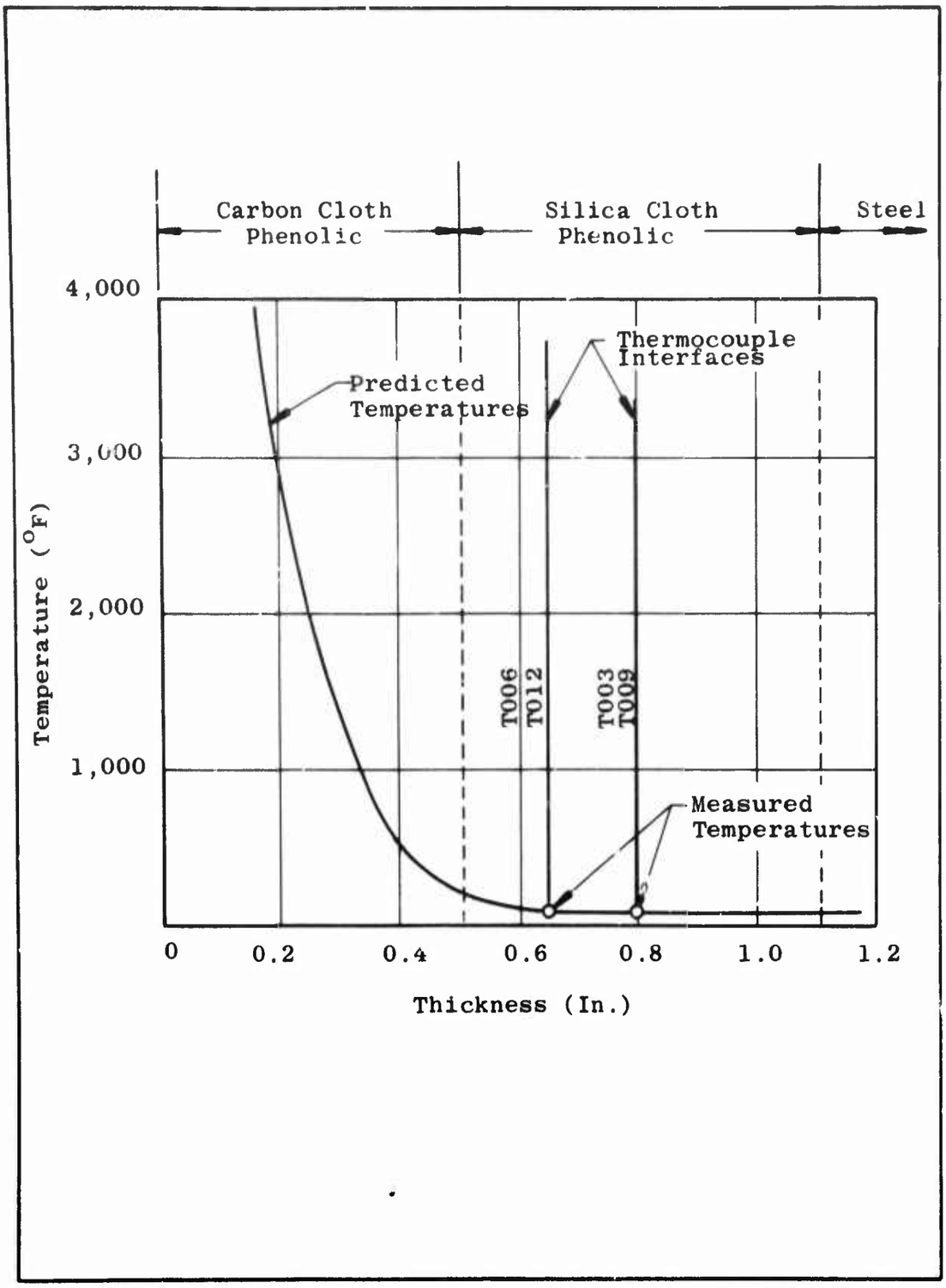

Figure 74. Thermal Profile, Nozzle No. 1, Station C, 30 Sec

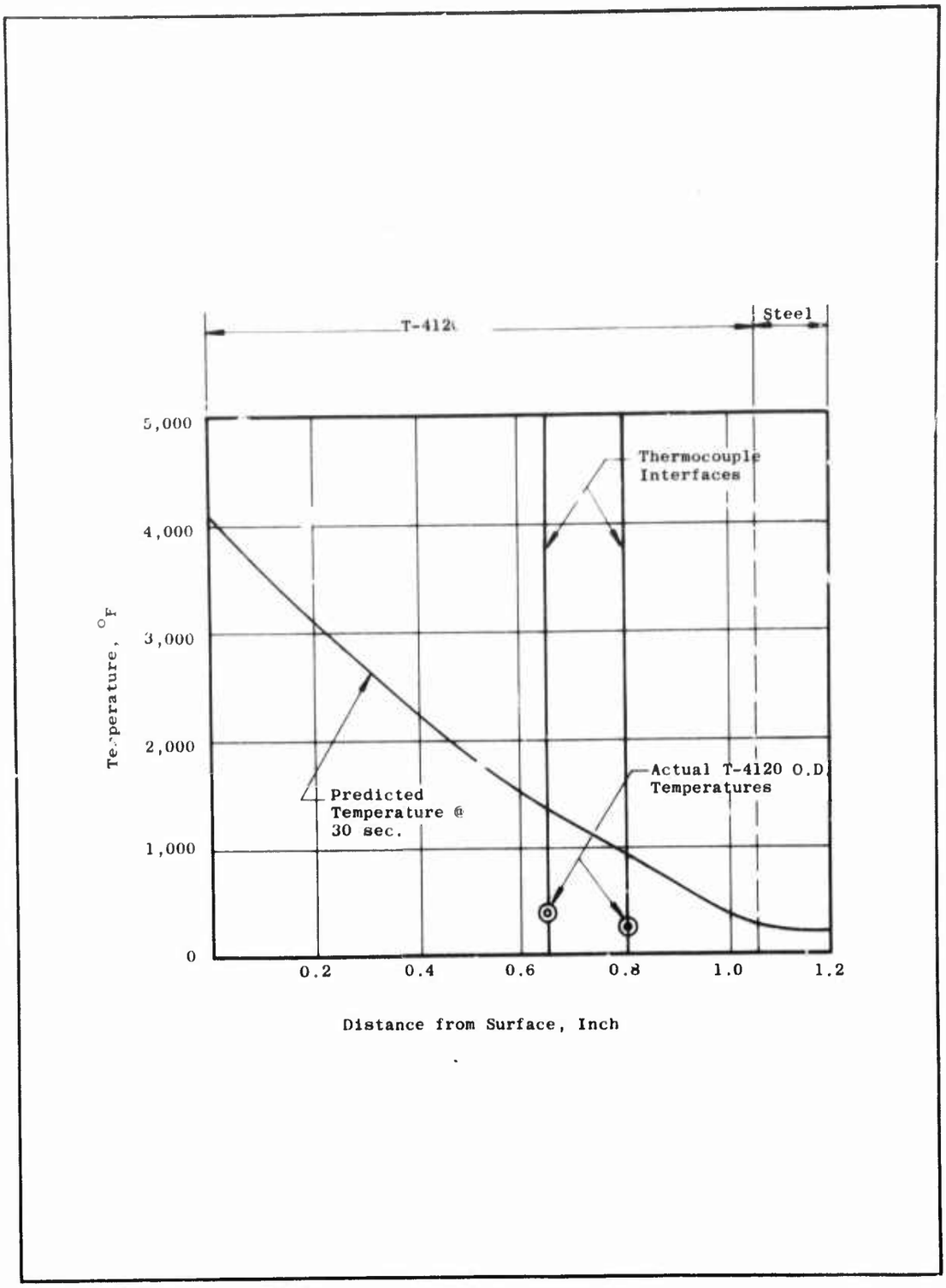

Figure 75. Thermal Profile, Nozzle No. 3, Station C, 30 Sec

C. NOZZLE NO. 4

Subscale Nozzle No. 4 in the original program plan was to be designed using the data obtained from the first three nozzle tests and the materials cure optimization and the process studies. A review of the data showed that the basic materials selected were satisfactory, lower pressure cures were adequate, and improvement in the inlet char retention and a reduction of exit cone thermal cracking was desirable. The design of Nozzle No. 4 is shown in Figure 76. The materials and design changes are compared to Nozzle No. 3 in Table XXIX.

The nozzle fabrication matrix is shown in Table XXII. The inlet, cured in place under vacuum bag pressure, was the same T-4113 material. The inlet had small holes drilled over 180 deg of the internal surface. This drilling technique has been used on ablative plastics to relieve thermal stresses and reduce spalling and cracking.

The throat backup material was the same as in Nozzle No. 3 except it was cured in place without any external pressure.

The throat was changed from a 1,000 psi cured T-2610 part to a 200 psi cured T-4120 part which was compatible with the aims of the program.

The exit cone was the same as in Nozzle No. 3 with the addition of an insulation to protect the steel shell and provide a bonding layer. The insulation used was UF-1149, an asbestos filled polyamide epoxy developed under the Minuteman Stage I Program. This insulation should allow direct cure in position of the T-4120, as a good bond is obtained between the two materials, either primed or unprimed and the UF-1149 has a high elongation. During fabrication of Nozzle No. 3, two attempts were made to cure the T-4120 material in the steel body. In both attempts, separations occurred between the steel shell and the insulation. These separations were attributed to poor adhesion of the T-4120 to the steel and/or to material shrinkage during cure. The physical properties and adhesion properties of UF-1149 are presented in Table XXX.

To confirm the design of Nozzle No. 4, thermal and erosion analyses were conducted (ref Appendix A). Figures 77 and 78 are the predicted thermal profiles through the throat and exit cone, respectively, at the thermocouple Stations B and C.

The nozzle was static tested during February 1967. Motor ignition and performance were normal for approximately 3 sec of operation, at which time a series of events occurred that resulted in a complete failure of the nozzle assembly. The failure sequence as established from film review is reflected in Table XXXI. The cause of malperformance was difficult to establish definitely; however, it is felt that a two part failure occurred.

1. There was possibly a joint failure between the nozzle aft flange/retainer ring interface. A poor seal between these two components could expose the retainer ring retention bolts to the exhaust

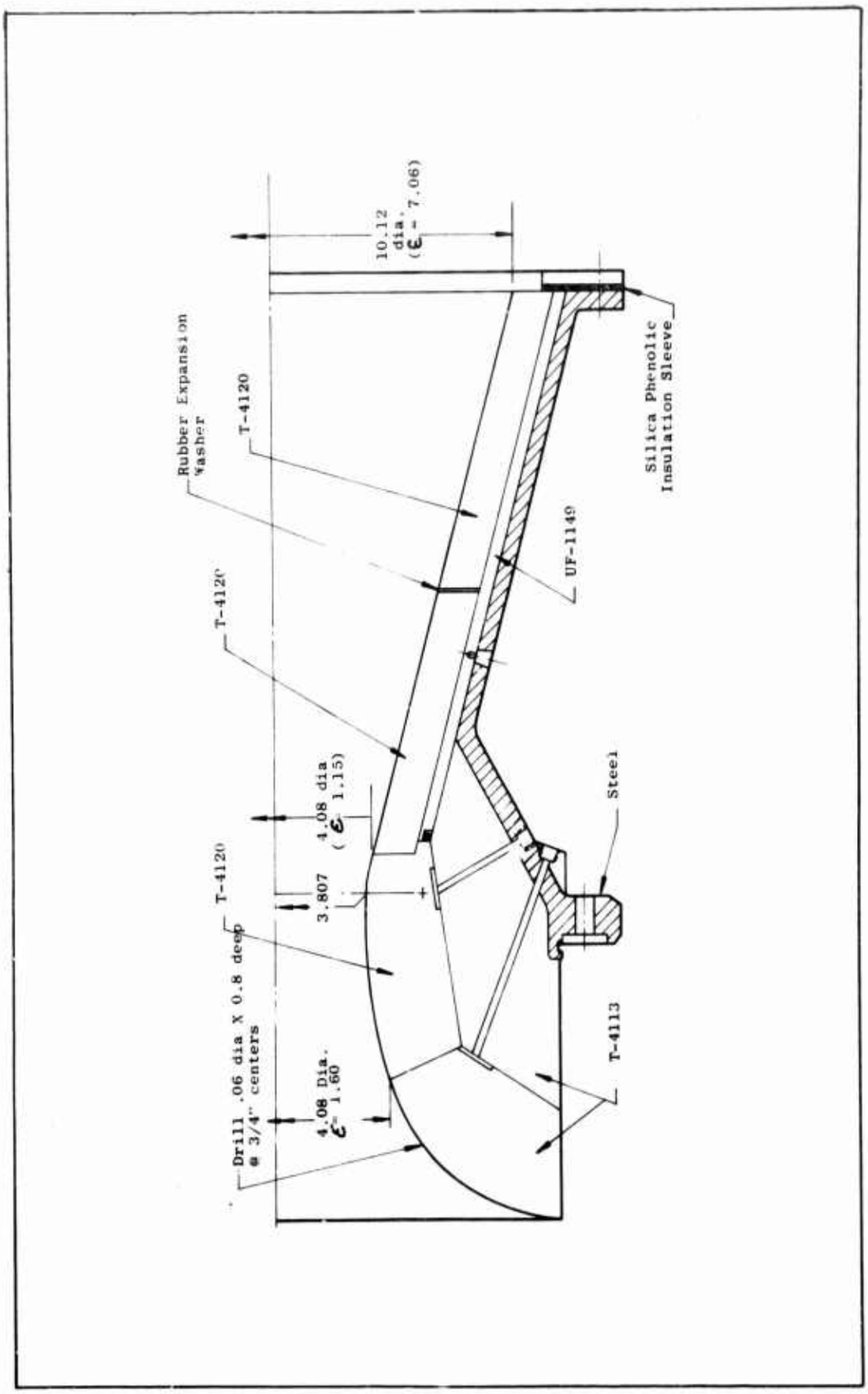

Figure 76. Nozzle No. 4

TABLE XXIX

NOZZLE DESIGN COMPARISON

Component	Nozzle No. 3 Material	Nozzle No. 3 Process	Nozzle No. 4 Material	Nozzle No. 4 Process	Design Changes
1. Inlet	T-4113	300°F, 200 psi	T-4113	170°F, 15 psi	Drill holes in surface over half of inlet.
2. Throat	T-2610	300°F, 1,000 psi	T-4120	300°F, 200 psi	Move inlet interface forward and normal to surface.
3. Throat Backup	T-4113	300°F, 200 psi	T-4113	170°F, 0 psi	None
4. Exit Cone	T-4120	170°F, 15 psi	T-4120	170°F, 15 psi	Thin down to allow backup insulation. Include rubber expansion washers.
5. Exit Cone	N/A	--	UF-1149*	80°F, 0 psi	To provide thermal insulation for 60 second test.

*Asbestos filled epoxy polyamide.

TABLE XXX

PHYSICAL PROPERTIES OF UF-1149

Test Temperature (°F)	Tensile Properties: Tensile Strength (psi)	Tensile Properties: Elongation (Percent)
75	580	89
300	60	15

Adhesion System: Base (Cured)	Adhesion System: Primer	Adhesion System: Adhesive (Uncured)	Adhesive Properties: Adhesive Strength (psi)	Adhesive Properties: Type of Failure
UF-1149	--	T-4120	612	100% in T-4120
UF-1149	UF-1149	T-4120	565	90% in T-4120
UF-1149	UF-1149 / T-4120	T-4120	565	100% in T-4120
Steel	--	UF-1149	630	100% in UF-1149

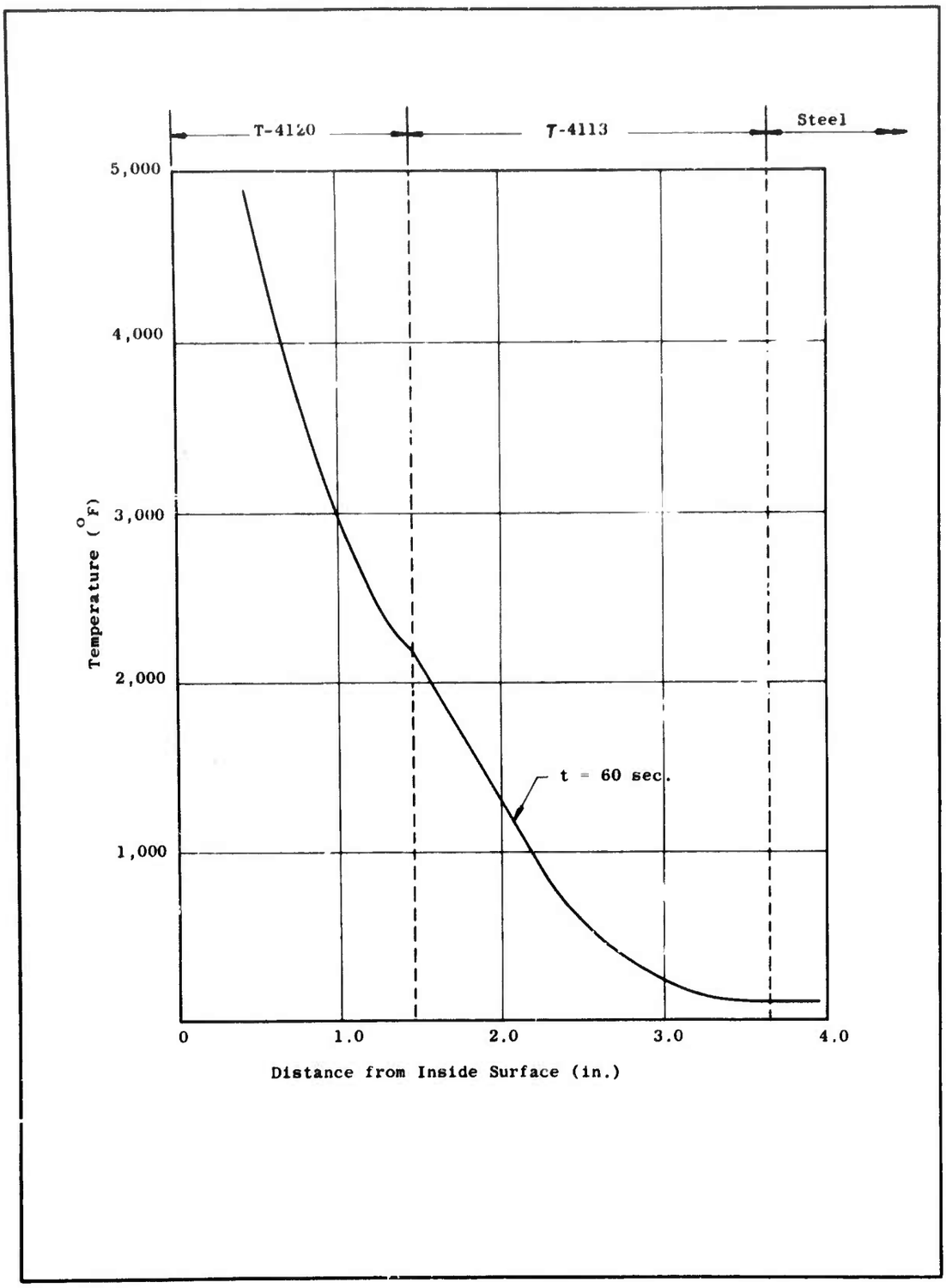

Figure 77. Predicted Temperature Profiles, Nozzle No. 4, Station B

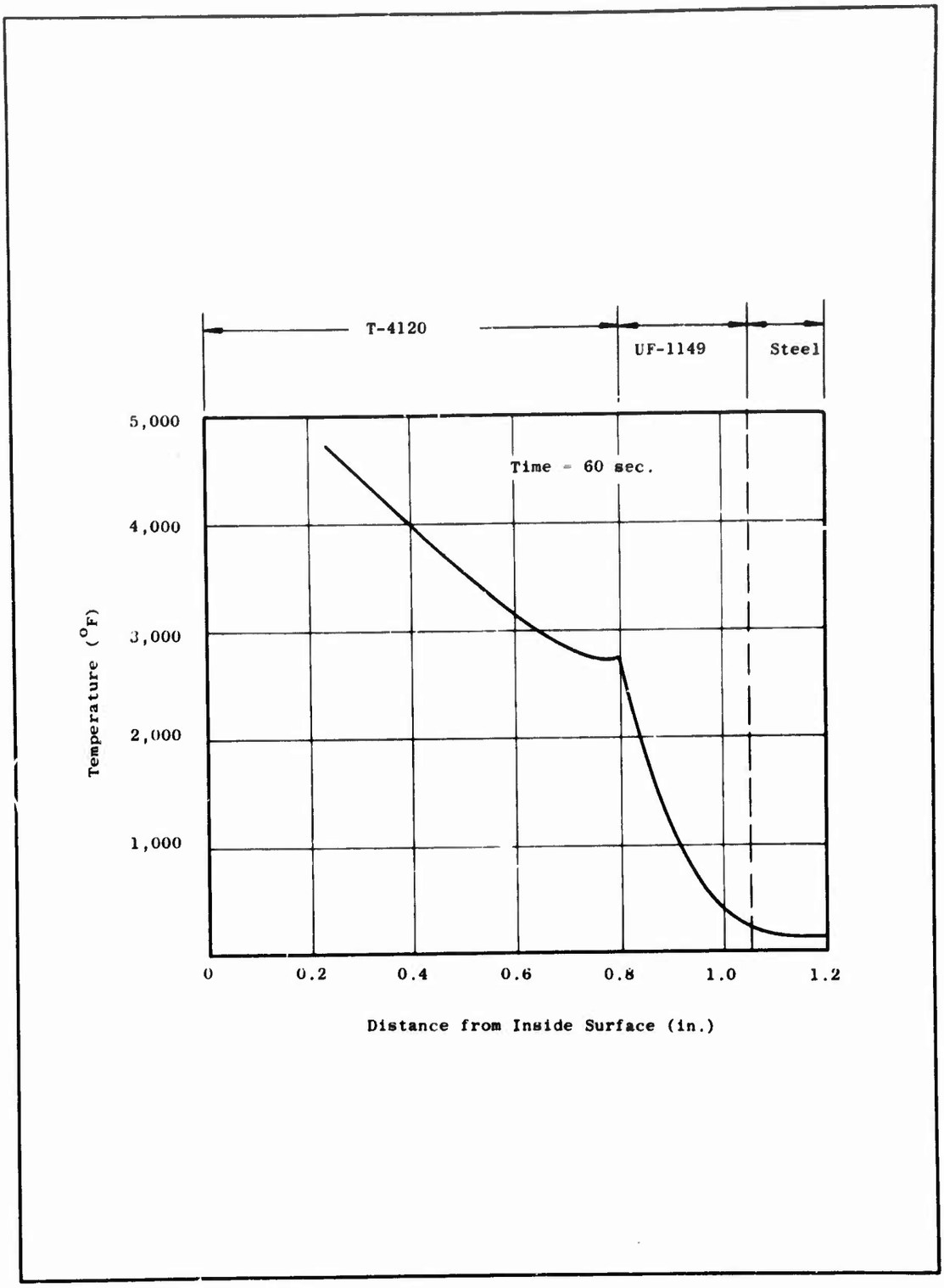

Figure 78. Predicted Temperature Profiles, Nozzle No. 4, Station C

TABLE XXXI

NOZZLE NO. 4 FAILURE SEQUENCE

	Failure Sequence	Film No. 1* Exit Burnthrough (sec)	Film No. 2** Flange Burnthrough (sec)
1.	Exit Plane Flame at Retainer Interface	2.89	3.57
2.	Exit Plane Retainer Lost Silica and Steel	7.10	8.47
3.	One Dark Large Object Ejected from Nozzle (Exit Cone Segment)	7.60	9.15
4.	Second Dark Large Object Ejected from Nozzle (Exit Cone Segment)	7.71	9.15
5.	Burnthrough at Forward Exit Cone (Knee Joint)	10.95	12.92
6.	Burnthrough at Aft of Flange Ring	11.15	13.15
7.	Some Thermocouple Leads are Lost	11.75	14.70
8.	Very Large Dark Object Ejected (Throat and Inlet Possibly)	12.60	--
9.	Exit Cone Steel Shell Ejected	27.20	32.30
10.	Nozzle Flange Steel and Bolts Ejected***	74.20	70.40

*Located on exit burnthrough side.
**Located on flange burnthrough side.
***Motor was still burning when film ended.

gases which in turn could have resulted in loss of the retaining ring at approximately 7 sec. Subsequently, two objects were observed leaving the nozzle assembly. These objects were believed to be the forward and aft exit cone components.

2. There was possibly a malperformance of the inlet. The inlet surface eroded to the instrumentation lead exposing the instrumentation channel to the gases. The gases escaped through the channel entrance, located at a point just aft of the nozzle-to-motor flange, resulting in burnthrough of the nozzle shell at approximately 11 sec. Shortly thereafter, objects (believed to be the throat and inlet components) were observed leaving the assembly.

D. NOZZLE NO. 5

1. DESIGN

The nozzle design and instrumentation configuration is illustrated in Figure 79. The nozzle liner included six different materials bonded into a nozzle structural shell. Twelve thermocouples and four strain gages were installed at three nozzle planes to complete the nozzle design.

The inlet section included the carbon cloth phenolic, the T-4113 material, and four thermocouples installed on the backside of the T-4113 ($\epsilon = 1.9$).

The throat section included the T-2610 throat and the T-4113 throat support with four thermocouples installed at the backside of the throat and two strain gages at the outer shell surface ($\epsilon = 1.0$).

The exit section included T-2610 and T-4120, plus silica cloth phenolic liners, a glass cloth phenolic structure insulation sleeve, and instrumentation. The instrumentation included four thermocouples at the backside of the T-4120 and two strain gages at the outer steel shell surface ($\epsilon = 2.4$).

Reinforced plastics were incorporated into the design for specific purposes. The carbon cloth inlet ring was used to eliminate the effect of the closure rubber erosion on the T-4113 inlet. The exit cone silica and glass cloth parts were used to insulate the steel shell and retainer plate.

The structural support and retainer were made from welded 1020 steel plate and rolled sheet stock, and formed into a shell and ring construction.

2. FABRICATION

The nozzle components, materials and fabrication processing methods are listed in Figure 80. The fabrication sequence is indicated as a step by step process flow sheet. In addition, the nozzle fabrication matrix is reflected in Table XXII.

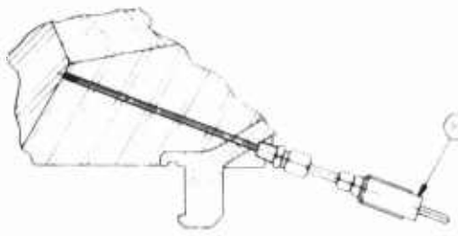

DETAIL A
TYP INSTL

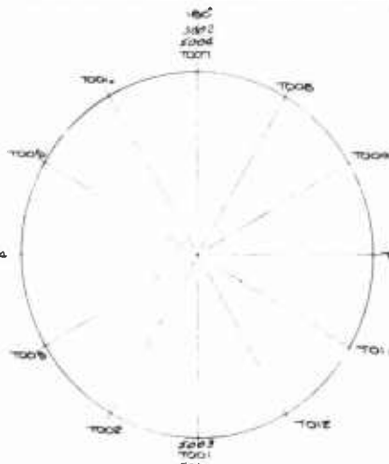

VIEW LOOKING FORWARD

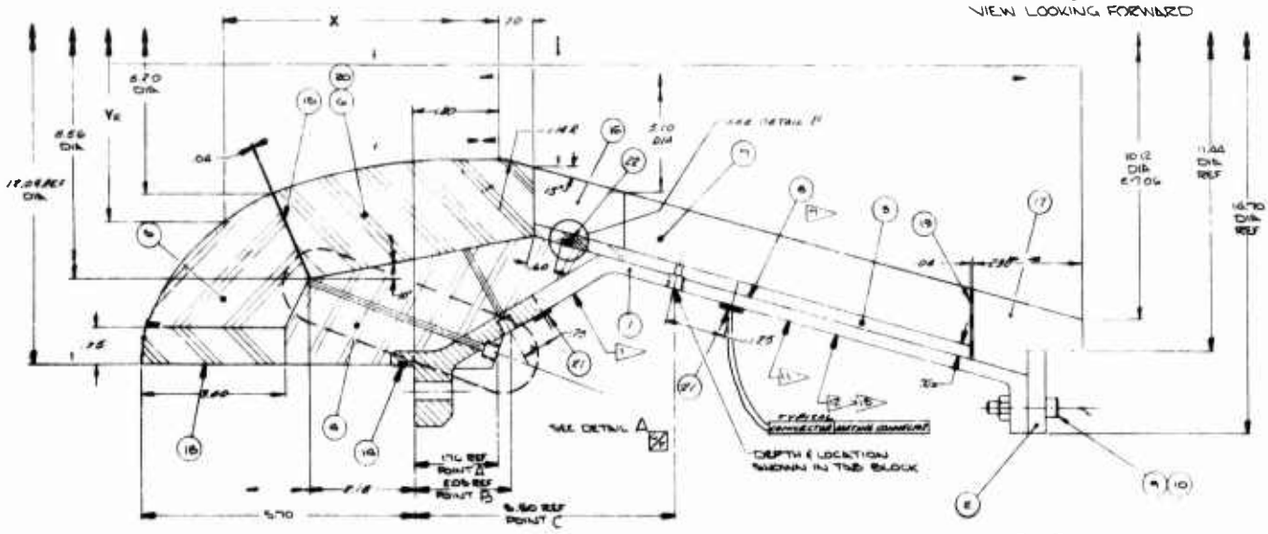

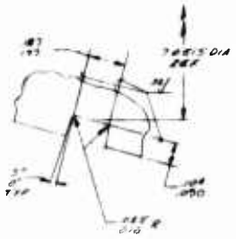

DETAIL B
SCALE NONE

NOZZLE INLET COORDINATES X	YR
.00	1.90
1.09	1.51
2.91	2.06
3.93	2.90
4.94	3.66
4.90	3.24
6.62	3.82
6.99	4.46
7.27	4.97
7.42	5.47
7.68	6.02

ITEM NO.	CODE NO	LOCATION	DRILL DEPTH
11	T001	POINT A @ 0°	THRU ITEM 4
12	T002	POINT B @ 30°	4
13	T003	POINT C @ 60°	3
11	T004	POINT A @ 90°	4
12	T005	POINT B @ 120°	4
13	T006	POINT C @ 150°	3
11	T007	POINT A @ 180°	
12	T008	POINT B @ 210°	4
13	T009	POINT C @ 240°	3
11	T010	POINT A @ 270°	4
12	T011	POINT B @ 300°	4
13	T012	POINT C @ 330°	THRU ITEM 5
21	S001	HEART PT @ @ 0°	
21	S002	HEART PT @ @ 180°	
21	S003	LFS APT PT A @ 0°	
21	S004	LFS APT PT B @ 180°	

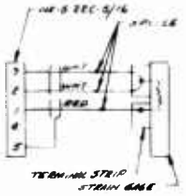

STANDARD - STRAIN GAGE CONNECTOR

A

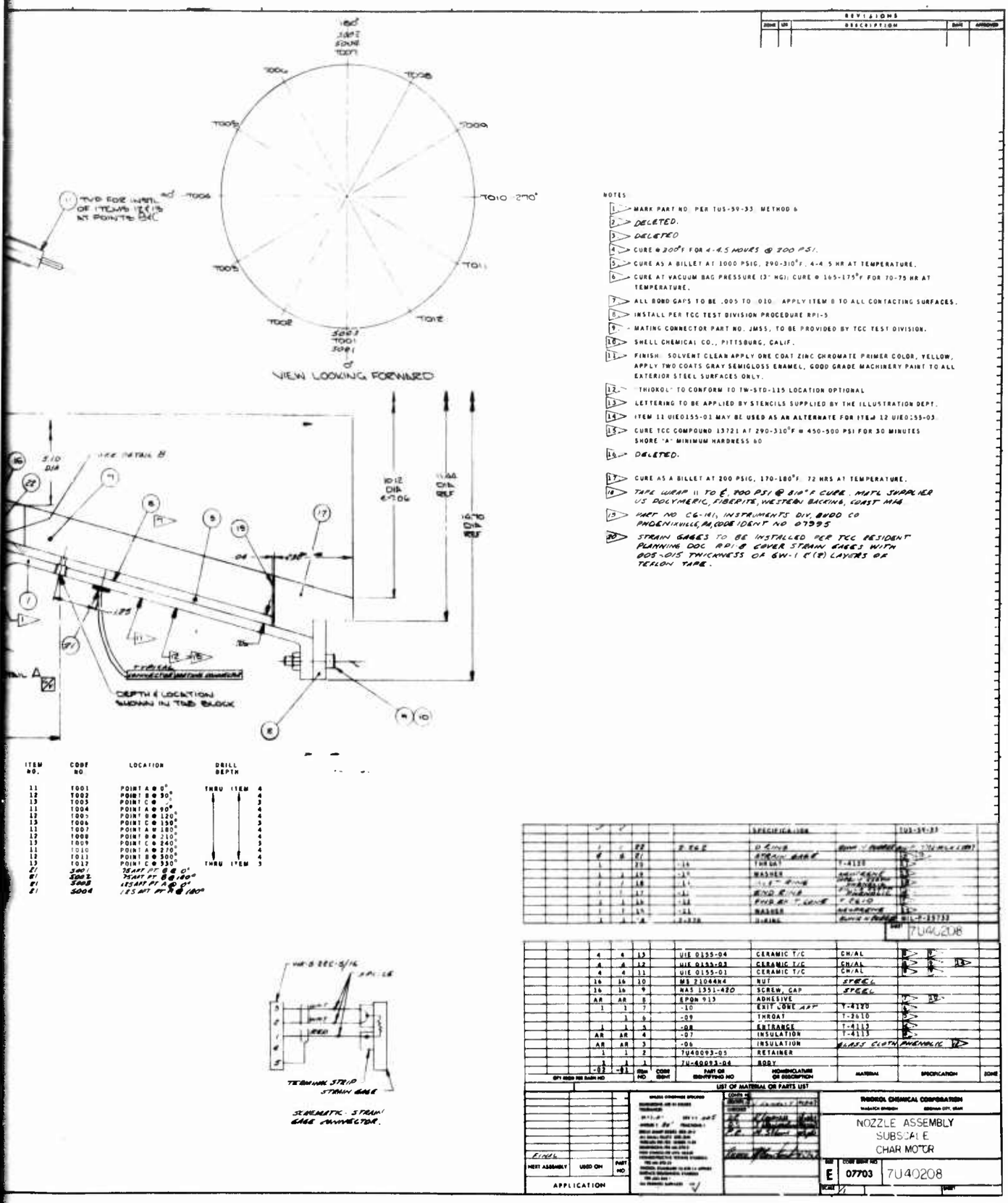

Figure 79. Nozzle Assembly, Subscale Char Motor

B

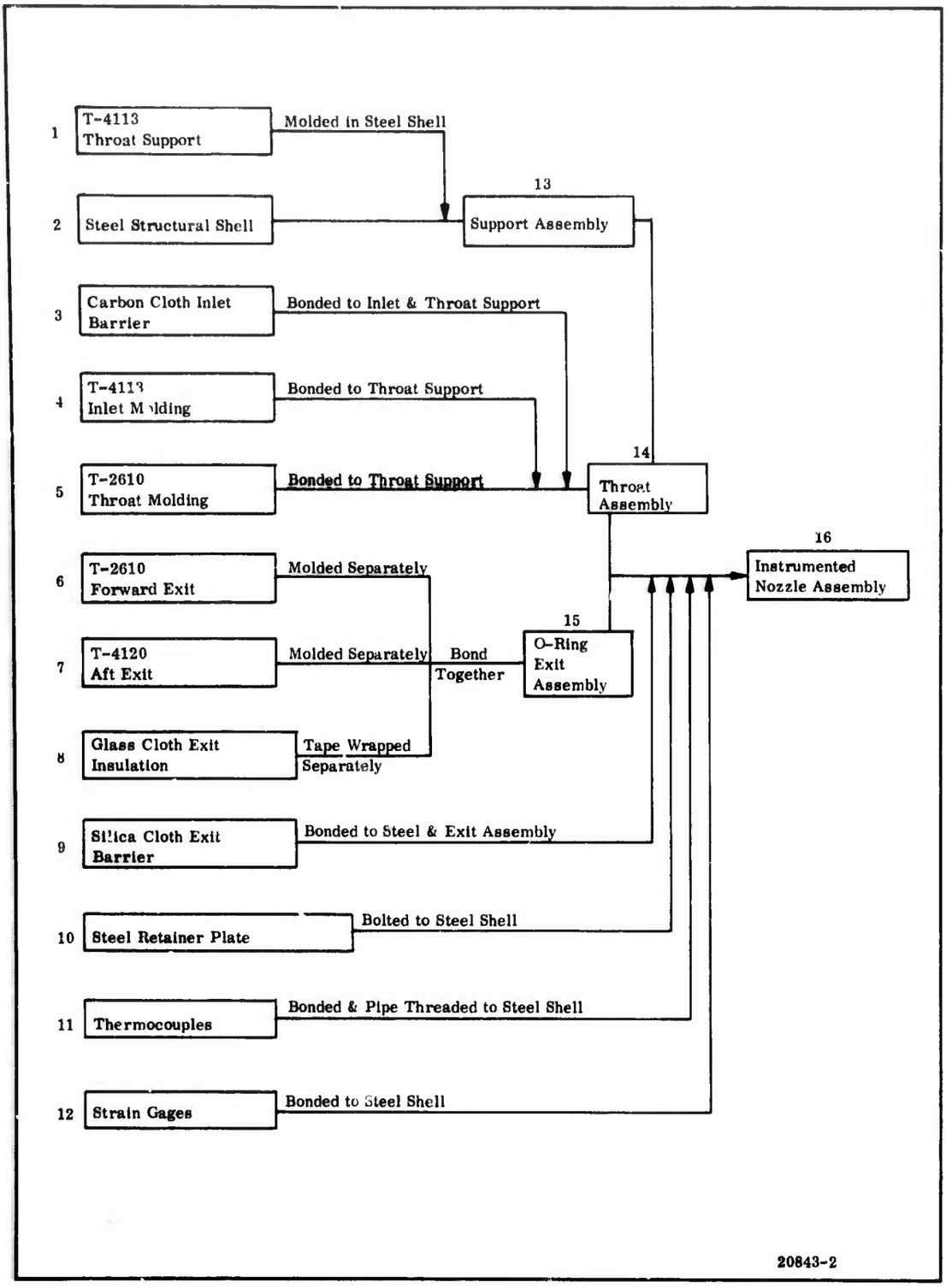

Figure 80. Nozzle No. 5 Components, Materials, and Fabrication Process

The first eight components were machined to fit three subassemblies (support, throat, and exit). The three subassemblies were bonded together, and items 8 thru 12 were added to complete the instrumented nozzle assembly.

3. ANALYSIS

The nozzle analysis includes the determination of an aerodynamic nozzle contour, heat transfer coefficients, material properties, thermodynamic nozzle wall thermal gradients, and structural thermomechanical stresses.

The results for each analytical effort are summarized briefly with comments limited to significant details. The nozzle design criteria used for the analysis follow.

Web time (sec)	60
Throat diameter (in.)	3.80
Exit cone expansion ratio	7.06
Propellant	LPC 556
Average web pressure (psia)	700
Maximum expected operating pressure (psia)	800

The average (eroded and uneroded), two dimensional, coldwall heat transfer coefficients for the nozzle design (illustrated in Figure 79) are shown in Figures 81 and 82 (ref Appendix A, Sections B, D, and E).

The LCCM material thermal and mechanical properties, shown in Figures 83 thru 85, are based on room temperature data that were projected to 6,000°F based on experience with graphite and graphite phenolic material properties.

The two dimensional thermal gradients without erosion depths were predicted for the inlet (A), throat (B), and exit (C) planes (Figures 86 thru 89) without carbon cloth in the inlet (A), and with T-4120 instead of T-2610 in the forward exit cone (C). The thermal gradients were projected to 40 and 60 sec after ignition for the longest scheduled burning time in the program at an average web pressure of 700 psia. The steel shell and bondlines are shown at room temperature, except at the exit cone liner bond. While the exit cone bond is heated by T-4120, retention is still maintained by the end silica cloth ring and steel retainer plate.

A symmetrical, two dimensional, thermal mechanical stress computer program was used to analyze the inlet and throat planes using the available material properties, pressures, and wall thermal gradients. The thermal mechanical stresses at t = 60 sec in two planes are plotted vs distance from the inside wall, and the factors of safety are calculated from the actual and allowable stresses (Figures 90 and 91).

Results of a preliminary thermal mechanical stress analysis, conducted at the exit cone section (C), is shown in Table XXXII.

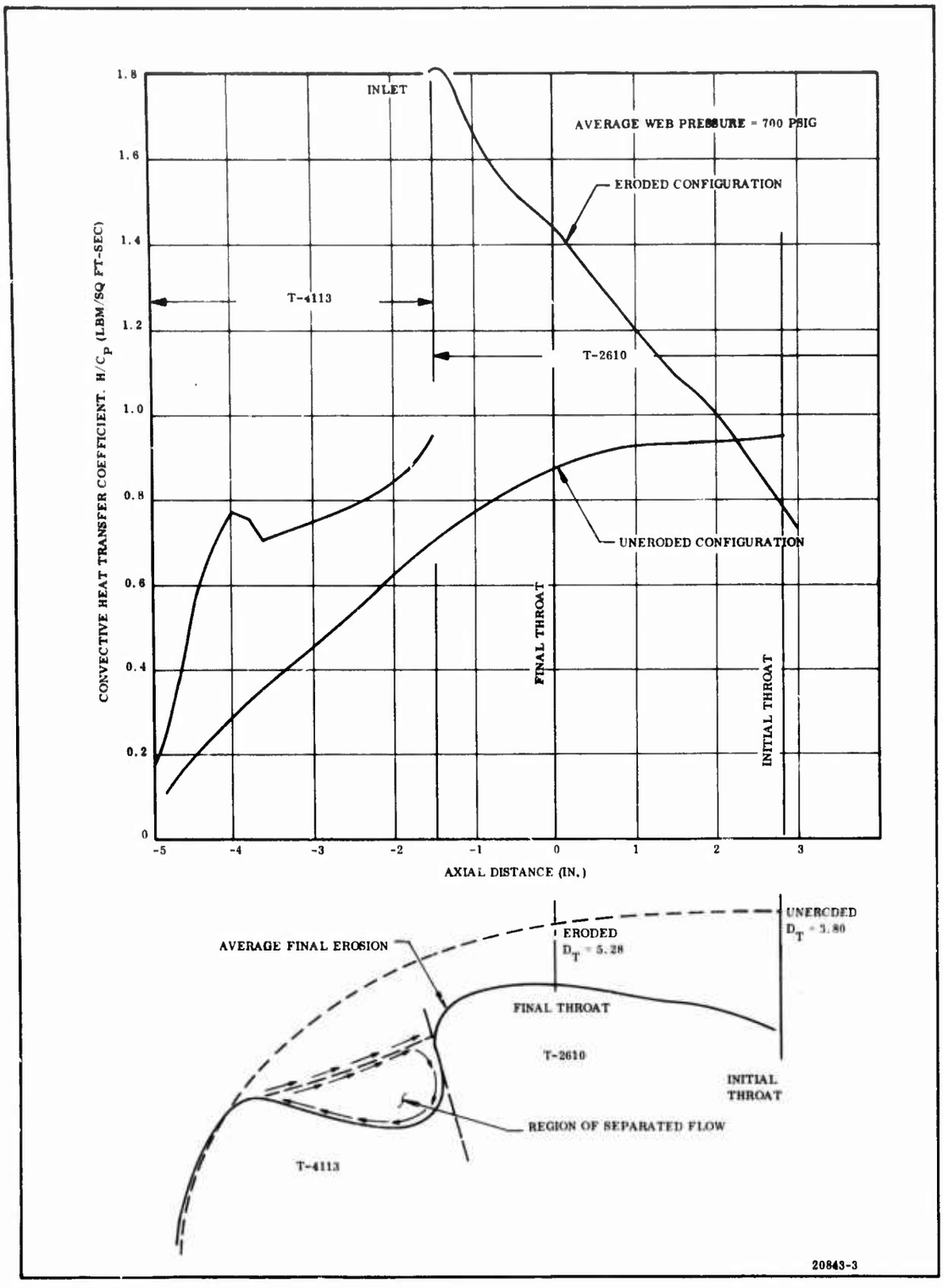

Figure 81. Subscale Char Motor No. 5 Convective Heat Transfer Coefficient vs Axial Location

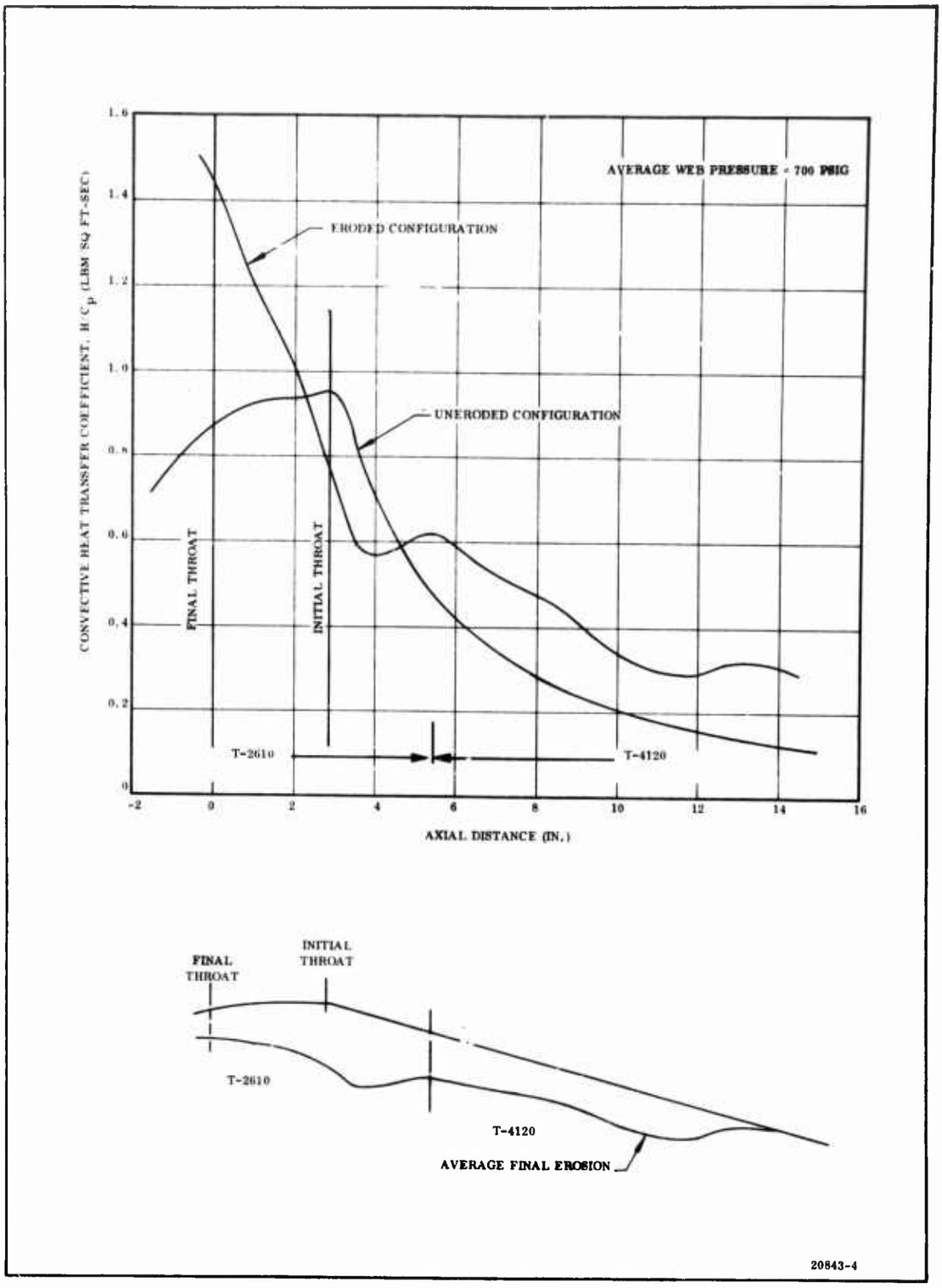

Figure 82. Subscale Char Motor No. 5, Throat and Exit Cone Convective Heat Transfer Coefficient

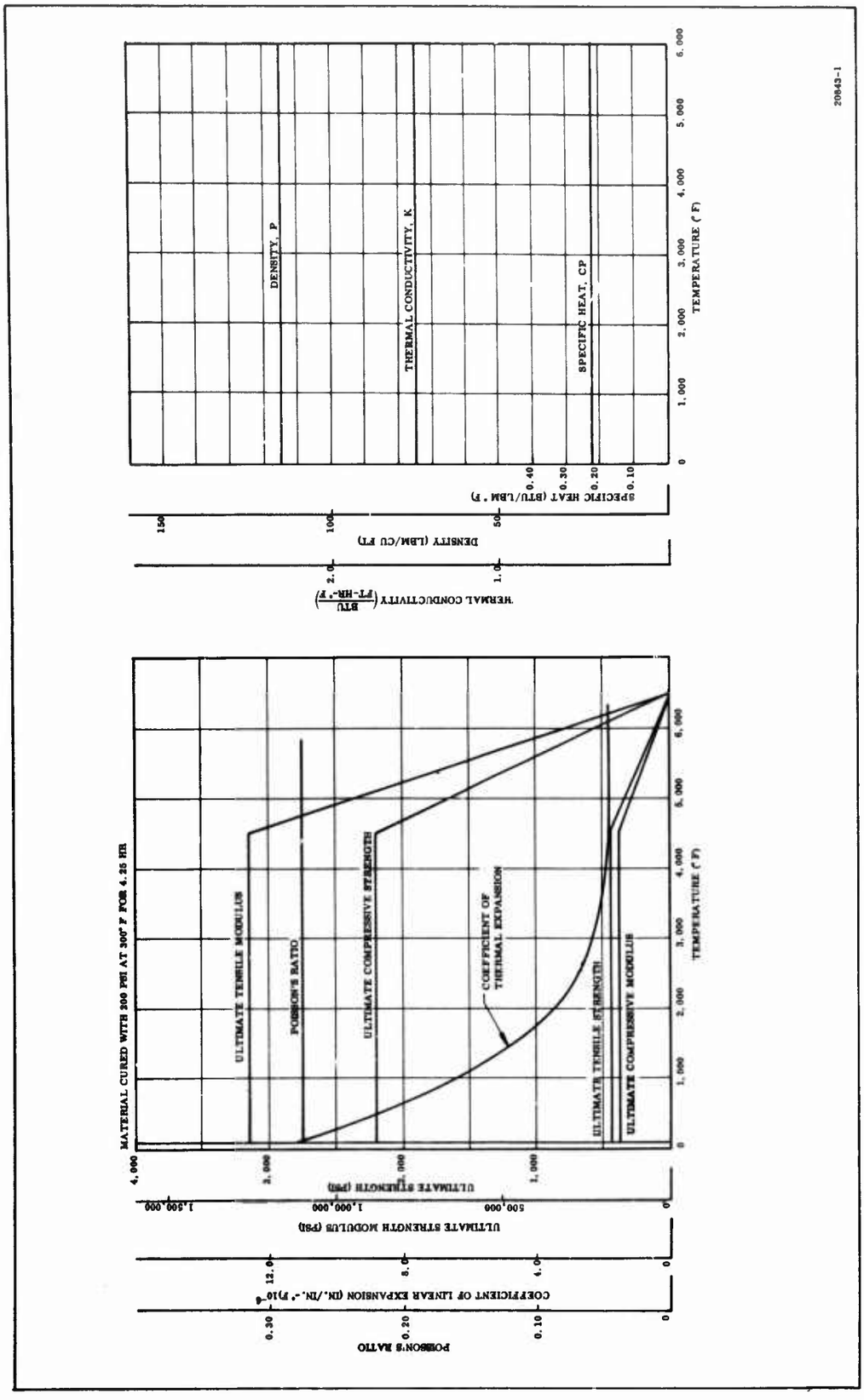

Figure 83. Estimated Mechanical Properties, T-4113

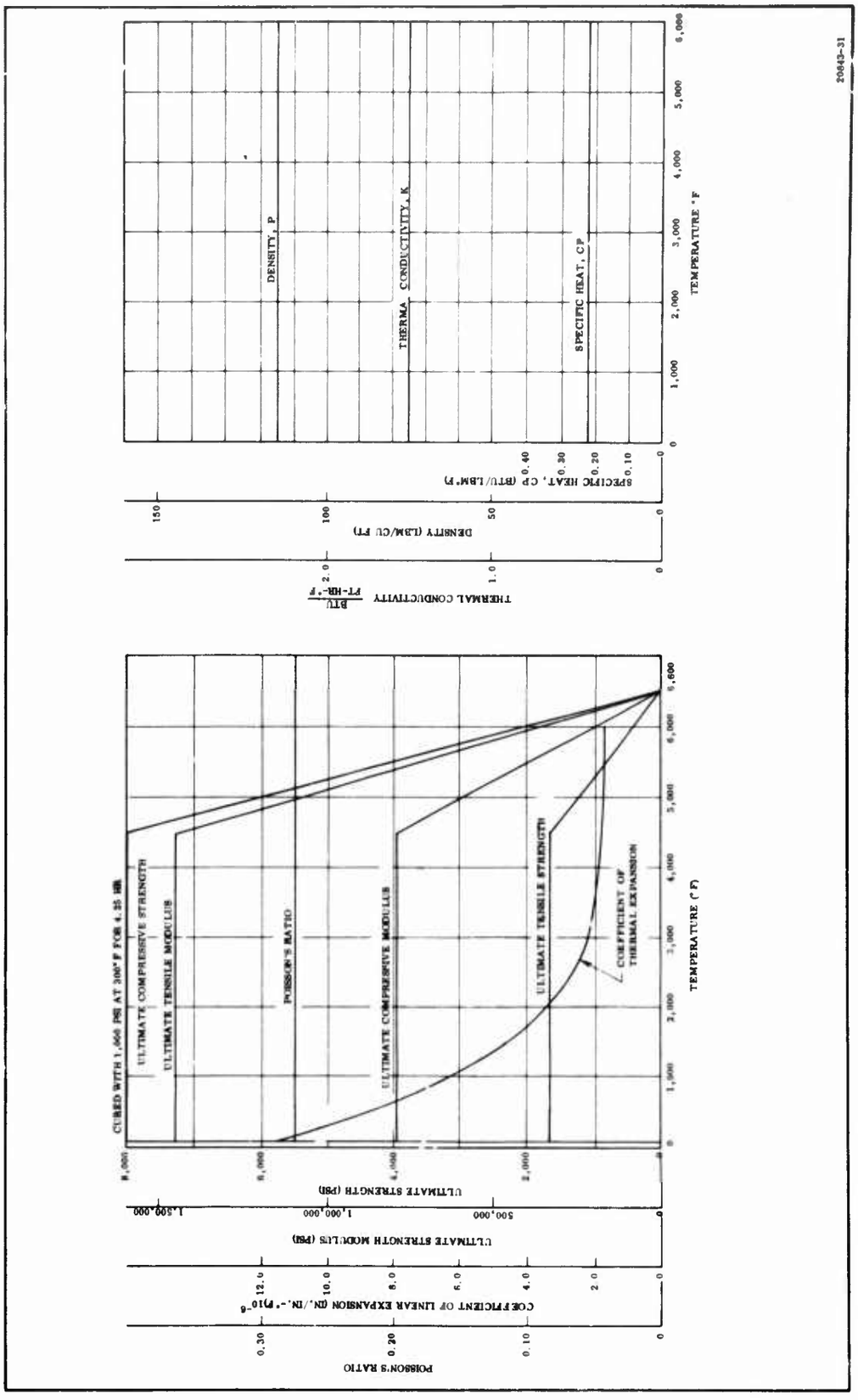

Figure 84. Estimated Mechanical Properties, T-2610

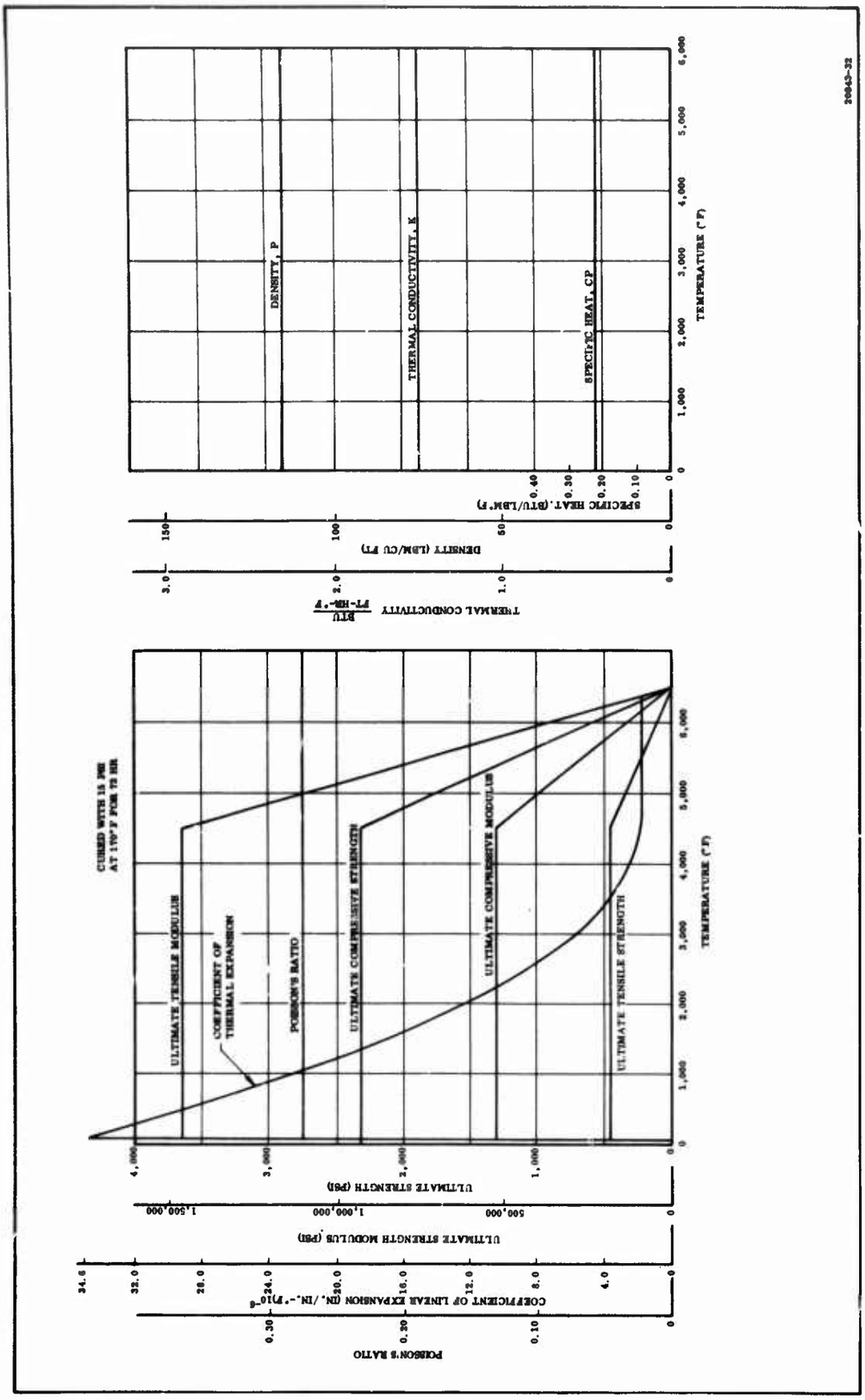

Figure 85. Estimated Mechanical Properties, T-4120

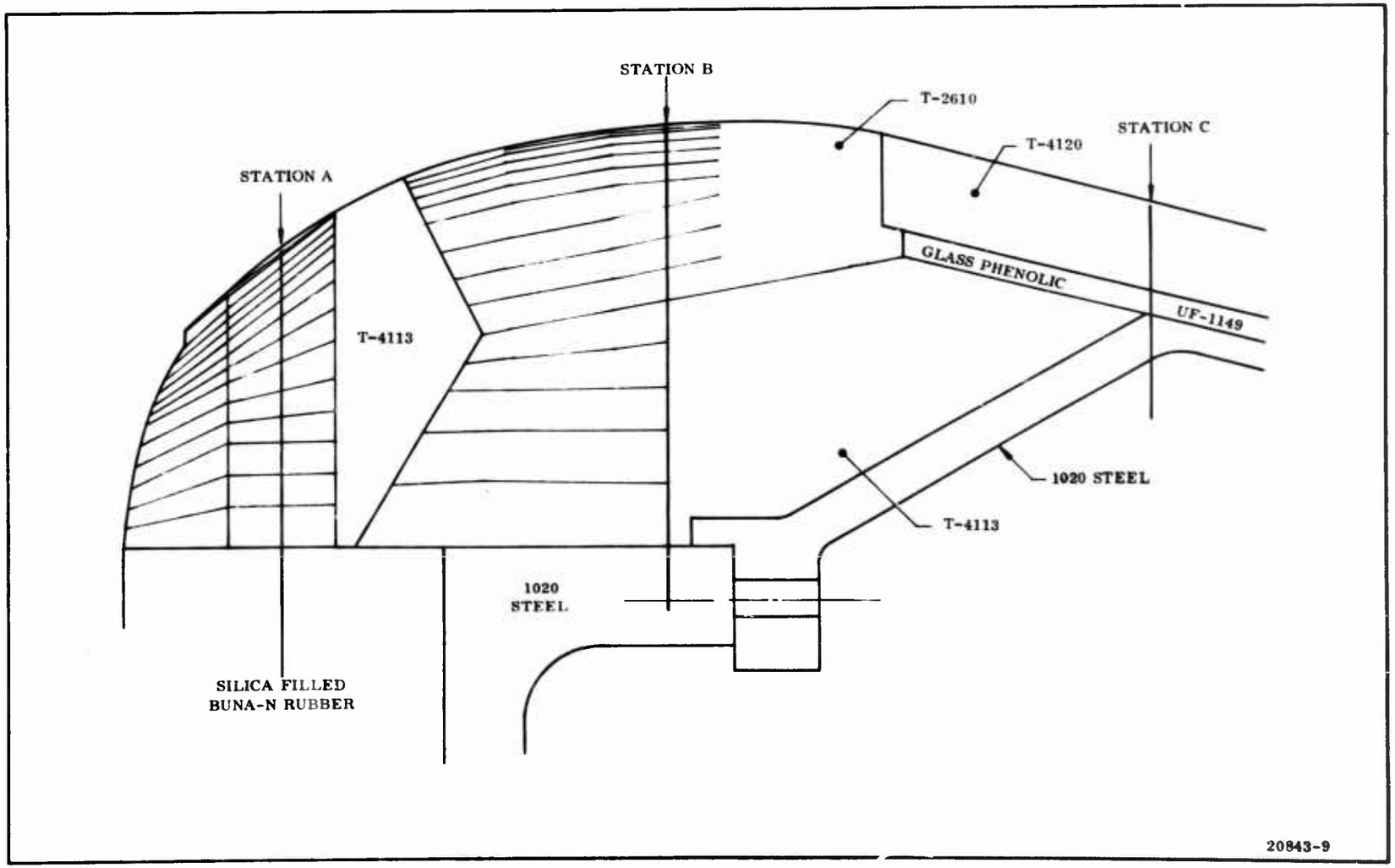

Figure 86. Thermal Gradient Planes

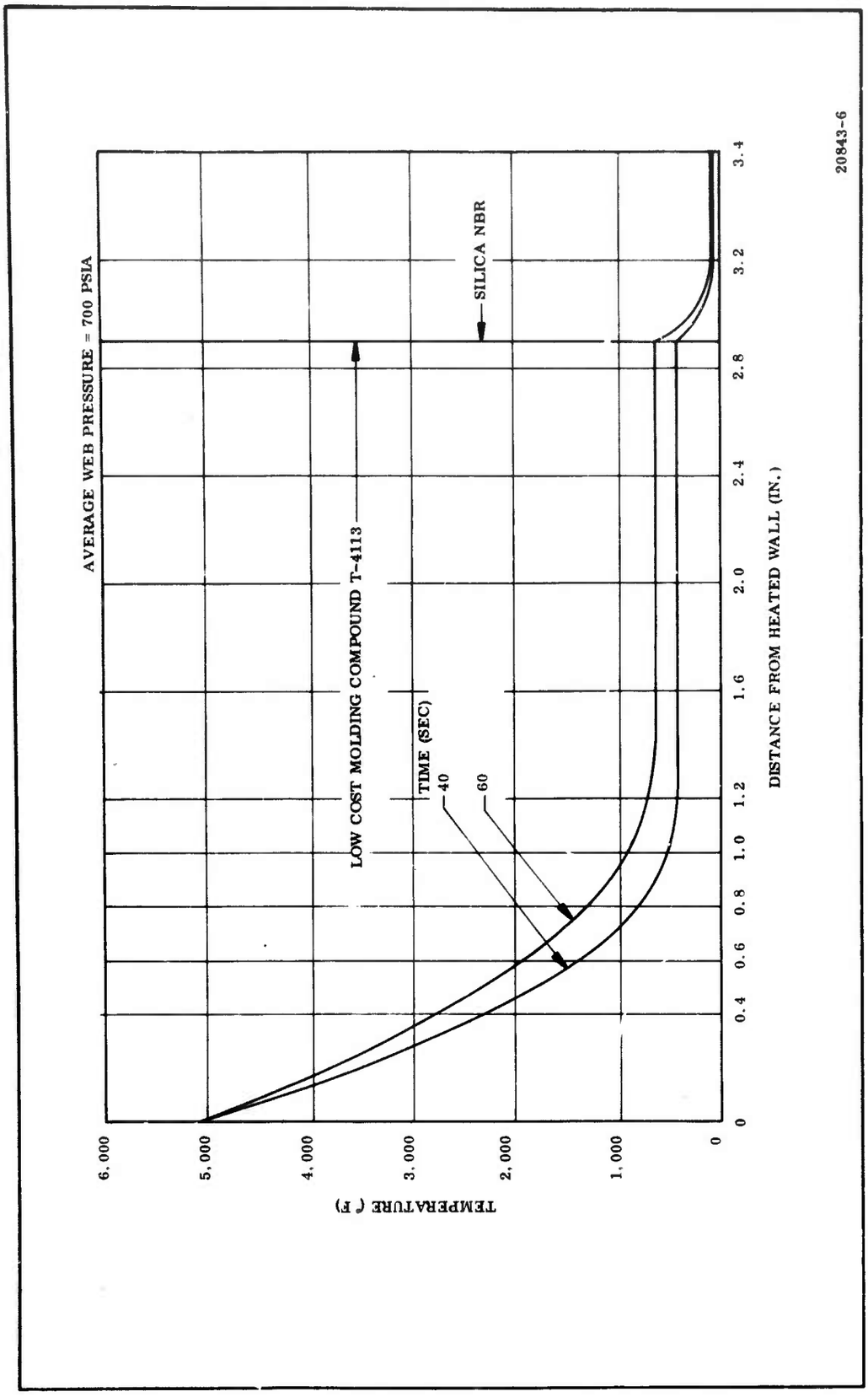

Figure 87. Temperature Gradients (Nose Section) vs Distance from Heated Wall

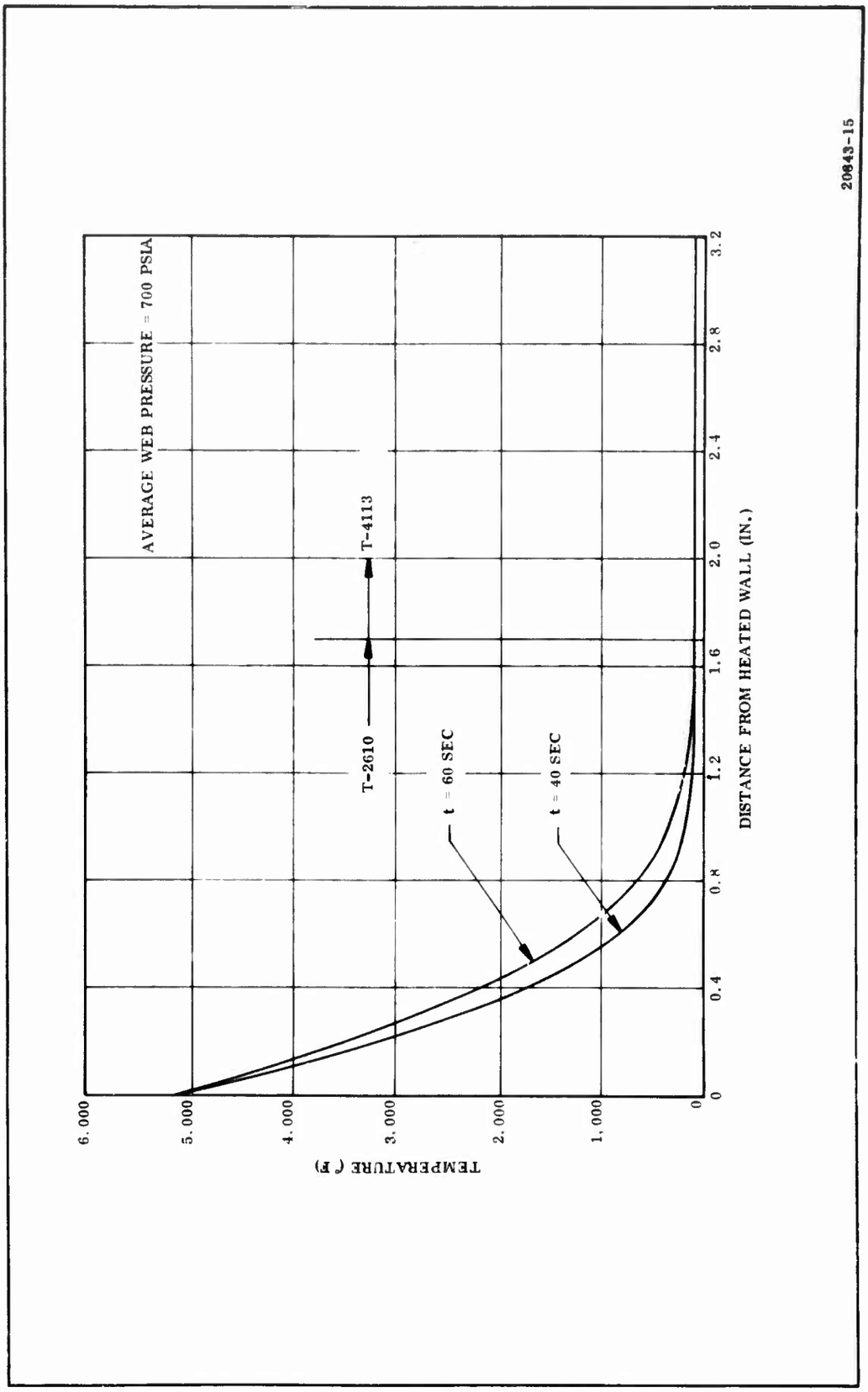

Figure 88. Temperature Gradients (Throat Section) ve Distance from Heated Wall

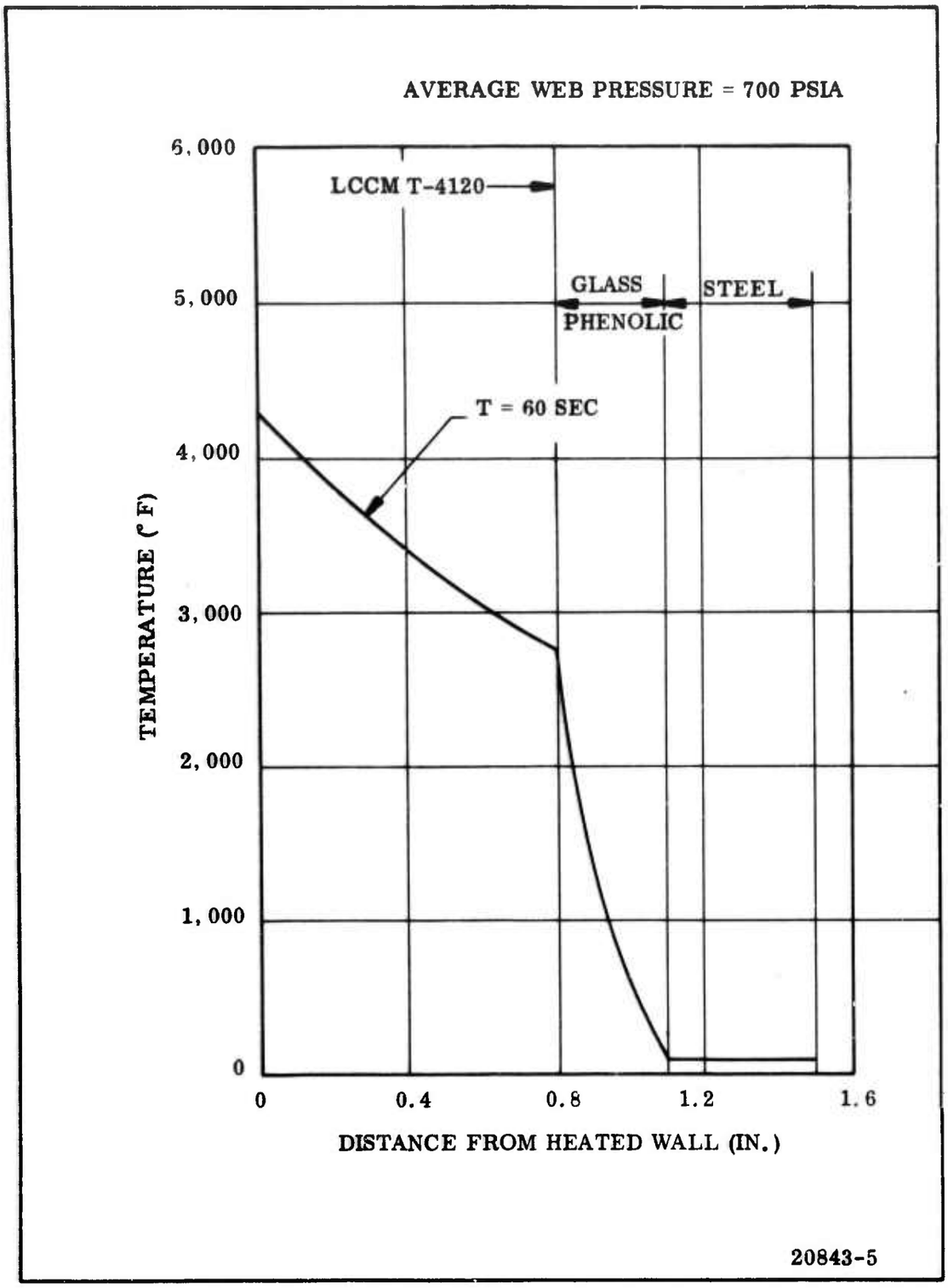

Figure 89. Temperature Gradients (Exit Section) vs Distance from Heated Wall

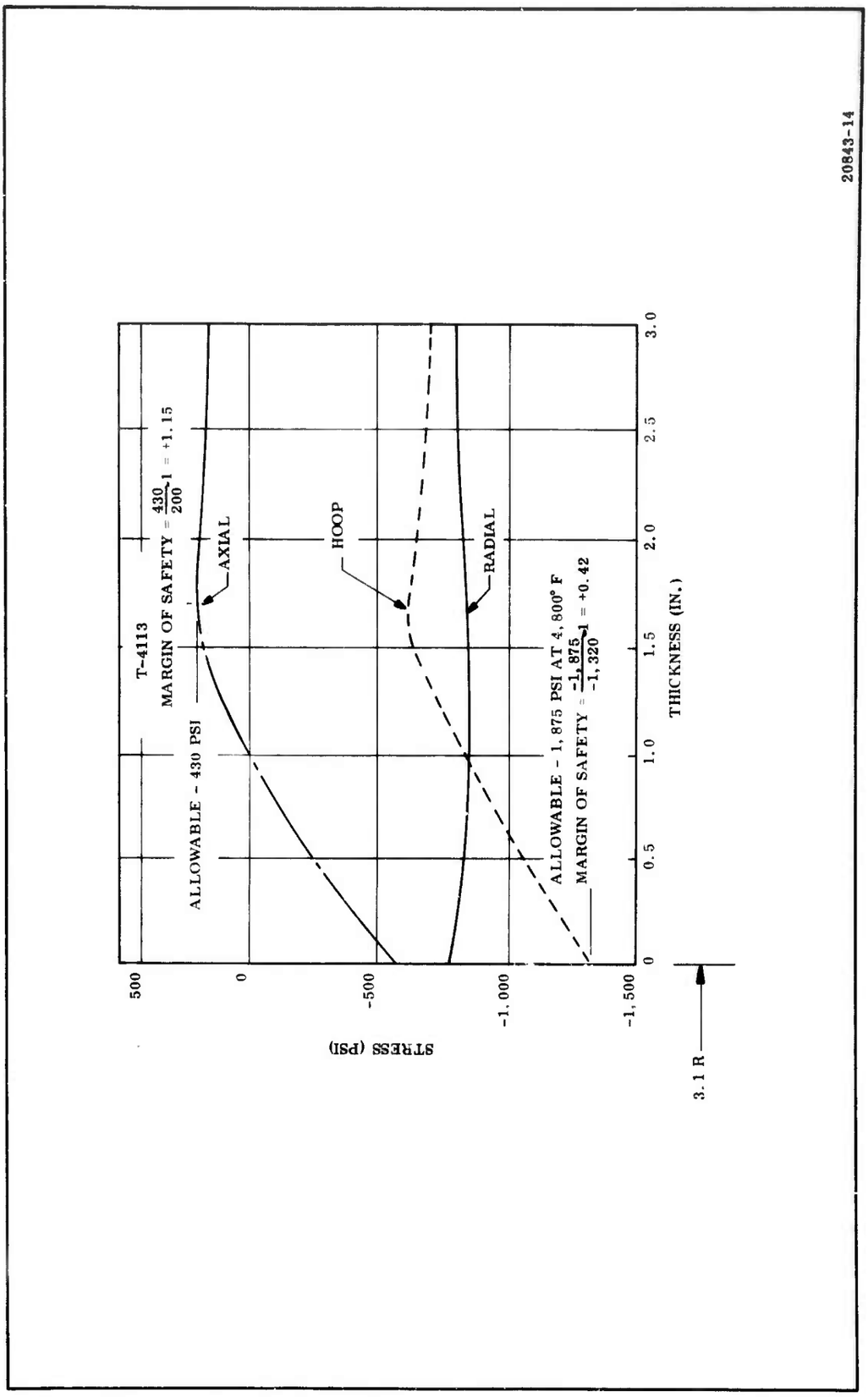

Figure 90. Thermal Mechanical Stresses, Station A

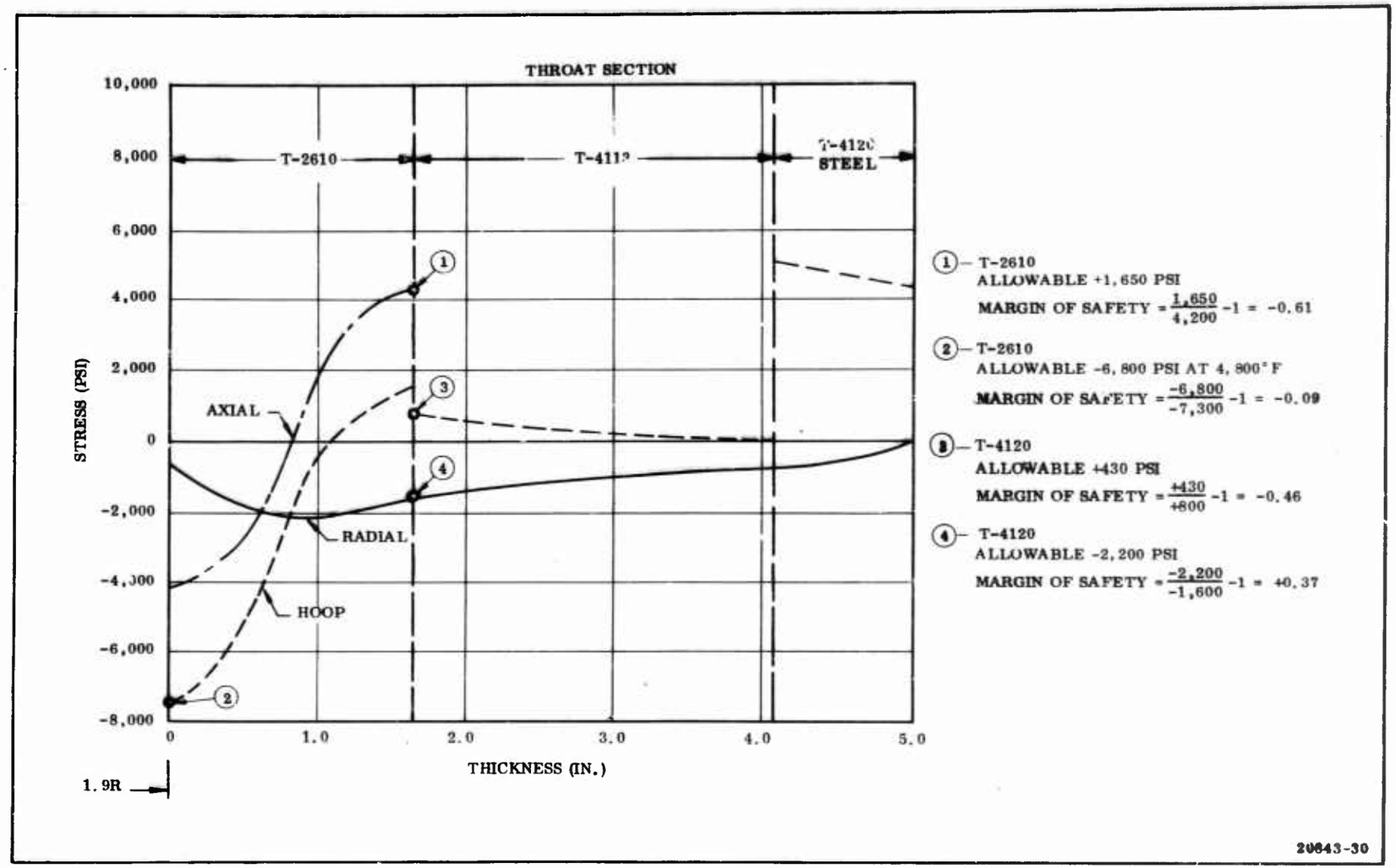

Figure 91. Thermal Mechanical Stresses, Station B

TABLE XXXII

THERMAL MECHANICAL STRESS ANALYSIS

Exit Cone Station C
Thermal Stress

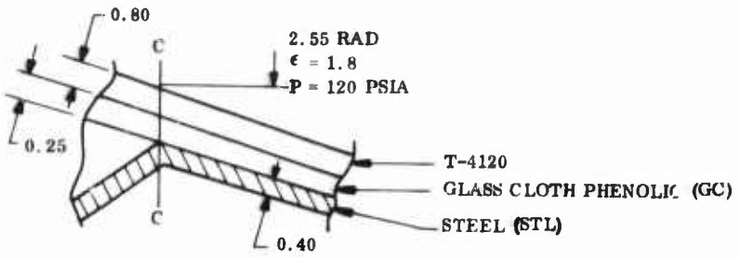

t = 60 sec

P_{max} = 800 psia

Material	Elastic Modulus $E(10^6)$ (psi)	Coefficient Thermal Expansion $\alpha(10^{-6})$ (in./in.°F)	ΔT Temperature Rise (°F)	Thickness (in.)	Allowable Stress (psi)	Actual Stress (psi)	Margin of Safety
T-4120	0.5	3.6	3,525 (4,300 / 2,750)	0.80	2,325C	4,870C	-0.52
Glass Cloth	0.5	0.2	1,425 (2,750 / 100)	0.25	$2,000^{T}_{C}$	1,630T	+0.22
1020 Steel	29.0	6.1	0	0.40	55,000T	9,480T	+ High

1 Additive Concentric Hoop Stress $\sigma_{LCCM}(0.80) + \sigma_{GC}(0.25) + \sigma_{STL}(0.40) = PR = 120(2.55) = 306$

2 Equal Concentric Radial Deflection $\frac{\Delta R}{R} = \left(0.013 + \frac{\sigma_{LCCM}}{0.50 \times 10^6}\right) = \left(0 + \frac{\sigma_{GC}}{0.50 \times 10^6}\right) = \left(0 + \frac{\sigma_{STL}}{29 \times 10^6}\right)$

$\sigma_{GC} = 0.172\,\sigma_{STL}$

$\sigma_{LCCM} = -0.013(0.50 \times 10^6) + 0.172\,\sigma_{STL} = -6,500 + 0.172\,\sigma_{STL}$

3 Sub 2 into 1

$0.80(-6,500 + 0.172\,\sigma_{STL}) + 0.25(0.172\,\sigma_{STL}) + 0.40\,\sigma_{STL} = 306$

$-5,200 + 0.138\,\sigma_{STL} + 0.043\,\sigma_{STL} + 0.40\,\sigma_{STL} = 306$

$0.581\,\sigma_{STL} = +5,506$

$\sigma_{STL} = +9,480$ psi

4 Sub 3 into 2

$\sigma_{GC} = 0.172(+9,480) = +1,630$ psi

$\sigma_{LCCM} = -6,500 + 0.172(+9,480) = -6,500 + 1,630 = -4,870$ psi

5 Sub 4 into Table for Margin of Safety = $\frac{\text{Allowable Stress}}{\text{Actual Stress}} - 1$

With the existing material properties and no predicted erosion depth, the margins of safety for the throat, inlet, and exit at a maximum expected operating chamber pressure of 800 psia are indicated as follows:

Stress Margins of Safety

Section	T-4120	T-4113	T-2610	Glass	Steel
Inlet	--	+0.42 Hoop Compressive Stress	--	--	--
Throat	--	-0.46 Hoop Tensile Stress	-0.61 Axial Tensile Stress	--	+ High Hoop Tensile Stress
Exit	-0.52 Hoop Compressive Stress	--	--	+0.24 Hoop Tensile Stress	+ High Hoop Tensile Stress

The negative stress margins of safety are at best, in this early development of the material processing and the mechanical thermal properties, indications of material acceptability and must be compared with strain gage and thermocouple data and test performance to insure prediction accuracy. The negative stress margins indicate that multiple material retention methods are required in addition to extensive backup standard reinforced plastic insulation materials to insure the integrity of the nozzle.

The nozzle and closure structural shells were analyzed for the average web pressure of 700 psia with a discontinuity computer analysis using short symmetrical free bodies which provided the stress and margins of safety shown in Figure 92. All margins of safety are positive and satisfactory.

4. INSPECTION

Visual and photographic inspections of the postfired nozzle, before and after static test, indicate high erosion in the inlet, throat, and forward exit, with localized severe erosion and chunking upstream (Figures 93, 94 and 95) and downstream of the throat (Figures 96, 97 and 98).

Figure 95 shows the start of the gas leak under the throat in the T-4113 inlet material while Figure 96 shows venting of the gas leak passage along the 277 deg plane. The inlet material (Figures 94 and 95) was eroded and gouged deeply for 360 deg, with the exit cone (Figure 96) affected for only 180 deg between the 30 and 210 deg planes.

Figures 93 and 94 show the nozzle to closure interface, potted over with an insulation material, and the entrance to the two burst disc assemblies before and after the static test.

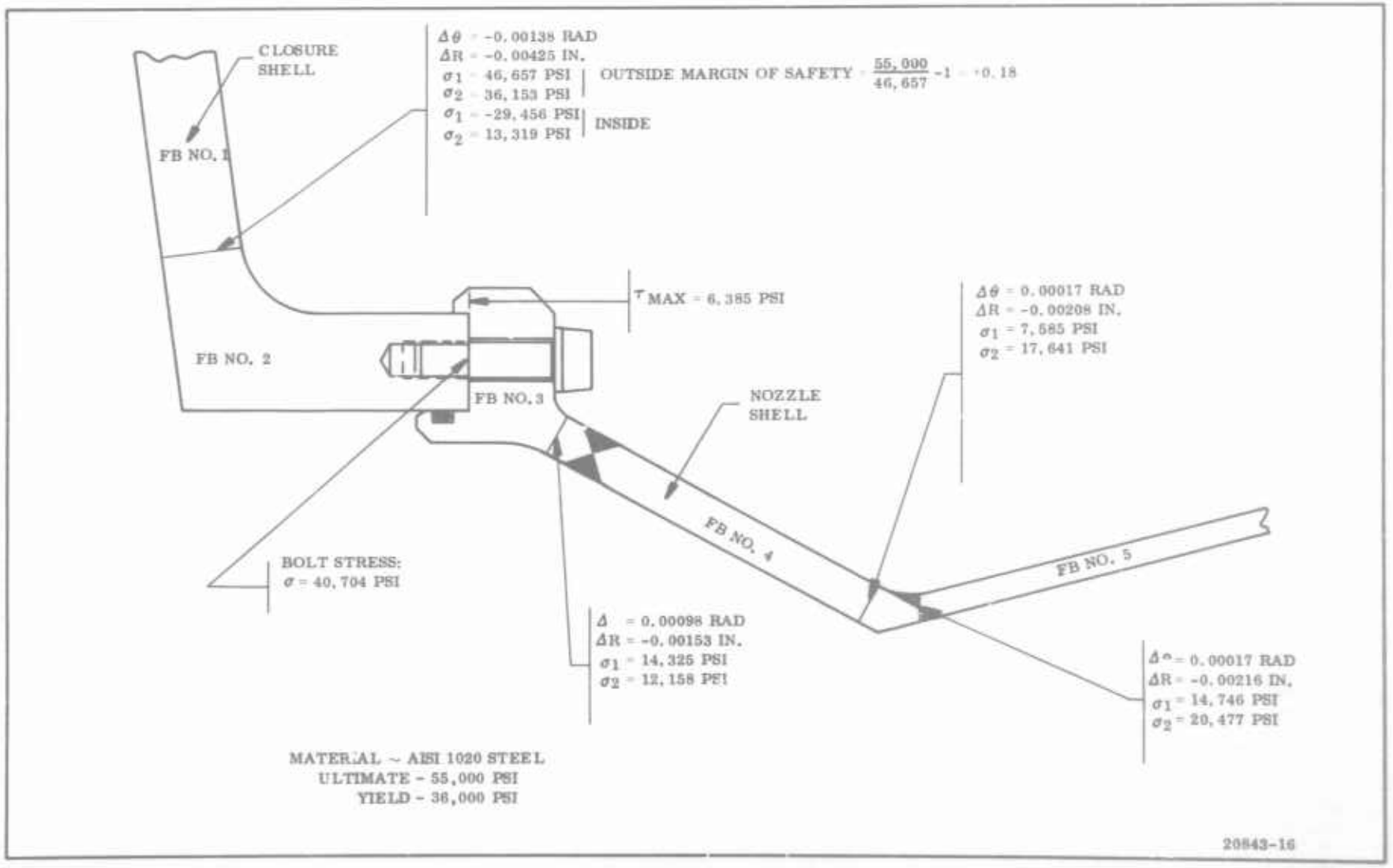

Figure 92. Housing Summary Analysis

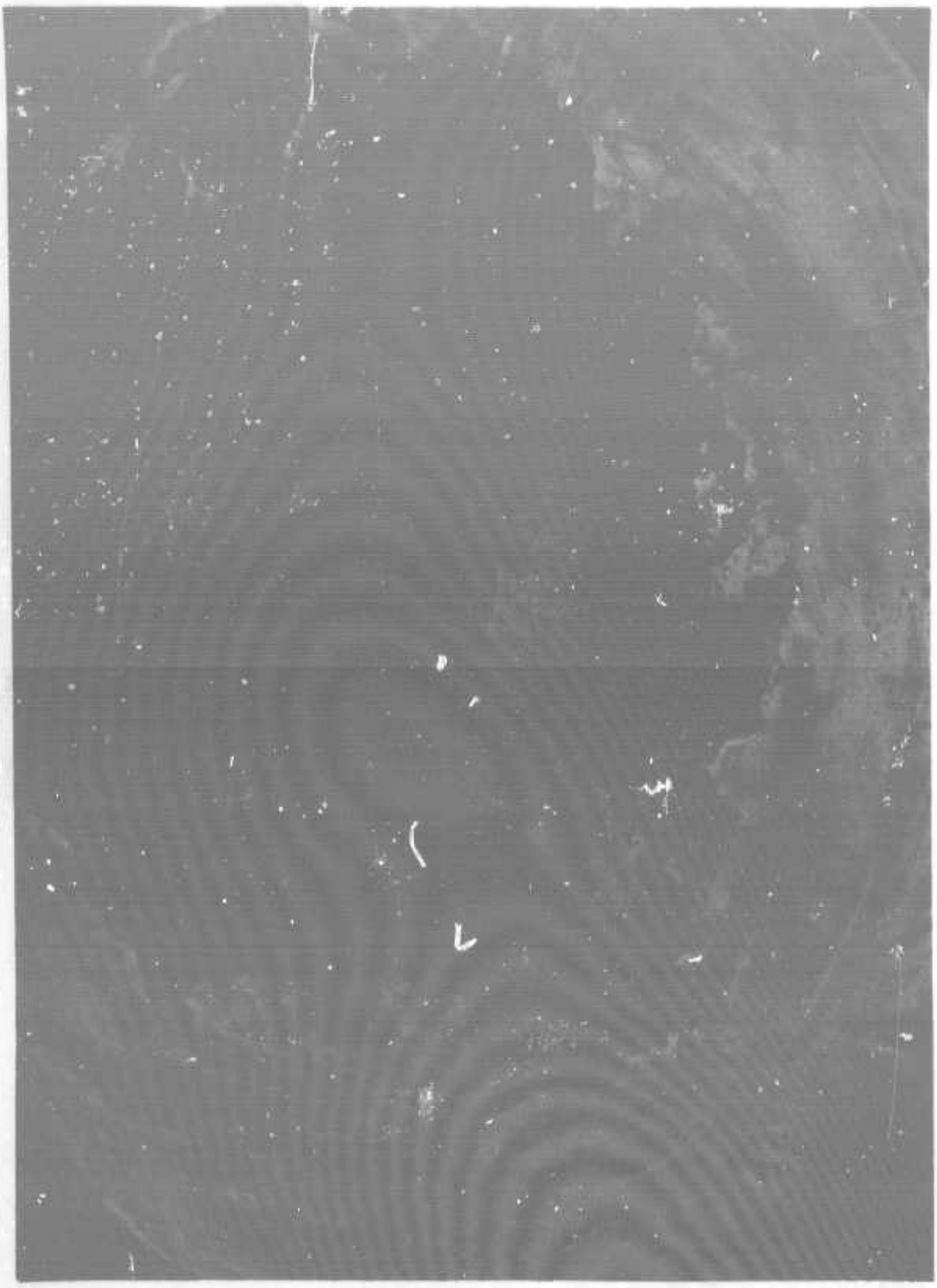

Figure 93. Nozzle No. 5 Inlet, Pretest

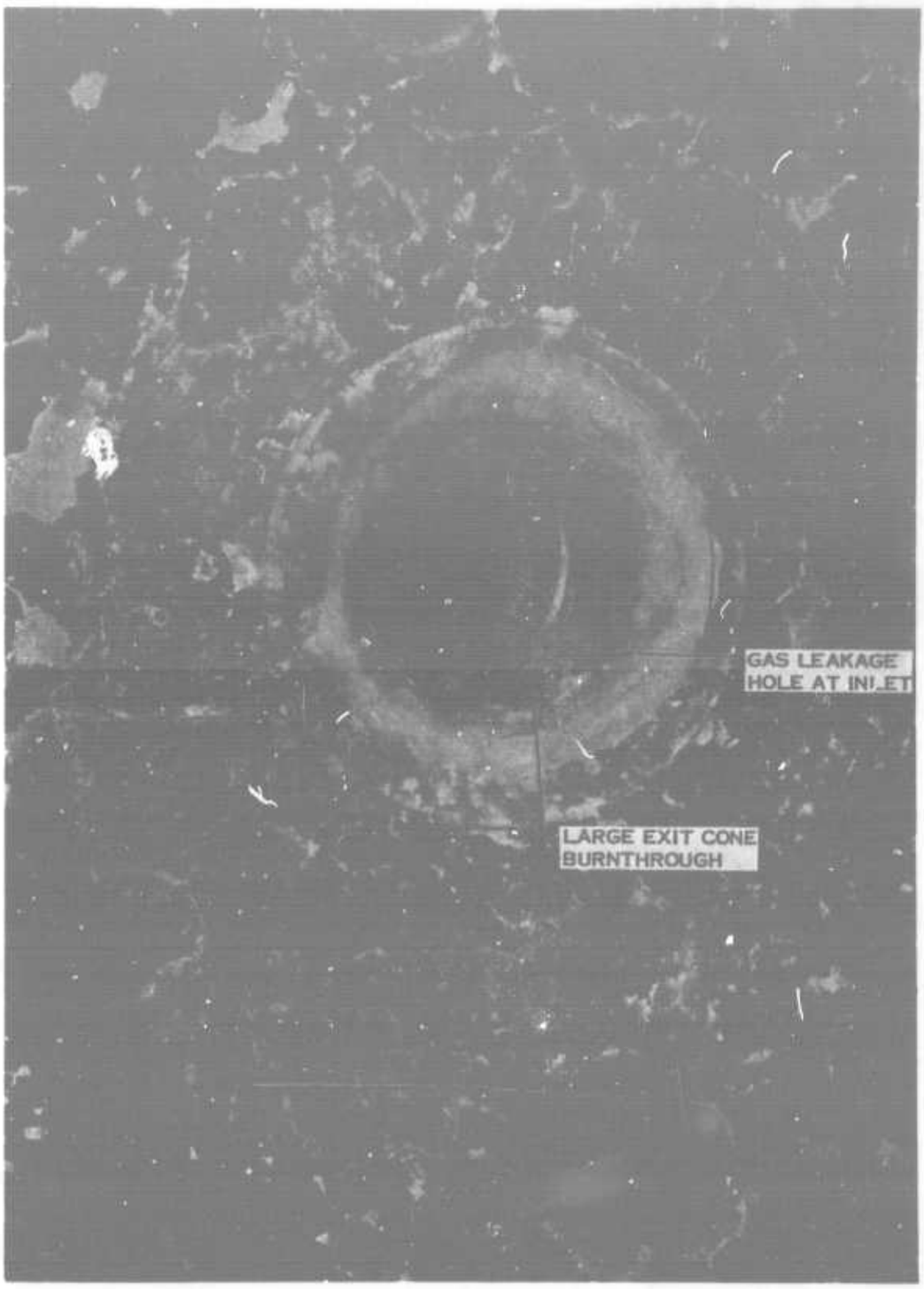

Figure 94. Nozzle No. 5 Inlet, Postfired Condition

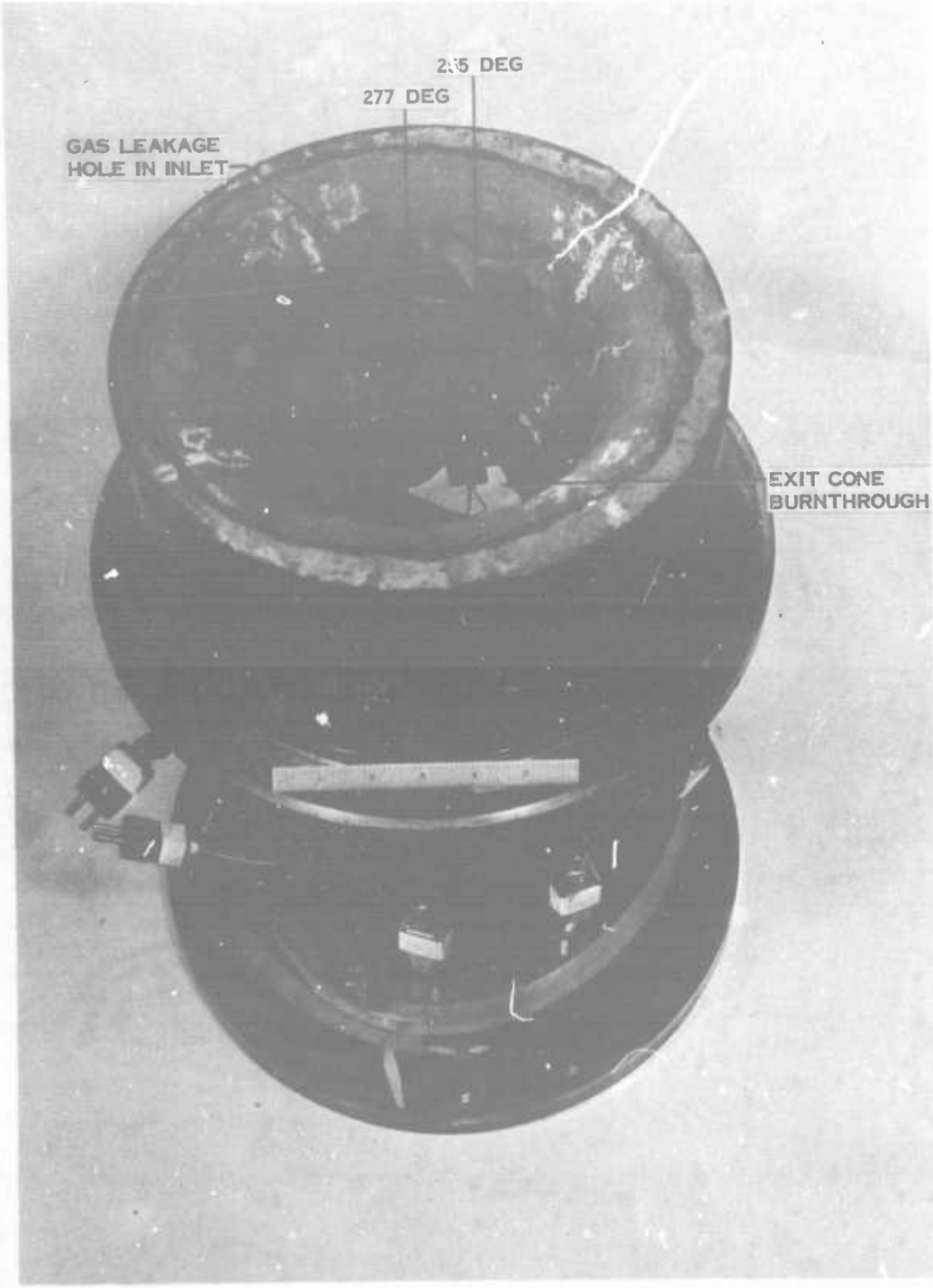

Figure 95. Nozzle No. 5 Postfired Condition

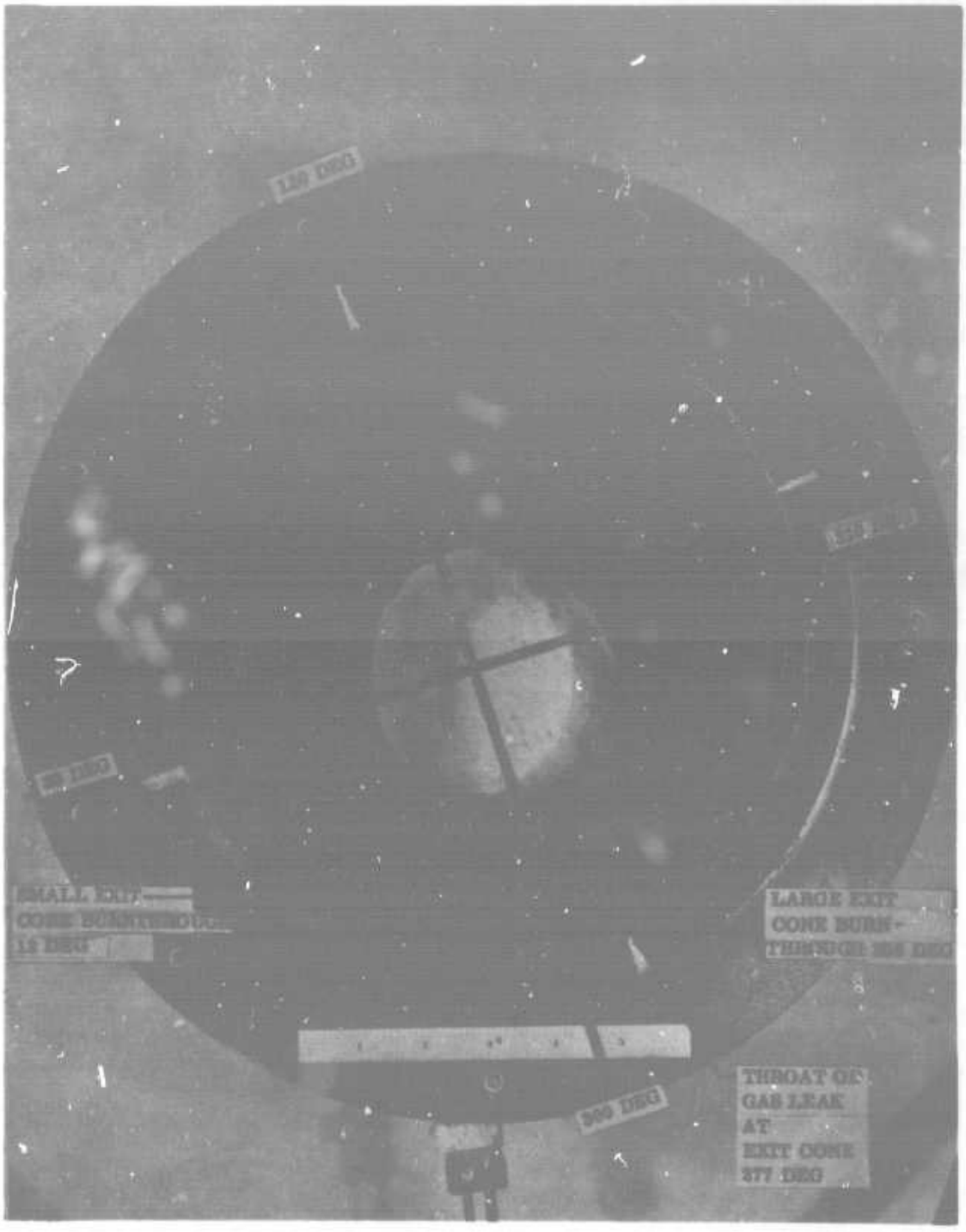

Figure 96. Nozzle No. 5 Exit Cone, Postfired Condition

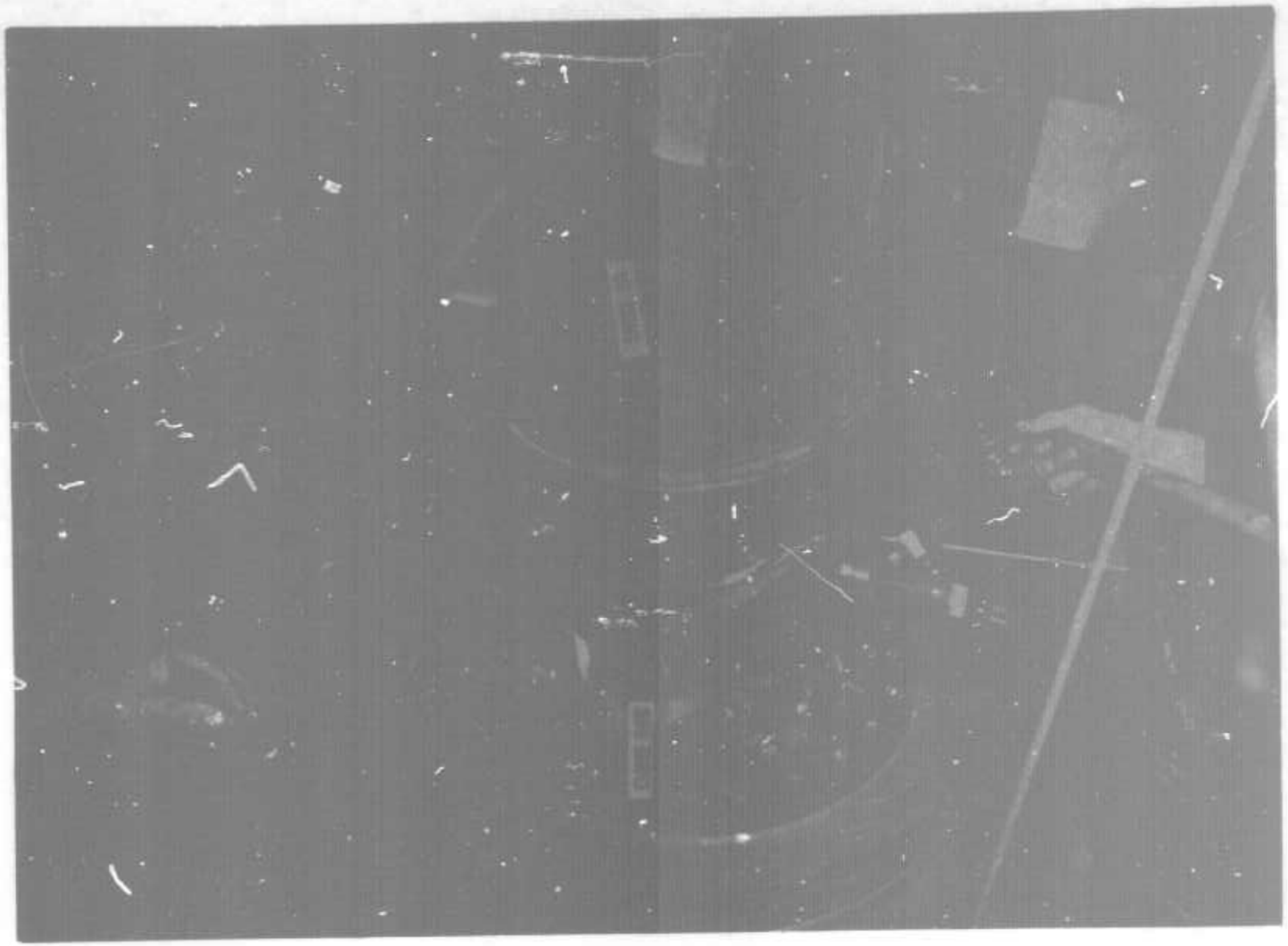

Figure 97. Nozzle No. 5, Large Exit Cone Burnthrough

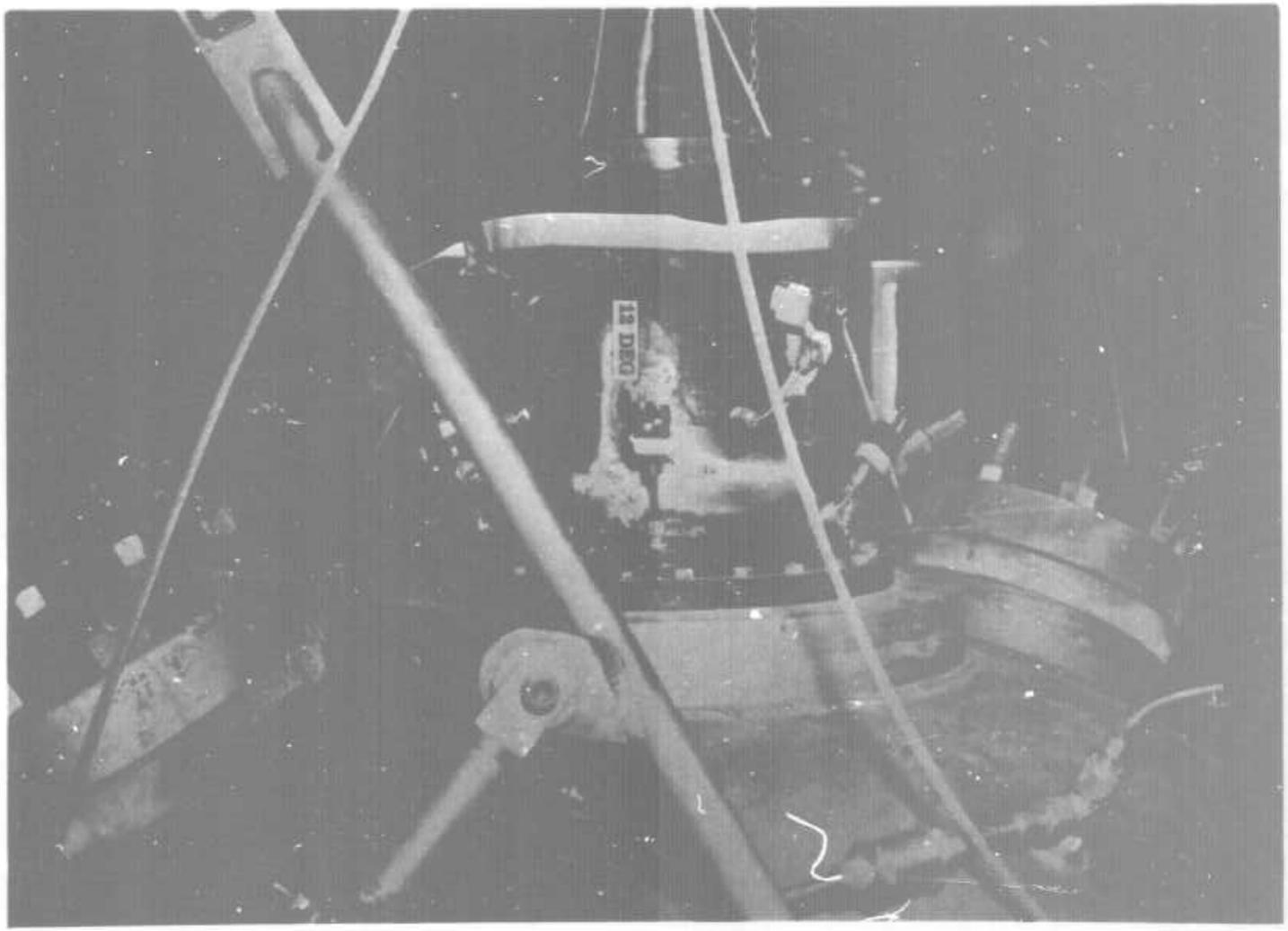

Figure 98. Nozzle No. 5, Small Exit Cone Burnthrough

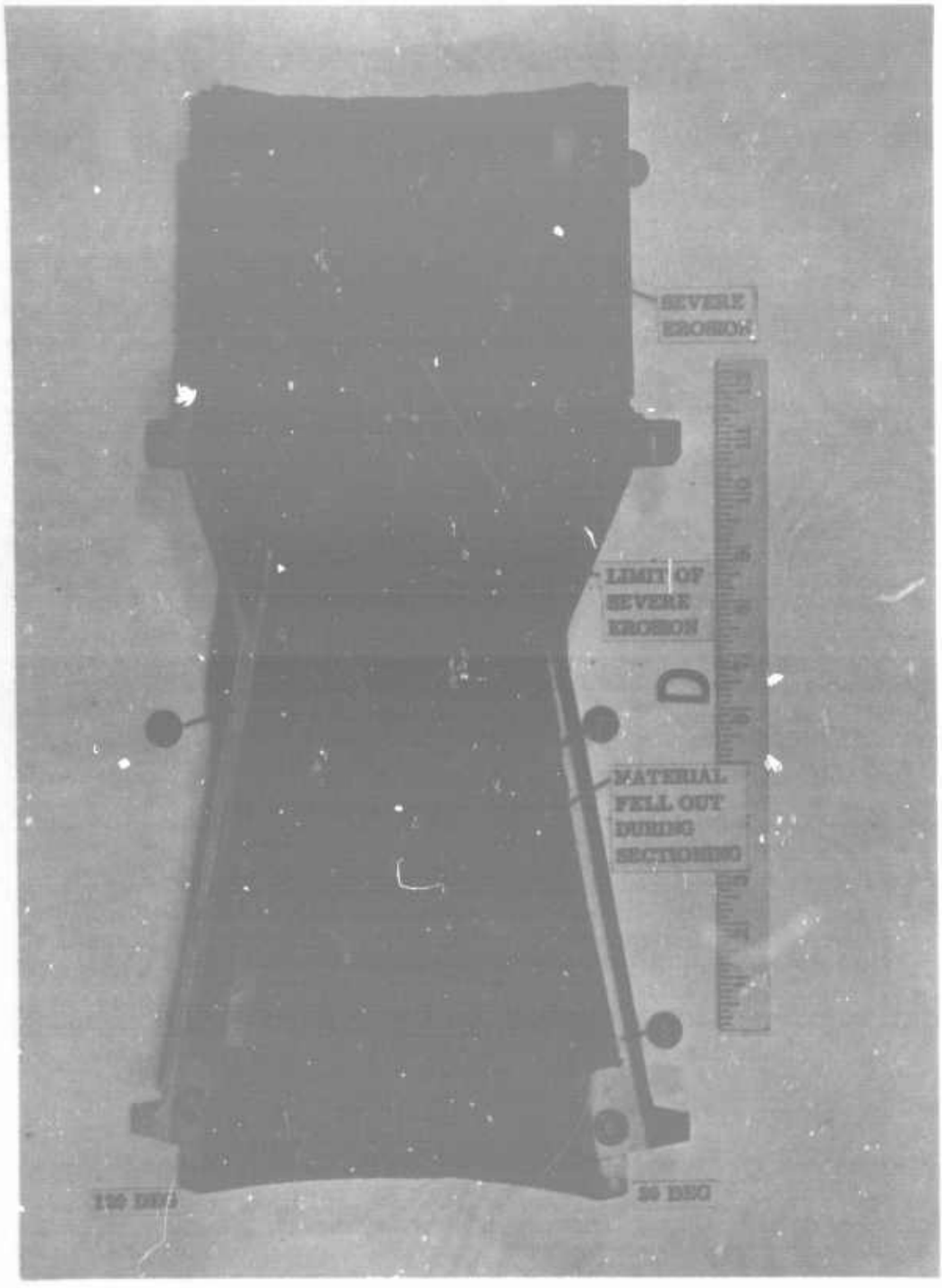

Figure 99. Nozzle No. 5, 30-120 Deg Exit Cone Section

Figures 97 and 98 show two nozzle burnthrough areas at 12 and 255 deg, the two burst disc assemblies, and the special AF material test panel that was tested in the nozzle exhaust plume.

After visual and photographic inspection, the postfired nozzle was cut into four 90 deg segments, as illustrated in Figures 99 thru 102. Inspection of the four segments resulted in the following comments.

Segment	T-4113	Throat and Forward Exit T-2610	Aft Exit T-4120
120 thru 30 deg (Figure 99)	Poor. Severe material erosion close to throat.	Fair. Severe erosion to steel at 30 deg in throat and forward exit. Uniform throat erosion.	Fair. Material fell out during nozzle segmenting at 30 deg. Some spalling of liner. Uniform erosion.
30 thru 300 deg (Figure 100)	Poor. Severe material erosion close to throat.	Poor. Severe aft throat and forward exit erosion and gouging to steel shell. Uniform throat erosion.	Poor. Small steel burnthrough at 12 deg. 4120 liner material gone around hole.
300 thru 210 deg (Figure 101)	Poor. Severe material erosion. Gouging and start of gas leak at 277 deg.	Poor. Severe aft throat and forward exit erosion and gouging to steel shell. Uniform throat erosion.	Poor. Large steel burnthrough at 255 deg. Gas leak at 277 deg.
210 thru 120 deg (Figure 102)	Poor. Severe material erosion close to throat.	Fair. High throat erosion.	Fair. Severe erosion to insulation at 210 deg. Some spalling of liner. Uniform erosion.

Generally, the T-4113 inlet material was severely and nonuniformly eroded close to the throat ring ($\epsilon = 2.0$) in all four segments, and was severely gouged at 277 deg where a gas leak started under the throat inlet.

The throat and forward exit material (T-2610) was eroded uniformly, with severe aft throat and forward exit erosion and gouging to the steel shell for half of the circumference in the two 90 deg segments (30 to 300 deg and 300 to 210 deg).

The eroded passage under the throat at 277 deg, as shown in Figures 103 and 104, allowed high pressure exhaust gas to leak through the throat to exit cone joint and create hot gas injection 0.70 in. downstream of the throat and at an area ratio of $\epsilon = 1.2$ (Figure 105).

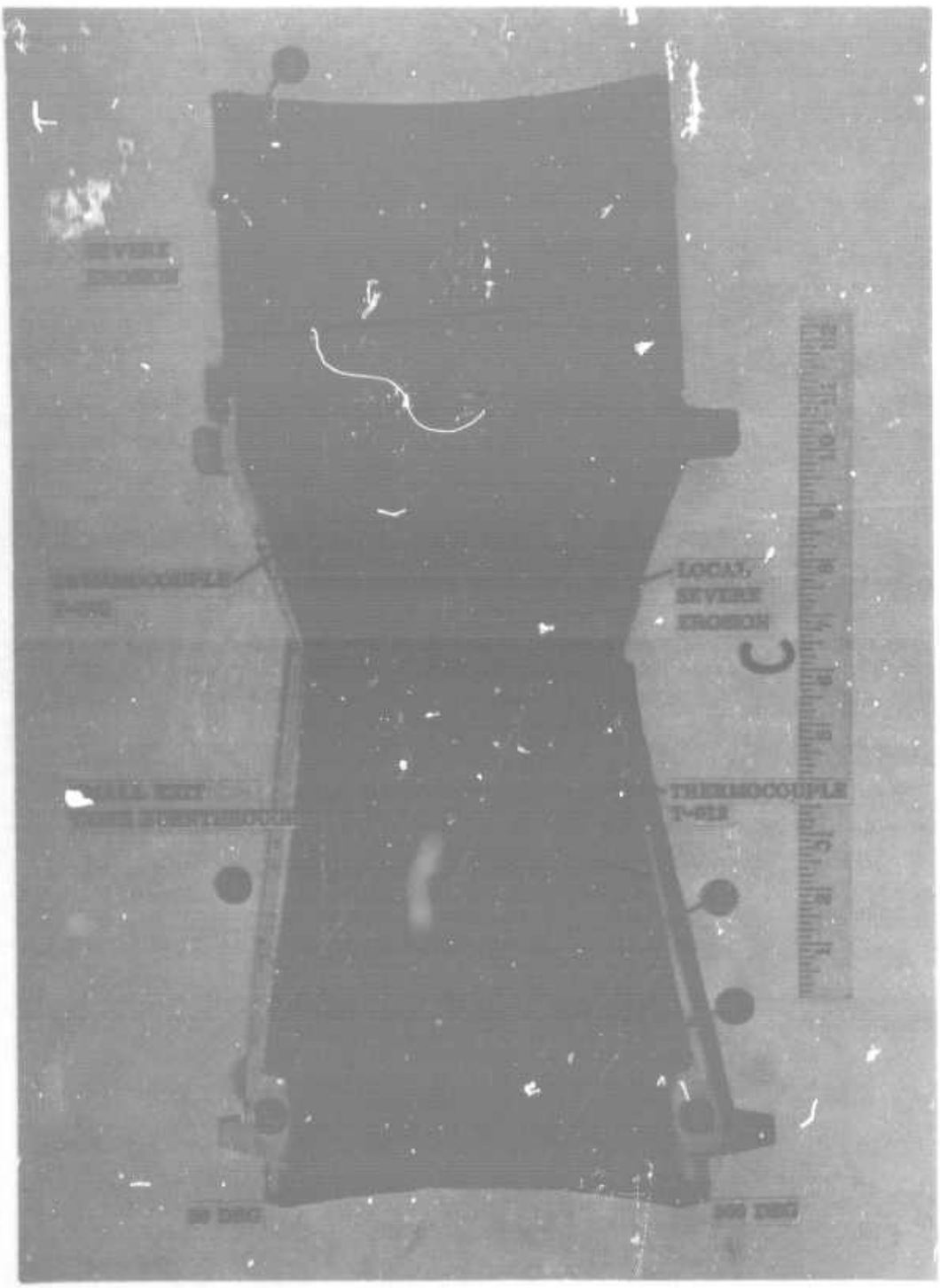

Figure 100. Nozzle No. 5, 30-300 Deg Exit Cone Section

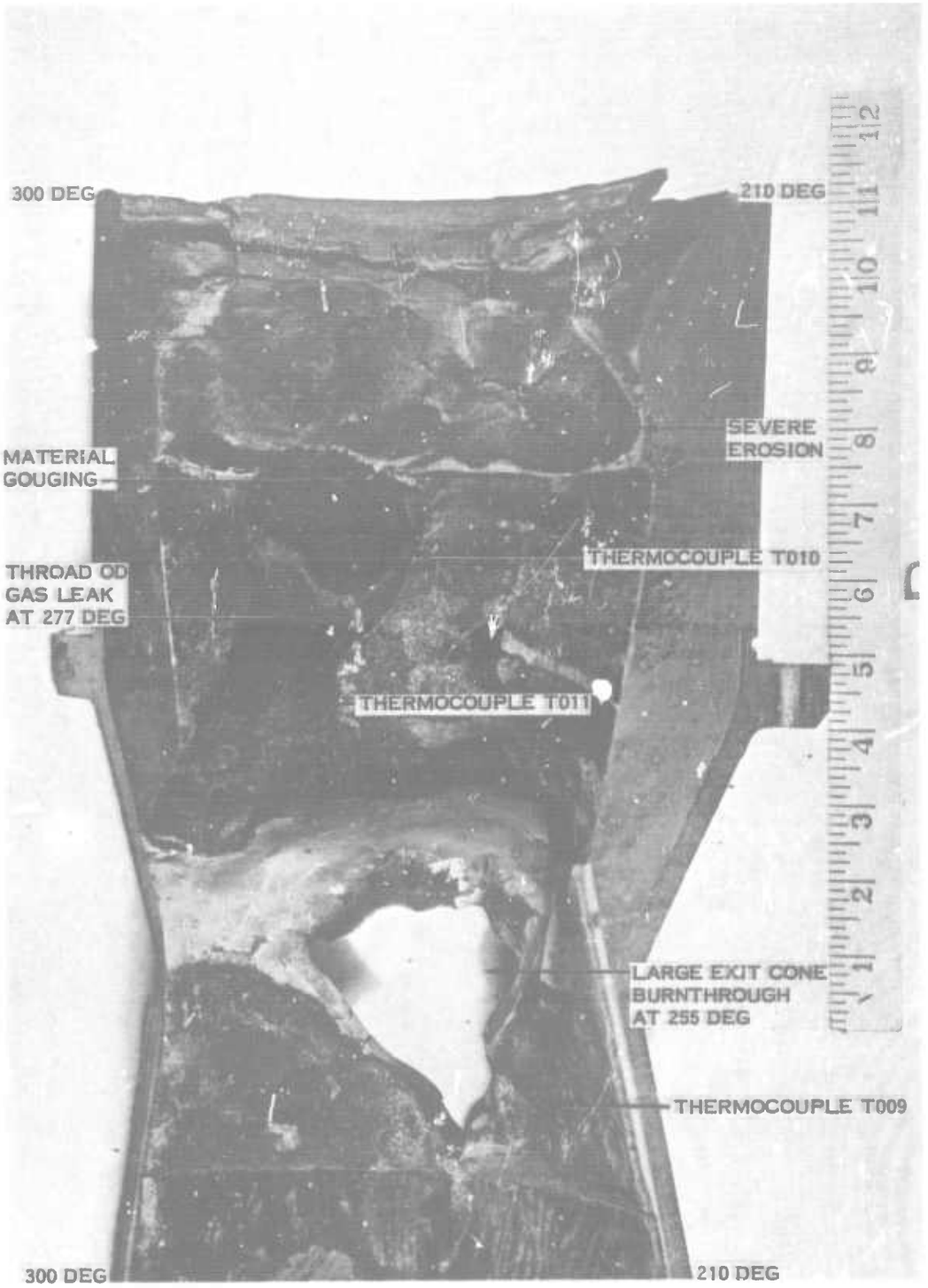

Figure 101. Nozzle No. 5, 210–300 Deg Exit Cone Section

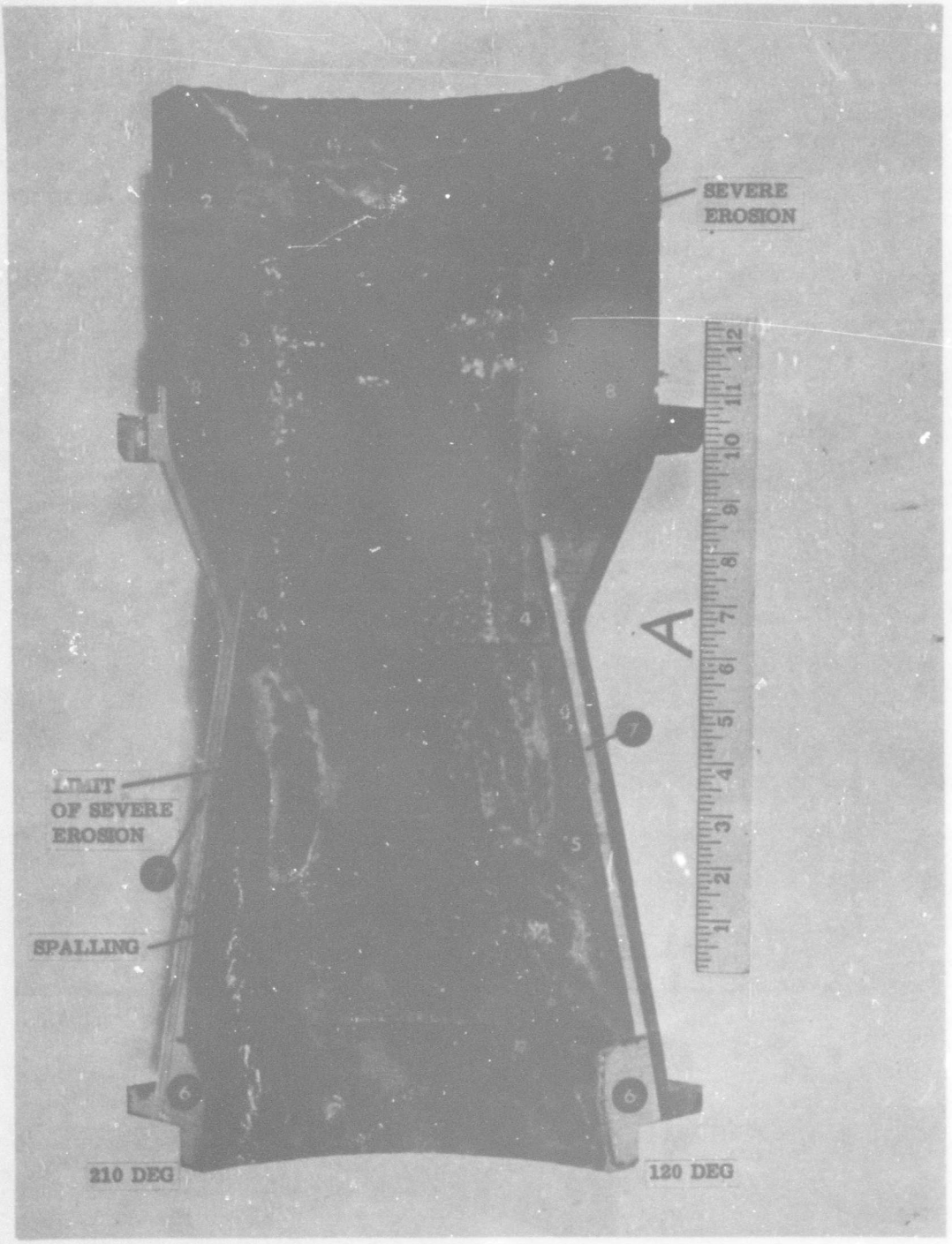

Figure 102. Nozzle No. 5, 120–210 Deg Exit Cone Section

Figure 103. Nozzle No. 5, Hole in Exit Cone

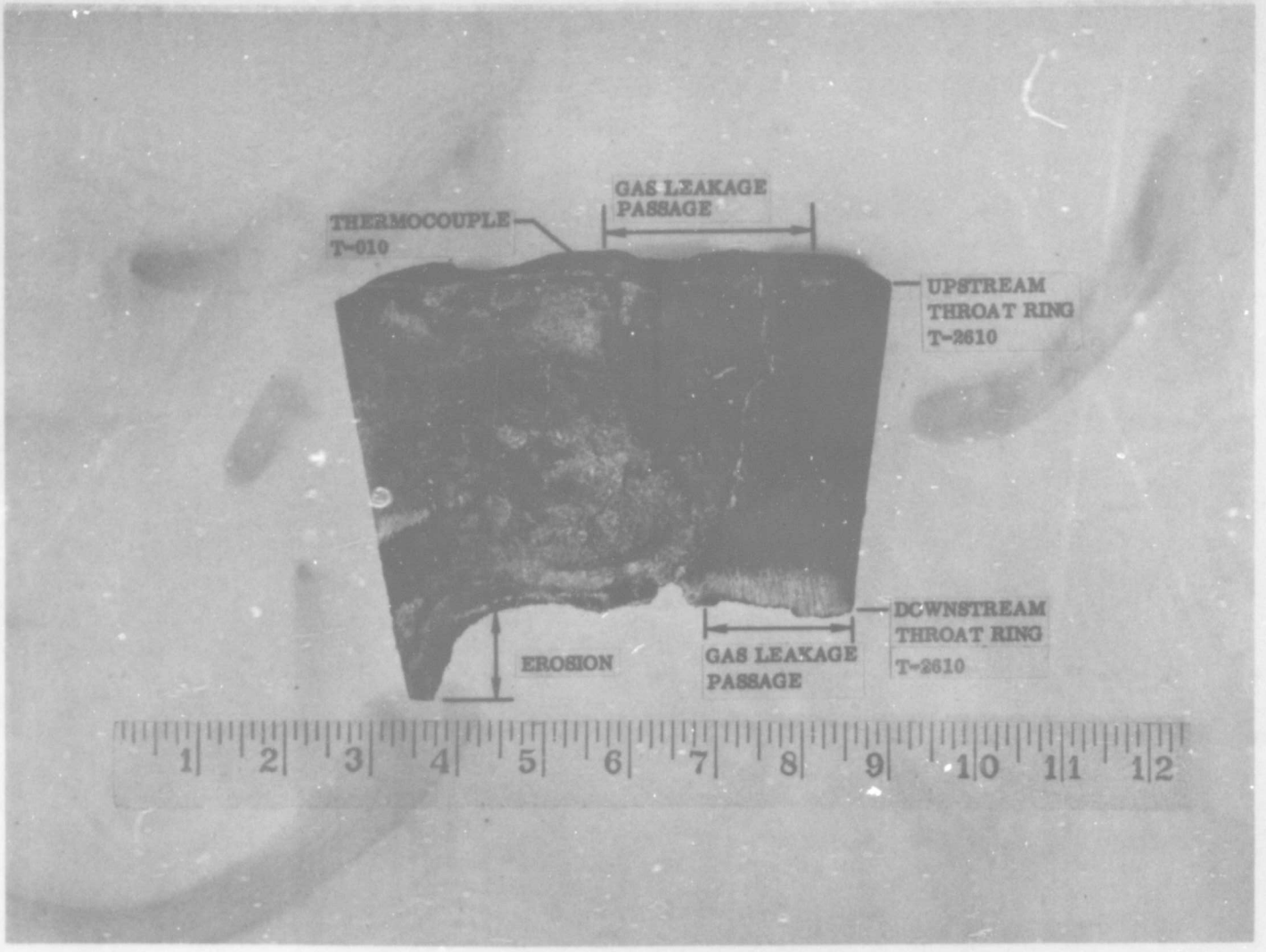

Figure 104. Nozzle No. 5 Throat Ring

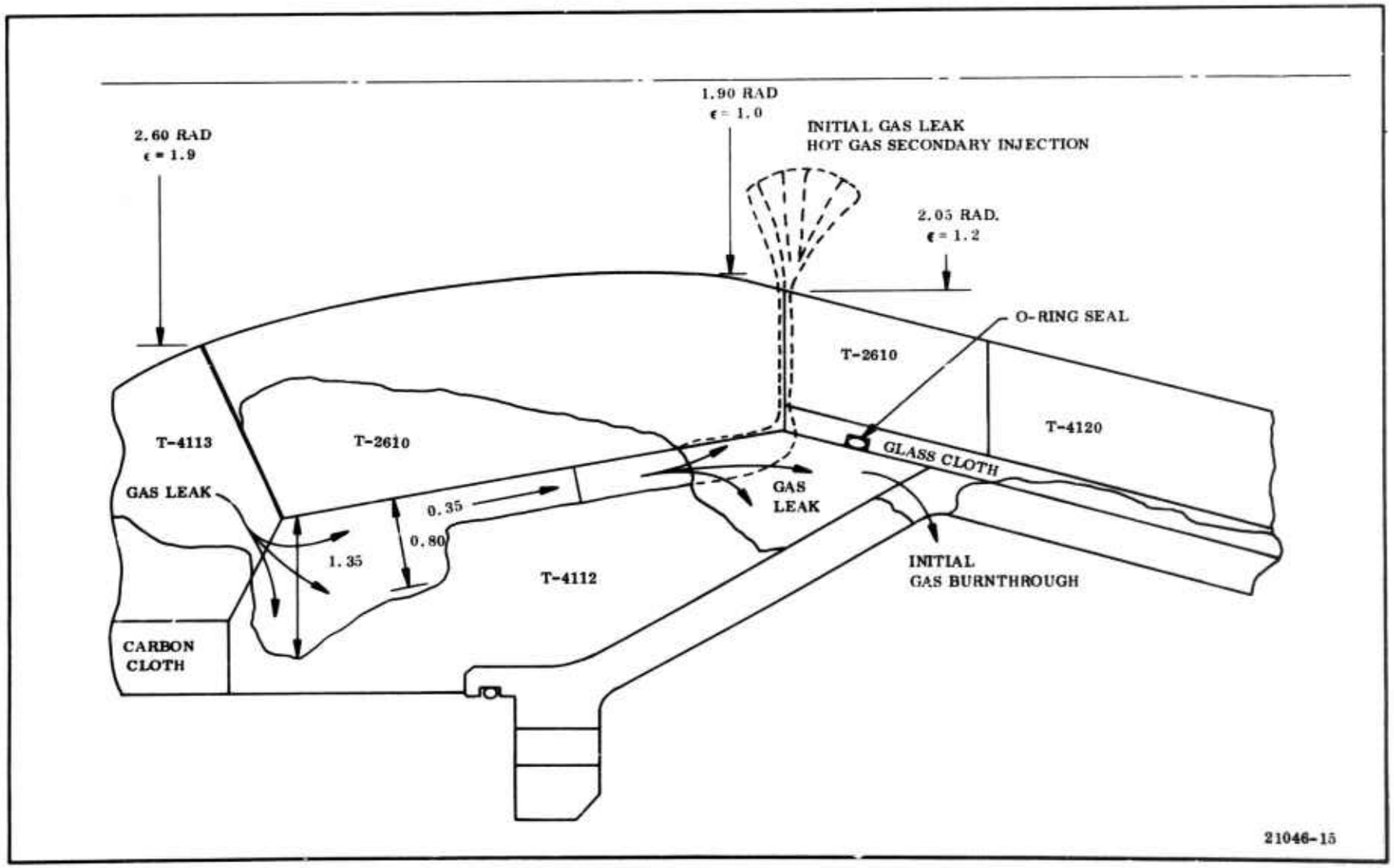

Figure 105. Nozzle No. 5, 277 Deg Plane Showing Gas Leak and Exit Cone Burnthrough

The large and small burnthroughs in the steel exit shell occurred on opposite sides of the gas leak passage at 12 and 277 deg, as indicated below and within the 180 deg arc of gouged exit cone

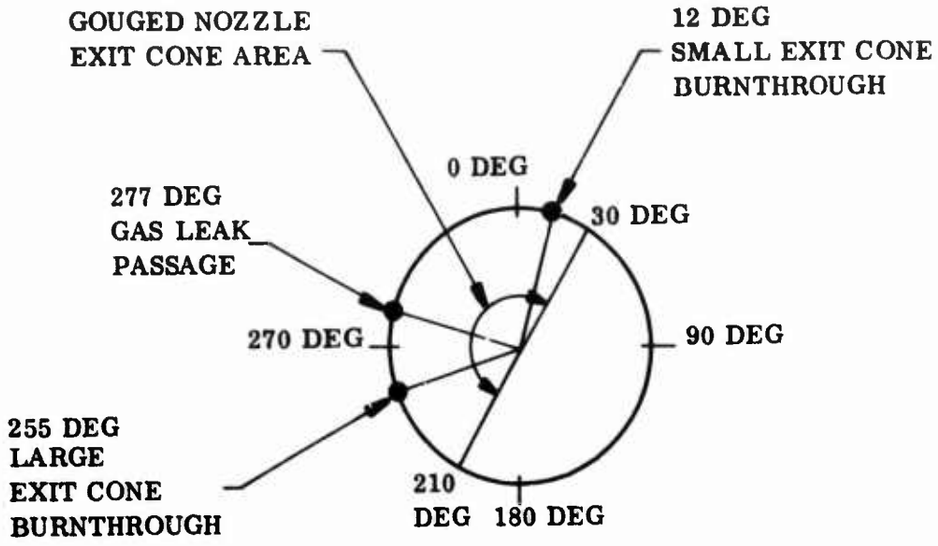

LOOKING UPSTREAM

The aft exit cone lost the majority of its T-4120 liner in the 30 to 210 deg segment, or half the circumference, as a result of the gas leakage and gas injection aft of the throat. The other half of the aft exit cone showed uniform erosion with some spalling (Figure 102).

The throat support material, T-4113, performed satisfactorily except for the gas leak passage at the 277 deg position, and the erosion-gouging at its downstream edge when the throat and forward exit cone no longer provided liner protection.

The reinforced plastics performed satisfactorily at the inlet, at the exit cone insulation sleeve and at the exit end ring. The inlet material was carbon cloth phenolic and the exit cone insulation sleeve and the exit end ring were silica cloth phenolic.

The erosion profiles for the four sectioned nozzle planes (30, 120, 210 and 300 deg) are illustrated in Figure 106. At selected area ratios, the minimum, nominal, and maximum erosion rates are shown. The location of the 12 thermocouples at points A, B, and C, with their heat affected times, also are shown.

The best plane of Nozzle No. 5, least affected by the gas leakage, was at 120 deg. The erosion at the selected area ratios is plotted in Figure 107. The erosion versus area ratio of Nozzle No. 3 of this program, using the same liner materials, also is shown in Figure 107 for comparison.

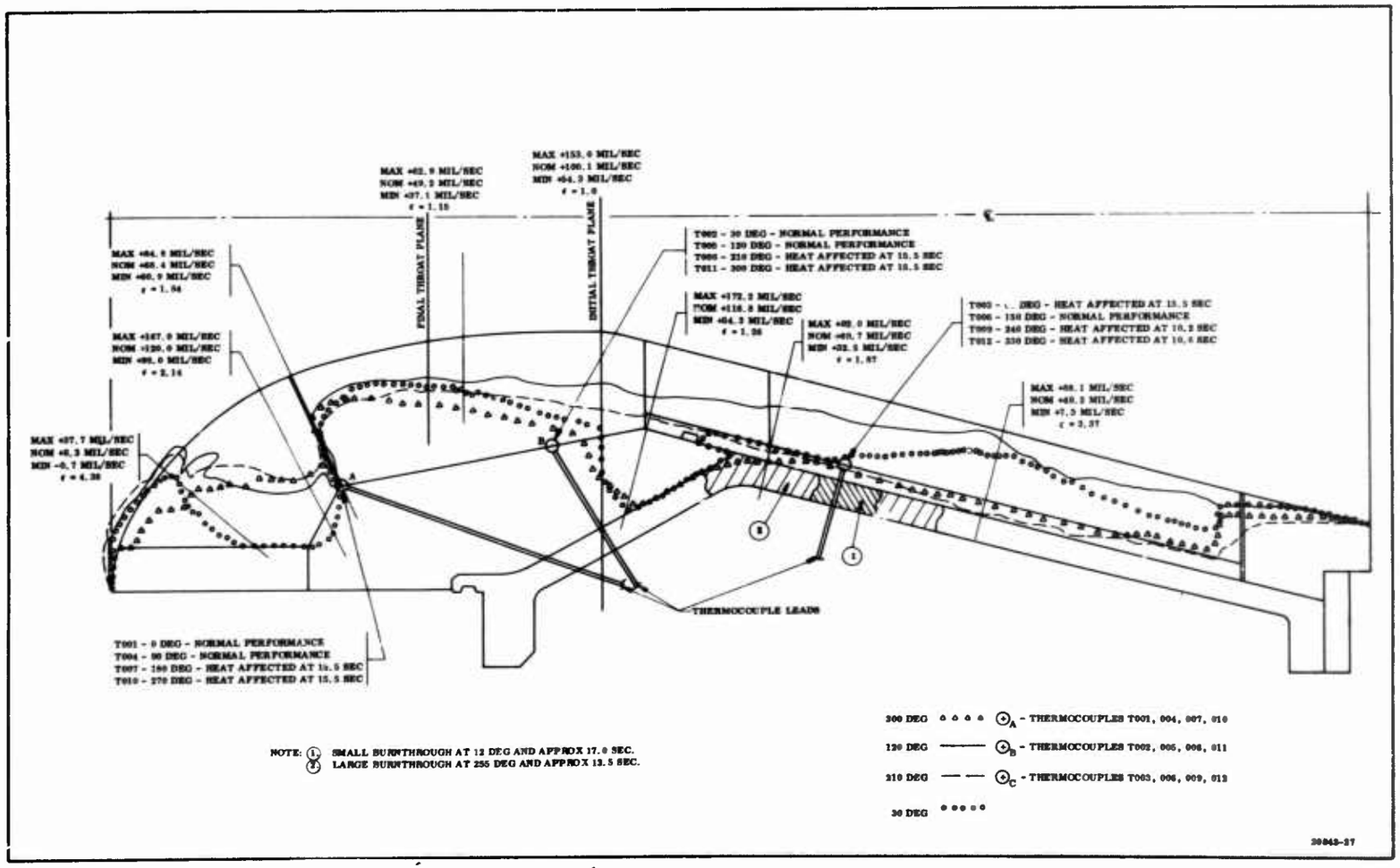

Figure 106. Nozzle No. 5 Material Erosion

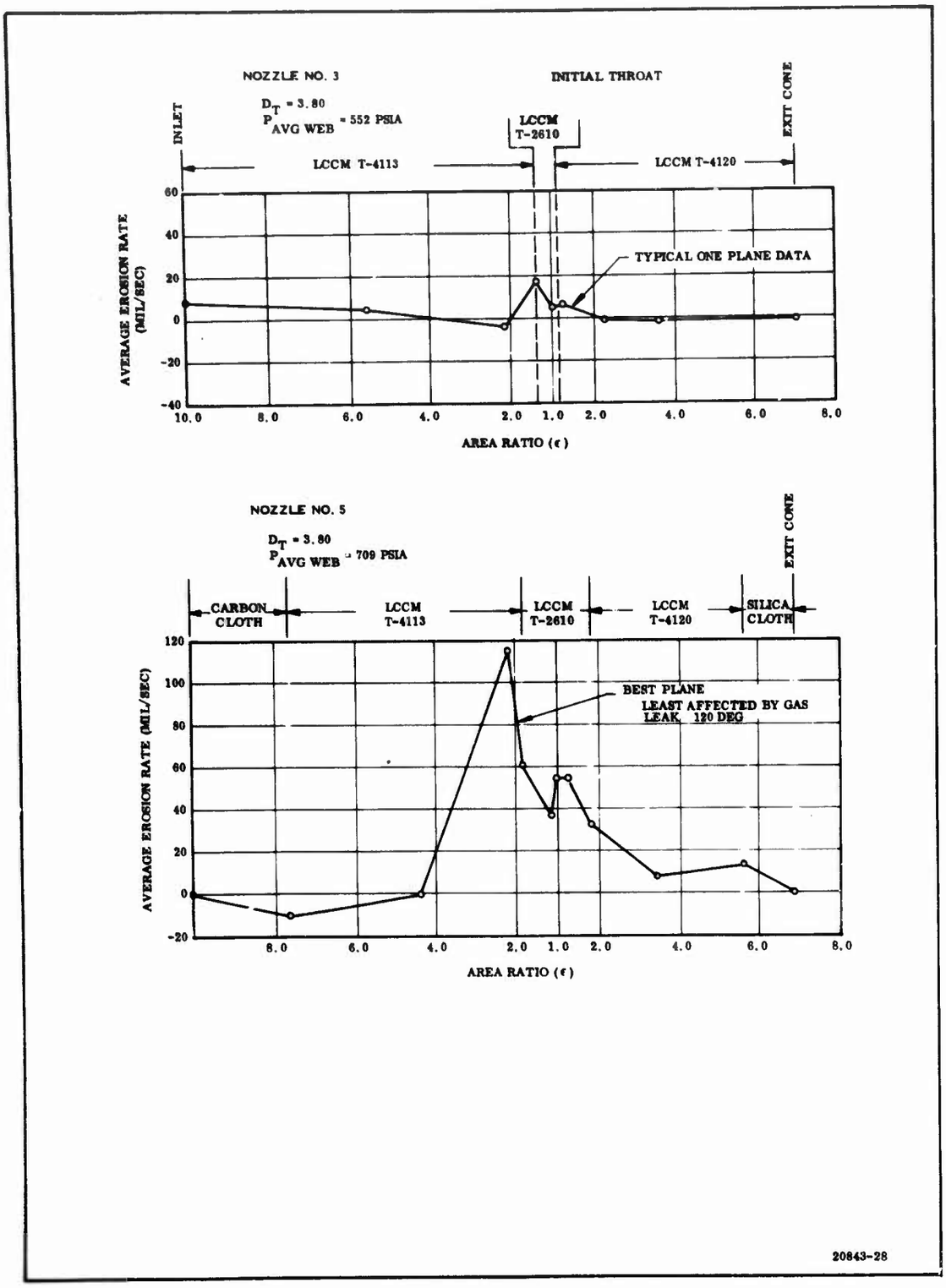

Figure 107. Actual Erosion Rate, Nozzle No. 5 vs Nozzle No. 3

The design of Nozzles No. 3 and 5 was similar except for material interface location and inlet contour. The motors operated at different pressures, as discussed later in the report.

5. INSTRUMENTATION

The motor instrumentation included two chamber pressure transducers, 12 nozzle thermocouples and four nozzle strain gages. The strain gages were inoperative for the entire motor static test, and therefore, are not mentioned in the analysis.

Pressure transducer P1 was selected as the representative gage. Data from this transducer are plotted versus time in Figure 108. The pressure traces for the test of Nozzle No. 1 (graphite cloth-phenolic throat) and Nozzle No. 3 (T-2610 throat) of this program are superimposed on the pressure trace for the Nozzle No. 5 test.

In the Nozzle No. 5 test, pressure rose at the rate of 56 psig/sec from 1.0 to 7.0 sec after ignition to a pressure of 910 psig, exceeding the pressure band width of the tests for Nozzles motors No. 1 and 3. Pressure in the Nozzle No. 5 test then falls at the rate of 63 psig/sec from 7.0 to 14.8 sec after ignition to a pressure of 420 psig, which is below the pressure band width of the tests for Nozzles No. 1 and 3.

After 14.8 sec of motor operation, the pressure rises at the rate of 1,280 psig/sec to a maximum pressure of 1,060 psig at 15.3 sec after ignition. Then the burst discs blew, decreasing chamber pressure to 10 psig at 19.2 sec after ignition.

The initial pressure rise probably resulted from an increase in propellant burning surface area by dishing or case to propellant interface separation. A possible alternative is that the hot gas leak under the throat to the forward exit plane (ϵ =1.2) partially choked the nozzle, creating a new smaller aerodynamic throat downstream of the initial throat by hot gas secondary injection.

The subsequent motor pressure decrease at 7 sec after ignition may have resulted from the throat area increasing because of material erosion at a faster rate than the change in propellant burning surface area. The final pressure spike rise at 14.8 sec after ignition represents a very rapid increase in the propellant burning surface area before blowing the burst discs at 15.3 sec after ignition.

Photographic camera coverage at the Edwards AFB test bay included three cameras with shutter speeds of 64, 200 and 1,000 frames per sec. After time sequencing the three cameras (Table XXXIII), the 200 fps camera appeared to obtain the most reliable data. Film coverage taken by this camera indicated that the exit cone was burned through at 12.8 sec, the burst discs were blown at 15.2 sec, and the test ended at 27.7 sec after ignition. The 1,000 fps camera was labeled incorrectly (probably 400 fps), but did indicate that some LCCM material was lost before the exit cone burnthrough, probably exit cone T-4120 material.

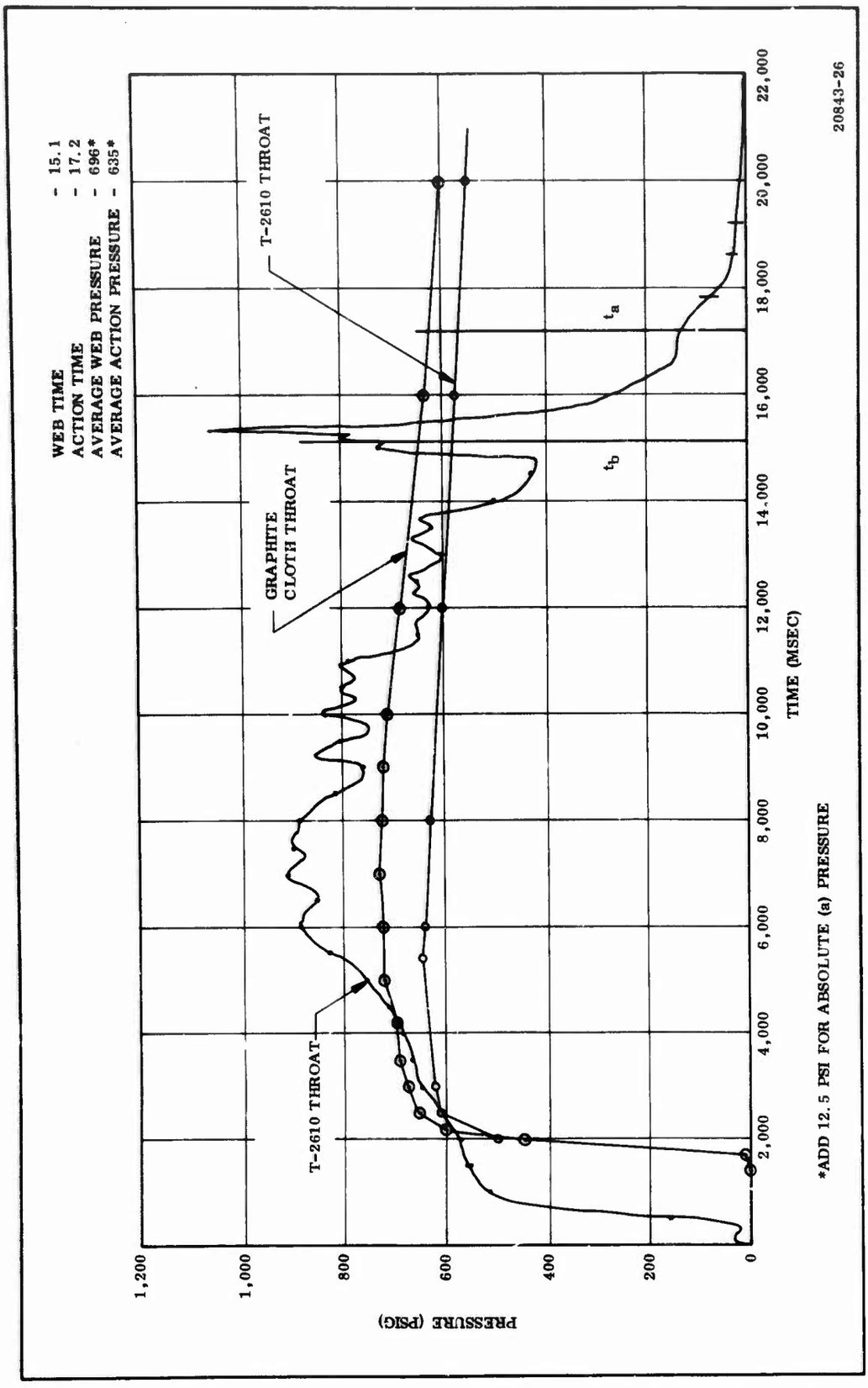

Figure 108. Motor Performance, Nozzle No. 5

TABLE XXXIII

CAMERA TIME SEQUENCING

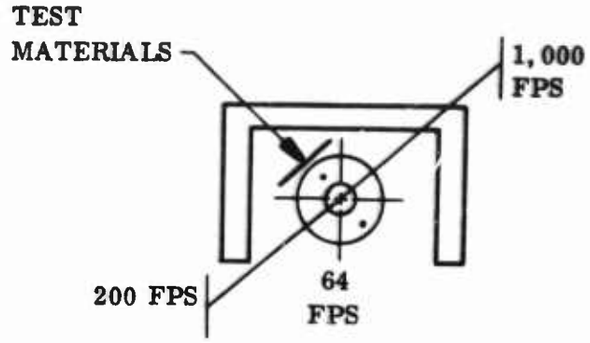

Event	64 fps Camera Time (Sec)	200 fps Camera Time (Sec)	1,000 fps Camera Time (Sec)
1. Loss of LCCM Liner Material	--	--	Before Exit Cone Burn-through
2. Large Exit Cone Burnthrough	14.2	12.8	
3. Ch .r Motor Burst Disc Blew an.. Pressure Dropped	16.7	15.2	
4. Small Exit Cone Burnthrough	17.8	16.2	
5. No Gas Exhaust at Large Exit Cone Hole	19.7	17.8	
6. No Gas Exhaust at Small Exit Cone Hole	21.6	18.6	
7. End of Test	29.9	27.7	

Best Camera Coverage and Timing of Sequences.

NOTES:

1. During static test, other Air Force materials were tested in nozzle exhaust plume. Between 9.7 and 16.2 the AF test panel acted as a jet tab on the exit plane.

2. 1,000 fps speed was erratic; no effort was made to correct the frame speed.

The thermocouples were located in the nozzles as shown in Figure 10[illegible]. The temperature versus time data are plotted for the inlet, throat, and exit planes in Figures 110, 111 and 112.

At the inlet, all thermocouples registered 55 to 65°F up to the first 12 sec after ignition. After 12 sec of motor operation, thermocouples T_7 and T_{10} started to increase in temperature faster than T_1 and T_4 due to the inlet material loss, the exit cone burnthrough, or the throat OD gas leak. The instruments were inoperative at 15.5 sec, after the burst discs were blown out.

The throat plane thermocouples all registered 55 to 65°F up to 12 sec after ignition when thermocouples T_8 and T_{11} started to increase in temperature faster than T_2 and T_5. The T_8 and T_{11} temperature rise could be attributed to the throat OD gas leak or the exit cone burnthrough. The instruments were inoperative at 15.5 sec, after the burst discs blew.

At the exit cone, all gages were 50°F up to 8 sec after ignition when T_9 and T_{12} started to increase in temperature and became inoperative at 10.2 and 10.6 sec after ignition due to loss of exit cone liner material T-4120 and resultant exposure to exhaust gas. (The maximum thermocouple temperature range for Chromel-Alumel is 2,200°F.) Thermocouple T_3 also increased in temperature at 8 sec after ignition only to become inoperative at 15.5 sec, when the burst disc blew. Thermocouple T_6, located in the 150 deg plane, recorded a normal temperature rise to 32 sec after ignition due to its location away from the exit cone burnthrough.

6. SPECIAL POST-TEST STUDIES

To assist in the post-test evaluation of Nozzle No. 5, the following special studies were conducted.

1. Nozzles No. 3 and 5 average two dimensional heat transfer coefficients and erosion were compared since both nozzles used the same materials in the same location.
2. LCCM properties of materials from the uncharred areas of Nozzle No. 5 were compared with properties of materials from Nozzle No. 3.
3. Changes from Nozzle No. 3 to No. 5 were evaluated.
4. LCCM material performance on this nozzle was compared with performance on other Thiokol nozzles (TU-379 motor nozzle for NASA, IR & D nozzle under Thiokol and Air Force sponsorship, and submerged nozzle).

a. Nozzle Comparison--Nozzles No. 3 and 5, with the same materials in the same motor design, were used to compare the average heat transfer coefficients and erosion rates for performance anomalies. The initial (uneroded) and final (eroded) heat transfer coefficients for Nozzle No. 5 inlet and exit cone are shown in Figures 81 and 82, with the Nozzle No. 3 coefficients shown in Figures 113 and 114.

NOTE:

1. LARGE EXIT CONE BURNTHROUGH OCCURRED AT 12.8 SEC IN THE 225 DEG PLANE.
2. BURST DISCS BLOW AT 15.3 SEC IN THE 75 DEG AND 225 DEG PLANE ON THE CLOSURE.
3. SMALL EXIT CONE BURNTHROUGH OCCURRED AT 16.2 SEC IN THE 12 DEG PLANE.
4. THROAT-THROAT SUPPORT INTERFACE LEAKED AT 277 DEG PLANE.

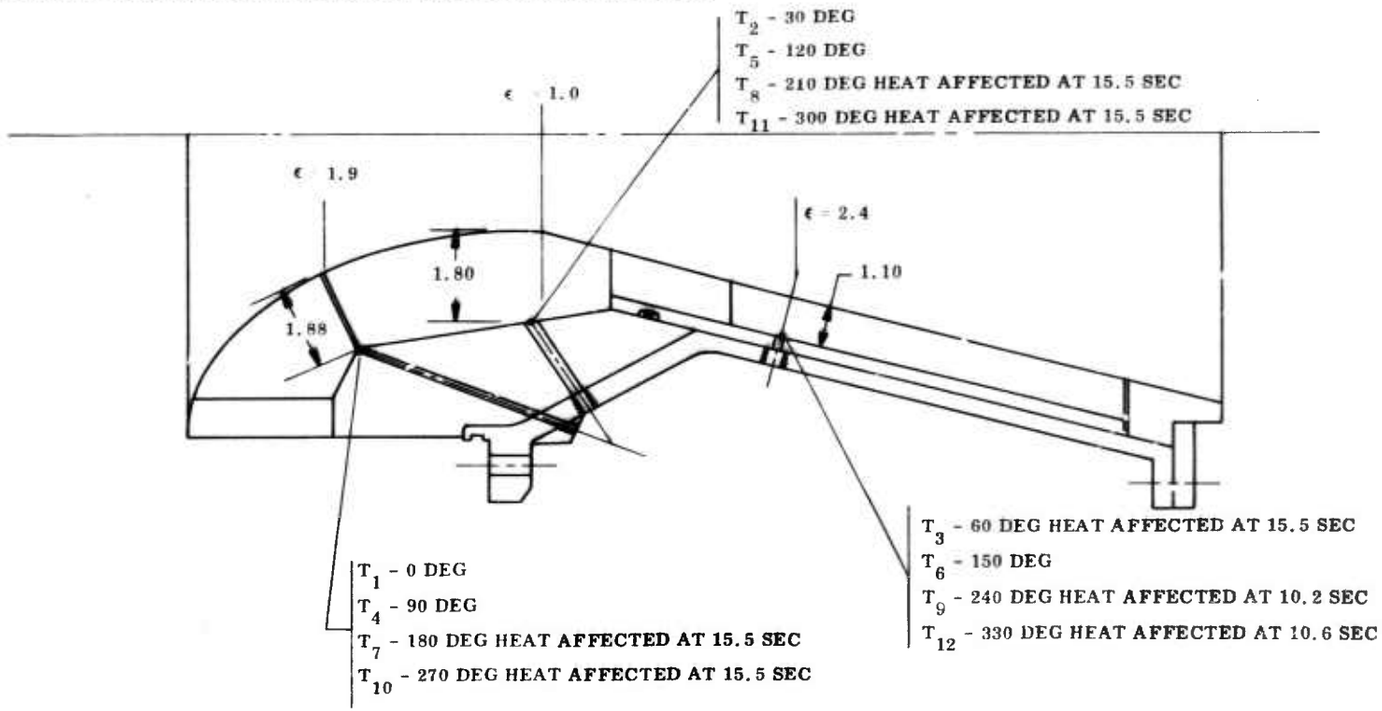

Figure 109. Instrumentation Location, Nozzle No. 5

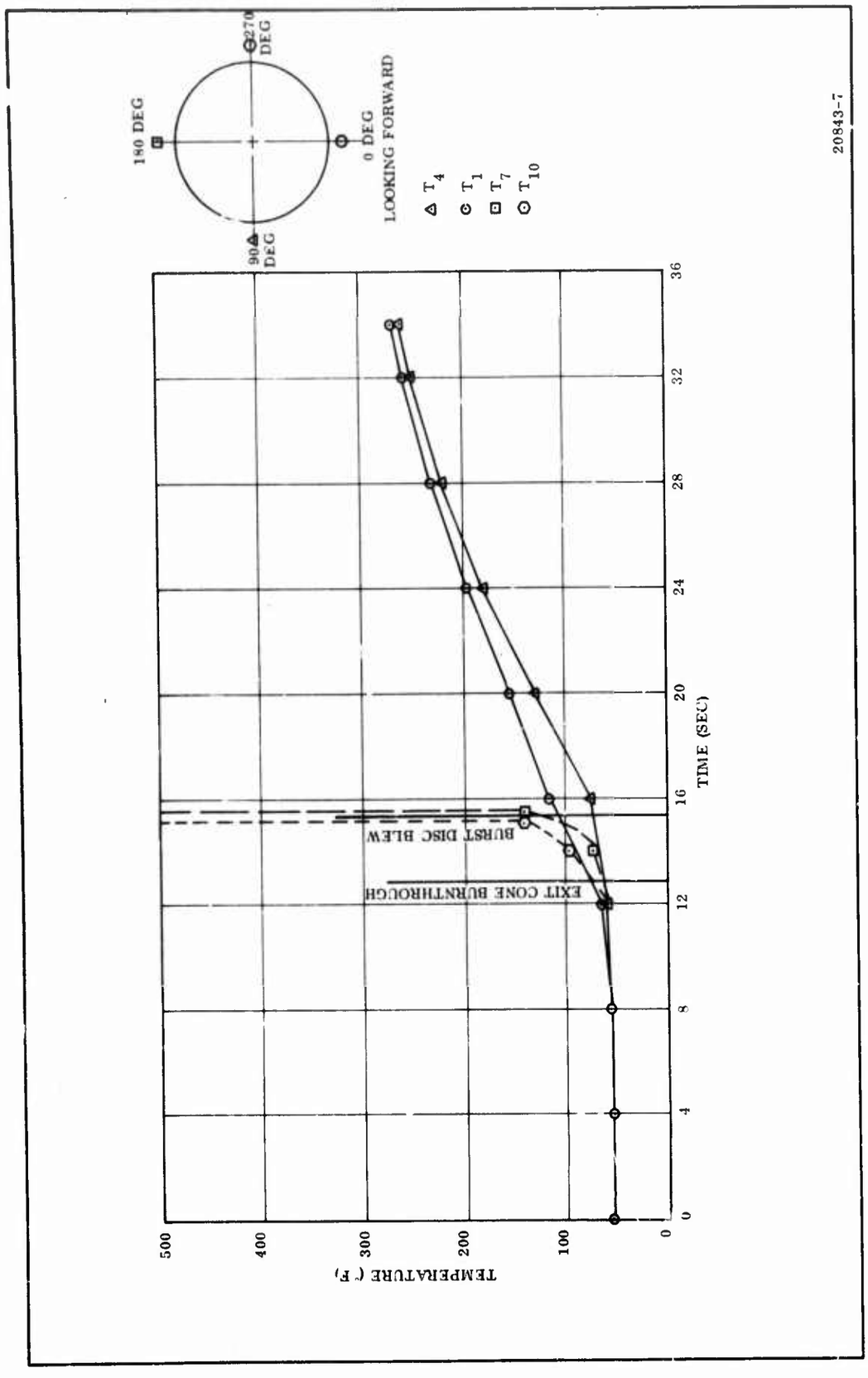

Figure 110. Thermocouple Data, Inlet, Nozzle No. 5

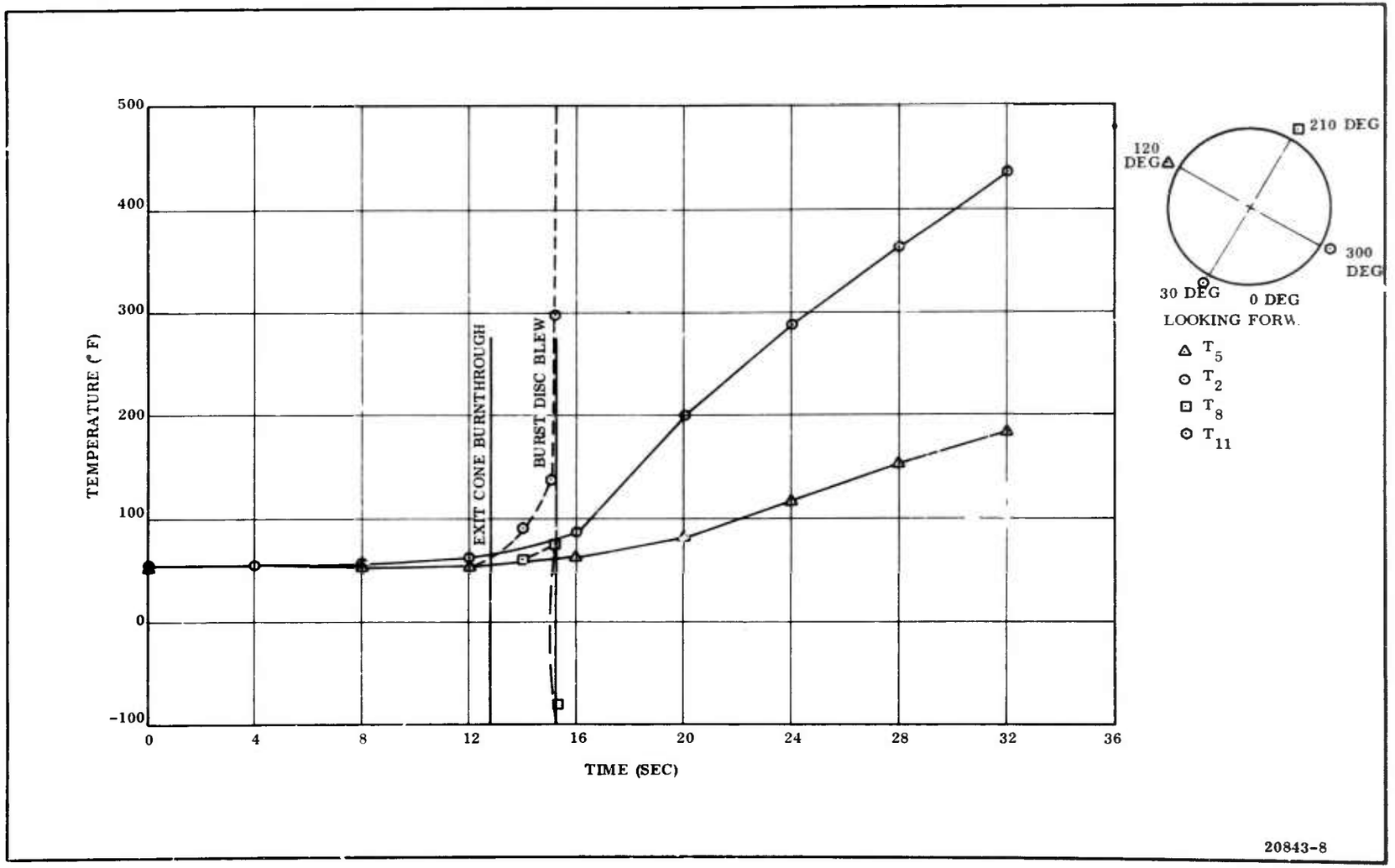

Figure 111. Thermocouple Data, Throat, Nozzle No. 5

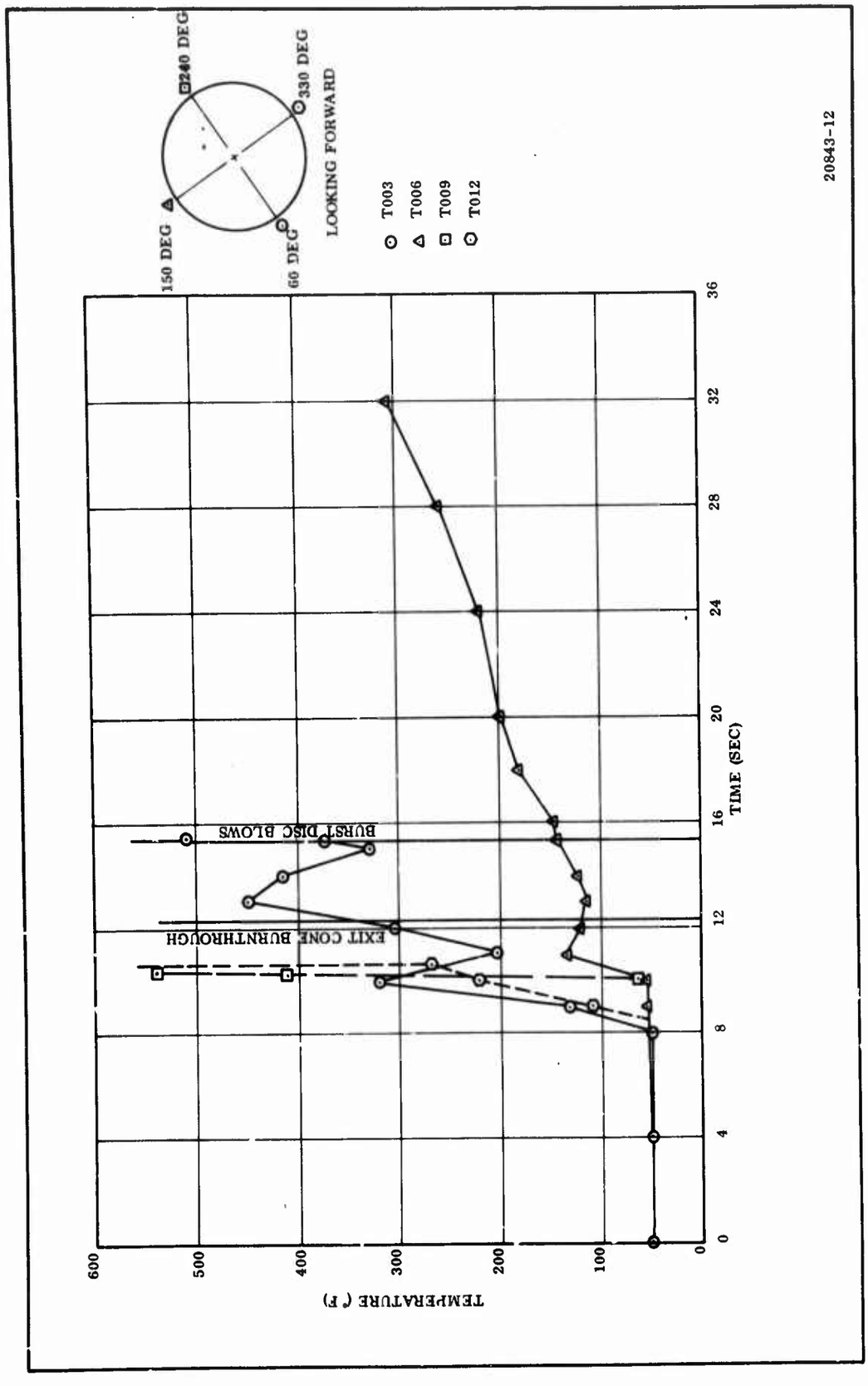

Figure 112. Thermocouple Data, Exit Cone, Nozzle No. 5

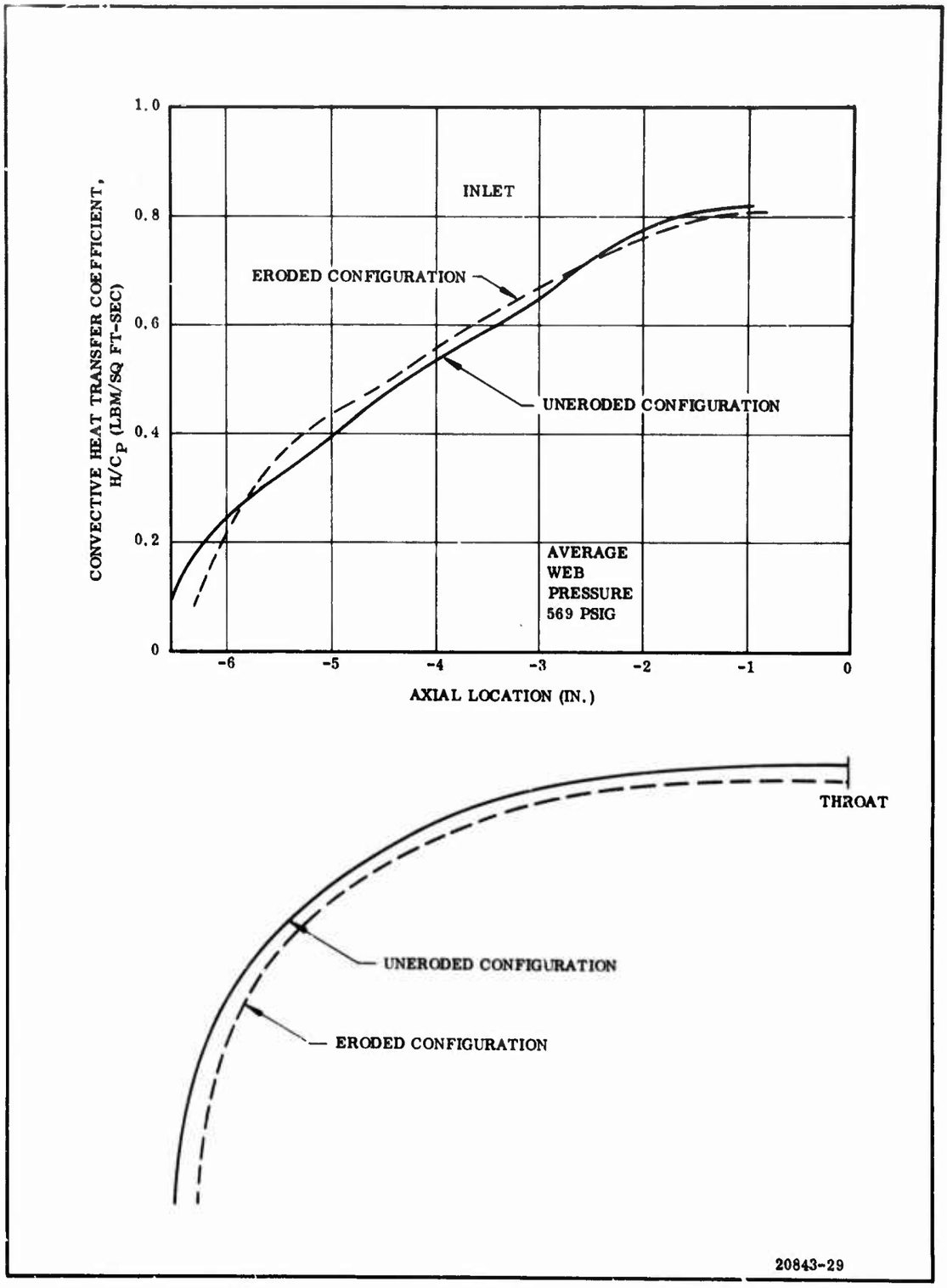

Figure 113. Convective Heat Transfer Coefficient, Nozzle No. 3

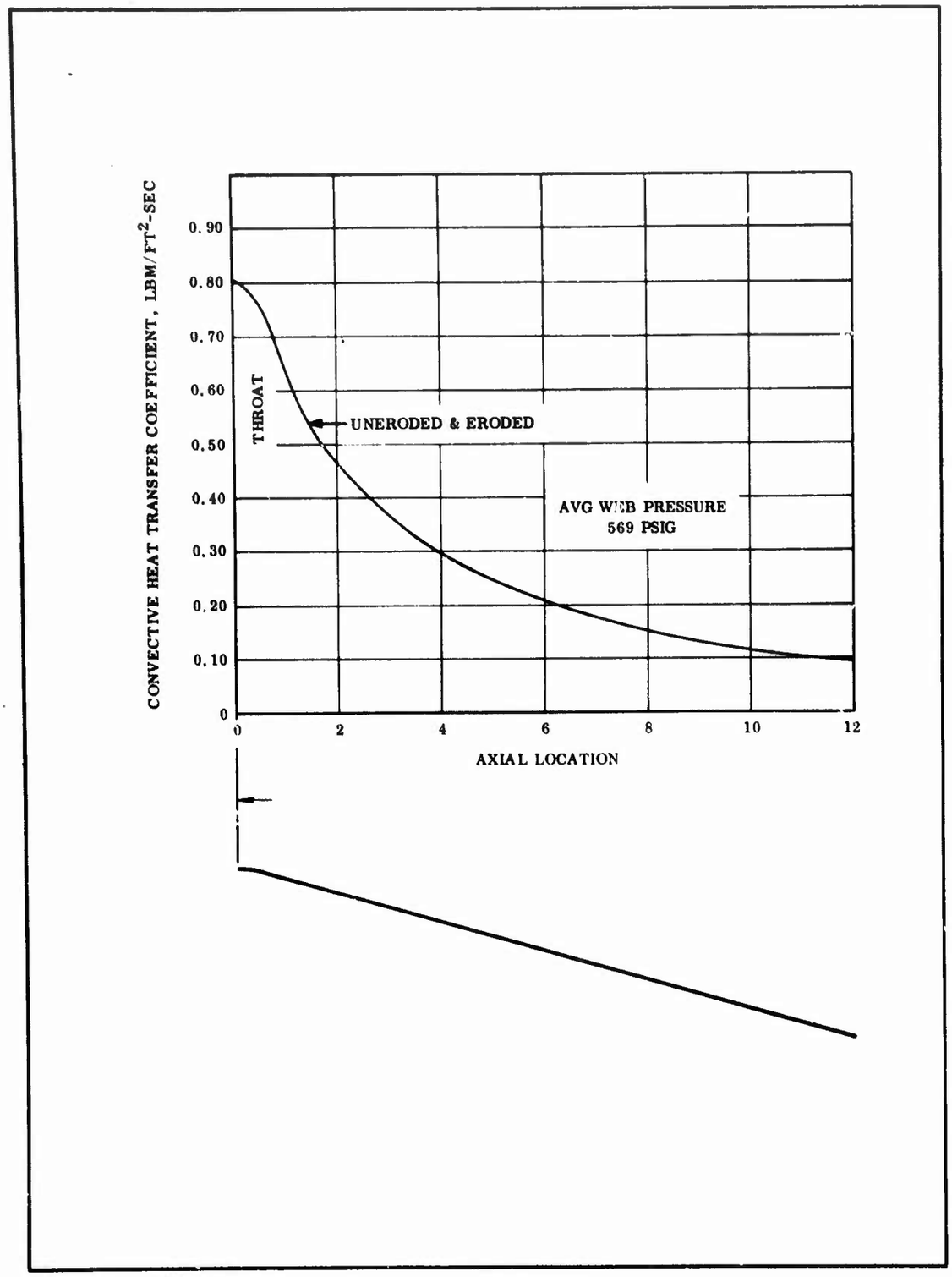

Figure 114. Convective Heat Transfer Coefficient, Throat and Exit Cone, Nozzle No. 3

In Figure 115 the contours, average heat transfer coefficients (initial and final), and average erosion rates versus axial location are compared for Nozzles No. 3 and 5. The maximum inlet diameter plane is the start of both nozzles, simulating the installed nozzles on the motor.

Since erosion is a function of the final heat transfer coefficient, the Nozzle No. 5 erosion rates (ER) can be predicted from the Nozzle No. 3 erosion rates using the average heat transfer coefficients for both nozzles. Thus, at any one axial location point:

$$\text{ER No. 5} = \text{ER No. 3} \left(\frac{\text{h/cp No. 5}}{\text{h/cp No. 3}} \right)$$

Predicted and actual erosion rates are shown below and in Figure 115.

Axial Location	Material	Nozzle No. 3 Erosion (mil/sec)	Predicted Nozzle No. 5 Erosion (mil/sec)	Actual Nozzle No. 5 Erosion (mil/sec)
-1 Inlet	T-2610	5.09	6.9	63.00
-3 Inlet	T-2610	15.00	28.4	61.00
-4 Inlet	T-4113	6.5	8.5	92.00
0 Throat	T-2610	5.0	6.3	82.00
+4 Exit	T-4120	0	0	68.00

The large disparity between the predicted and actual values in the inlet throat and exit cone locations indicates anomalies, possibly resulting from changes in material processing or fabrication, a sensitivity to higher chamber pressures, or the effects of the gas leak under the throat into the forward exit cone.

Many assumptions are made in presenting the data shown in Figure 115 such as uniform erosion rate and uniform rate of heat transfer coefficient change, but the large disparity between actual and predicted values indicates the effects of abnormal motor test conditions and material inconsistencies.

b. Material Tests--The material for Nozzles No. 3 and 5 were identical and were used in the same location on each nozzle. The only process change between the two nozzles appeared to be the way T-4113 inlet material was partially staged ("B" condition) after mixing the graphite granules, NBR rubber, and the phenolic resin. The T-4113 material for Nozzle No. 3 was "B" staged in a heated open tray to drive off the volatiles, while the T-4113 material for Nozzle No. 5 was heated in tray with a vacuum to increase the rate of volatiles loss.

Density, ultimate compression, and resin content tests were conducted on tested virgin or representative laboratory specimens of Nozzles No. 3 and 5 materials. Results are compared in Table XXXIV.

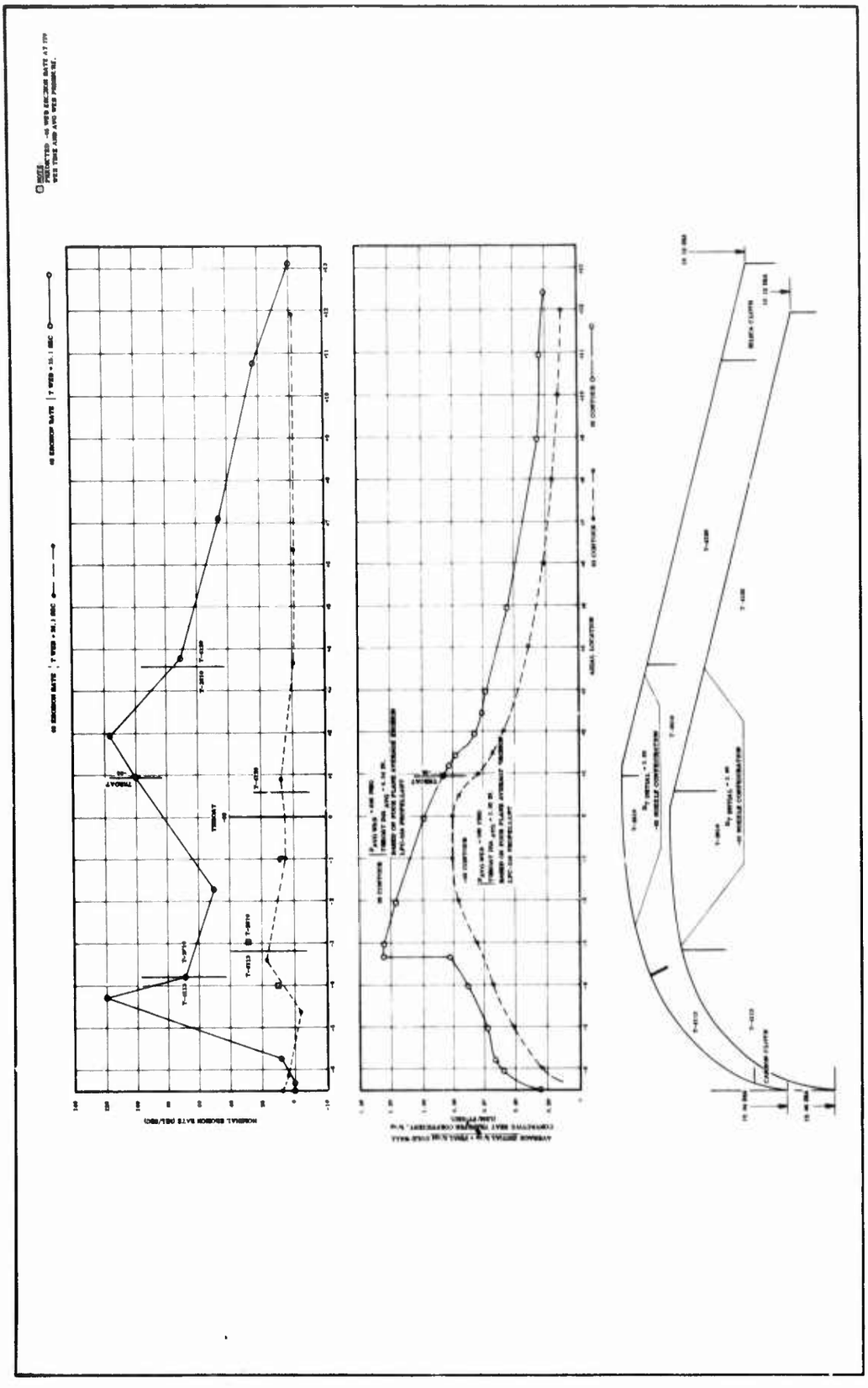

Figure 115. Performance Comparison Between Nozzles No. 3 and 5

TABLE XXXIV

NOZZLE MATERIAL SPECIMEN TEST RESULTS

Properties	Inlet T4113 (200 psi and 300°F)		Throat T2610 (1,000 psi and 300°F)		Exit T4120 (15 psi and 170°F)	
	Nozzle No. 3	Nozzle No. 5	Nozzle No. 3	Nozzle No. 5	Nozzle No. 3	Nozzle No. 5
Density (gm/cc)	1.44*	1.56*	1.57*	1.71*	1.42*	1.47*
Ultimate Compression (psi)	130 at Room Temperature** 30 at 300°F	1,593 Exposed to 260°F During Test* (TC-001 Ref)	12,000 at Room Temperature** 5,000 at 300°F	7,490 Exposed to 300°F During Test* (TC-002 Ref) -005	8,200 at Room Temperature** 2,000 at 300°F	4,923 Exposed to 300°F During Test* (TC-006 Ref)
Resin Content						
Process Specification Requirement (% of Specimen)	25** Phenolic Resin and Rubber	25** Phenolic Resin and Rubber	25** Phenolic Resin	25** Phenolic Resin	25** Phenolic Resin	25** Phenolic Resin
Test Value (% of Specimen)	No Data	25* Exposed Only To Room Temp	No Data	11* Exposed To Elevated Temp	No Data	8* Exposed To Elevated Temp

*Post-Tested Specimen
**Nonfired Laboratory Specimen

The comparison of Nozzles No. 3 and 5 material sample densities, ultimate compressions, and resin contents seems to be in agreement except for the differences listed in the following tabulation.

1. T-4113 material elevated temperature strength comparison.

Nozzle No. 3	Nozzle No. 5
30 psi at 300° F	1,593 psi at 260° F

The change in "B" staging of the T-4113 material apparently increases compression strength by a factor of 50+.

2. The T-4120 material resin content, compared to specification requirements, was lower than that expected of postfired test specimens.

Nozzle No. 5 Specification Requirement Resin Content	Nozzle No. 5 Material Resin Content
25 percent	11 percent

3. The T-2610 material resin content, compared to specification requirements, was lower than that expected of postfired test specimens.

Nozzle No. 5 Specification Requirement Resin Content	Nozzle No. 5 Material Resin Content
25 percent	8 percent

E. NOZZLE NO. 6

1. DESIGN

The nozzle design and instrumentation configuration is illustrated in Figure 116. The nozzle liner included three different materials bonded into a nozzle structural shell and retainer plate. Twelve thermocouples and four strain gages were installed at three nozzle planes to complete the nozzle design.

The inlet section included the silica cloth phenolic and the T-2610 materials, and four thermocouples installed on the backside of the T-2610.

The throat section included the Graphite H-205-85 throat and glass phenolic throat support, with four thermocouples installed at the backside of the throat and two strain gages at the outer steel shell surface ($\epsilon = 1.0$).

The exit section included T-2610 and silica cloth phenolic liners, a glass cloth phenolic structure insulation sleeve, and instrumentation. The instrumentation included four thermocouples at the backside of the T-2610 and two strain gages at the outer steel shell surface ($\epsilon = 2.4$).

The structural support and retainer were made from welded 1020 steel plate and rolled sheet stock and formed into a shell and ring construction.

2. FABRICATION

The nozzle components, materials, and fabrication processing methods are listed in Figure 117. The fabrication sequence is indicated as a step by step process flow sheet. In addition, the nozzle fabrication is reflected in Table XXII.

The first six items were machined to mate each other and the steel shell and then bonded to form the throat assembly. The last six items were also machined and bonded into the steel shell and throat assembly.

Nozzle No. 6 was the same as Nozzle No. 5 except for material and component length changes. The changes are listed below.

		Nozzle No. 5	Nozzle No. 6
1.	Throat support	T-4113	Silica phenolic
2.	Inlet barrier	Carbon phenolic	Silica phenolic
3.	Inlet	T-4113	T-2610 Length increased
4.	Throat	T-2610	H-205-85 Length decreased
5.	Exit cone	T-2610 Unequal length cones T-4120	T-2610 Equal length cones
6.	Exit cone insulation	Glass phenolic	Silica phenolic

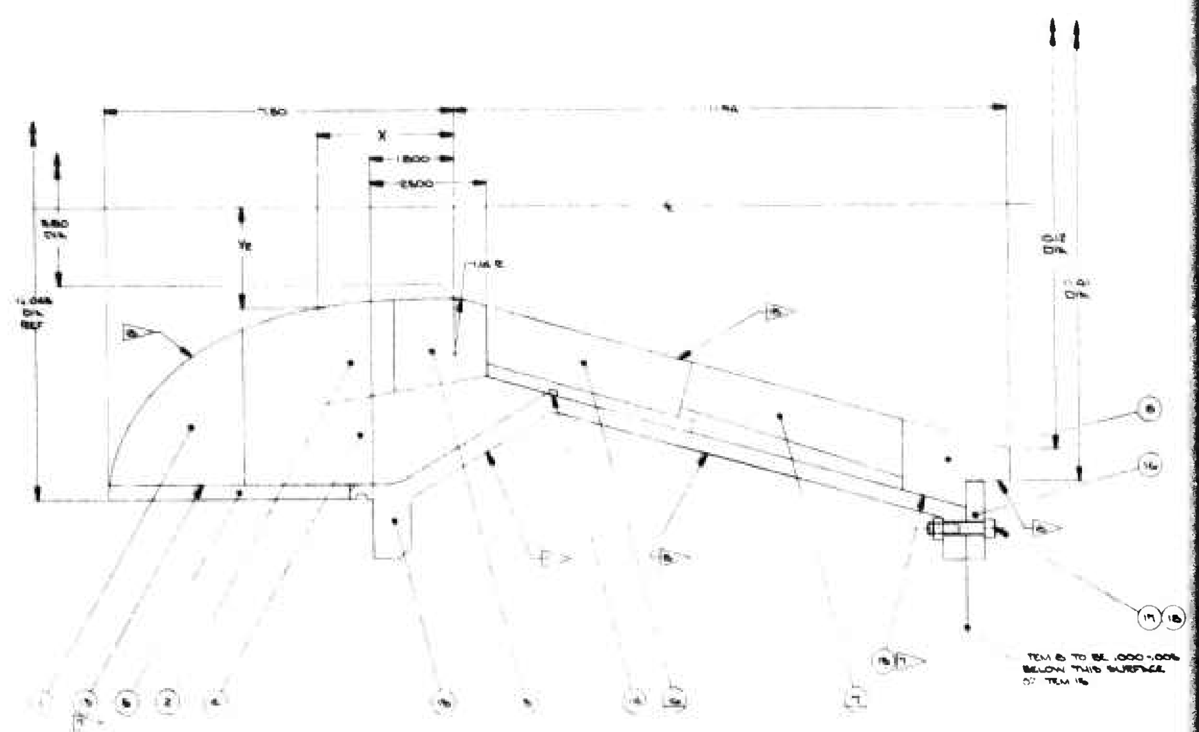

INLET COORDINATES	
X	Y
.00	1.90 REF
1.09	1.91
2.91	[illegible]
3.98	[illegible]
4.99	[illegible]
5.80	[illegible]
6.52	[illegible]
6.99	4.46
7.27	4.97
7.62	5.47
7.80 REF	6.02 REF

A

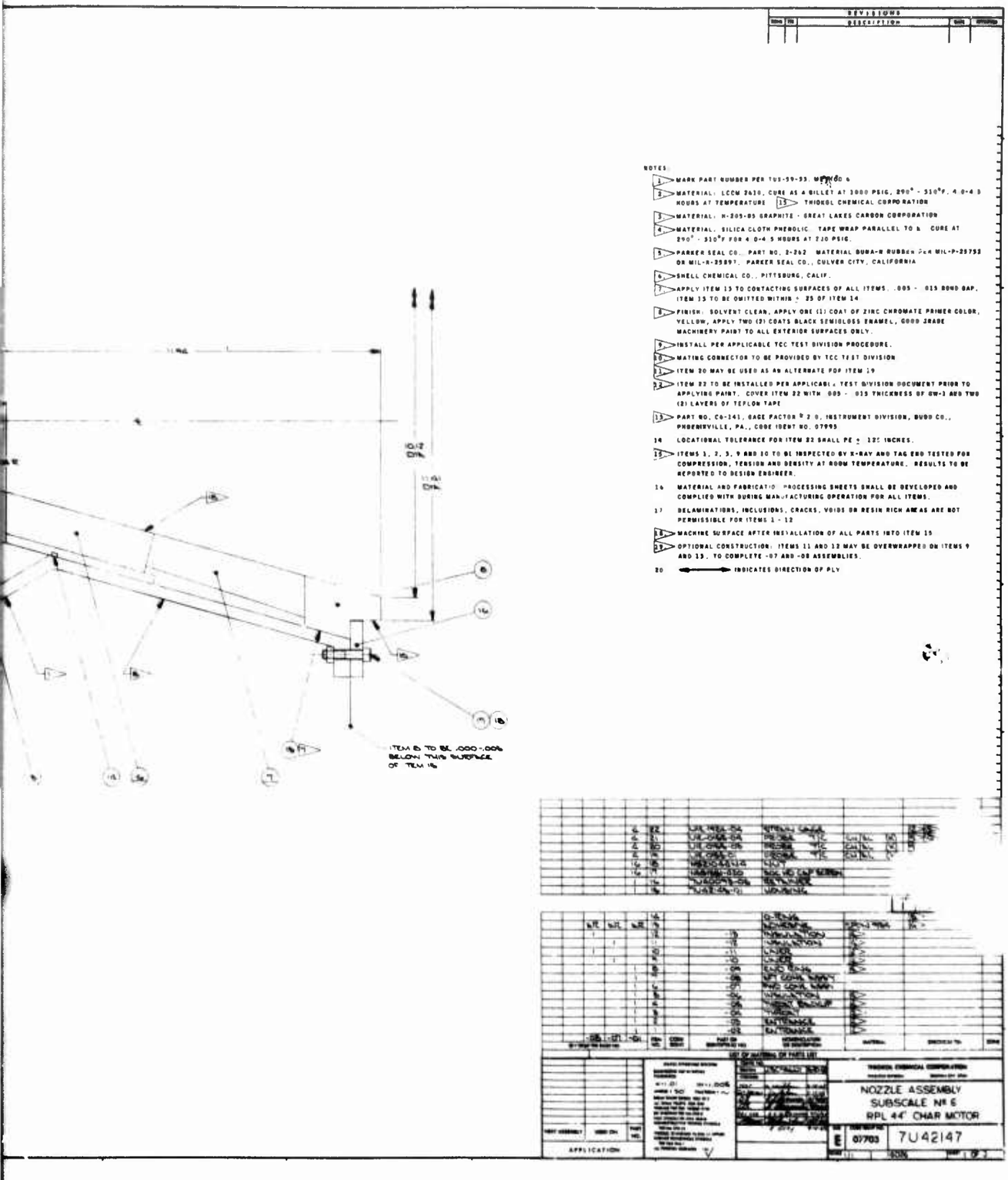

Figure 116. Nozzle No. 6 Assembly Drawing

B

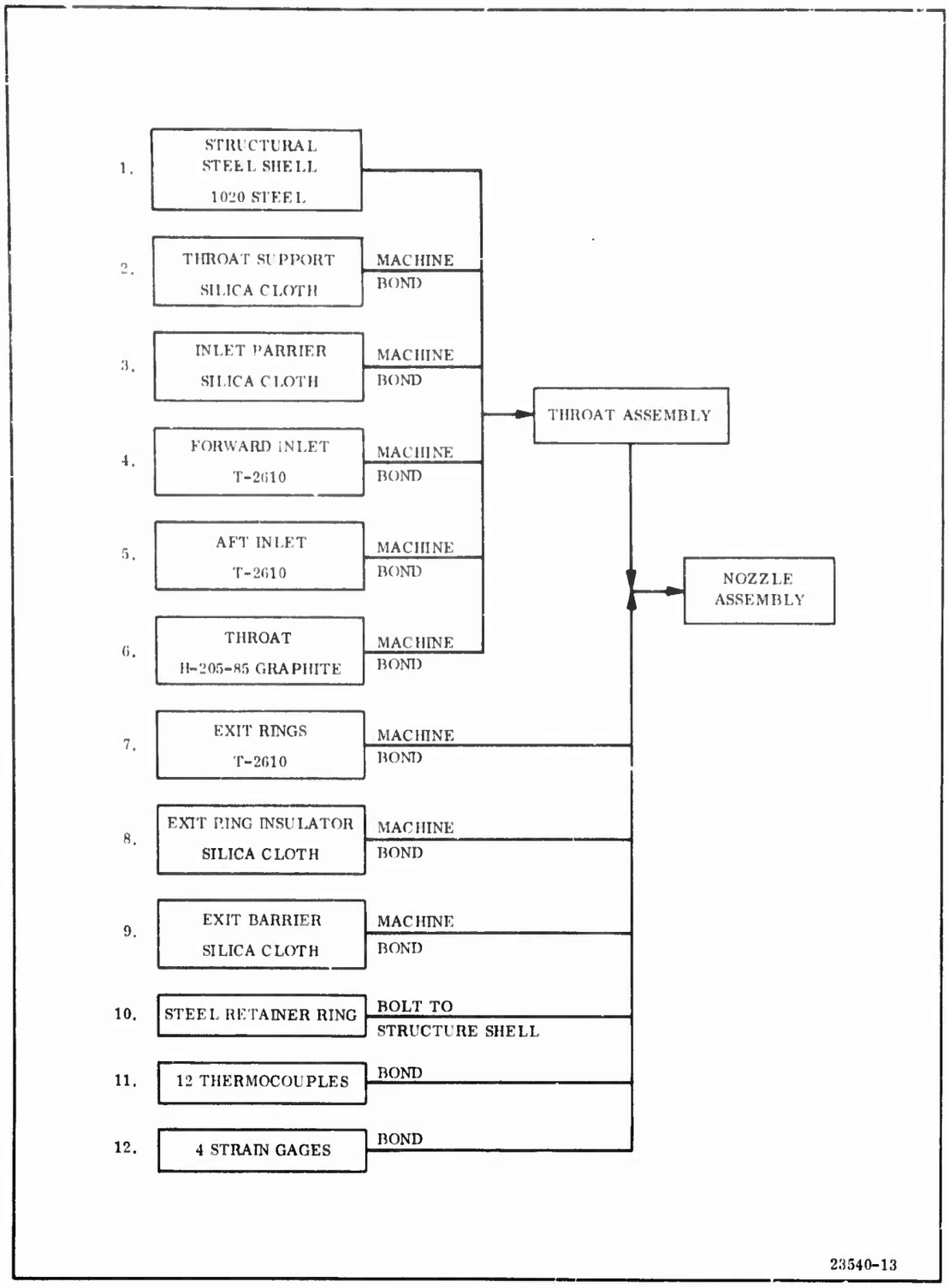

Figure 117. Nozzle No. 6 Fabrication Process

The T-2610 nozzle components were fabricated as solid billets at 1,000 psi and 300°F, with the reinforced plastics processed at 200 psi and 300°F. All the billets exposed to motor exhaust gas were X-rayed and met the Quality Assurance requirements. Tag end specimens were taken from Thiokol fabricated components and tested for density, compression, and tensile strength. Results of these tests are presented on Table XXXV. All material properties were acceptable but the forward exit cone ring of T-2610 with a 1.32 gm/cc density was considerably lower than the other T-2610 billets at 1.80 to 1.82 gm/cc.

3. ANALYSIS

The Nozzle No. 6 design criteria listed below were the same as for Nozzle No. 5.

Throat diameter	3.80 in.
Web time	60 sec
Average web pressure	700 psia
MEOP pressure	800 psia
Propellant	LPC-556

No further analyses were made for Nozzle No. 6 except the structural discontinuity stress analysis of the steel shell attached to the new aft closure boss of the 44 in. RPL char motor (Figure 118). The minimum safety factor of +1.25 occurred at the closure boss interface. The maximum shell hoop strain at strain gages S001 and S002 was calculated equal to 252×10^{-6} for an MEOP of 798 psi. The strain values do not include the induced strain of the heated insulation liners.

4. MOTOR OPERATION

The motor for the Nozzle No. 6 test operated in a normal mode up to 8 sec after ignition. After 8 sec, smoke and flames were observed at the case-closure joint. Also, after 8 sec, the motor pressure trace indicated a sharp rise to 1,382 psig at 10.6 sec. Between 16 and 18 sec the motor lurched left and right on the six component stand. At 19.3 sec the closure and nozzle were ejected at the case-closure bolted joint with a recorded motor pressure of 1,000 psig (Figure 119). The nozzle successfully survived motor operation, ejection, and ground impact.

The liner materials--T-2610 low cost graphite particle molding compound (inlet and exit) and H205-85 molded graphite (throat)--performed satisfactorily during motor operation and during nozzle-closure ejection and ground impact. The T-2610 lost more material than expected in the inlet and forward exit cone. The absence of an inlet and forward exit cone char layer and localized char layer loss in the aft exit cone indicate a possible loss of the char layer during the nozzle-closure ejection and ground impact. The low density forward exit cone (T-2610) may have also contributed to the loss of the forward exit cone char layer. In the final evaluation of the liner

TABLE XXXV

PHYSICAL PROPERTIES, NOZZLE NO. 6

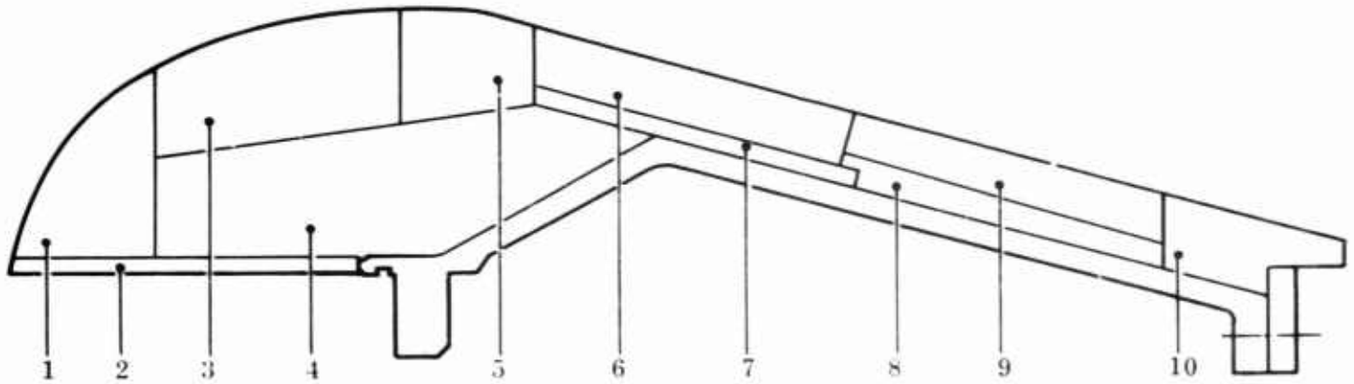

Location Index	Material	Density (gm/cc)	Mechanical Properties At Room Temperature: Compression (psi)	Tensile Strength (psi)
1	T-2610	1.80	12,900	2,845
2	Silica Cloth Phenolic	--	--	--
3	T-2610	1.81	13,020	2,785
4	Silica Cloth Phenolic	1.69	13,380	--
5	High Density Graphite	--	--	--
6	T-2610	1.32	12,362	--
7	Silica Cloth Phenolic	--	--	--
8	Silica Cloth Phenolic	--	--	--
9	T-2610	1.81	10,653	--
10	Silica Cloth	1.70	16,521	--

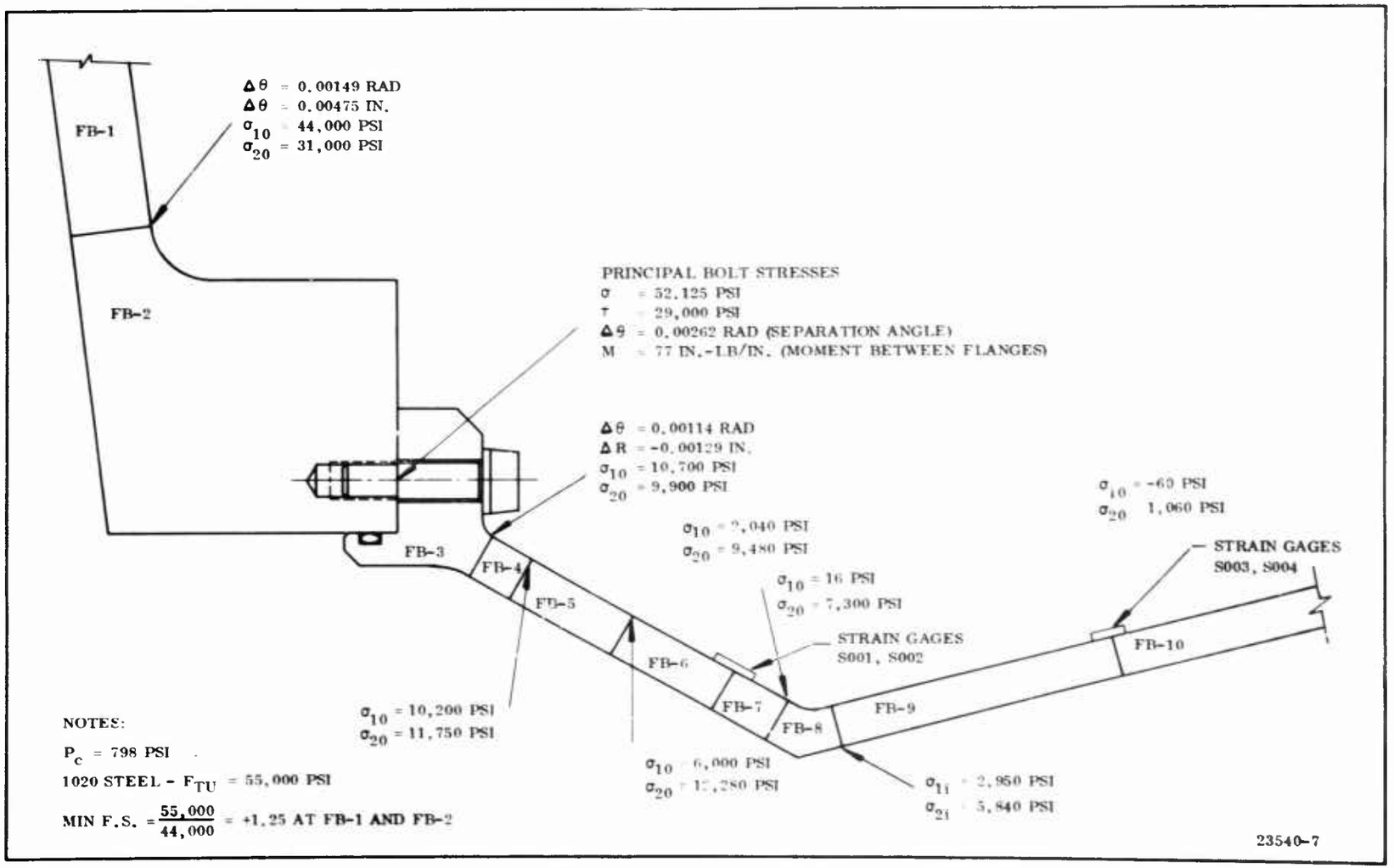

Figure 118. Housing, Nozzle No. 6 (RPL Char Motor)

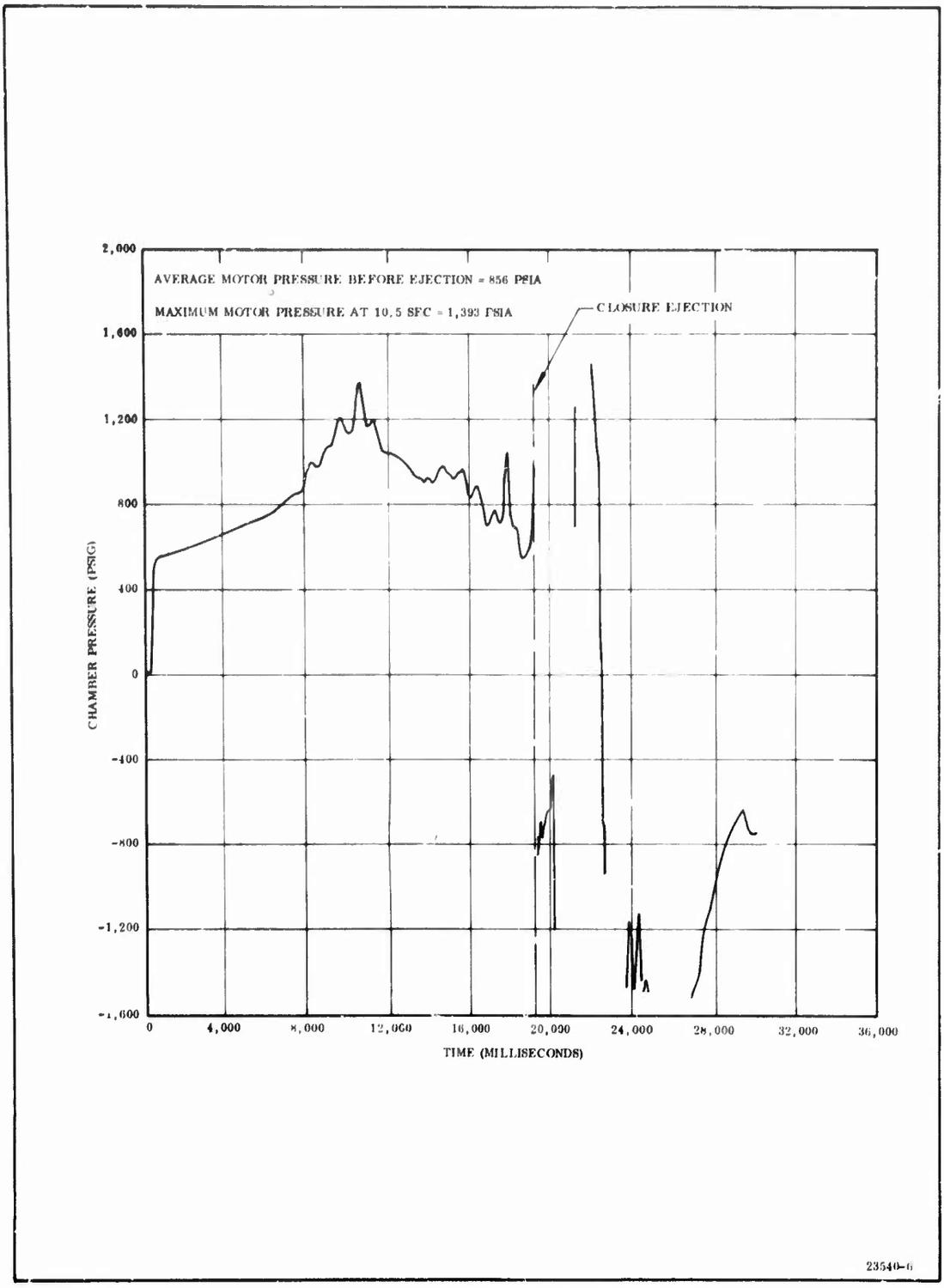

Figure 119. Pressure Trace, Test of Nozzle No. 6

materials, a depth of material loss was reported, but no erosion rates were calculated. The erosion rates were omitted because no information was available to indicate whether the T-2610 char layer was lost during motor operation or nozzle-closure ejection and ground impact.

The thermocouple traces of the backside aft inlet, throat and forward inlet were normal until motor malfunction caused erratic readings.

The strain gage results were also in agreement with the predicted structural shell stresses under 800 psia motor pressure.

Early in the motor operation (2 to 7 sec) a secondary material test was conducted by RPL personnel. A stack of materials, supported by an inverted U-bar hinged frame, was thrust into the nozzle exhaust gas plume for high temperature evaluation.

5. POST-TEST INSPECTION

Visual and photographic inspections of the fired nozzle indicated a high uniform material loss in the inlet (T-2610), an irregular, high material loss in the forward exit (T-2610), and spalling in the aft exit (T-2610). The throat ring H-205-85 graphite performed satisfactorily with low uniform erosion. Figures 120 and 121 show the irregular inlet material (T-2610) surface with a high material loss. Figures 122, 123, and 124 show the gouged and spalled exit cone rings of T-2610 also with a high material loss. A summary of material performance is shown on Table XXXVI.

The nozzle liner and insulators were sectioned into four gradients as shown in Figures 125 thru 128 to show the loose charred layers in the LCCM material.

The nozzle material loss in the four cut planes is shown in Figure 129. No erosion rates for the T-2610 were calculated due to the uncertainty of the amount of material loss before and after nozzle-closure ejection. The maximum and minimum radial throat erosion rates were 8.29/3.11 mils/sec. The aft exit cone ring of T-2610 shrunk and swelled after testing to a smaller conical surface than after final fabrication machining.

6. INSTRUMENTATION

The nozzle assembly included twelve thermocouples and four strain gages attached to the nozzle as shown in Figure 130. One thermocouple (T001) and one strain gage (S001) were inoperative during the test. At 17.0 sec the instrumentation malfunctioned due to the motor lurching in the test stand or the case-closure flame leak.

The maximum temperatures all occurred at the time of instrumentation malfunction. The maximum average backside temperature for the T-2610 aft inlet, the H-205-85 throat, and T-2610 forward exit are listed below.

TABLE XXXVI

MATERIAL PERFORMANCE, NOZZLE NO. 6

Component	Material	Comments
Forward inlet	T-2610 Graphite phenolic	Medium uniform material loss. Light spalling all around inner edge. Irregular rough surface with some pitting.
Aft inlet	T-2610 Graphite phenolic	Deep spalling at aft edge near edge of the throat. Some gouges and spalling, which created a rough surface.
Throat	H-205-85 Graphite	Light uniform erosion at both edges. Forward edges still sharp except for 90 deg section. Very good appearance. Smooth surface, free of cracks, gouges and spalling.
Forward exit	T-2610 Graphite phenolic	Normal material loss at forward edge developing into gouges all around starting 0.5 to 1.5 in. aft of forward edge all through the length and stretching into part of the forward edge of the aft exit piece. Average depth of spall, approximately 0.5 inch.
Aft exit	T-2610 Graphite phenolic	Some spalling as a continuation from the forward exit section tapering off towards exit plane. Two places, one spall area in middle ring. Uniform swelling of the material causing delaminations, 1/8 to 1/4 in. under surface, permitting escape of hot gases towards end ring. Possible leaking through delaminations near aft exit.
End ring	Silica cloth phenolic	Light uniform erosion. Smooth surface. Some discoloration and flow patterns. Very good condition. Some delaminations at forward edge and away from spalled aft exit area.

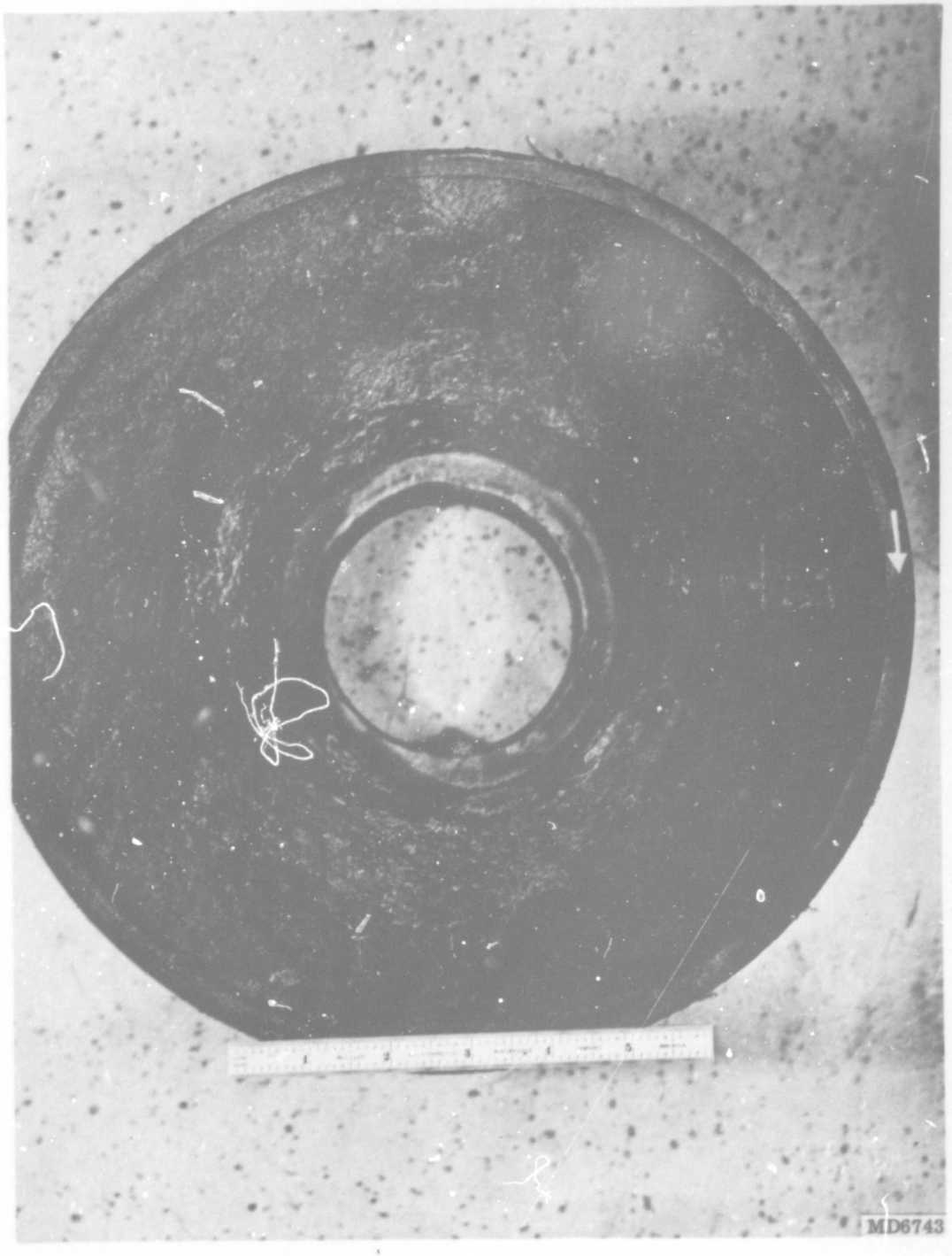

Figure 120. Nozzle No. 6 Postfired Inlet (View A)

Figure 121. Nozzle No. 6 Postfired Inlet (View B)

Figure 122. Nozzle No. 6 Postfired Exit Cone (View A)

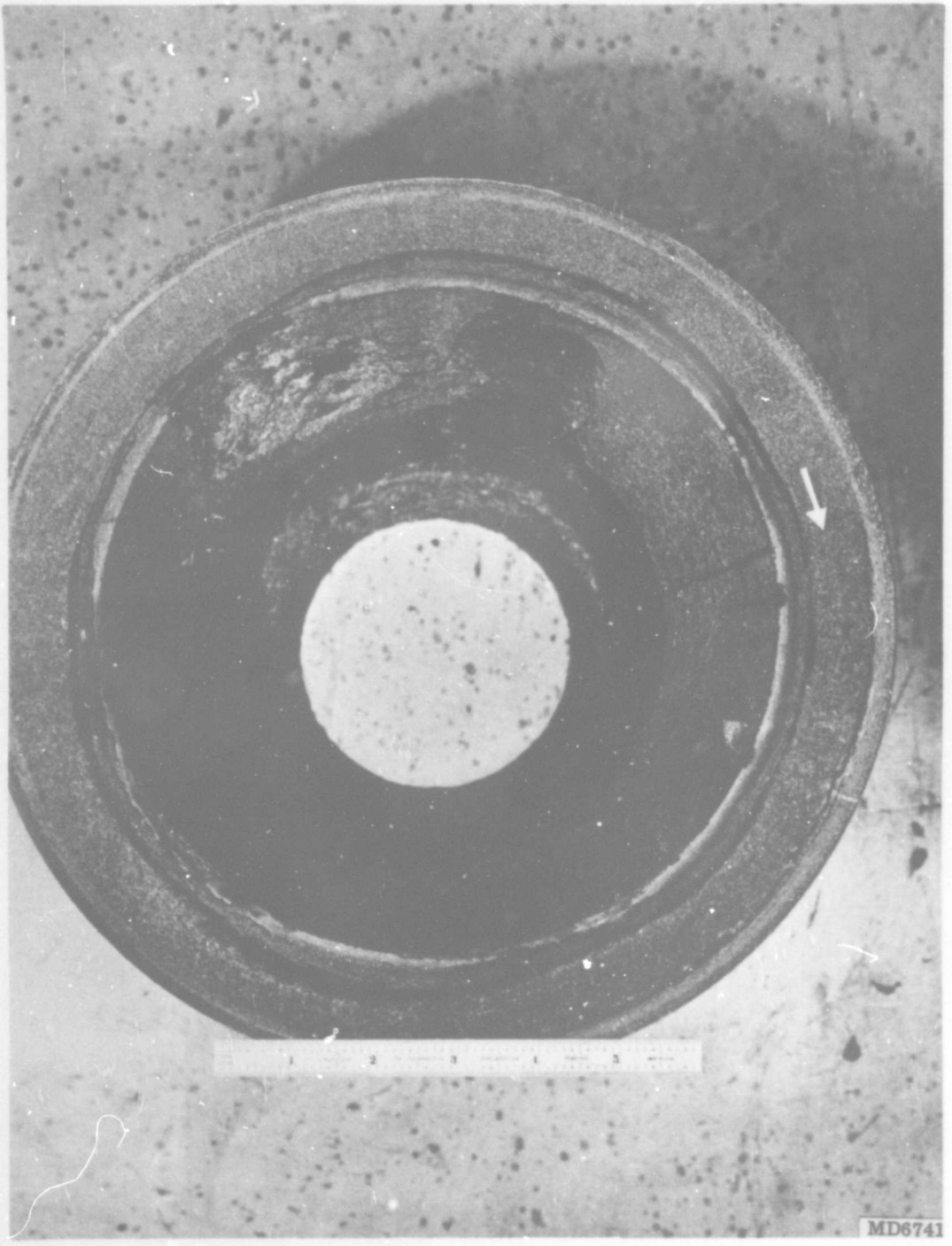

Figure 123. Nozzle No. 6 Postfired Exit Cone (View B)

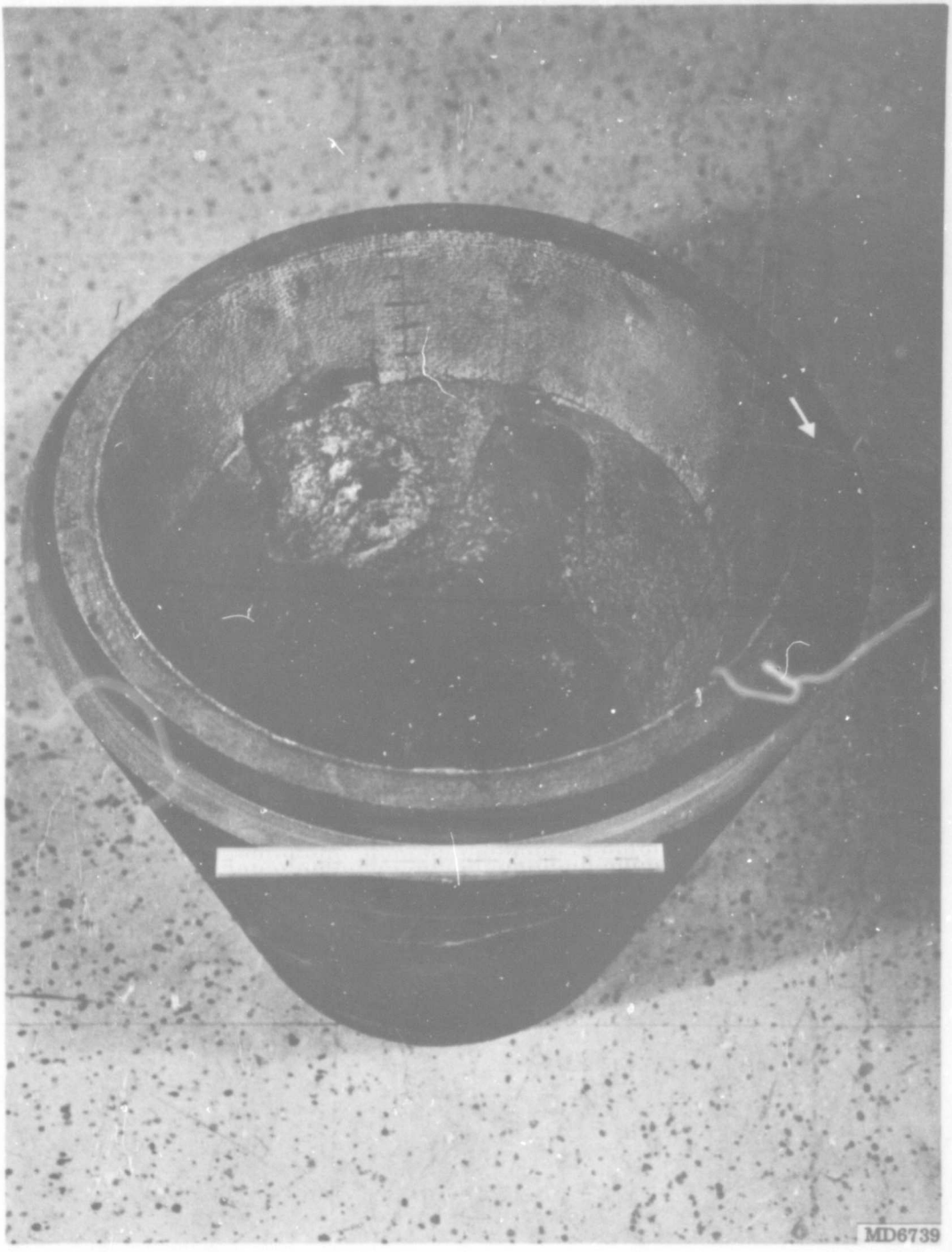

Figure 124. Nozzle No. 6 Postfired Throat Exit Ring

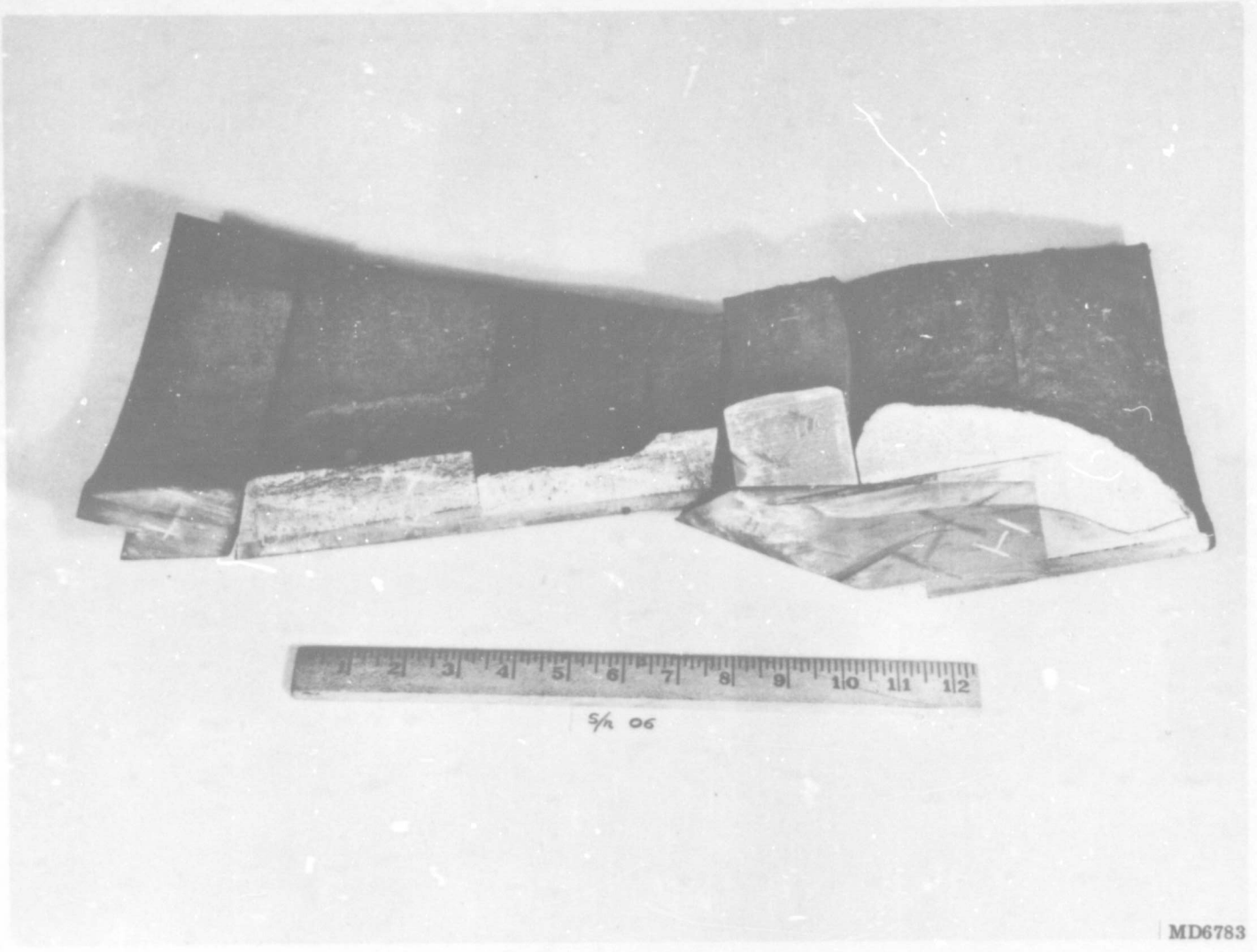

Figure 125. Nozzle No. 6 Postfired Segment (A)

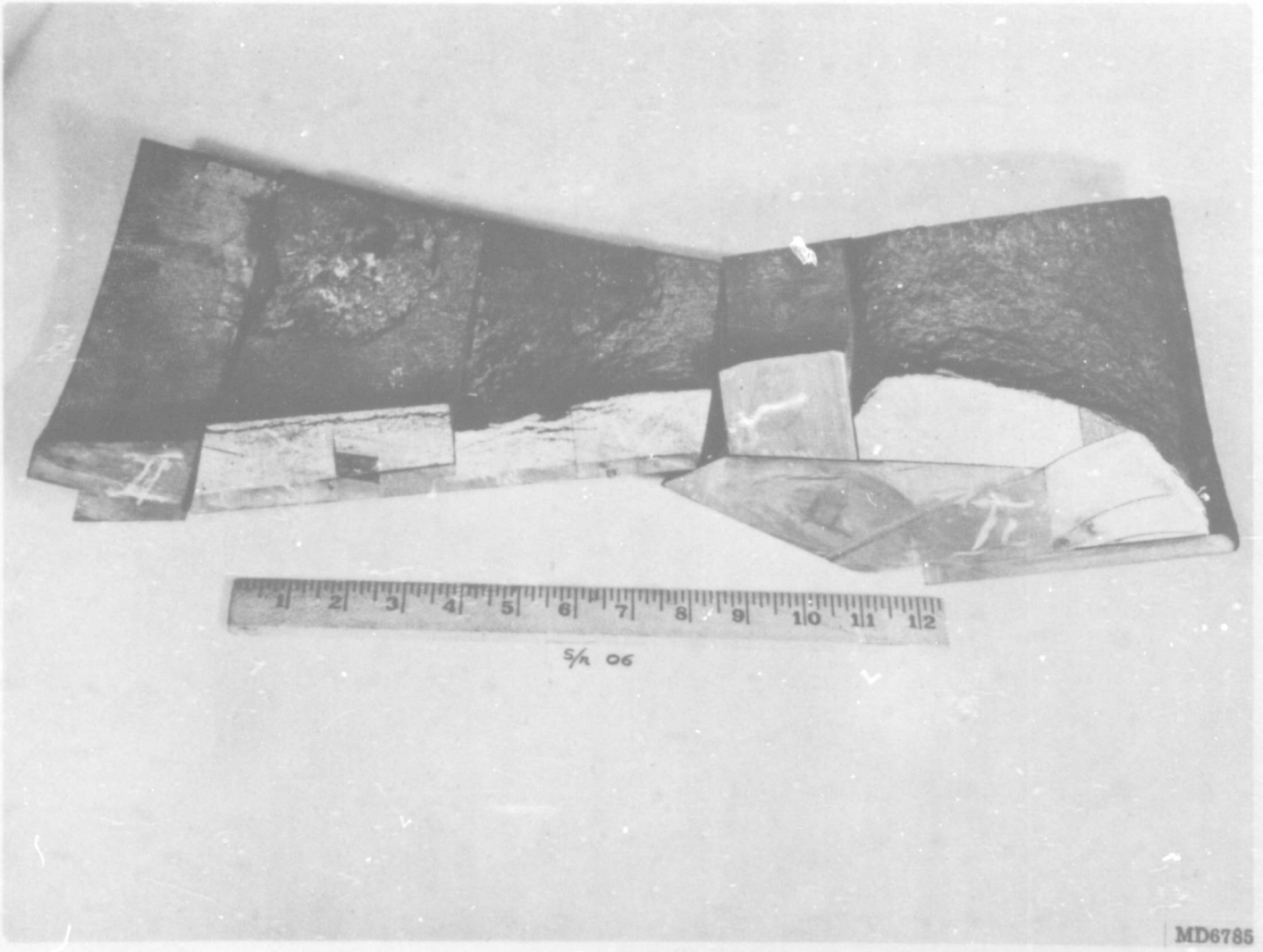

Figure 126. Nozzle No. 6 Postfired Segment (B)

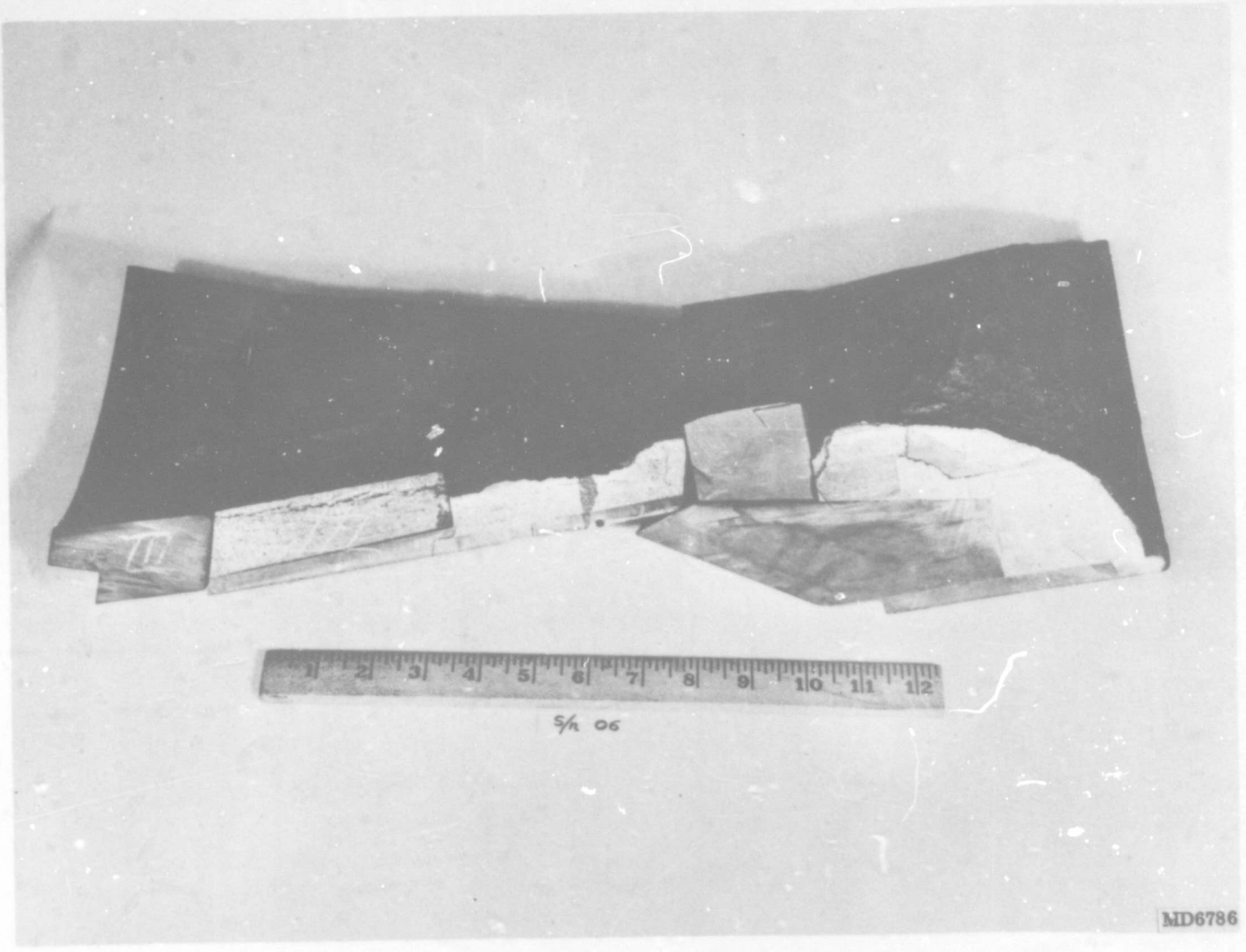

Figure 127. Nozzle No. 6 Postfired Segment (C)

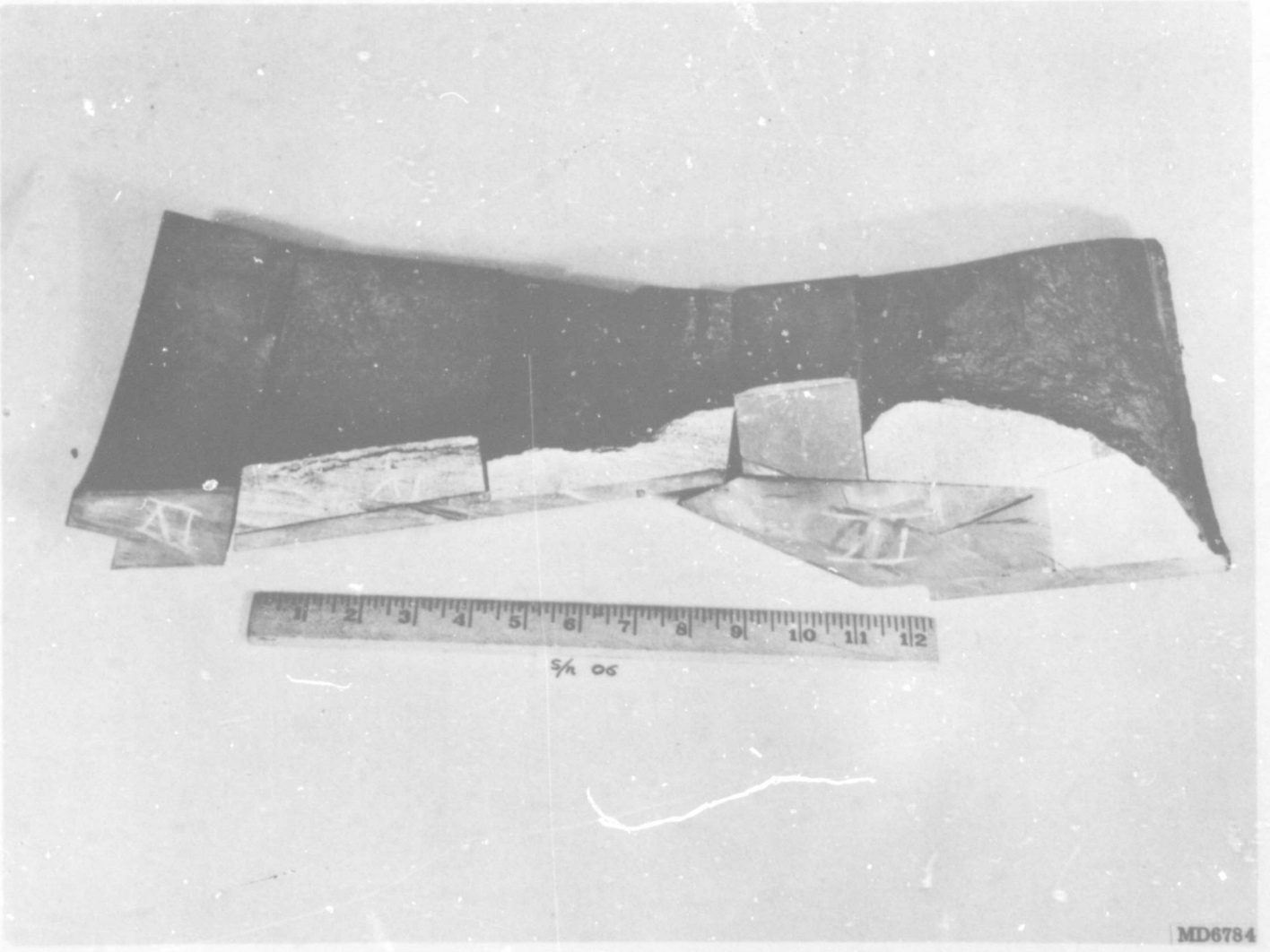

Figure 128. Nozzle No. 6 Postfired Segment (D)

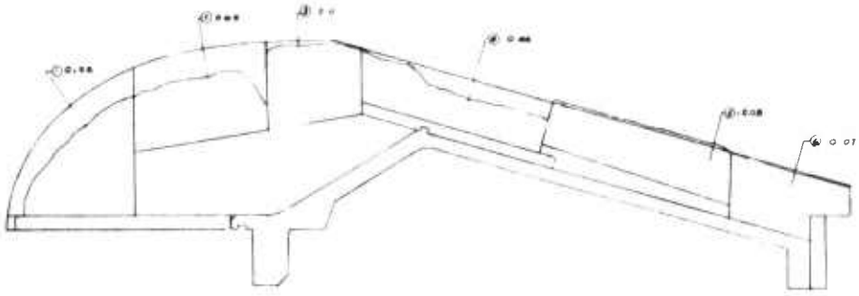

EROSION PROFILE SECTION-I

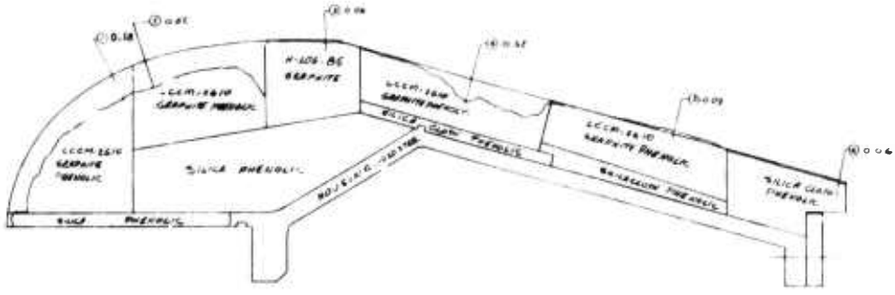

EROSION PROFILE SECTION II

A

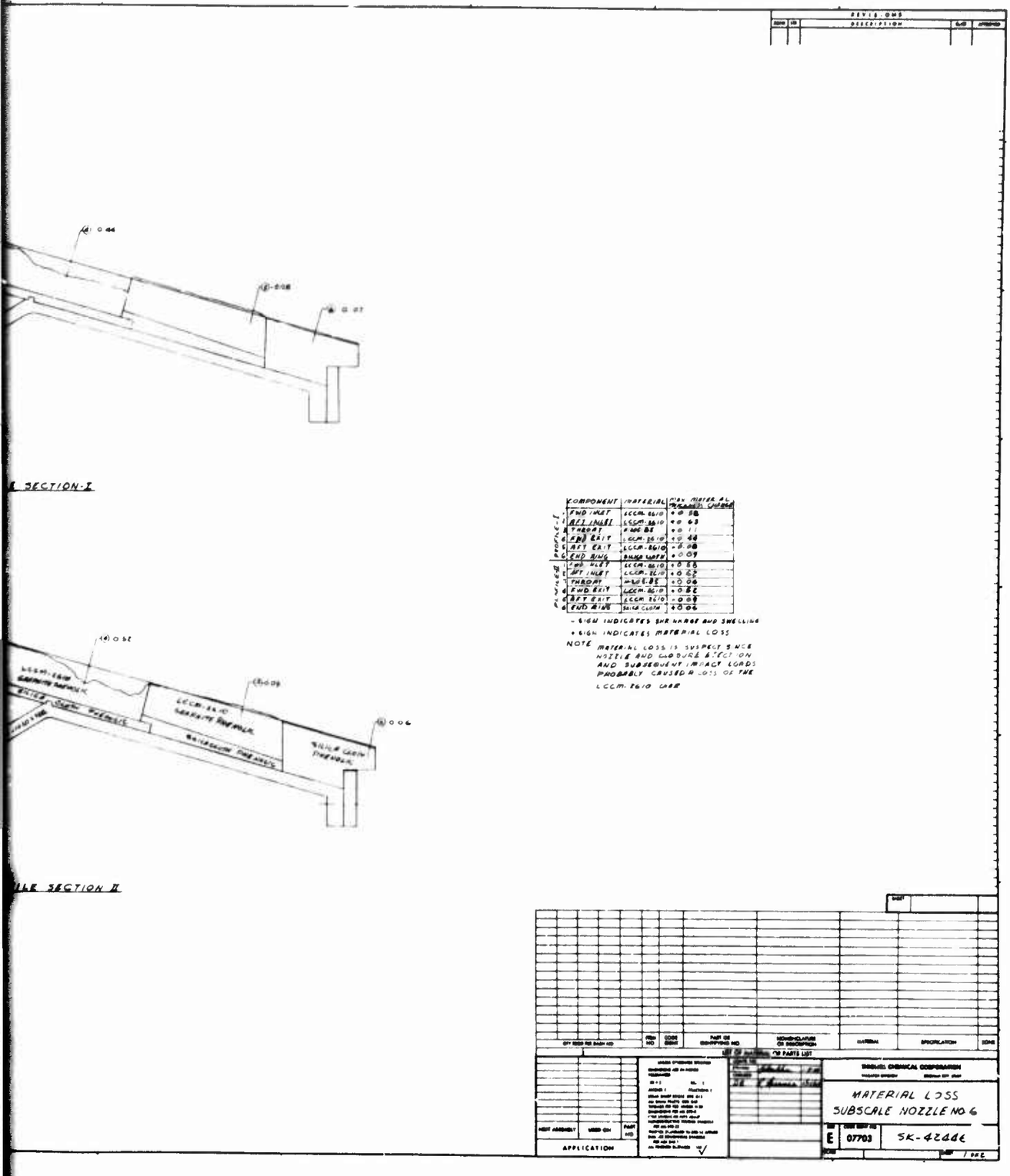

Figure 129. Nozzle No. 6 Material Loss

B

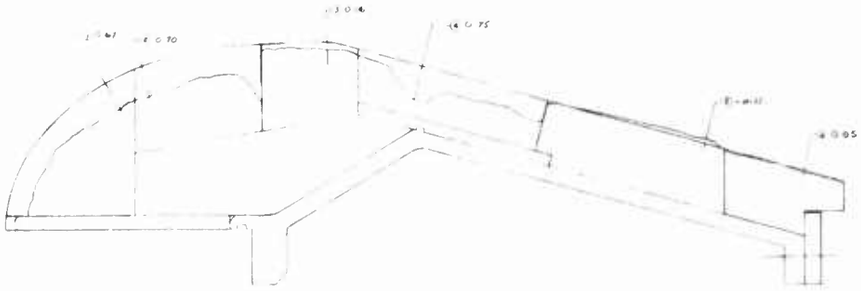

EROSION PROFILE SECTION III

	COMPONENT	MATERIAL	MAX. MATERIAL ALLOWABLE SUBMERGE
PROFILE III	1	FWD INLET	LCCM EG10	+ 0.67
	2	AFT INLET	LCCM EG10	+ 0.70
	3	THROAT	W-208 BS	+ 0.16
	4	FWD EXIT	LCCM-EG10	+ 0.75
	5	AFT EXIT	LCCM-EG10	- 0.11
	6	END RING	SILICA CLOTH	+ 0.05
PROFILE IV	1	FWD INLET	LCCM EG10	+ 0.88
	2	AFT INLET	LCCM EG10	+ 0.61
	3	THROAT	W-208 BS	+ 0.18
	4	FWD EXIT	LCCM-EG10	+ 0.78
	5	AFT EXIT	LCCM EG10	- 0.09
	6	END RING	SILICA CLOTH	+ 0.88

- SIGN INDICATES SUBMERGE AND

+ SIGN INDICATES MATERIAL LOSS

NOTE

MATERIAL LOSS IS SUSPECT
NOZZLE AND CLOSURE EJE
AND SUBSEQUENT IMPACT
PROBABLY CAUSED ACOSS
LCCM-EG10 CHAR

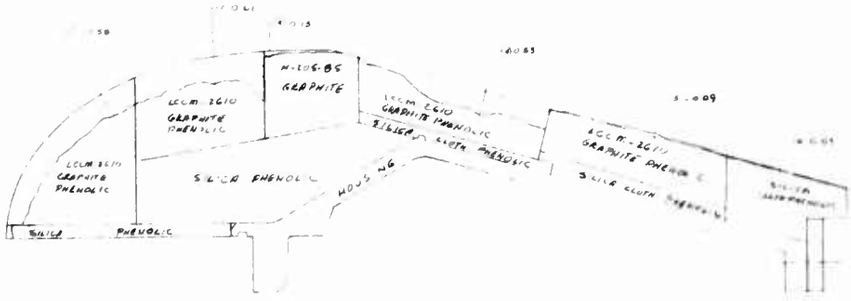

EROSION PROFILE SECTION IV

Figure 12

A

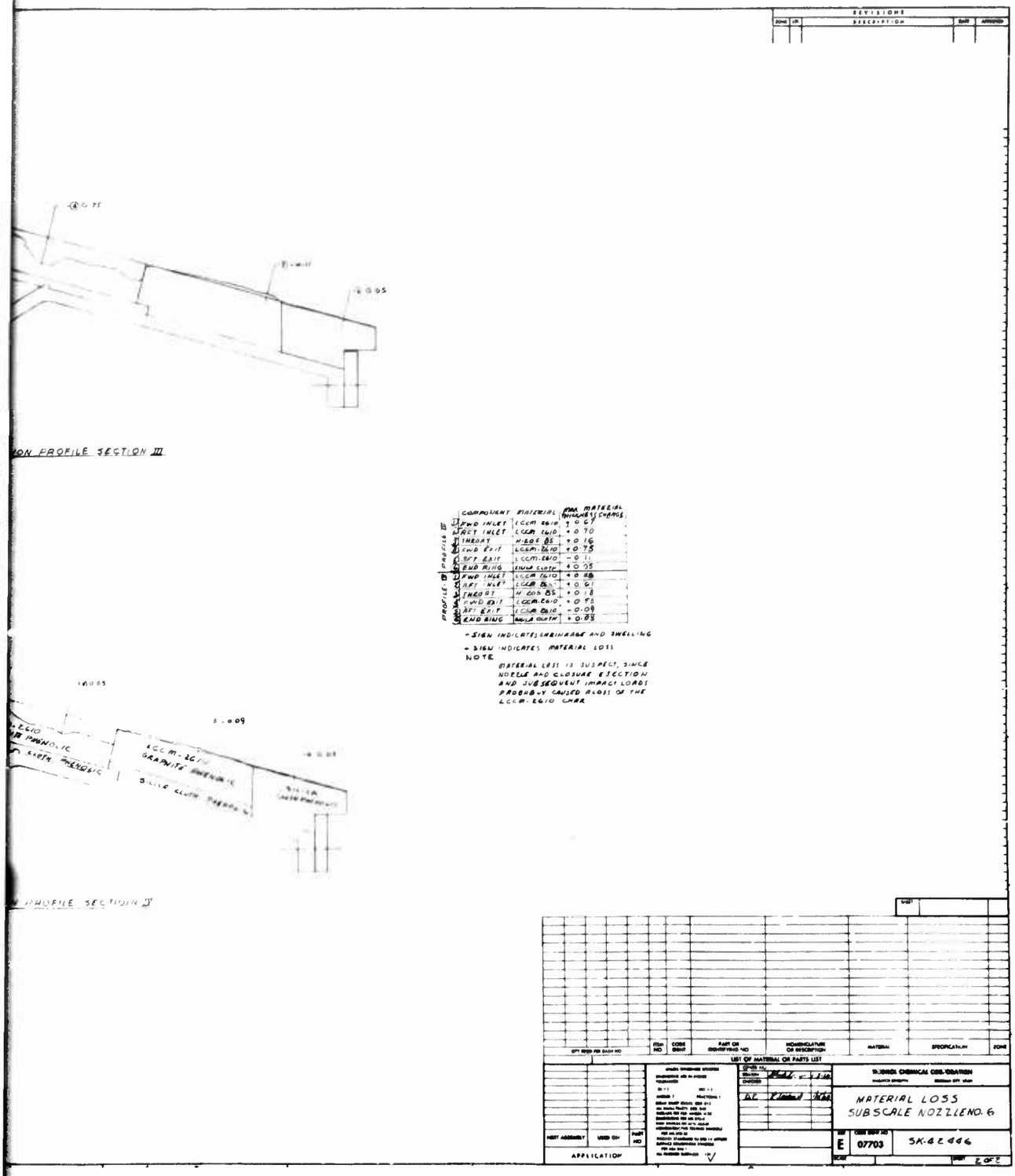

Figure 129. Nozzle No. 6 Material Loss (Cont)

B

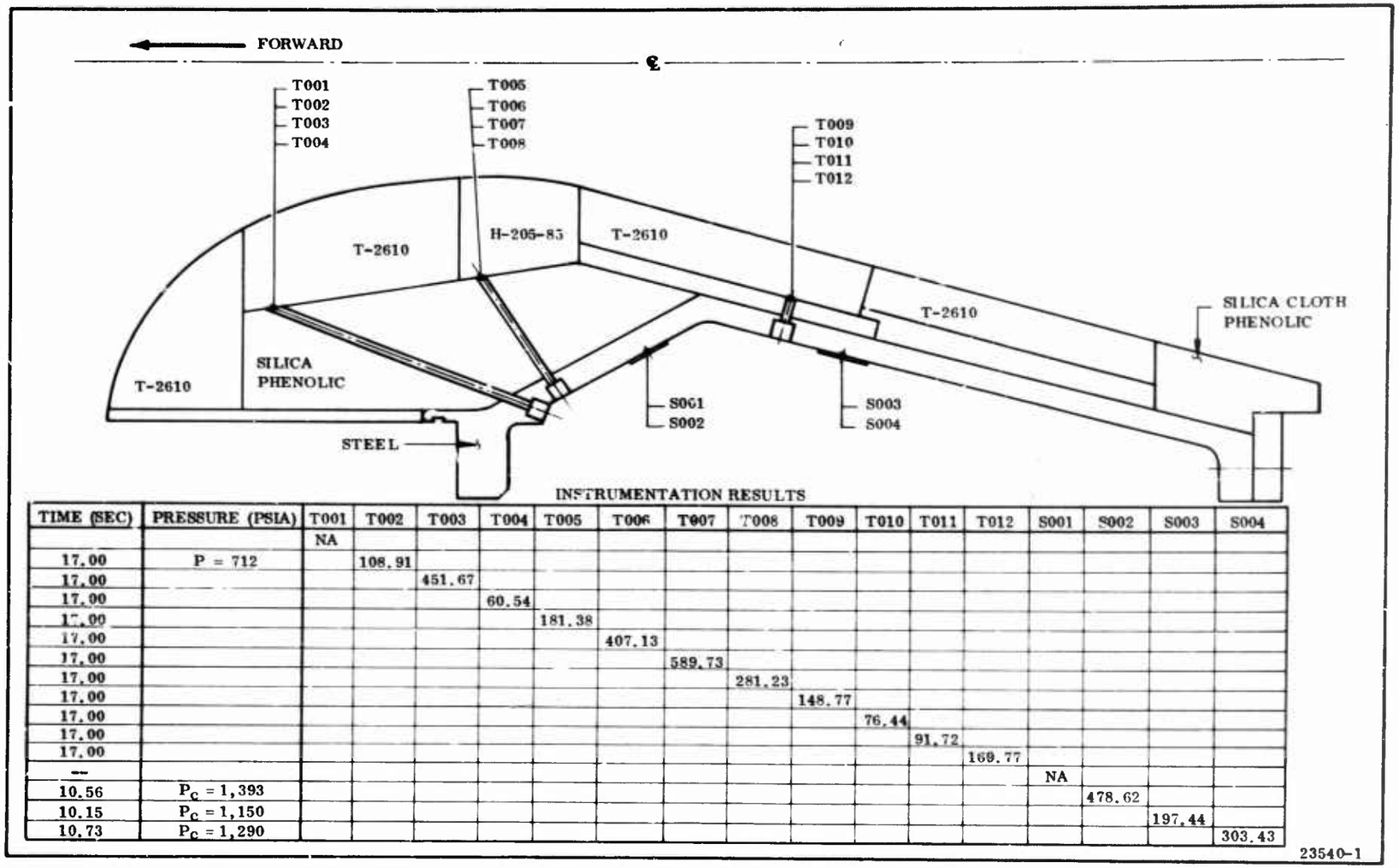

TIME (SEC)	PRESSURE (PSIA)	T001	T002	T003	T004	T005	T006	T007	T008	T009	T010	T011	T012	S001	S002	S003	S004
		NA															
17.00	P = 712		108.91														
17.00				451.67													
17.00					60.54												
17.00						181.38											
17.00							407.13										
17.00								589.73									
17.00									281.23								
17.00										148.77							
17.00											76.44						
17.00												91.72					
17.00													169.77				
—														NA			
10.56	P_c = 1,393														478.62		
10.15	P_c = 1,150															197.44	
10.73	P_c = 1,290																303.43

Figure 130. Maximum Instrumentation Readings, Nozzle No. 6

	Max Avg Temperature (°F)
Aft inlet (T-2610)	207
Aft throat (H-205-85)	365
Forward exit (T-2610)	122

The thermocouples at the inlet, throat and exit are plotted versus motor time in Figures 131 thru 133.

Strain gages located on the steel shell back of the forward exit cone are plotted versus motor time in Figure 134. The maximum average stress and strain are shown below.

Location	Time (sec)	Motor Pressure (psia)	Max Avg Strain (in./in. x 10^{-6})	Max Avg Stress (psi)
Convergent steel cone	10.56	1,393	479	13,900
Divergent steel cone	10.73	1,290	226	6,550

The maximum average strain at the design pressure (800 psi) is compared with the predicted strain levels:

	Time (sec)	Actual Max Avg Strain (in./in. x 10^{-6})	Predicted Max Avg Strain (in./in. x 10^{-6})
Convergent steel cone	6.8	303	252
Divergent steel cone	6.8	185	37

Good agreement between actual and predicted strain levels are shown for both the divergent and convergent steel strain gages.

7. DISCUSSION OF NOZZLE NO. 6 TEST RESULTS

Nozzle No. 6 was fired 30 Oct 1968 at Edwards Air Force Base for the purpose of evaluating the performance and quality of LCCM components. The test was not completed due to a malfunction of the aft motor closure which was blown off with the nozzle. Results of the analysis indicated that the material loss was due to:

1. Impact loads on the nozzle which may have caused some loss of the T-2610 char.
2. Erratic motor operating pressures (Figure 119).

However, analysis results of components for the firing period prior to the malfunction indicates:

1. The T-2610 used in the forward and aft inlet showed high uniform material loss with some light pitting.
2. The H-205-85 graphite used in the throat was in excellent condition.
3. The forward and aft exit cone sections were also manufactured from T-2610. The forward section exhibited heavy localized spalling and gouges extending into the aft exit section. The aft exit cone also showed some swelling and possible gas leaks through the char layer (Figures 123 and 124). The low density forward exit ring may have contributed to the heavy irregular material loss.
4. The end ring of silica cloth phenolic was in very good condition.
5. The thermocouple and strain gage instrumentation results appeared normal when compared with previous successful subscale nozzle tests.

Nozzle No. 6 operated satisfactory until the motor aft closure separated from the motor assembly at 19.3 sec of motor operation.

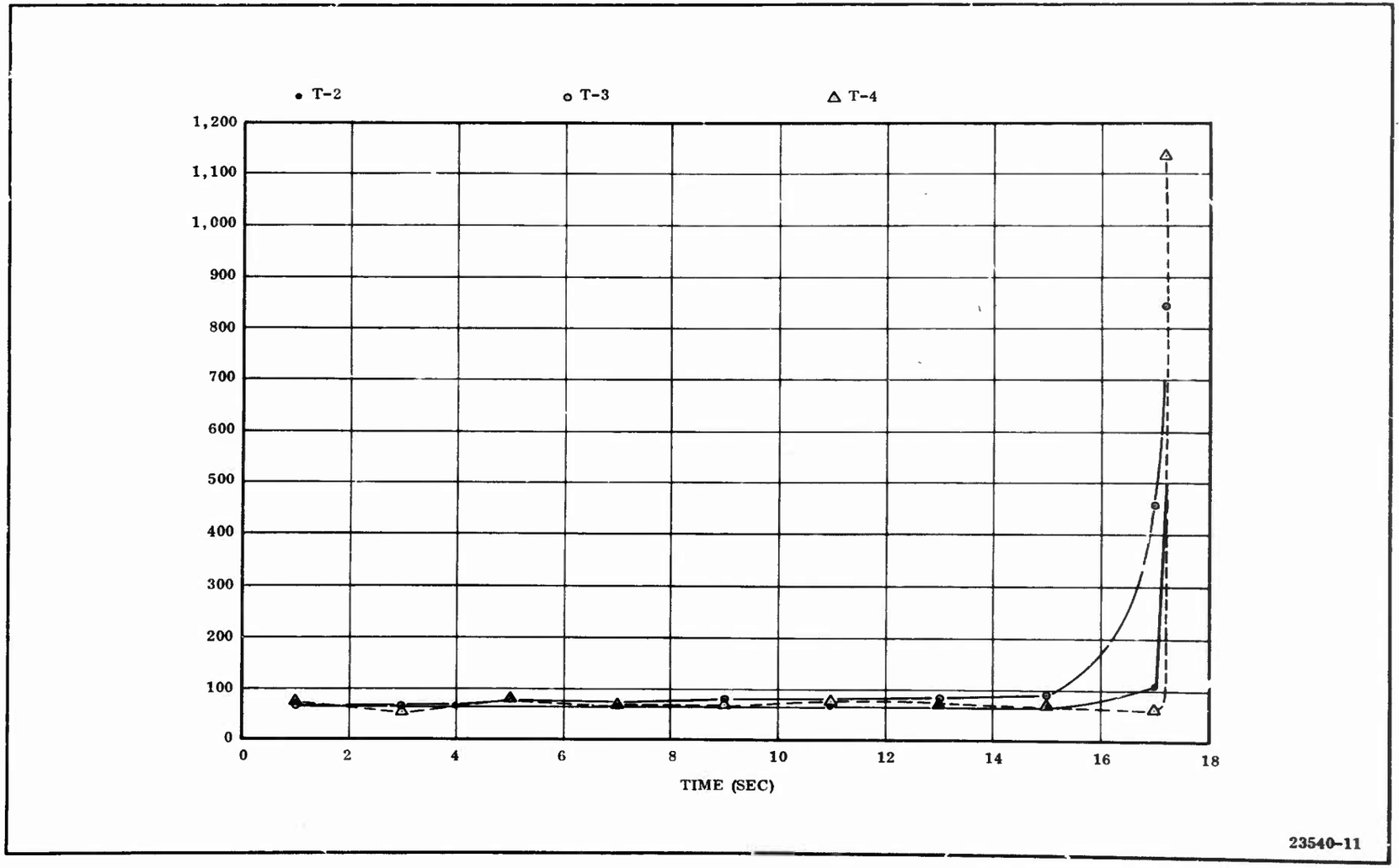

Figure 131. Nozzle No. 6 Inlet Thermocouple Reading

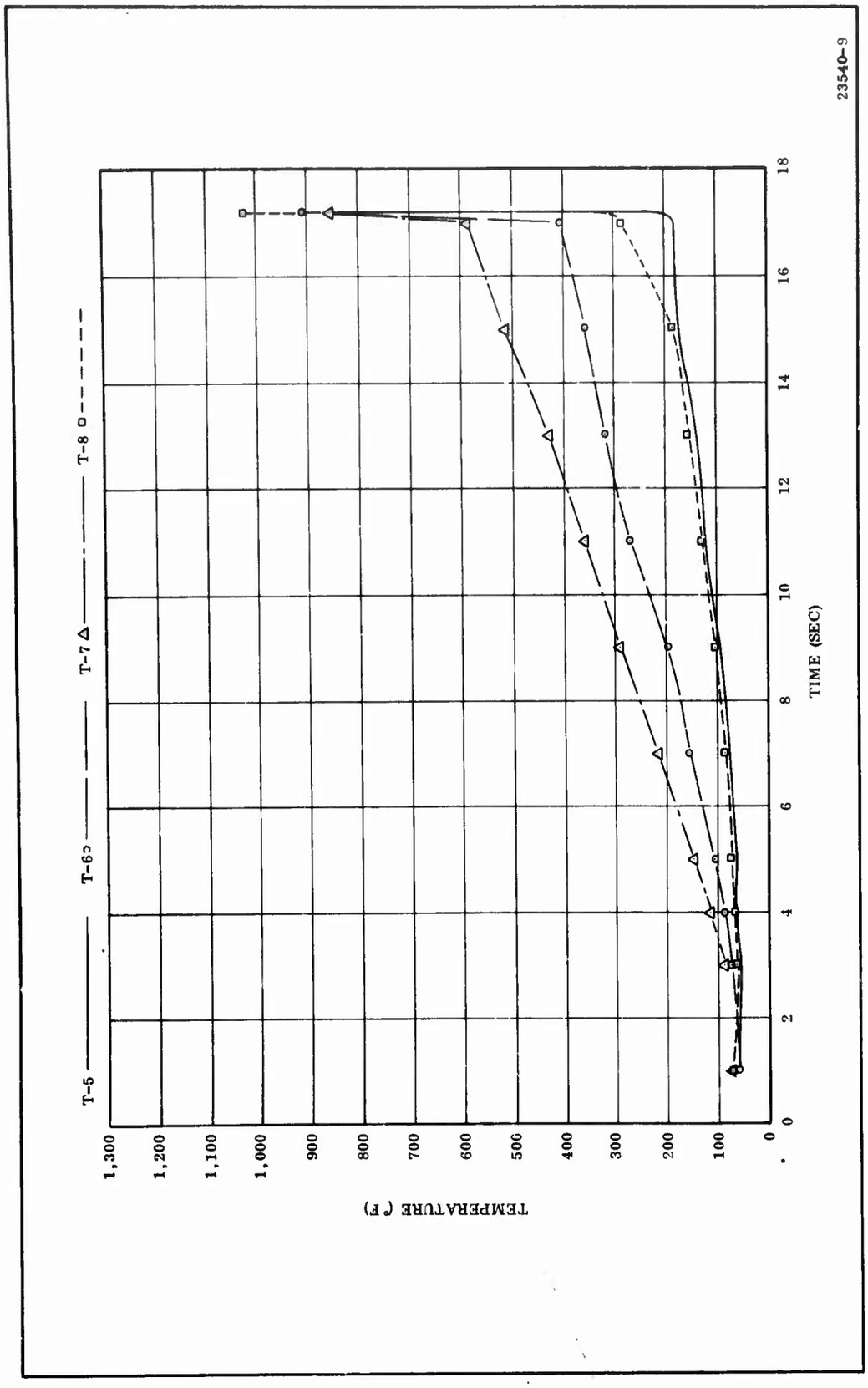

Figure 132. Nozzle No. 6 Throat Thermocouple Reading

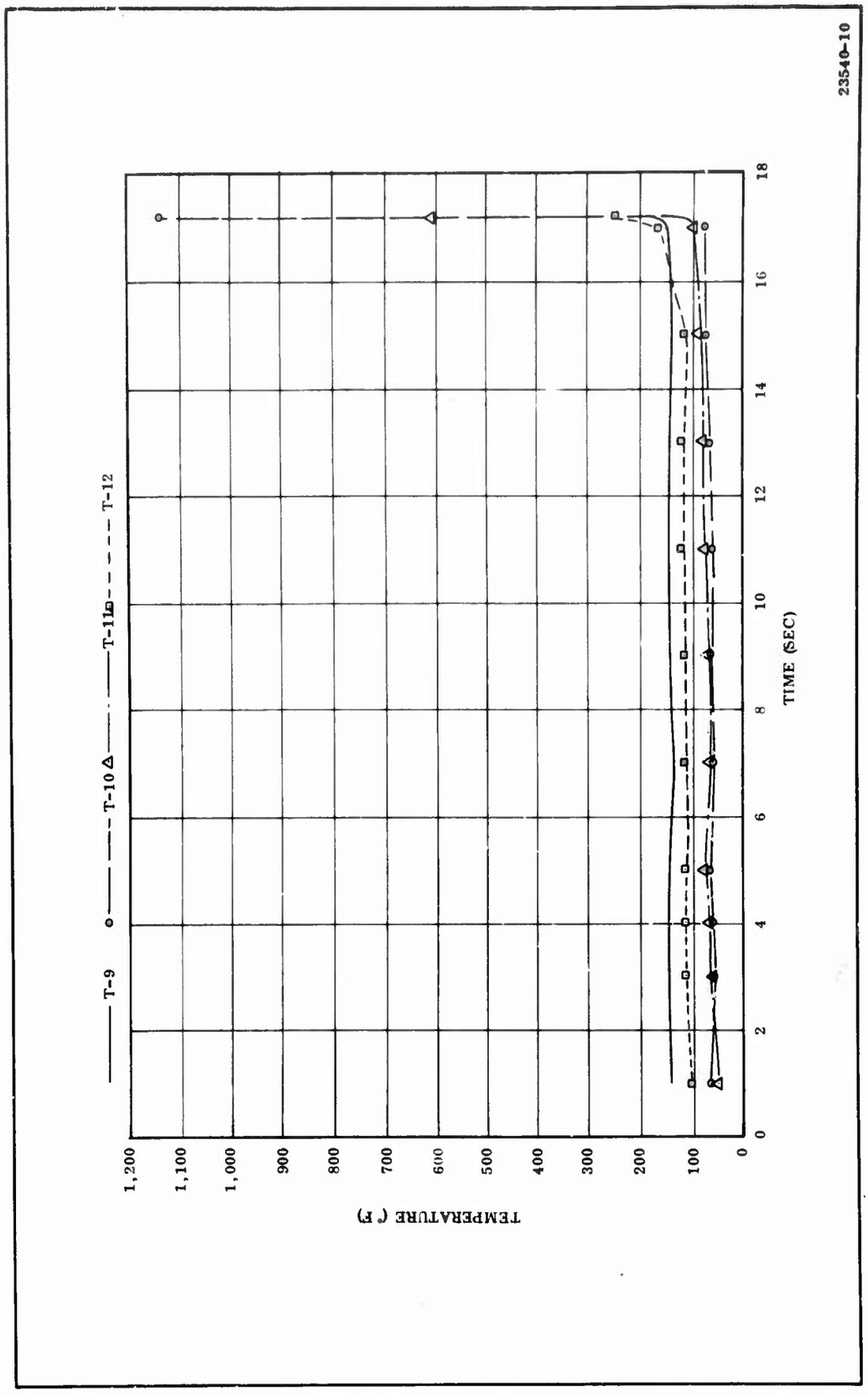

Figure 133. Nozzle No. 6 Exit Cone Thermocouple Reading

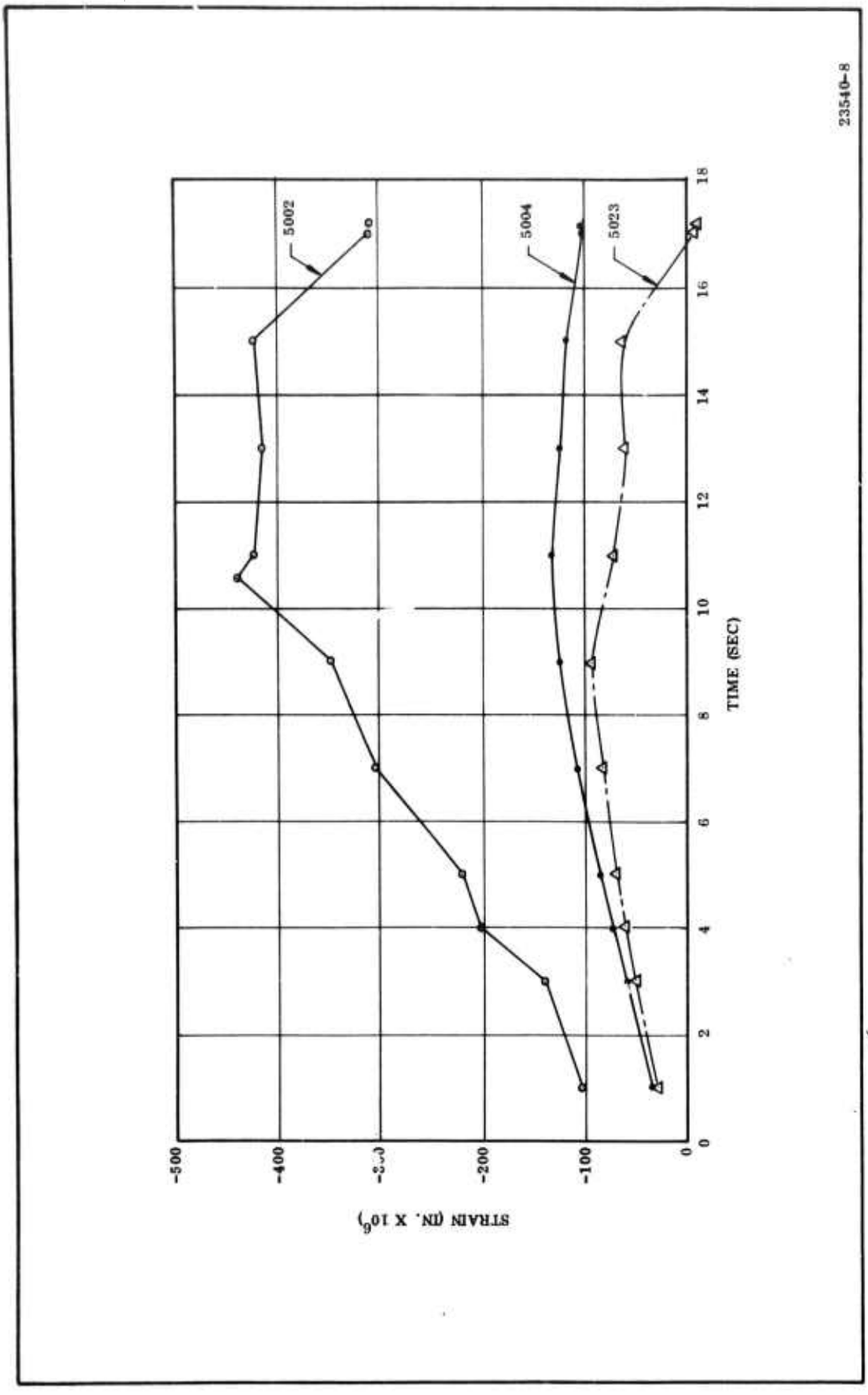

Figure 134. Nozzle No. 6 Strain Gage Readings

SECTION IV
CONCLUSIONS AND RECOMMENDATIONS

This program encompassed material and process optimization and motor static test evaluation of three graphite-particle phenolic ablative materials (T-2610, T-4120, and T-4113). The accumulative results of this family of low cost materials are very encouraging as demonstrated by the erosion resistance of T-2610 as a nozzle throat component in test Nozzle No. 3, and the general performance of T-4120 in the higher expansion ratios of the exit cone in Nozzles No. 2 and 3. However, performance data from the six motor firings substantiate that these carbonaceous materials will require additional development effort and performance evaluation before they can be recommended for use as reliable ablative materials in a large solid propellant motor environment. Based on these results, the following conclusions are offered.

1. T-2610 exhibited acceptable performance as a throat component when evaluated at moderate pressures (550-575 psi avg).
2. T-4120 performs well in the exit cone at the higher expansion ratio when cured at low temperature and pressure (170° F, 15 psi).
3. T-4113 as an ablative liner is unacceptable; however, the material may be utilized as a liner backup component.
4. Laboratory and small screening motor tests indicate that T-4120 can be used as an ablative liner defect repair material on components fabricated from the three materials evaluated in this program.
5. In general the reliability and performance uniformity of these materials must be improved to be comparable in performance with the more expensive reinforced phenolic ablative materials that are commonly used.

Based on the accumulative results of the T-2610 and T-4120 tests, additional development and evaluation effort is recommended.

APPENDIX A

NOZZLE AEROTHERMODYNAMIC ANALYSES

The theoretical aerothermodynamic analyses of the liner wall material in a nozzle considers several steps in defining the flow field, the environmental conditions near the wall, and the response of the materials to these environments.

This analysis is performed in eight separate steps, five of which are programed for high speed digital computers.

A. Thermochemical analysis

B. Nozzle configuration

C. Wall erosion prediction

D. Flow field calculation

E. Boundary layer

F. Wall material properties

G. Wall transient temperature

H. Wall transient temperature check

This method of analysis, while essentially theoretical, does provide for the introduction of empirical data (wall erosion prediction) and design information (nozzle configuration and wall material properties) to supplement theory. The analysis steps are summarized in Figure A-1 and discussed in detail below.

A. THERMOCHEMICAL ANALYSIS

From the basic propellant formulations and a specified chamber pressure, the equilibrium and/or frozen composition and thermodynamic properties are calculated during gas expansion. The original version of the program in use at Thiokol was based on one by Zeleznik and Gordon described in NASA TND-1454. The analysis is primarily based on satisfying conservation of mass, Dalton's Law of partial pressures, adiabatic combustion, and an isentropic combustion process. The enthalpy, heat of formation, and free energy data are obtained from an up-to-date file of JANAF data. The species system is usually set to allow every gaseous species, including ions if desired, to be in the system of products that are selected from the thermodynamic tape. Gaseous or liquid species are allowed to change phase at their equilibrium temperature.

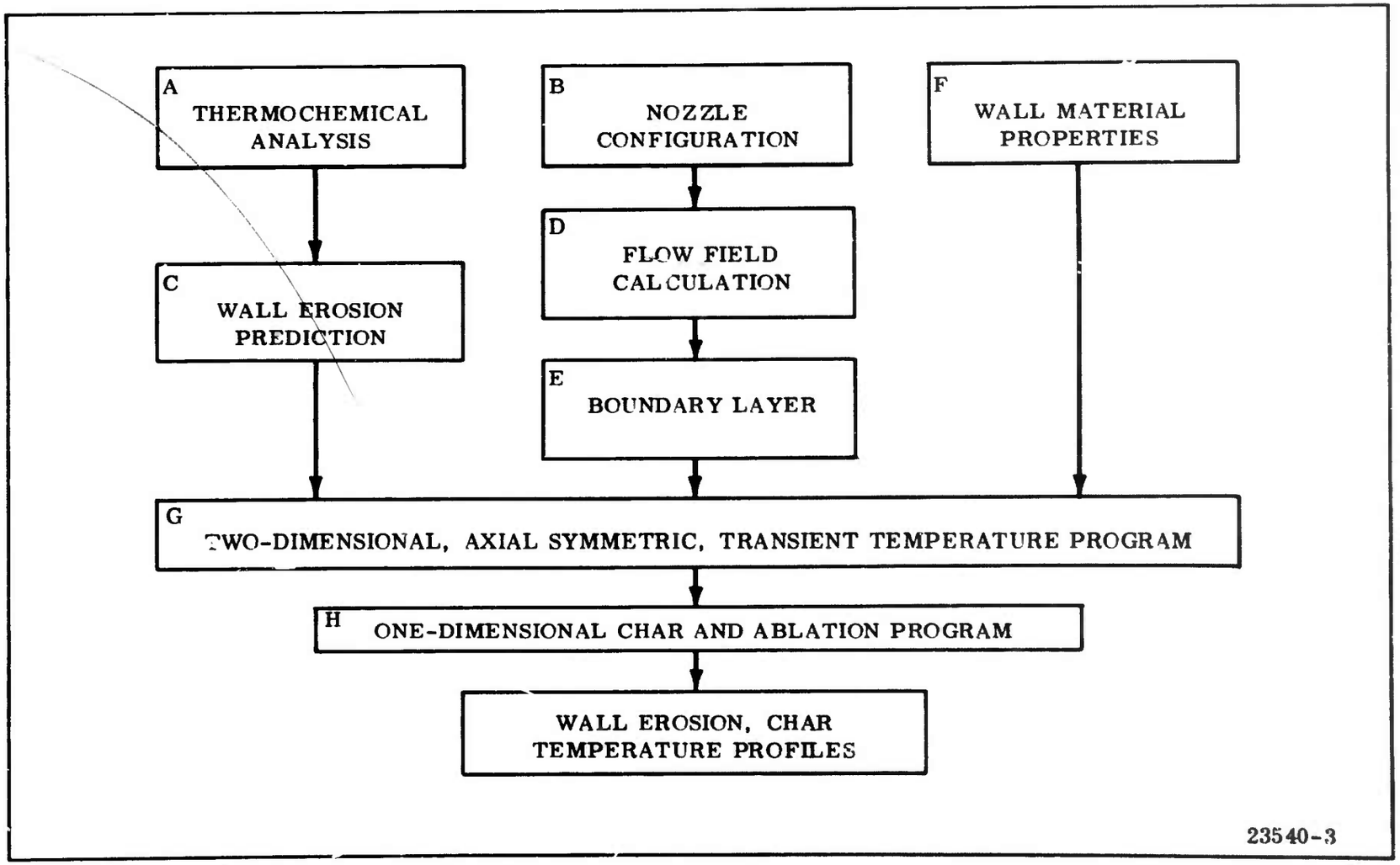

Figure A-1. Aerothermal Analysis in Wall Material Response Calculations

The output parameters, which are subsequently used in the aerothermo analysis, are the gas thermodynamic properties, the composition, and the blowing coefficient.

B. NOZZLE CONFIGURATION

The nozzle configuration (inlet, throat and exit diameters, inlet coordinates and exit cone half angle) defines the boundaries for the wall erosion prediction and flow field calculations.

C. WALL EROSION PREDICTION

To provide wall erosion predictions the following motor information must be available.

1. Grain configuration.
2. Propellant blowing coefficient.
3. Nozzle configuration.
4. Throat diameter.
5. Average web pressure.
6. Liner materials selected.

The following steps outlined in Thiokol-Wasatch Document TWR-1710 "A Method for Preliminary Sizing of Nozzle Liner" and shown in Figure A-2 are followed for an empirical prediction of wall erosion rate.

1. Enter Bartz simplified convective heat transfer coefficient chart with the area ratio of the wall plane where the erosion rate is required and read out the convective heat transfer coefficient for the reference conditions of 1,000 psi, D_T = 10.00 in., blowing coefficient = 0.108, and wall temperature = 5,790° F.
2. Modify the convective heat transfer coefficient to the required motor average web pressure and throat diameter as shown:

$$\text{Modified } h/cp = hc/p \left(\frac{\bar{P}}{1,000}\right)^{1/1.25} \left(\frac{10}{D_T}\right)^{1/5}$$

where $\bar{p}$ = Required motor average web pressure

D_T = Required nozzle throat diameter

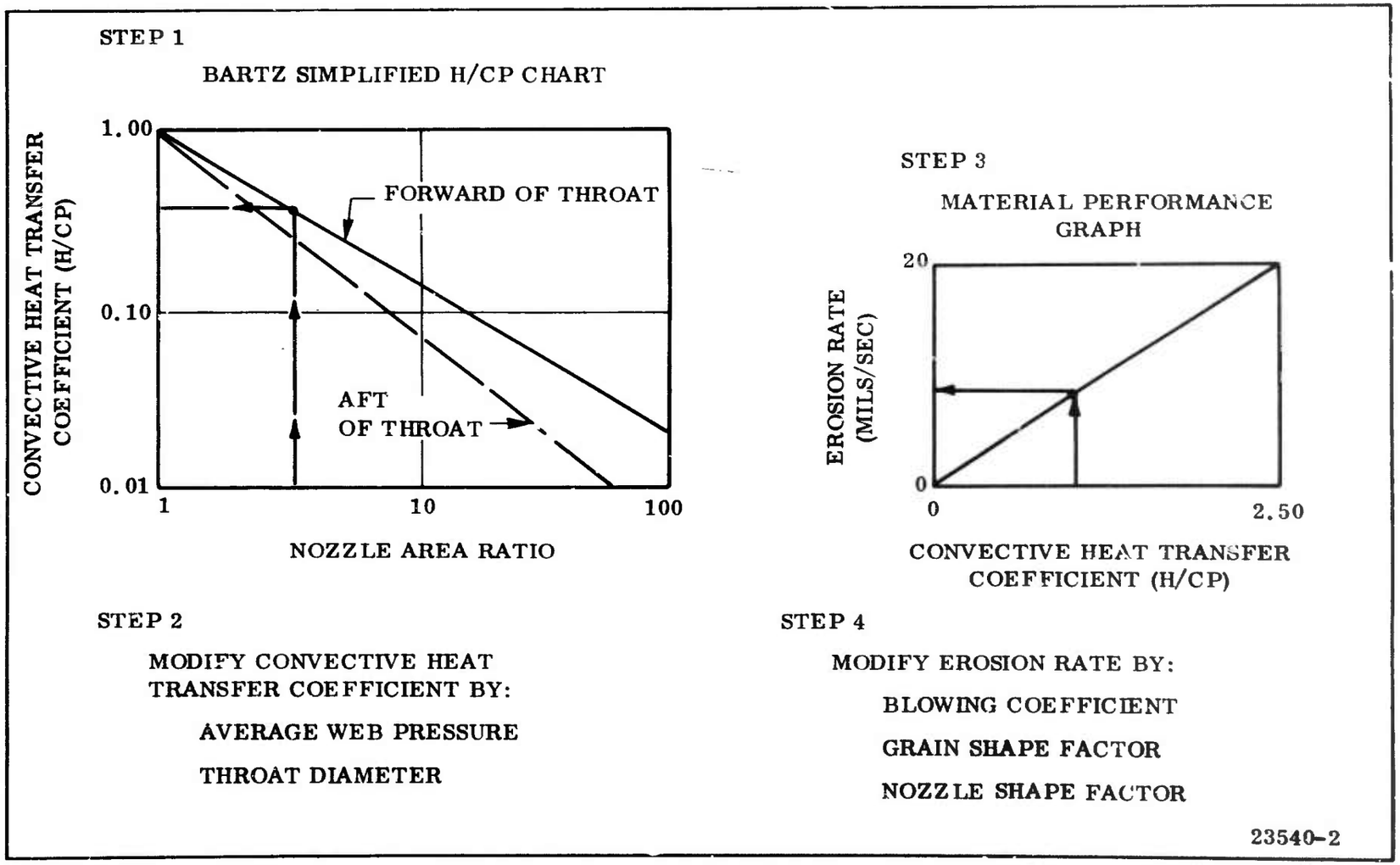

Figure A-2. Wall Erosion Rate Prediction Calculation Steps

3. Enter a material performance graph of the same material as the liner wall with the modified convective heat transfer coefficient and read out the predicted wall erosion rate.
4. Modify the predicted erosion rate by the grain shape factor (GSF), end burner; Star or CP; the propellant blowing coefficient (PBC); and the nozzle shape factor (NSF), external or submerged and type of TVC control.

$$\text{Modified erosion rate} = \text{erosion rate (GSF)} \left(\frac{\text{PBC}}{0.108}\right) \text{(NSF)}$$

D. FLOW FIELD CALCULATION

The flow field is divided into two regimes of subsonic flow and supersonic flow in calculating the wall flow conditions.

1. SUBSONIC FLOW NET (INLET)

The subsonic flow field is calculated by a solution of the Euler equation, the continuity equation, the condition of irrotational flow, and an expression for the speed of sound in an isentropic flow.

The inviscid, steady state flow field is calculated by a relaxation solution of the finite difference equation in terms of the stream function. The density is corrected at each mesh point in the calculation to account for compressibility.

Arbitrarily prescribed inlets, outlets, and channel boundaries are allowed with few restrictions. Mass addition (from burning or ablation) is allowed along any boundary and is input as a gradient in the stream function. This is particularly useful where the propellant surface is near the nozzle. The output consists of streamlines for specified values of the stream function and values of velocity, flow angle, pressure ratio, and Mach number along the streamlines.

An option allows the calculation of the uncoupled particle trajectories for any diameter and density and for any set of starting conditions at an inlet. The program calculates the trajectory and the conditions at impact (if necessary).

This program well defines the inviscid flow field at the edge of the boundary layer.

2. SUPERSONIC FLOW FIELD (EXIT)

On a conical nozzle, the wall flow conditions are not widely different from one-dimensional; therefore, this assumption was used for the exit cone.

E. TURBULENT BOUNDARY LAYER

In solid rocket motors the boundary layer is generally turbulent in the critical areas for analysis; therefore, this discussion considers turbulent boundary layer only. In a nozzle evaluation, the Reynolds number is checked to insure turbulent flow.

The boundary layer program calculates boundary layer thicknesses, skin-friction, and heat flux in axisymmetric nozzles. The method solves simultaneously the integral momentum and energy equations. Boundary layer shape parameters are based on a one-seventh power profile of velocity and stagnation temperature. The program is based on a program developed by Elliott, Bartz, and Silver at JPL on Contract NAS7-100*.

The program either calculates one-dimensional Mach numbers or accepts input values from the subsonic and supersonic flow calculations. The outputs are displacement thickness, momentum thickness, convective heat transfer coefficient, convective and radiative heat fluxes, skin friction coefficient, and the wall shear force.

F. WALL MATERIALS

In order to generate erosion, char, and material temperature profiles, the following material properties versus temperature must be provided for all the nozzle liner materials used as input for the 2-D Axisymmetric Transient Temperature Prediction Program.

1. Density.
2. Specific heat.
3. Thermal conductivity.
4. Emissivity.

G. WALL TRANSIENT TEMPERATURE

The material response program is called the 2-D Axisymmetric Transient Temperature Prediction Program (3148). It is used to predict nozzle liner wall thermal gradients from internal gas heating.

The program has two options: Option one predicts internal wall temperatures from prescribed heating boundary conditions. Option two determines heating boundary conditions and internal wall temperatures from prescribed temperature histories.

*Elliott, D. G., et al.: Calculation of Turbulent Boundary Layer Growth and Heat Transfer in Axisymmetric Nozzles, JPL Technical Report No. 32-387, February 1963.

The program inputs include material properties, convective heat transfer coefficients, and predicted wall erosion rates. The program will allow predicted erosion depths by processing the input data for preselected time spans, stopping, receiving erosion depth input, continuing to the next programed stop, and receiving erosion depth input. The pyrolysis of the resin is also simulated by a high heat capacity about the pyrolysis temperature.

The program output includes internal wall temperatures which are plotted with erosion and char versus radial wall thickness as shown in Figure A-3.

H. WALL TRANSIENT TEMPERATURE CHECK

The One-Dimensional Char and Ablation Program (3132) considers the resin pyrolysis and erosion in the energy balance and an input erosion rate. The empirical data were used for the erosion rates and several one-dimensional runs were made to check the accuracy of the 2-D Axisymmetric Temperature Prediction Program.

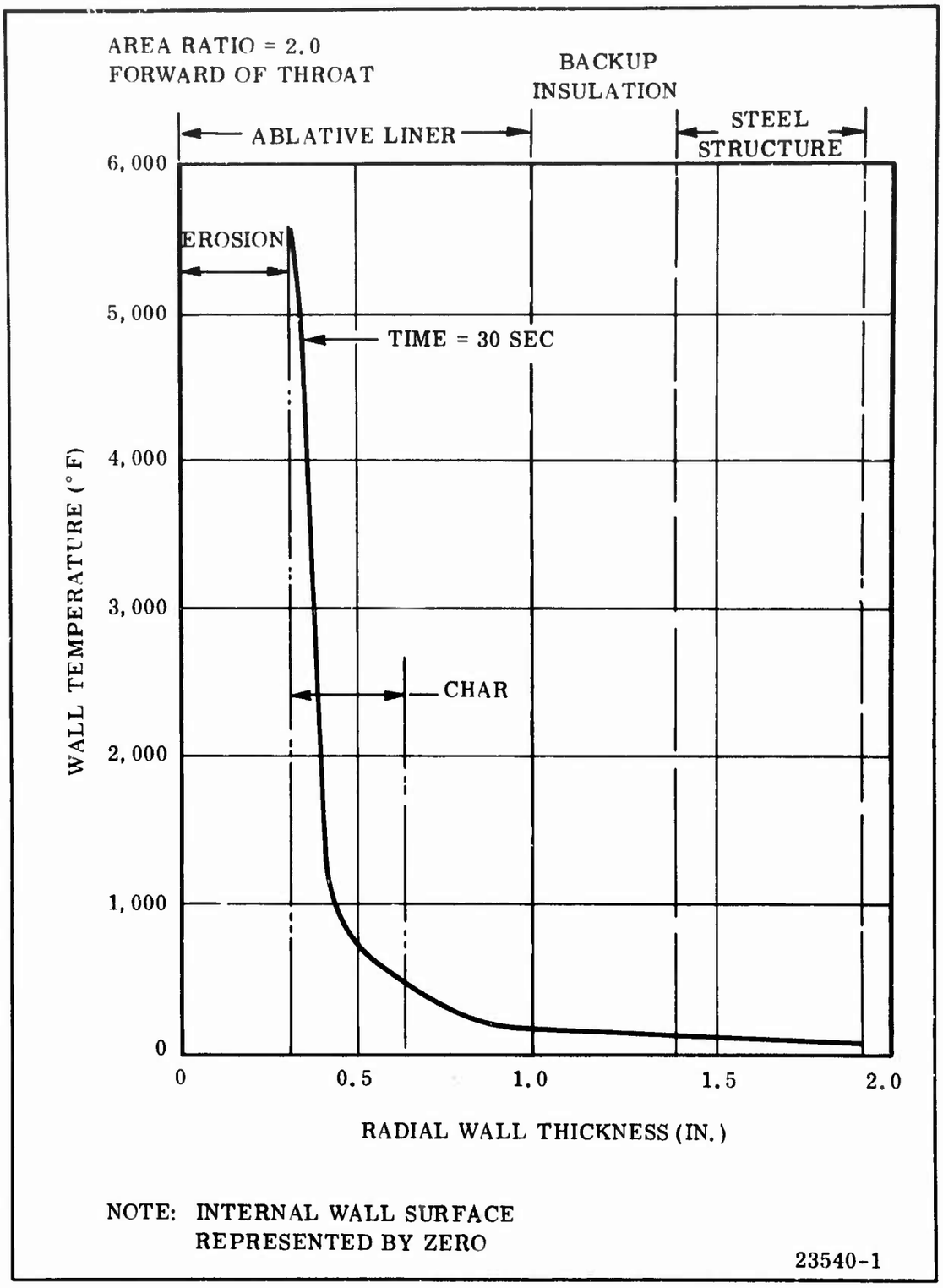

Figure A-3. Wall Temperature Profile

Unclassified
Security Classification

DOCUMENT CONTROL DATA - R & D

(Security classification of title, body of abstract and indexing annotation must be entered when the overall report is classified)

1. ORIGINATING ACTIVITY (Corporate author)	2a. REPORT SECURITY CLASSIFICATION
Thiokol Chemical Corporation Wasatch Division Brigham City, Utah	Unclassified 2b. GROUP

3. REPORT TITLE

Final Report, Development of Castable Carbonaceous Materials for Solid Rocket Nozzles

4. DESCRIPTIVE NOTES (Type of report and inclusive dates)

Final Report (March 1966 thru March 1969)

5. AUTHOR(S) (First name, middle initial, last name)

Stanley H. Cardall

Richard C. Laramee

6. REPORT DATE	7a. TOTAL NO. OF PAGES	7b. NO. OF REFS
March 1969	229	

8a. CONTRACT OR GRANT NO.	9a. ORIGINATOR'S REPORT NUMBER(S)
AF 04(611)-11417 b. PROJECT NO.	Publications No. 0469-23540
c. d.	9b. OTHER REPORT NO(S) (Any other numbers that may be assigned this report)

10. DISTRIBUTION STATEMENT

This document is subject to special export controls and each transmittal to foreign governments or foreign nationals may be made only with prior approval of AFRPL (RPOR/STINFO), Edwards AFB, California 93523.

11. SUPPLEMENTARY NOTES	12. SPONSORING MILITARY ACTIVITY
	Motor Component Development Branch, Rocket Propulsion Laboratory, Air Force Systems Command, Edwards, Calif

13. ABSTRACT

Three basic material formulations ~~designated T-2610, T-4120, and T-4113~~ were evaluated by laboratory testing and static firing in test motors with nozzles having a throat diameter of approximately 4 inches. In total, six nozzles were fabricated and static tested. ~~Nozzle No. 6~~, which was fabricated of conventional nozzle materials, was used as a baseline. The remaining five nozzles were constructed using the castable carbonaceous materials. Nozzles No. 1, 2, and 3 functioned successfully. Nozzle No. 4 malfunctioned due to material failure. Both a motor and nozzle malfunction occurred during the test of Nozzle No. 5. A motor failure prevented accurate evaluation of Nozzle No. 6. Performance data from the six nozzle tests indicate that the materials will require additional development effort; however, the accumulative results for materials T-2610 and T-4120 continue to be encouraging and warrant additional evaluation effort.

DD FORM 1 NOV 65 1473

Unclassified
Security Classification